INSIGHTS INTO GREAT LAKES BASIN WATER RESOURCES THROUGH FIELD DATA AND HYDROLOGIC MODEL INTEGRATION

By

Brent Porter Heerspink

A DISSERTATION

Submitted to
Michigan State University
in partial fulfillment of the requirements
for the degree of

Earth and Environmental Sciences—Doctor of Philosophy

2025

ABSTRACT

The Laurentian Great Lakes are the largest system of connected surface water lakes in the world. Fresh surface and groundwater totaling approximately 27,000 km^3 stored within the Great Lake Basin are a critical resource for the region and the rest of North America. However, anthropogenic contaminants, invasive species, increasing water use demands and a changing climate threaten these water resources in the Great Lakes Basin. To mitigate these threats, a better understanding of the processes controlling water resources, and hydrologic modeling frameworks capable of simulating past, current and future conditions are required. This dissertation seeks to apply both of these methods to study water quality and groundwater-surface water interactions within the state of Michigan region. Two primary research questions are addressed in this dissertation. First, what are the landscape and hydrologic factors which control stream nutrient concentrations? This question is addressed in Chapter 2 through the analysis of regional scale repeated synoptic stream chemistry sampling data and statistical analysis. Second, how are groundwater dynamics linked to Great Lakes lake levels, either indirectly through regional climate or directly through boundary condition effects? This topic is investigated in Chapters 3 and 4 using a coupled, process-based surface and groundwater model. Results from Chapter 2 suggest that landscape characteristics are a powerful predictor of stream chemistry early in the year during snowmelt, but that the landscape becomes decoupled from stream chemistry as the seasons progress. Relationships between streamflow and water chemistry during the spring and summer high flow events indicate distinct water chemistry patterns despite similar flow conditions when compared to baseflow. Chapter 3 investigates how groundwater storage changed during a period of extreme lake level variations. Simulations of surface hydrology and groundwater elevations from 2000-2023 using the Landscape Hydrology Model indicate that groundwater elevations increased along with lake elevations between 2013-2020, but that the onset of these storage increases lagged the onset of lake level changes by 2-4 years. In Chapter 4, this model is applied to investigate how coastal wetland connectivity to surface and groundwater changes as lake and groundwater elevations fluctuate. Modeling analysis suggests that rising groundwater elevations between 2000-2023 increased the amount of connected coastal wetland area by 18% when compared to estimates of surface water connectivity change alone. Finally, Chapter 5 provides a summary and proposes a method for more closely integrating field data collection and hydrologic models to groundwater nutrient transport through the use of a model-experiment framework

This Dissertation is dedicated to my Grandparents: William and Lorone Porter, and Donald and Angelyn Heerspink, from whom I learned an invaluable amount, and who inspired the determination and dedication needed to finish this PhD.
"To strive, to seek, to find and not to yield" – Ulysses, Alfred, Lord Tennyson

ACKNOWLEDGMENTS

I would first like to thank my family, starting with my parents, Brent D. Heerspink and Julie Porter, who both instilled in me a love for nature. As potters, they've created art from natural materials: clay from the Ohio River valley and the eastern UP, ash glazes from firewood cut on their property, sand from the beaches of Lake Michigan. In their free time, my parents seek to be outside, by gardening, horse-back riding, hunting, fishing, trapping and almost anything else that gets them in touch with the natural world. I inherited my parents' love for the outdoors, their appreciation for nature, and their curiosity. My interest in water science can be traced back to standing along a trout stream wondering where the water in a small spring came from. My parents have always supported my academic interests, from a middle school science fair project on water quality, to a college degree in biology, an internship in New Mexico, a Master's Degree that took me to Brazil and now through the ups and downs of my PhD. My parents have always been there when I needed them; their particular brand of steady encouragement has helped me throughout this PhD and the rest of my life. I wouldn't be the person, or the scientist I am today without them. I would like to thank my partner Alex Kuhl for her unwavering love and support. Our shared interest in science and the outdoors is what brought Alex and I together. She has listened to me complain, helped me solve problems, comforted me when things went wrong, encouraged me when I felt like quitting, and never stopped believing in my ability to climb this mountain, even when I did. In addition to Alex, her mother Diane Kuhl has been a constant source of encouragement, and worked hard to help me see the light at the end of the tunnel. I could not have made it through this journey without a group of close friends who have become family: Justin Pollard, Trent Pitko, Tori Malus and Chanse Ford. All four of them have been a source of love and support when I've needed it most; whether I needed a break, a laugh, a word of encouragement, or a reality check, they have always been there for me. Finally, I would like to thank my friend and lab mate Jake Stid. Jake and I went on the adventure that is earning a PhD together, we were there for each other in the most difficult days while trying to finish, and defended our dissertations just a month apart. I would not have made it through this program without him.

Next I would like to thank my advisor, Dr. Anthony Kendall. The first ideas of my PhD project were created in Anthony's office; his willingness to help me develop a PhD that met both my personal and academic interests is a major reason I stayed at MSU for my PhD. Developing the work in this dissertation has been a truly collaborative process, and I've deeply enjoyed the

work we got to do together. Anthony has been a wonderful advisor who's helped me grow as both a scientist and a mentor, and has become a dear friend. I also want to thank the rest of my advisory committee: David Hyndman, Dalton Hardisty, Matt Schrenk and Randall Hunt. Each of them have taught me important lessons about my science, and have looked out for me both personally and professionally. I owe a special thanks to Dave, who was my Master's degree advisor, and whose advice was critical in my decision to pursue a PhD. I also owe a special thanks to Randy, who opened the door to an internship at the U.S. Geological Survey which enriched my PhD experience immensely.

I could not have made it through my degree without my fellow Hydrogeology Lab members, both past and present including: Luwen Wan, Alexis Lanier, Jeremy Rapp, Quercus Hamlin, Behnaz Mirzendehdel, Samin Abolmaali, Maddie Sigler, and Noah Bohl. The Hydrolab has always had a wonderful culture of peer support and encouragement, and without the support of my peers this dissertation would not have been possible. This sentiment extends to the rest of the Earth and Environmental Sciences Department as well. I have received an invaluable amount of support and encouragement from faculty, staff and other students in the department. I also owe a great deal of thanks to my colleagues at the U.S. Geological Survey Upper Midwest Water Science Center including Chanse Ford, Howard Reeves, Mike Fienen, and Sherry Martin. I would also like to say a special thanks to Chanse and Sherry, with whom I've worked with at both MSU and USGS. Sherry has helped me to keep perspective on my work, push forward when things seemed bleak, and taught me to remember that people are why our science matters and how it gets done. Chanse and I have been both students together at MSU, and now colleagues at USGS. We've learned and worked together for seven years, and his advice and encouragement has been invaluable.

I would also like to thank my previous research mentors, who have helped guide me along the journey to getting my PhD. Timothy Lincoln was my undergraduate research advisor, who along with professors Vanessa McCaffrey and Ola Olapade helped me develop and complete my undergraduate thesis. They jumpstarted my career as a scientist, and all sought to look out for me during my time at Albion and beyond. While at Albion, I was introduced to an alumni, Paul Dixon, who offered me a post-bachelors internship at Los Alamos National Lab. Moving to New Mexico and working at Los Alamos was one of the defining events in my life. I learned technical skills, perspective and the attitude toward research that l needed to succeed in graduate school. I also owe

a special thanks to former MSU grad students Erin Haacker and Joe Lee-Cullin, who have become both good friends and wonderful mentors, providing a wealth of advice and support during my PhD

I would like to say a special thank you to three people who have become dear friends in addition to scientific mentors: Florie Caporuscio, Dan Haye and Mike Rearick. Florie and I worked together at LANL and bonded quickly over a shared love for fly fishing. I've learned invaluable lessons, both personal and professional from Florie, who has faithfully called me at least once a month during my dissertation to check on me, and remind me to focus on the finish line. Mike and I similarly met at LANL and connected through fly fishing. Mike and I put on a ton of miles in the field together and built a friendship that's lasted far beyond the short time I spent in New Mexico. Mike helped facilitate my first mule deer hunt, chasing some of the most astounding animals I've ever seen. Mike's been a steadfast friend since my time in New Mexico, and his determination in the woods has pushed me to become a better outdoorsman.

I finally like to thank the many other family and friends who have supported me during this journey including: Martha Ford, Casey Pollard, Brian and Crystal Eustice, Mark Zabrowski and Jana Burke, Leanne Hancock, Blaze and Megan Budd, Justin Ware, Jacob Roush, Autumn Parish, Sally and Randy Wiener, and Nancy Porter. I've been very blessed throughout my life to have a large group of people who've supported me, and I've leaned on all of them at one time or another during this PhD.

TABLE OF CONTENTS

LIST OF TABLES

LIST OF FIGURES

LIST OF ABBREVIATIONS

3DEP	3-Dimensional Elevation Program
DEM	Digital Elevation Model
ET	Evapotranspiration
GCM	Global Circulation Model
GLAHF	Great Lakes Aquatic Habitat Framework
GLB	Great Lakes Basin
GLERL	Great Lakes Environmental Research Laboratory
GRACE	Gravity Recovery and Climate Experiment
GPS	Global Positioning System
HK	Hydraulic Conductivity
LHM	Landscape Hydrology Model
LMB	Lake Michigan Basin
LP	Lower Peninsula
ModEx	Model-Experiment
N	Nitrogen
NASA	National Aeronautics and Space Administration
NED	National Elevation Dataset
NNSE	Normalized Nash-Sutcliffe Efficiency
NOAA	National Oceanographic and Atmospheric Administration
NSF	National Science Foundation
OLS	Ordinary Least Squares
P	Phosphorus (Chapter 2)
P	Precipitation (Chapter 3)
PET	Potential Evapotranspiration
RCM	Regional Climate Model
RMSE	Root Mean Square Error
TN	Total Nitrogen
TP	Total Phosphorus
USDA	United Stated Department of Agriculture
USGS	United States Geological Survey

UP	Upper Peninsula
WWTP	Wastewater Treatment Plant

CHAPTER 1: INTRODUCTION

The Laurentian Great Lakes are the largest system of freshwater connected lakes in the world. The Great Lakes Basin (GLB) covers portions of eight U.S. states and the Canadian province of Ontario, home to more than 30 million people, or ~10% of the US and ~30% of the Canadian population (Gronewold et al., 2013). Approximately 40 million people in the US and Canada get their drinking water from the GLB (Polidori et al., 2024). The Great Lakes region contains a diverse range of ecosystems including boreal forests, prairies, coastal wetlands and aquatic systems which support over 3,500 species of plants and animals (Michigan Sea Grant). The water resources of this region are a major driver of economic productivity contributing through sectors including tourism, manufacturing, shipping, and commercial fishing (NOAA, 2020).

Together the five lakes, Superior, Michigan, Huron, Erie and Ontario, contain approximately 23,000 km^3 of surface water or about 21% of the world's available freshwater (Hunter et al., 2015, Norton et al., 2019). In addition to the abundant surface waters, the GLB also contains about 4,000 km^3 of groundwater (Grannemann et al., 2010). The modern Great Lakes were formed by the advance and retreat of glaciers during the Quaternary Period (Larson and Schaetzl, 2001). These glaciers also deposited glacial sediments which define surficial geology in the southern portion of the basin. There is significant groundwater storage in these sediments, and in underlying permeable limestone and sandstone bedrock units (Feinstein et al., 2010, Grannemann et al., 2010). Groundwater is an important source of drinking water in the basin, providing water to both large urban areas and rural communities. It also provides up to 90% of streamflow (Neff et al., 2005), and contributes ~45% of the total inputs to the Great Lakes both directly through discharge to the lakes and indirectly as stream baseflow (Neff and Nichols, 2005). The Great Lakes play an important role in the climate of the region. Their large surface area and thermal inertia result in significant water recycling (evaporation, condensation, and precipitation) within the basin. This results in distinct lake effect precipitation patterns of concentrated snow and rainfall on the southern and eastern sides of the lakes (Notaro et al., 2013). However, the quality and quantity of ground and surface water resources in the Great Lakes Basin, are threatened by changing climate and land use, increased water use demands, and the release of anthropogenic contaminants.

The release of nitrogen and phosphorus compounds into the environment has resulted in

elevated nutrient concentrations in rivers (Singh et al., 2023), groundwater (Hamlin et al., 2022), wetlands (Hannah et al., 2020), inland lakes, and the Great Lakes (Ho and Michalak, 2015). Eutrophic conditions in Lake Erie have resulted in anoxia and harmful algal blooms, impacting aquatic ecosystems and municipal water resources for coastal human communities (Ho and Michalak, 2015). Nitrate leaching to groundwater has resulted in the contamination of drinking water wells in Michigan's Lower Peninsula, threatening human health (Hamlin et al., 2022). Considerable work has been done to study anthropogenic nutrient contamination, ranging from intense monitoring at the field to watershed scale, to regional scale modeling and data synthesis efforts (Byrnes et al., 2020, Gentry et al., 1998, Knapp et al., 2020, Knapp et al., 2022, Robertson et al., 2019). Despite these efforts, heterogeneous nutrient sources, transport and cycling processes prevent effective management (Van Meter et al., 2018). An increased understanding of both seasonal and spatial variability in nutrient concentrations, and the role of legacy nutrients delivered by groundwater flow paths with long transit times are needed to better address this issue.

Recent climate shifts have resulted in historic changes in lake levels (Gronewold et al., 2023). These rapid changes in lake levels have altered coastal ecosystems, impeded commerce and damaged coastal infrastructure (Gronewold et al., 2013, Theuerkauf and Braun, 2021). However, the effects of these recent climate shifts on terrestrial hydrology and groundwater dynamics within the basin are largely unquantified. Significant efforts have been undertaken to understand groundwater dynamics within the GLB, through a combination of observational data and hydrologic models. The scope of these investigations range from the county (Luukkonen et al., 2004 , Holtschlag et al., 1998), and watershed (Curtis et al., 2019, Hunt et al., 2013) to the Lake Michigan Basin scale (Feinstein et al., 2010). Yet, groundwater is largely underrepresented in regional scale hydrologic models, including those used for operational forecasting of climate, terrestrial hydrology, and lake levels in the Great Lakes (Fry et al., 2020). An improved understanding of how groundwater has responded to regional climate shifts, and its interactions with the Great Lakes, are necessary to effective water resource management within the GLB.

This dissertation seeks to better understand the processes controlling water quality and water resources in the GLB, through a combination of field data and hydrologic models, with a particular focus on groundwater-surface water interactions. Two major questions are addressed herein. First, what are the landscape and hydrologic factors that control stream nutrient concentrations? This topic is addressed though statistical analysis of regional scale repeated

synoptic stream sampling data. Second, how are groundwater dynamics linked to Great Lakes levels, either indirectly through regional climate or directly though boundary condition effects along the Great Lakes coastline? This topic is investigated using a coupled, process-based surface and groundwater model. Both of these investigations are focused on the state of Michigan region. Michigan, comprised of the Upper and Lower Peninsulas, is located in the central portion of the GLB, and has coastline along four of the five Great Lakes. Michigan has strong gradients in climate, ecosystems, hydrology, surficial geology and land use that encompasses conditions spanning a large portion of the GLB. The following three chapters of this dissertation detail these investigations.

Chapter 2 studies how water quality varies across seasons within Michigan's Lower Peninsula as a result of landscape characteristics and hydrological processes. Specifically, data from a repeated synoptic stream sampling campaign which targeted specific hydrologic conditions are used to understand how relationships between land cover and stream nutrient concentrations vary across seasons and flow conditions.

While developing this work, it became clear that the role of hydrologic processes in determining stream chemistry could not be fully characterized with field data alone; a hydrologic modeling framework capable of describing both surface and subsurface processes was needed. Thus, a coupled surface and groundwater model was developed to quantify how the sources of streamflow changed though time within a given catchment, and how this may affect water quality. During the development of this model, the Great Lakes reached historic highs following a period of unprecedentedly rapid water level increases. This phenomenon raised questions about how groundwater storage and discharge had changed during this period, and about the degree to which rising lake levels directly affect groundwater.

Subsequently, Chapters 3 and 4 focus on simulating groundwater at the regional scale within the GLB. Chapter 3 describes the development of this regional scale hydrology model, and it' use to quantify how groundwater storage has changed across the state of Michigan region from 2000-2024. This is the first regional scale, coupled surface and groundwater modeling effort to specifically investigate changes in groundwater storage coincident with the recent lake level variability. The fourth Chapter of this dissertation focuses on characterizing the direct interactions between the Great Lakes and the adjacent groundwater system, and how this may have affected coastal wetland habitats during swings in lake levels.

Finally, Chapter 5 concludes this dissertation and describes how the insights and tools develop here could be applied in a model-experiment (ModEx) framework to improve our understanding of stream water quality. The ModEx approach consists of closely integrating field data during model development, and use of the model to develop targeted filed data collection efforts. Specifically, it details a proposed hydrologic model-informed field sampling effort to better characterize the role of groundwater nutrient legacies in surface water quality.

.

REFERENCES

Byrnes, D.K., Meter, K.J.V., Basu, N.B., 2020. Long-Term Shifts in U.S. Nitrogen Sources and Sinks Revealed by the New TREND-Nitrogen Data Set (1930–2017). Global Biogeochem Cy 34. https://doi.org/10.1029/2020gb006626

Curtis, Z.K., Liao, H., Li, S., Sampath, P.V., Lusch, D.P., 2019. A Multiscale Assessment of Shallow Groundwater Salinization in Michigan. Groundwater 57, 784–806. https://doi.org/10.1111/gwat.12873

Feinstein, D.T., Hunt, R.J., Reeves, H.W., 2010. Regional groundwater-flow model of the Lake Michigan Basin in support of Great Lakes Basin water availability and use studies, Scientific Investigations Report 2010-5109. U.S. Geological Survey.

Fry, L.M., Apps, D., Gronewold, A.D., 2020. Operational Seasonal Water Supply and Water Level Forecasting for the Laurentian Great Lakes. J. Water Resour. Plan. Manag. 146. https://doi.org/10.1061/(asce)wr.1943-5452.0001214

Gentry, L.E., David, M.B., Smith, K.M., Kovacic, D.A., 1998. Nitrogen cycling and tile drainage nitrate loss in a corn/soybean watershed. Agric Ecosyst Environ 68, 85–97. https://doi.org/10.1016/s0167-8809(97)00139-4

Grannemann, N.G., Hunt, R.J., Nicholas, J.R., Reilly, T.E., Winter, T.C., 2000. The Importance of Ground Water in the Great Lakes Region, Water-Resources Investigations Report 2000-4008. U.S. Geological Survey.

Gronewold, A.D., Fortin, V., Lofgren, B., Clites, A., Stow, C.A., Quinn, F., 2013. Coasts, water levels, and climate change: A Great Lakes perspective. Climatic Change 120, 697–711. https://doi.org/10.1007/s10584-013-0840-2

Hamlin, Q.F., Martin, S.L., Kendall, A.D., Hyndman, D.W., 2022. Examining Relationships Between Groundwater Nitrate Concentrations in Drinking Water and Landscape Characteristics to Understand Health Risks. Geohealth 6, e2021GH000524. https://doi.org/10.1029/2021gh000524

Hannah, B.A., Kendall, A.D., Martin, S.L., Hyndman, D.W., 2020. Quantifying linkages between watershed factors and coastal wetland plant invasion in the US Great Lakes. Landscape Ecol 35, 2843–2861. https://doi.org/10.1007/s10980-020-01124-3

Ho, J.C., Michalak, A.M., 2015. Challenges in tracking harmful algal blooms: A synthesis of evidence from Lake Erie. J Great Lakes Res 41, 317–325. https://doi.org/10.1016/j.jglr.2015.01.001

Holtschlag, D.J., Luukkonen, C.L., Nicholas, J.R., 1996. Simulation of ground-water flow in the Saginaw Aquifer, Clinton, Eaton, and Ingham counties, Michigan, Water Supply Paper 2480. U.S. Geological Survey, Washington, D.C.

Hunt, R.J., Walker, J.F., Selbig, W.R., Westenbroek, S.M., Regan, R.S., 2013. Simulation of Climate-Change Effects on Streamflow, Lake Water Budgets, and Stream Temperature Using GSFLOW and SNTEMP, Trout Lake Watershed, Wisconsin, U.S. Geological Survey Scientific Investigations Report 2013–5159. U.S. Geological Survey, Reston, Virginia:

Hunter, T.S., Clites, A.H., Campbell, K.B., Gronewold, A.D., 2015. Development and application of a North American Great Lakes hydrometeorological database — Part I: Precipitation, evaporation, runoff, and air temperature. J Great Lakes Res 41, 65–77. https://doi.org/10.1016/j.jglr.2014.12.006

Knapp, J.L.A., Freyberg, J. von, Studer, B., Kiewiet, L., Kirchner, J.W., 2020. Concentration–discharge relationships vary among hydrological events, reflecting differences in event characteristics. Hydrol Earth Syst Sc 24, 2561–2576. https://doi.org/10.5194/hess-24-2561-2020

Knapp, J.L.A., Li, L., Musolff, A., 2022. Hydrologic connectivity and source heterogeneity control concentration–discharge relationships. Hydrol. Process. 36. https://doi.org/10.1002/hyp.14683

Larson, G., Schaetzl, R., 2001. Origin and Evolution of the Great Lakes. J Great Lakes Res 27, 518–546. https://doi.org/10.1016/s0380-1330(01)70665-x

Luukkonen, C.L., Blumer, S.P., Weaver, T.L., Jean, J., 2004. Simulation of the ground-water-flow system in the Kalamazoo County area, Michigan, U.S. Geological Survey Scientific Investigations Report 2004-5054. U.S. Geological Survey, Reston, VA.

Meter, K.J.V., Cappellen, P.V., Basu, N.B., 2018. Legacy nitrogen may prevent achievement of water quality goals in the Gulf of Mexico. Science 360, 427–430. https://doi.org/10.1126/science.aar4462

Michigan Sea Grant. Great Lakes Fast Facts. Michigan Sea Grant, https://www.michiganseagrant.org/topics/great-lakes-fast-facts/.

Neff, B.P., Day, S.M., Piggott, A.R., Fuller, L.M., 2005. Base flow in the Great Lakes Basin, Scientific Investigations Report 2005-5217. U.S. Geological Suvey, Reston, VA.

Neff, B.P., Nicholas, J.R., 2005. Uncertainty in the Great Lakes Water Balance, Scientific Investigations Report 2004-5100. U.S. Geological Survey, Reston, Virginia.

National Oceanic and Atmospheric Administration (NOAA). 2020. Great Lakes environmental indicators: A baseline for managing water quality and ecosystem health. National Oceanic and Atmospheric Administration. https://repository.library.noaa.gov/view/noaa/3861

Norton, P.A., Driscoll, D.G., Carter, J.M., 2019. Climate, Streamflow, and Lake-Level Trends in the Great Lakes Basin of the United States and Canada, Water Years 1960–2015, Scientific Investigations Report 2019–5003. U.S. Geological Survey, Reston Virginia.

Notaro, M., Holman, K., Zarrin, A., Fluck, E., Vavrus, S., Bennington, V., 2013. Influence of the Laurentian Great Lakes on Regional Climate*. J. Clim. 26, 789–804. https://doi.org/10.1175/jcli-d-12-00140.1

Polidori, J.A., Paulson, H.L., Gronewold, A.D., 2024. Assessing trends in urban municipal water use across the Great Lakes Basin. J. Gt. Lakes Res. 50, 102243. https://doi.org/10.1016/j.jglr.2023.102243

Robertson, D.M., Saad, D.A., Benoy, G.A., Vouk, I., Schwarz, G.E., Laitta, M.T., 2019. Phosphorus and Nitrogen Transport in the Binational Great Lakes Basin Estimated Using SPARROW Watershed Models. Jawra J Am Water Resour Assoc 55, 1401–1424. https://doi.org/10.1111/1752-1688.12792

Singh, N.K., Meter, K.J.V., Basu, N.B., 2023. Widespread increases in soluble phosphorus concentrations in streams across the transboundary Great Lakes Basin. Nat. Geosci. 16, 893–900. https://doi.org/10.1038/s41561-023-01257-5

Theuerkauf, E.J., Braun, K.N., 2021. Rapid water level rise drives unprecedented coastal habitat loss along the Great Lakes of North America. J Great Lakes Res 47, 945–954. https://doi.org/10.1016/j.jglr.2021.05.004

CHAPTER 2: SEASONALLY VARIABLE RELATIONSHIPS BETWEEN LANDSCAPE CHARACTERISTICS, HYDROLOGY, AND STREAM NUTRIENT CONCENTRATIONS REVEALED THROUGH STRATEGIC SYNOPTIC SAMPLING

Abstract

The spatial and temporal heterogeneity of nutrient (nitrogen (N) and phosphorus (P)) sources, cycling, and transport poses a significant barrier to accurately predicting their concentrations and impedes effective water quality management. A better understanding of how nutrient sources, landscape characteristics, and hydrologic processes affect nutrient fluxes is needed to improve predictive capability. To investigate these seasonal dynamics, stream chemistry data from 64 Great Lakes tributaries across Michigan's Lower Peninsula were collected through synoptic sampling efforts conducted during three hydrologic conditions: snowmelt, post-planting summer rainfall, and fall baseflow. Observed concentrations of N and P species increased from north to south in the study region, corresponding to increasing urban and agricultural land uses. On average, concentrations were highest during snowmelt, elevated during summer rainfall, and lowest during baseflow. Linear models describing stream nutrient concentrations using landscape characteristics performed best for snowmelt samples ($R^2 \leq 0.83$), moderately for summer rainfall ($R^2 \leq 0.73$), and most poorly for baseflow ($R^2 \leq 0.70$). This progressive decoupling between landscape characteristics and stream nutrient concentrations indicates a regime shift from landscape-dominated concentrations in the Spring, to stream process-dominant in the late summer and early fall. This shift corresponds to changing concentration-discharge relationships and aligns with reduced influence of surface runoff relative to groundwater discharge, decreased nutrient availability, and increased biogeochemical cycling as the seasons progress. Explicitly considering this seasonal switch from landscape-dominated to instream process-dominated nutrient controls may provide insights to predict nutrient delivery to waters impacted by eutrophication.

1. Introduction

The global development of agricultural, industrial, and wastewater infrastructure in response to growing human population has resulted in release of nutrients (specifically nitrogen (N) and phosphorus (P)) to the landscape far in excess of natural conditions (Byrnes et al., 2020, Carey and Migliaccio 2009, Hamlin et al., 2022, Vitousek et al., 2009). These anthropogenic nutrients pose a significant threat to the quality of groundwater and surface water in developed regions across the globe (Vörösmarty et al., 2010). This threat is widely recognized and has been extensively studied, with recent examples from North America (Basu et al., 2023, Wan et al., 2023), South America (Figueiredo et al., 2020), South Africa (Mararakanye et al., 2022), India (Bowes et al., 2020), Europe (Ebeling et al., 2021), China (Zhang et al., 2019), and New Zealand (Rogers et al., 2023). Nutrient accumulation in surface waters has caused increases in the occurrence and severity of anoxic conditions and harmful algal blooms in regions including the Gulf of Mexico (Rabalais et al., 2002), Chesapeake Bay (Boesch et al., 2001) and Lake Erie (Ho and Michalak, 2015). Anthropogenic nutrients also accumulate in the subsurface, contaminating shallow groundwater (DeSimone et al., 2014, Knoll et al., 2019, Lockheart et al., 2013, Nolan et al., 1997) and posing a threat to drinking water and human health, especially in heavily agricultural regions (Hamlin et al. 2022, Pennino et al., 2017, Ward et al., 2018). Tackling this problem has been hindered by factors including generally unknown nutrient inputs, complex biogeochemical cycles, and species-dependent transport via both surface and groundwater pathways—all of which vary seasonally. Further complicating this issue are the long lag times between nutrient release and delivery along subsurface flowpaths, which can provide sustained nutrient inputs to surface waters even after nutrients inputs have been reduced (Martin et al., 2021, Van Meter et al., 2018). Advancing the capability to accurately describe and predict landscape nutrient fluxes to surface waters requires a deeper understanding of relationships among these landscape, hydrologic and biogeochemical processes.

Studying patterns in stream nutrient concentrations across gradients in landscape characteristics and hydrologic conditions through careful sampling campaign design can enhance this understanding. Stream catchments integrate seasonally variable landscape inputs, runoff flowpaths, solute transport mechanisms and nutrient cycling processes across the landscapes they drain. Stream chemistry also provides an ecologically relevant monitoring and management target, as rivers are important natural ecosystems, and a major conduit by which nutrients are transported

from uplands to wetlands, inland lakes, and ultimately the Great Lakes coastline (Mooney et al., 2020, Robertson and Saad, 2011). As a result, measuring and monitoring stream chemistry has been, and continues to be, a powerful tool to understand how the landscape affects water quality.

Land use and land cover determine the nutrient sources within a watershed (Hamlin et al., 2020, Luscz et al., 2015, 2017), which are a strong control on observed surface water nutrient concentrations (Allen, 2004, Robertson and Saad, 2011). Specifically, the amount of agricultural and urban areas within a watershed have been correlated to increased nutrient concentrations in surface waters systems ranging from headwater streams in Oregon (Poor and McDonnel, 2007) to reservoirs in the Missouri River basin (Jones et al., 2004). Conversely, the presence of forested areas is correlated with decreased stream nutrient concentrations, due to lower nutrient inputs (Jones et al., 2004).

Watershed landscape characteristics also exert control on nutrient cycling and transport processes. The presence of riparian wetlands, which are hotspots of biogeochemical activity, has been correlated to decreases in stream nutrient concentrations relative to landscape inputs (Hansen et al., 2018; Martin et al., 2011). Tile drainage is widespread across the agricultural Midwest, and creates a direct conduit between the root zone and surface waters, short circuiting natural transport and cycling processes in the shallow subsurface (Gorski and Zimmer, 2021). This results in flashy streamflow responses and increased nutrient export during storm flow events in extensively drained landscapes (Gentry et al., 2007, Miller and Lyon 2021, Royer et al., 2006). In urban watersheds, wastewater treatment plant (WWTP) effluent high in nutrients can comprise a significant proportion of streamflow, especially during low flows in heavily urban influenced watersheds (Carey and Migliaccio, 2009, Ledford et al., 2021).

Hydrologic processes affect nutrient transport and biogeochemical cycling within a watershed, and play an important role in determining stream chemistry. Specifically, variations in the active flowpaths by which water moves from uplands to streams, can mobilize different pools of stored nutrients, change residence times between mobilization and delivery, and affect the degree of nutrient cycling. Overland flow can mobilize nutrients stored on or near the surface, and quickly transport them to surface waters (Want et al., 2023). Groundwater flowpaths can result in long delays from moralization to delivery (Martin et al., 2017, Van Meter and Basu, 2017), and may result in increased biogeochemical cycling both within aquifers (Lin et al., 2019) and the hyporheic zone of rivers (Zarnetske et al., 2011). While hard to characterize directly, the relative

contribution of flowpaths and the size of contributing areas have both been correlated to changes in streamflow conditions (Jones et al., 2017, Gorski et al., 2021, Zimmer et al., 2019).

Extensive research has been conducted to explore the connections between streamflow dynamics and stream nutrient concentrations. These relationships are highly variable across events (Knapp et al., 2020, Gorski and Zimmer, 2021), seasons (Zimmer et al., 2017), nutrient sources (Jones et al., 2017), antecedent conditions (Knapp et al., 2020), and dominant land use in the watershed (Kincaid et al., 2020). For example, increased streamflow has been correlated to increased nutrient concentrations in agricultural watersheds due to the mobilization of these solutes stored on the landscape, and decreased concentrations in urban watersheds due to the dilution of WWTP effluent high in N and P (Van Meter et al., 2020). Seasonal changes to nutrient sources and bioavailability can result in different concentration-discharge relationships for events of similar magnitudes within a watershed (Knapp et al., 2020). While these and other studies using high-frequency data provide valuable insights into nutrient transport processes, the equipment costs, site access needs, and maintenance requirements limit the potential to collect high-resolution data in many locations at regional scales.

Synoptic sampling provides a snapshot of physical parameters under similar environmental conditions by collecting samples from multiple locations over a short, defined sampling period. Though synoptic sampling lacks high temporal resolution, its low cost (relative to continuous sampling), spatial coverage, and ability to target specific conditions of interest make it a powerful tool to interpret landscape-scale patterns in stream chemistry. Within hydrology, this approach has been applied across a range of spatial and temporal scales, from sampling multiple locations in a single catchment over hours or days (Runkel et al., 2013, 2023), to sampling a large number of watersheds at a regional scale during multi-day sample collection campaigns (Mooney et al., 2020, Verhougstraete et al., 2015). Synoptic sampling methods have also been applied to investigate how stream chemistry evolves along a river corridor (Hensley et al., 2020, Malin et al., 2024). The data from such synoptic sampling campaigns can be used for a range of applications, including investigating relationships between the landscape and stream chemistry (Wayland et al., 2003), monitoring for the presence of contaminants such as acid mine drainage (Messer et al., 1988, Runkel et al., 2013, 2023) or characterizing physical processes, such as identifying the groundwater flowpaths active within stream reaches (Semrdon and Gardner, 2022). Recent work by Abbot et al., (2017) showed that spatial patterns in stream chemistry were stable across years

to decades, suggesting that synoptic sampling data may be representative of landscape scale patterns in stream chemistry beyond the year or season sampled.

Despite extensive study, the complex interplay between landscape characteristics, nutrient inputs, hydrologic processes and biogeochemical cycles limits our understanding of the dominant controls of nutrient export and often prevents effective management (Martin et al., 2021, Van Meter et al., 2018). Many previous publications that investigated how landscape characteristic and hydrologic processes affect seasons stream water quality relied on high frequency water quality monitoring data in a limited number of small catchments. Studies at larger spatial scales also often rely on high frequency data from a few locations on large streams (e.g. Van Meter et al., 2020) or provide a single snapshot in time (e.g. Mooney et al., 2020). An opportunity exists therefore, to explore methods to investigate spatial and seasonal variability in stream nutrient dynamics at regional scales without the need for high frequency monitoring equipment.

Here, a repeated synoptic sampling campaign of 64 watersheds across Michigan's Lower Peninsula was employed to study spatial and seasonal dynamics in stream chemistry. This effort was designed to sample three key portions of the stream hydrograph (hereafter "seasons"): early spring snowmelt, summer rain, and fall low flows (hereafter "baseflow"). Selection of these three seasons was based on prior observations of distinct hydrologic and landscape nutrient source conditions occurring annually in this region. These observations include: high flows and the presence of stored nutrients from agricultural applications the previous fall during snowmelt; elevated flow conditions and recent nutrient applications during summer rainfall; and groundwater dominated low flows and depleted nutrient storage on the landscape during baseflow. Based on these observations, the following hypotheses were developed: 1) in agricultural and rural regions, streamflow and nutrient concentrations would be highest during snowmelt, moderate during summer rainfall, and lowest during baseflow; 2) in urban areas, where the primary nutrient source is municipal WWTP effluent (Carey and Migliaccio, 2009), reduced seasonality in nutrient concentrations relative to agricultural landscapes would occur, and 3) for more reactive nutrient species such as nitrate or soluble reactive phosphorus, seasonal variability may be considerably more complex across landscape types. Data analysis was guided by three primary research questions: 1) how do nutrient concentrations vary during snowmelt, summer rainfall, and baseflow conditions across watersheds with a range of dominant land cover types? 2) What are the dominant landscape and hydrogeologic characteristics that affect seasonal nutrient concentrations across

seasons? 3) How do changing hydrologic processes affect seasonal nutrient concentrations? Testing these hypotheses and answering these questions can provide a deeper understanding of the driving factors behind the spatial and seasonal variations in stream nutrient fluxes and subsequent delivery of nutrients to the Great Lakes, and within similar landscapes more broadly.

2. Methods

2.1 Study Area

This study examined in-stream nutrient dynamics in 64 Great Lakes tributaries draining 82% of Michigan's Lower Peninsula (including small portions of neighboring Indiana and Ohio, Figure 1). This region is characterized by gradients in climate, hydrogeology, nutrient inputs and land cover representative of large portions of the upper Midwestern United States. The rivers in Michigan's Lower Peninsula drain to the Laurentian Great Lakes, which are the largest system of connected freshwater lakes in the world and contain about 20% of the world's fresh surface water (Hunter et al., 2015). This critical resource is threatened by water quality issues, including the widespread addition of anthropogenic nutrients to the landscape, leading to elevated nutrient fluxes (Hamlin et al., 2020, Robertson and Saad 2011) and groundwater nitrate concentrations (Hamlin et al., 2022), as well as increased establishment of invasive species (Hannah et al., 2020), harmful algal blooms (Ho and Michalak 2015), and other deleterious effects.

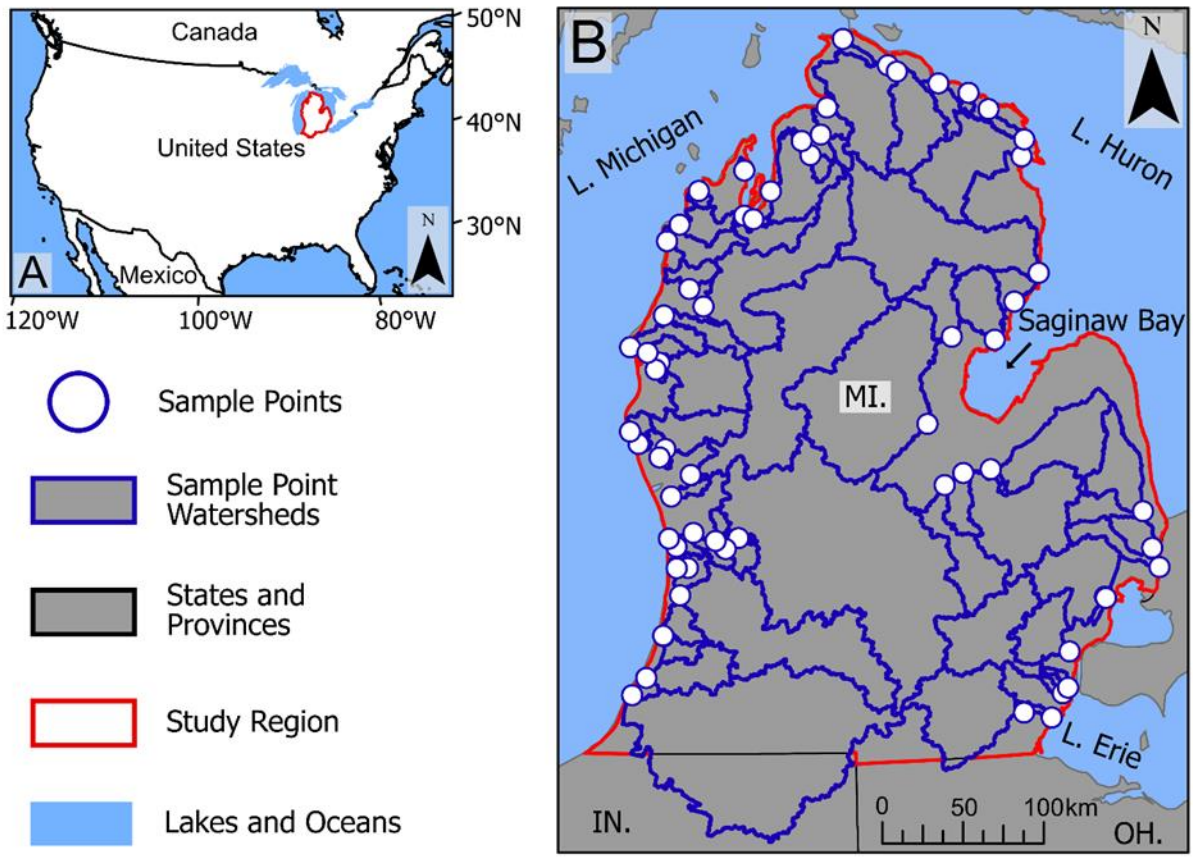

Figure 1: Seasonal Strategic Synoptic Sampling Study Region. The location of (A) the study domain within the United States and (B) the locations of the sample points and their associated watersheds for the 64 Great Lakes tributaries examined in this study. None of the watersheds included in this study overlap or are nested.

Michigan's Lower Peninsula has a temperate and strongly seasonal climate, with warm temperatures and periodic rainfall during spring and summer (April-October), and colder temperatures and periodic snowfall during fall and winter (November-March). Mean annual precipitation decreases from southwest to northeast (Figure 2B), and mean annual temperature (Figure 2C) decreases from south to north in the region. Snowfall, snowpack thickness, and snowmelt all also increase from south to north in the state (Ford et al., 2020). The amount and timing of snowmelt are closely linked to the magnitude and timing of peak spring streamflows across the region.

Land use and land cover range from temperate forest-dominated regions in the north, to strongly urbanized and agricultural regions in the south and southeast (Figure 2A). Hamlin et al., (2020) quantified source-specific nutrient inputs across the U.S. Great Lakes Basin for 2010. In

the Lower Peninsula, total N and P loads to the landscape are highest in Central Michigan and lowest in the Northern Lower Peninsula. Nutrient inputs are dominated by chemical fertilizer and manure inputs in agricultural regions, by atmospheric deposition and septic leaching in rural areas, and by non-agricultural fertilizer, septic, and wastewater sources in urban areas (Hamlin et al., 2020). Since 2010, little has changed in terms of both land use (Dewitz and U.S. Geological Survey, 2021) and nutrient loading (Byrnes et al., 2020) in the region; thus the landscape conditions present for this study are similar to those today.

The county-scale N mass balance calculated by Byrnes et al. (2020) shows increasing N surplus rates north to south across the study region, and that these rates are comparable to those in large portions of the agricultural Midwest, Central and Eastern United States (Byrnes et al., 2020). Peak N surplus rates of greater than 100 kg-N/ha/y are observed within the study region, but occur less often than in the most agriculturally intensive regions of the US (e.g., portions of Illinois, Indiana, Wisconsin and Iowa).

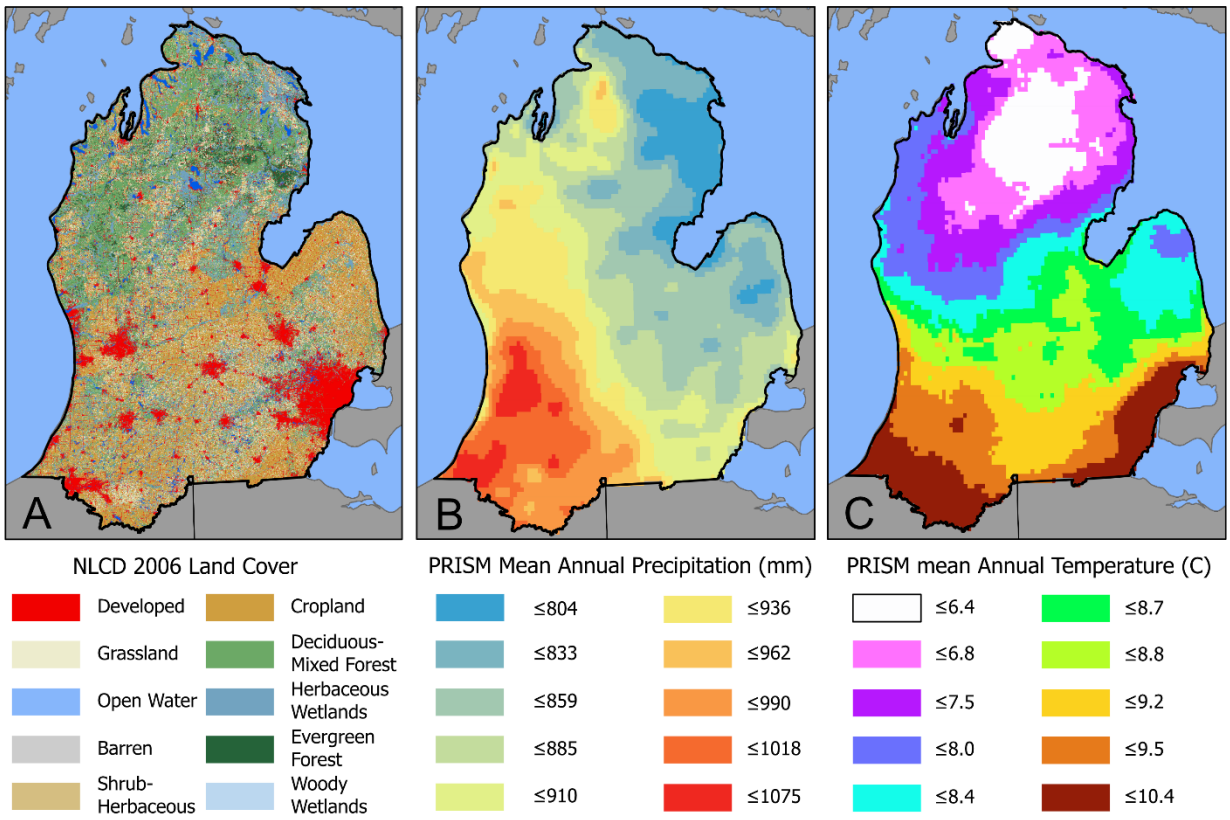

Figure 2: Land Cover, Precipitation and Temperature in Michigan's Lower Peninsula. Landscape and climate gradients across the study region of A) reclassified 2006 NLCD land cover (Fry et al., 2011), B) 30-year (1990-2019) mean annual precipitation normals, and C) annual temperature normals, both from PRISM (Prism Climate Group, 2020).

The hydrogeologic setting of Michigan's Lower Peninsula is characterized by thick recently deposited (Pleistocene era) glacial sediments overlying much older (Silurian through Jurassic) bedrock units of the Michigan Basin. There are four primary aquifers in Michigan's Lower Peninsula: three in the sedimentary bedrock units and one in the overlying unconsolidated glacial sediments (Milstein 1987, Soller and Garrity 2018, Westjohn and Weaver 1998). A USGS investigation showed very high baseflow index values (ratio of groundwater-sourced to total annual streamflow) across the Lower Peninsula, from ~40% to > 90%. The highest baseflow indices occur in areas with thick glacial deposits including in the northern Lower Peninsula. In contrast, baseflow index values were lowest in the Saginaw Bay to southern Lake Huron area and in the south-eastern corner of the state where glacial deposits are thin (Neff et al., 2005).

2.2 Three-Season Study Design, Sample Collection, and Analysis

To assess these hypotheses, 64 stream sampling locations across Michigan's Lower

Peninsula were selected, representing a diverse range of nutrient inputs, landscape characteristics, and dominant hydrologic processes. Sample watersheds were identified using three primary criteria. First, only rivers which drain directly to the Great Lakes were considered. Second, the 30 largest streams by watershed area in the Lower Peninsula were chosen. Third, 34 smaller streams evenly distributed around the Lower Peninsula, not overlapping the 30 largest watersheds, were chosen to provide greater variability in land cover characteristics. In total, these sample locations capture 84% of the Lower Peninsula land area. For each watershed, a sampling point was selected by identifying road crossing (bridge) locations that: 1) maximized upstream watershed area while avoiding hydraulic backwater effects from the Great Lakes, 2) had adequate flow predominantly sourced from river discharge (as opposed to municipal outfalls or other artificial discharge sources), 3) provided clear access for water sampling and flow measurement instruments, and 4) was safely accessible. Samples were collected from the bridges at the center of the stream channel. Both whole water and filtered samples were collected, stored either refrigerated or frozen, and held prior to analysis according to standard methods. Further details on the site selection, sample collection, and analytical processes can be found in the methods and supplementary material of Verhougstraete et al. (2015).

For each hydrologic condition, a target sampling window was defined based on regional streamflows and land cover practices: October 1st to 13th, 2010 for baseflow; March 4th to 23rd, 2011 for snowmelt; and June 1st to 28th, 2011 for summer rainfall. Within each window, streamflow, temperature, and precipitation conditions were monitored to ensure that the desired conditions were met. The baseflow sampling event occurred during a period of relatively little precipitation across the study region, indicated by both weather radar and streamflow hydrographs at USGS stream gauging stations within the study region. Snowmelt, which occurred earlier in the southern portion of the study region, was identified by observing several days of warm temperatures and precipitation and subsequent hydrograph rise. Summer rainfall sampling in June happened in two campaigns, as substantial rain events occurred separately in the northern and southern portions of the study region. For four sites, discharge measurements and sample collection could not be completed due to access issues or conditions during one of the three seasons. Of the 60 sites where data were collected during all three seasons, event flows were higher than baseflow at 52 locations during snowmelt, and 56 locations during summer rainfall, indicating distinct hydrologic conditions were captured.

At each sampling site, streamflow discharge was measured, physical stream water parameters were quantified, and samples were collected and preserved for various laboratory analyses. Table A1 provides a list of analytes and the analytical methods for their quantification. No a priori assumptions were made about the speciation of N and P species during the design of this sampling campaign. Rather, a series of N and P species that are related but differ in terms of solubility and reactivity were quantified. For N, Total Nitrogen (TN), nitrate plus nitrite (NO_X), Nitrite (NO_3) and Ammonium (NH_4) are reported. For phosphorus, total Phosphorus (TP), total dissolved phosphorus (TDP), soluble reactive phosphorus (SRP) are reported. TP represents all P, both bound to particulate matter and dissolved in water. TDP is assessed on a filtered and digested fraction of a water sample, representing both dissolved P and P bound to particles smaller than 0.45 um. Soluble reactive phosphorus is assessed on filtered, undigested samples and represents only dissolved, unbound phosphorus. In addition to the species listed in Table A1, pH and non-particulate organic carbon data were also collected, however these parameters were not explicitly included in this analysis. Summary statistics of their value are provided in Table A3 to provide additional geochemical context for the nutrient values reported.

Results from this sampling campaign have provided insights into variations in fecal contamination (Verhougstraete et al., 2015) and microbial source tracking (Wilson et al., 2022). Here, the spatial and seasonal patterns in observed TN and TP are presented. Results for other nutrient species are summarized in the text, with figures provided in the supplemental material. The maximum (max.), mean, median (med.), minimum (min.), and standard deviation (stdev.) for each analyte were calculated using the Python packages NumPy (Harris et al., 2020) and Pandas (McKinney, 2010) and are reported in Table A3. The significance of differences between median concentrations between seasons for each analyte was evaluated using a chi-squared test on the results of Mood's median test, implemented in the Python package SciPy (Virtanen et al., 2020).

2.3 Linear Modeling

Ordinary least squares (OLS) linear modeling was used to investigate how landscape characteristics (including land use, nutrient sources, and hydrologic characteristics) relate to stream nutrient concentrations, and how these relationships change across seasons. This method was chosen over more complex linear or non-linear methods due to the relative ease of interpretation, well-developed methods to assess model performance and significance, and generally strong model performance. OLS modeling and associated significance tests were

conducted using the Python package *StatsModels* (Seabold and Perktold, 2010).

For each combination of nutrient species and season, two sets of OLS models were created using different sets of driver variables. Models were also created for the major ion species Na, Cl, Ca, K, SO_4, and Mg (Table A1), which provide a reference of model performance for non-reactive species that are sourced from the landscape (Na, Cl, K and SO_4) or from water-rock interactions in the subsurface (Ca and Mg). For example, chloride has a non-point anthropogenic source (used broadly as a paved surface deicer) similar to N and P, but unlike nutrient species it is transported relatively conservatively via both surface and subsurface flowpaths. Driver variables for the two sets of linear models were: 1) *land cover model*: proportions of major land cover types within sample catchments, and 2) *land cover and hydrogeology model:* land cover proportions along with catchment-average hydrologic properties (soil hydraulic conductivity, groundwater travel time, and annual recharge). The *land cover model* was chosen to investigate how landscape characteristics (as a proxy for nutrient sources and surface processes) affect stream nutrient concentrations, while the *land cover and hydrology model* was used to investigate if hydrologic characteristics as a proxy for subsurface processes may help to explain the observed stream nutrient concentrations. Each model considers only one species as its independent variable. Therefore, while some parameters such as TDP and SRP are closely related, they are modeled independently and the results interpreted independently. The spatial predictor variables for both models are described in greater detail in the next section. Analyte concentrations and some driver variables were normalized to achieve near-normal distribution of the independent and dependent variables. Specifically, nutrient concentrations were log-transformed, and land cover proportions were logit-transformed following the methods used in Hannah et al. (2020).

Adjusted R-squared (R^2) values were used to assess the relative performances of each model, which allow for comparison of linear model performance across models with varying structures (i.e., numbers of predictors). Adjusted R^2 penalizes the addition of additional predictor variables if they do not add predictive power to the model (Seabold and Perktold, 2010, Yin and Fan, 2001). Adjusted R^2 values were compared across species, seasons, and model structures, giving insights into which species are most correlated to landscape characteristics, how those relationships shift across seasons, and whether incorporating hydrologic variables better explains concentrations than land covers alone. The p-value of the F statistic provided by *StatsModels*, was used to assess the significance of each season/species model with 0.05 as the significance

threshold.

A chi-squared test on the Likelihood Ratio Static (LRS) (Lewis et al., 2010) is used to assess whether adding increased model complexity significantly improved performance. The LRS is defined in Equation 1, where, L_a is the log-likelihood of the original model, and L_b is the log-likelihood of the model with added parameters. The log-likelihoods for each model were output as part of the ordinary least squared model function in *StatsModels*.

[1] $$LRS = -2(L_b - L_a)$$

The degrees of freedom for the chi-squared test were equal to the difference in the number of independent variables between the model with the added variable and the original model. Here, a p-value < 0.05 indicates that the model with added parameters performed significantly better.

2.4 Spatial Predictor Datasets

The spatial predictor variables for the linear model were quantified within sample point watersheds using either the *Tabulate Area* (for proportions of land use) or *Zonal Statistics* (for hydrologic characteristics) tools in the ArcGIS Spatial Analysis toolbox. These sample point watersheds were derived from the National Elevations Dataset 1 arc-second DEM product, as described in Verhougstraete et al. (2015). Briefly, watersheds were generated using sample locations manually snapped to flowlines generated from a D8 flow direction grid computed from a sink-filled DEM.

The 2006 National Land Cover Database (NLCD) was processed into summary land cover classes, as shown in Table A2. In addition to using land cover proportions as drivers in the linear model, each sample watershed was also classified into a dominant land cover type for visualization and other analyses. Forested, Agricultural, and Urban watersheds were defined as having greater than 50% watershed area occupied by each land cover type, while Mixed was defined as no single land cover class covering > 50% of the watershed area. Forested landscapes were most common in the north, agricultural watersheds in the south, and urban watersheds in and around the larger metropolitan areas (Figure A1). While dominant land covers were summarized by these three categories, all study watersheds contain some degree of mixed land use and land cover characteristics, a trait common to Midwestern drainage basins. Tables A7 and A8 show watershed characteristics including watershed size, land cover proportions and dominant land cover classes for all 64 sample point watersheds.

Gridded estimates of three hydrogeologic characteristics were quantified across the entire

sampling domain: groundwater travel time, average groundwater recharge, and soil hydraulic conductivity. Groundwater travel time estimates were created by Martin et al. (2021) using aquifer hydraulic conductivity estimates and interpolated groundwater levels to estimate velocities along 2-D subsurface flowpaths. Groundwater recharge was estimated for the domain using linear relationships between soil hydraulic conductivity and annual precipitation, each computed from an integrated surface and groundwater hydrologic model (Kendall 2009). These linear models can then be readily applied to a broader spatial domain (e.g. Wan et al., 2023). Soil hydraulic conductivity was estimated using the gSSURGO database along with the ROSETTA pedotransfer functions (Schaap et al., 2001). Watershed summaries of these hydrogeologic characteristics are shown in Figure A2.

2.5 Baseflow Normalized Concentrations

To assess how relationships between stream discharge and solute concentrations change across seasons, the log baseflow-normalized concentration, Cn, was calculated using Equation 2, where Ce is the event (i.e., snowmelt or spring rain) concentration, Cb is the baseflow concentration.

[2] $$Cn = log10(Ce/Cb)$$

Calculating baseflow-normalized concentrations allows for the classification of solutes as enriched, diluted, or unchanged in response to snowmelt or spring rain event flows. Values of log-normalized concentrations above 0 indicate enrichment, while those less than 0 indicate dilution. Development of this metric was inspired by the analysis of concentration-discharge relationships and their use to classify river systems as chemostatic or chemodynamic. Similar to the interpretation of chemodynamic behavior in continuously monitored catchments, changes to the baseflow normalized concentration are attributed to the activation of different flowpaths, nutrient sources, or in-stream processes.

3. Results and Discussion

3.1 Seasonal and Spatial Variations in Nutrient Concentrations

Median nutrient concentrations across the sites were highest during snowmelt, elevated during summer rainfall, and lowest during baseflow, supporting our first hypothesis. Spatial patterns in TN and TP concentrations during the three seasons are shown in Figure 3. Median TN concentrations were significantly higher at snowmelt (1.3 mg/L) than during summer rainfall (0.92 mg/L, $p \leq 0.030$) or baseflow (0.69 mg/L, $p \leq 0.001$), but baseflow and summer rain concentrations

were not significantly different ($p \leq 0.070$). Median TP concentrations were also significantly higher during snowmelt (0.076 mg/L) than during summer rainfall (0.036 mg/L, $p \leq 0.004$) and baseflow events (0.025 mg/L, $p \leq 6.8E-09$). For TP however, summer rainfall TP concentrations were also significantly higher ($p \leq 0.011$) than during baseflow. Descriptive statistics for each analyte are listed in Table A3, while Table A4 shows the p-values for median concertation compared across the three seasons.

This seasonal pattern of decreasing median concentrations from snowmelt, through summer rainfall to baseflow was observed for TDP, NH_4, NO_X, TDN, and NO_3, however, the significance in these seasonal differences is variable. Median NH_4 (Figure A3) and TDP concentrations (Figure A4) were significantly different across all three seasons, while median NO_3 (Figure A5) and TDN (Figure A6) concentrations were not significantly different during any of the three seasons. Median NO_X concentrations (Figure A7) were only significantly different between snowmelt (0.86 mg/L) and baseflow (0.34 mg/L, $p \leq 0.045$). The only exception to this seasonal pattern is for SRP (Figure A8), which had similar median concentrations during snowmelt (0.0092 mg/L) and baseflow (0.097 mg/L) and lowest concentrations during summer rainfall (0.006), with the only significant difference between summer rainfall and baseflow ($p \leq 0.007$).

The observed pattern of peak nutrient concentrations during snowmelt, greater mobilization of phosphorus relative to N during rainfall and low baseflow concentrations are supported by other studies of nutrient seasonality across North America. Recent work by Basu et al. (2023) used a random forest model to predict annual and seasonal stream nutrient concentrations, showing similar seasonal patterns of stream nutrient concentrations as were observed in this study. They also observed different seasonal patterns for N and P species, with summer TP and SRP concentrations shown to be moderate, while dissolved inorganic nitrogen concentrations during summer were near those observed at baseflow. Wilson et al. (2019) studied nutrient flux during snowmelt and rainfall events in watersheds of the Canadian Great Plains, finding elevated TP concentrations during both snowmelt and rainfall, while TN concentrations were higher during snowmelt and lower during rainfall events. These results support the observation of significantly elevated TP but not TN during summer rainfall found in this study. Basu et al. (2023) attributed the observed increase of TP relative to TN during summer rainfall to wet antecedent conditions and the extensive presence of tile drains in their study watersheds (Wilson et al., 2019).

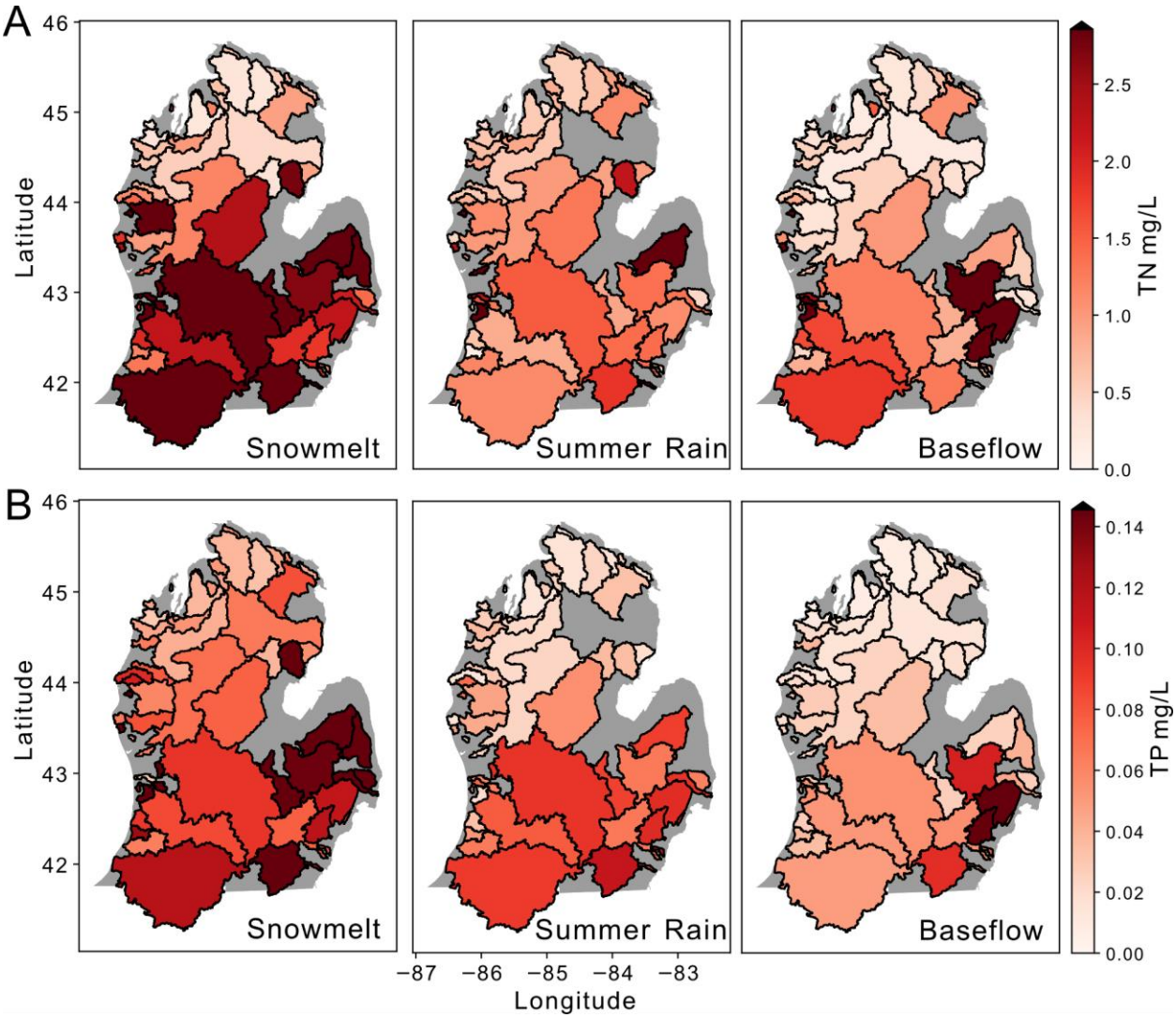

Figure 3: Seasonal TN and TP Concentrations Maps. Concentrations of (A) Total Nitrogen and (B) Total Phosphorus for the three hydrologic conditions sampled. Both TN and TP had strong north-to-south gradients in concentrations and different seasonal behavior across the region.

There was a strong north-south gradient of increasing nutrient concentrations (Figure 3), reflecting gradients in both land use and climate (Figure 2). Dominant land use transitions from forested in the northern watersheds toward agricultural and urban in the southern watersheds (Figure A2), leading to an increase in the proportion of developed land within a watershed from north to south in the region (Figure A9). This land cover transition corresponded to higher median and maximum TN and TP concentrations in the southern half of the state (42 to 44° latitude) than in the northern half (44 to 46° latitude), as shown by the violin plots in Figure A10. For TN, this trend was strongest during snowmelt, while it was strongest for TP during summer rainfall (Figure

A11).

The observed variations in the spatial and seasonal patterns of nutrient concentrations are attributed to the activation of different nutrient sources, transport pathways, and uptake processes across seasons and landscape types. Streamflows (Figure A12) were similar during the two event flows, though concentrations were significantly different for TN, TP, TDP, and NH_4. These observed differences in concentration despite similar streamflow conditions were likely related to: 1) the mobilization of additional nutrient sources through the activation of different flowpaths during snowmelt events relative to summer rain and baseflow, 2) increased cycling of nutrients during summer rainfall relative to snowmelt, or 3) a combination of the two. This interpretation is supported by previous studies using high-frequency monitoring data. Knapp et al. (2020) observed that the variation in event scale concentration-discharge relationships is controlled by a solutes source (e.g., groundwater vs. landscape sources) and its dominant transport processes. Knapp et al. (2020), along with Kapp et al. (2022) demonstrate that seasonal variations in catchment wetness (the amount of antecedent moisture in the watershed) also affects the transport mechanisms active during hydrologic events (i.e., snowmelt or rainfall) and the resulting solute mobilization.

The lack of significant seasonal difference in TDN and NO_3 concentrations may have been due to the influence of legacy N species in the system. Large inputs of N to the landscape (Hamlin et al., 2020), and long transit times for N species transported via subsurface flowpaths can lead to consistent, elevated N inputs to streams from groundwater (Martin et al., 2017, Van Meter et al., 2017). The consistent addition of legacy nutrients sustaining elevated nutrient N inputs from the event flows through baseflow may account for the steady yet insignificant decrease in concentration between the three seasons for these two nutrient species.

3.2 Seasonal Nutrient Dynamics across Dominant Land Covers

Streams with different dominant watershed land cover types (Figure A1) had distinct seasonal patterns in TN and TP concentrations (Figure 4). As expected, given the few sources of nutrients, forested watersheds consistently had the lowest average TN and TP concentrations across the three seasons. Agricultural watersheds generally had the highest TN and TP concentrations during snowmelt and summer rainfall, while urban watersheds tended to have greater concentrations during baseflow. Notably urban watersheds also had high TP concentrations during summer rainfall. N species showed generally similar patterns (Figures A13 – A15), except NH_4 which exhibited distinctly different seasonal patterns across watershed types (Figure A16)

with concentrations similar in agricultural and urban watersheds during snowmelt and summer rainfall, and highest concentrations in mixed watersheds during baseflow. Phosphorus species had generally similar patters to TP, (Figures A17 and A18), except during summer rainfall SRP concentrations were highest in agricultural watersheds. Van Meter et al. (2020) analyzed long-term stream chemistry monitoring data from over 200 sites across the Great Lakes Basin and observed a similar pattern of seasonal nutrient flux patterns across watersheds with different dominant land covers. Specifically, they observe that nutrient concentrations were highest during event flows in forested and agricultural watersheds, while urban watersheds frequently have the highest concentrations during low flow periods.

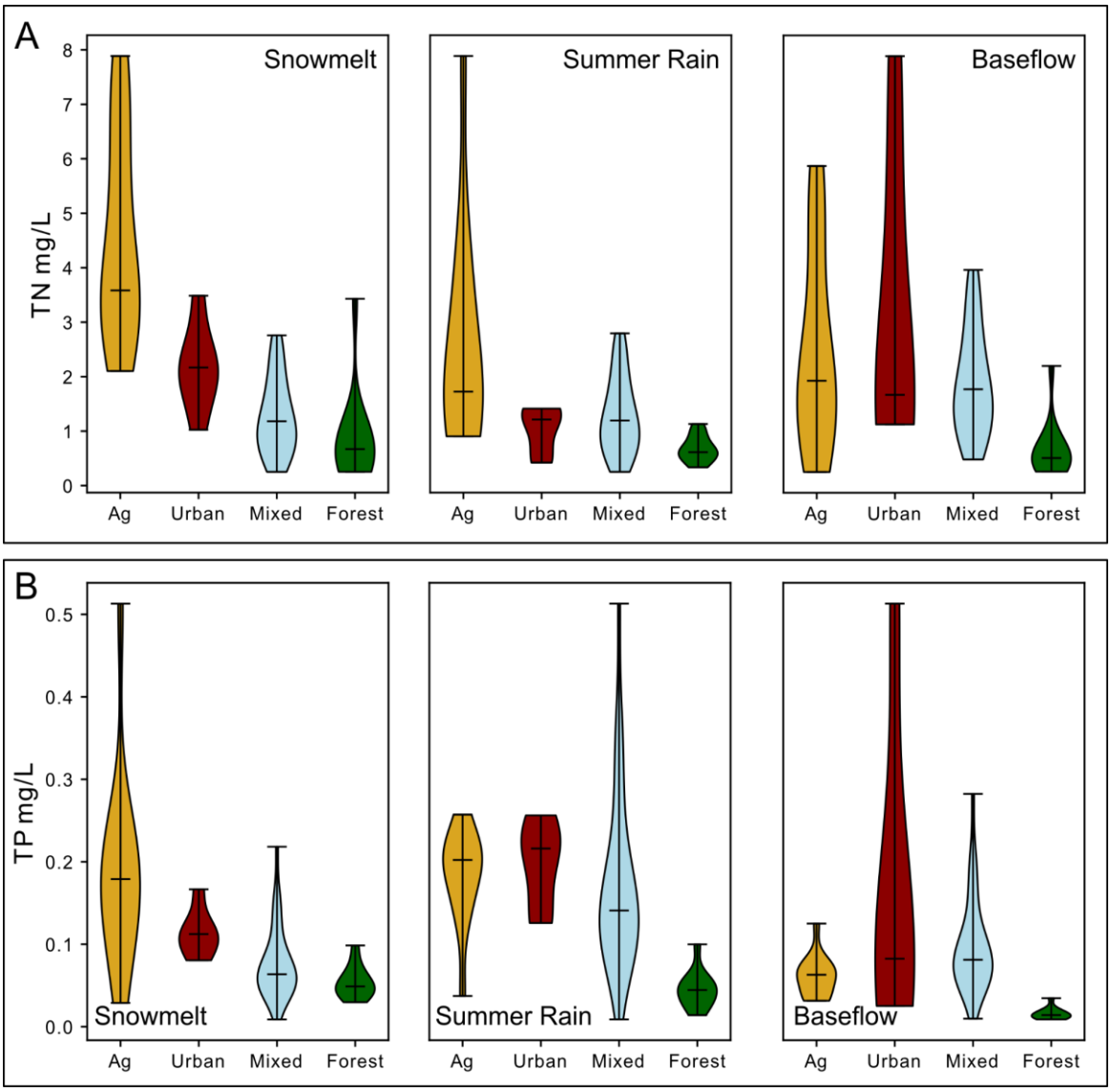

Figure 4: Seasonal TN and TP Concentration Distributions by Land Cover. Distribution of TN and TP concentrations across the three seasons in the four classified watershed land cover types (Figure A2). In these violin plots, the shaded regions are mirrored probability distribution functions for each group. The central line is the median concentration, with the top and bottom lines indicating the maximum and minimum sample, respectively. TN concentrations were highest in agricultural watersheds during both snowmelt and summer rainfall, and highest in urban watersheds during baseflow. TP concentrations were highest in agricultural watersheds during snowmelt, and in urban watersheds during summer rain and baseflow.

The differences in seasonality of peak concentrations between urban and agricultural areas highlight the importance of both nutrient sources and streamflow generation processes on stream nutrient fluxes. Peak concentrations in agricultural watersheds occurring during snowmelt suggest that some of the nutrients stored at or near-surface from the prior planting and growing seasons

were flushed out during snowmelt. Decreases in concentrations through summer rainfall and baseflow conditions may be due to accompanying shifts in streamflow sources toward subsurface flowpaths that typically have lower nutrient concentrations and greater rates of nutrient uptake than direct surface runoff. This interpretation is supported by a recent study in the Illinois River Basin that used nitrate isotope composition to trace sources of nitrate in streamflow across seasons in the Illinois River (Lin et al., 2019). They demonstrated that decreases in stream nutrient concentrations throughout the year coincide with decreasing $\delta^{15}N$ and increasing $\delta^{18}O$ values, which is consistent with a shift toward older, denitrified groundwater, resulting in lower nitrate concentrations during baseflow in agricultural tributaries of the Illinois River. In urban areas, peak nutrient concentrations at baseflow for most nutrient species are attributed to generally steady WWTP effluent volumes constituting a greater proportion of streamflow. Ledford et al. (2021) found that WWTP effluent contributed up to 90% of baseflow in an urban watershed near Philadelphia, PA. This is also supported by the findings of Lin et al. (2019), with nitrate isotope composition in the Illinois River more closely matching that of the Chicago WWTP effluent during low flow conditions.

3.3 Drivers of Nutrient Concentrations across Seasons

The land cover-only linear models demonstrate that land cover proportions alone were strong predictors of stream ion concentrations, with up to 83% of variation across sites explained within a given season (Figure 5). All adjusted R^2 values for all species, seasons, and both sets of models are listed in Table A5. Model performance was consistently strong for the less-reactive species (Na, K, Cl, SO_4) across all three seasons, with adjusted R^2 values between 0.63 and 0.83. Model performance for the species primarily sourced from subsurface water-rock interactions (Ca, Mg) was relatively uniform across the three seasons, but with lower adjusted R^2 values (0.35 to 0.52).

For nutrients, land cover is generally a stronger predictor of concentrations during snowmelt than during other seasons (except for TP), with adjusted R values ranging from 0.38 (NH_4) to 0.81 (TDN). As the seasons progress, the relationship between land cover and stream nutrient chemistry weakens. During summer rainfall, model performance is moderate but highly variable, with adjusted R^2 values between 0.02 and 0.70. Model performance is weakest at baseflow, with the lowest R^2 values (0.002 to 0.68). TP is a notable exception to this pattern, which has the strongest model performance during baseflow (adjusted R^2 = 0.68) and the weakest

performance during snowmelt (adjusted $R^2 = 0.45$). This degradation of model performance as the season's progress is attributed to increased nutrient cycling and shifting hydrologic processes throughout the growing season and into fall.

Model performance is highly variable for individual P species, but was strongest for SRP during snowmelt and summer rainfall, and TP during baseflow. Model performance for P species generally increases with solubility during snowmelt and decreases with solubility during baseflow, while no trends with solubility are observed during summer rainfall. For N species, performance is consistently highest for TDN and NO_3 across the three seasons and no trend in model performance with respect to solubility is observed. Note that the models for SRP and NH_4 during baseflow, and NH_4 during summer rainfall did not pass the 5% significance threshold (indicated by open circles in Figure 5).

During snowmelt and summer rainfall, surface and shallow subsurface flowpaths are activated, creating a direct connection between the landscape and surface waters (Freeze 1974, Stottlemyer and Toczydlowski, 1991, Zimmer et al., 2019). This direct connection is likely responsible for the relatively high percent of variance in stream nutrient concentrations explained by land cover during snowmelt and summer rainfall events. Increases in nutrient cycling during the summer may help explain the overall decreased model performance and increased variability in performance observed for the summer rainfall model. A study of nutrient uptake seasonality in three watersheds in Michigan's Upper Peninsula showed that both gross primary production and community respiration were higher during early summer (May to July) than during late summer/fall (August to October) (Hoellein et a., 2007). These highly seasonal changes to nutrient uptake processes are not well represented by land cover alone (Gorski and Zimmer 2021, Marinos et al., 2020). As streamflow sources become groundwater dominated during baseflow, the loss of direct connection to the landscape surface may drive the decreased model performance. Specifically, the significant lag times between solute loading at the surface, and its delivery to streams via saturated groundwater flowpaths with long transport times (e.g., Martin et al., 2017, Van Meter and Basu 2017), were not well captured in the linear model. Additionally, vadose zone transport, sorption, and cycling processes affect the chemistry of waters prior to their recharge to the saturated groundwater table (Green et al., 2018, Lee et al., 2006). This interpretation is also supported by results from Kincaid et al. (2020) who monitored nitrate and SRP in 3 headwater catchments to calculate hysteresis patterns in concentration-discharge relationships over 400 storm

flow events. Differences in observed C-Q hysteresis patterns indicate that nutrient sources and transport pathways vary across seasons, dominant land cover types, and constituents.

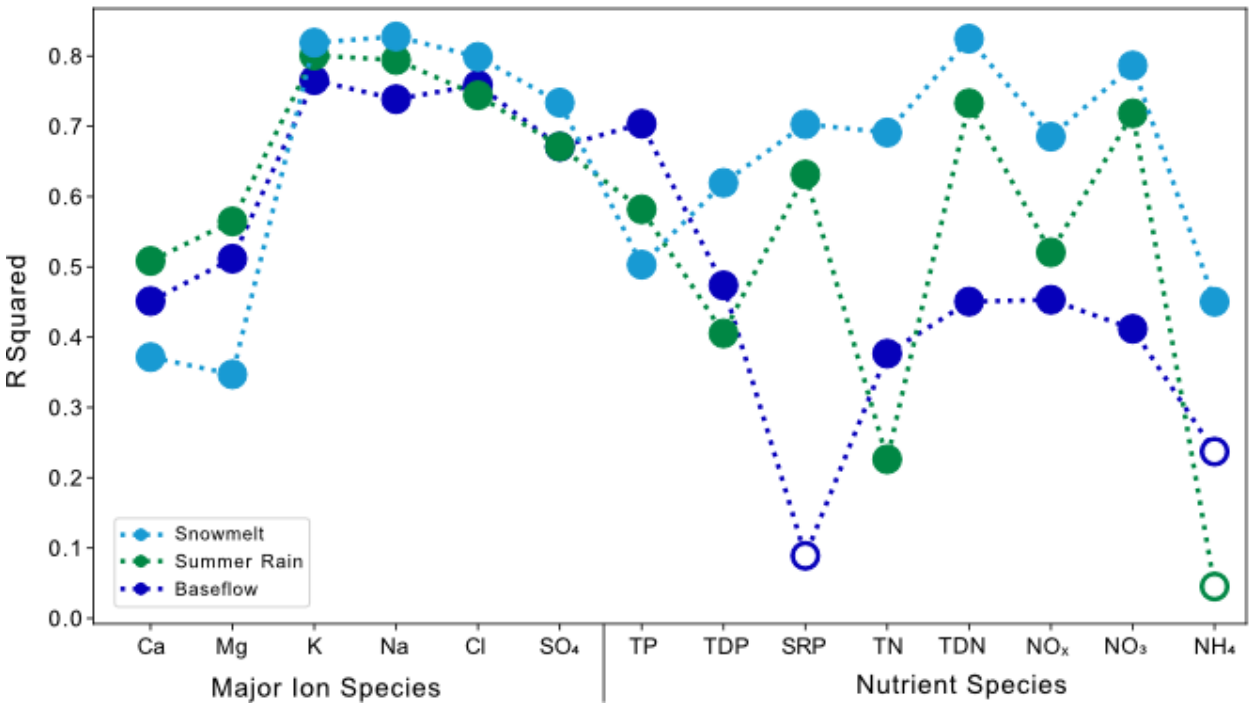

Figure 5: Land Cover Linear Model for Stream Chemistry. Performance for the OLS relating observed nutrient concentrations across the three seasons to land cover proportions in the sample watershed. For nutrient species, model performance decreased as the seasons progressed from snowmelt to summer rainfall and baseflow. For the conservative species Na, K, Cl, and SO^4 model performance was consistently high across seasons, while it was consistently moderate for Ca and Mg. Open circles indicate models for the given element and season fell below the significance threshold for the F-test, indicating no significant relationship between the driver variables and observed concentrations.

The second set of linear models, which added hydrogeologic variables, increased performance significantly for several non-reactive species across all three seasons (Figure 6B). Specifically, model performance improved for Ca, Mg, and K with increases in adjusted R^2 values between 0.05-0.14. This improvement is attributed to the abundance of these solutes in groundwater, sourced from water-rock interactions in the subsurface (Langmuir, 1997, Williams et al., 2007). Model performance was not significantly increased for the already high-performing Na, Cl, or SO_4 models during any of the three seasons, except for a very small yet significant increase of 0.02 for Cl during snowmelt.

In contrast to major ion species, adding hydrogeologic characteristics to the models

produced variable and limited improvements in model performance for the nutrient species. Generally, the additional model complexity produced lower adjusted R^2 values for many of the nutrients (although not significantly). Significant improvements in model performance occurred for the dissolved P species TDP and SRP (adjusted R^2 increases of 0.06 and 0.03 respectively) during snowmelt. The only significant improvements for N species were for TN, NO_x, and NO_3 during baseflow by 0.073, 0.067, and 0.082 respectively.

The improvement in model performance with the *hydrogeology model* for some nutrient species is attributed to the added hydrologic characteristics acting as proxies for groundwater nutrient transport mechanisms. For example, the improvements in performance for NO_3 and TN may be due to the inclusion of mean groundwater travel time, which has a significant regression coefficient for these two species only during baseflow. N compounds have been shown to travel through groundwater (Lin et al., 2019, Martin et al., 2017, Van Meter et al., 2018) and baseflow samples are representative of groundwater flowpaths due to the design of the seasonal synoptic sampling campaign. During snowmelt, improvements in TDP and SRP performance are attributed to the inclusion of hydrologic characteristics with significant regression coefficients during this season; recharge for TDP and soil K for SRP. These parameters are both related to the presence and function of tile drainage systems shown to transport significant amounts of phosphorus species in agricultural regions (Cain et al., 2022, King et al., 2015, Wan et al., 2023). Table A6 lists these and other significant model predictor variables for the models using both hydrologic and land cover characteristics. The limited improvements however indicate that the inclusion of proxies for groundwater processes is insufficient to increase performance during summer rainfall and baseflow. Explicit consideration of how runoff and nutrient transport processes change across seasons is likely required to better understand the observed variability in nutrient concentrations.

While the linear modeling approach used here cannot capture the complex interactions between all major factors affecting steam chemistry, the findings do help fill a gap in the understanding of how nutrient fluxes vary across seasons and landscape types. Previous studies that have focused on seasonal dynamics have largely done so in a small number of watersheds and rely on high-frequency water chemistry monitoring (e.g., Kincaid et al., 2020, Knapp et al., 2020, Poor and McDonnell, 2007, Wilson et al., 2019). Most of these studies focus primarily on event flows and do not expressly consider baseflow conditions or groundwater transport of nutrients. Studies focusing on how landscape characteristics influence stream chemistry (Allen, 2004,

Fraterrigo and Downing 2008, Hansen et al., 2018, Jarvie et al., 2008, Kincaid et al., 2020, Poor and McDonnell, 2007, Vidon and Hill, 2004, Wilson et al., 2019) often do not consider how these controls vary seasonally, instead focusing on long term average conditions. Recent work by Van Meter et al. (2020) investigated nutrient seasonality at the regional (Great Lakes basin) scale but relied on high-frequency data, and related landscape characteristics to changes in concentration-discharge relationships across a whole year, not at multiple points within a year. Due to the design of the seasonal synoptic sampling campaign, the approach of this study was able to investigate the seasonality of factors controlling stream nutrient concentrations using low-frequency data. Specifically, our models indicate a strong connection between the landscape and stream concentrations during snowmelt, and a progressive decoupling of this relationship during summer rainfall and baseflow. Furthermore, this decoupling is attributed to seasonally variable runoff, transport and cycling processes, as described in our conceptual model (section 3.4).

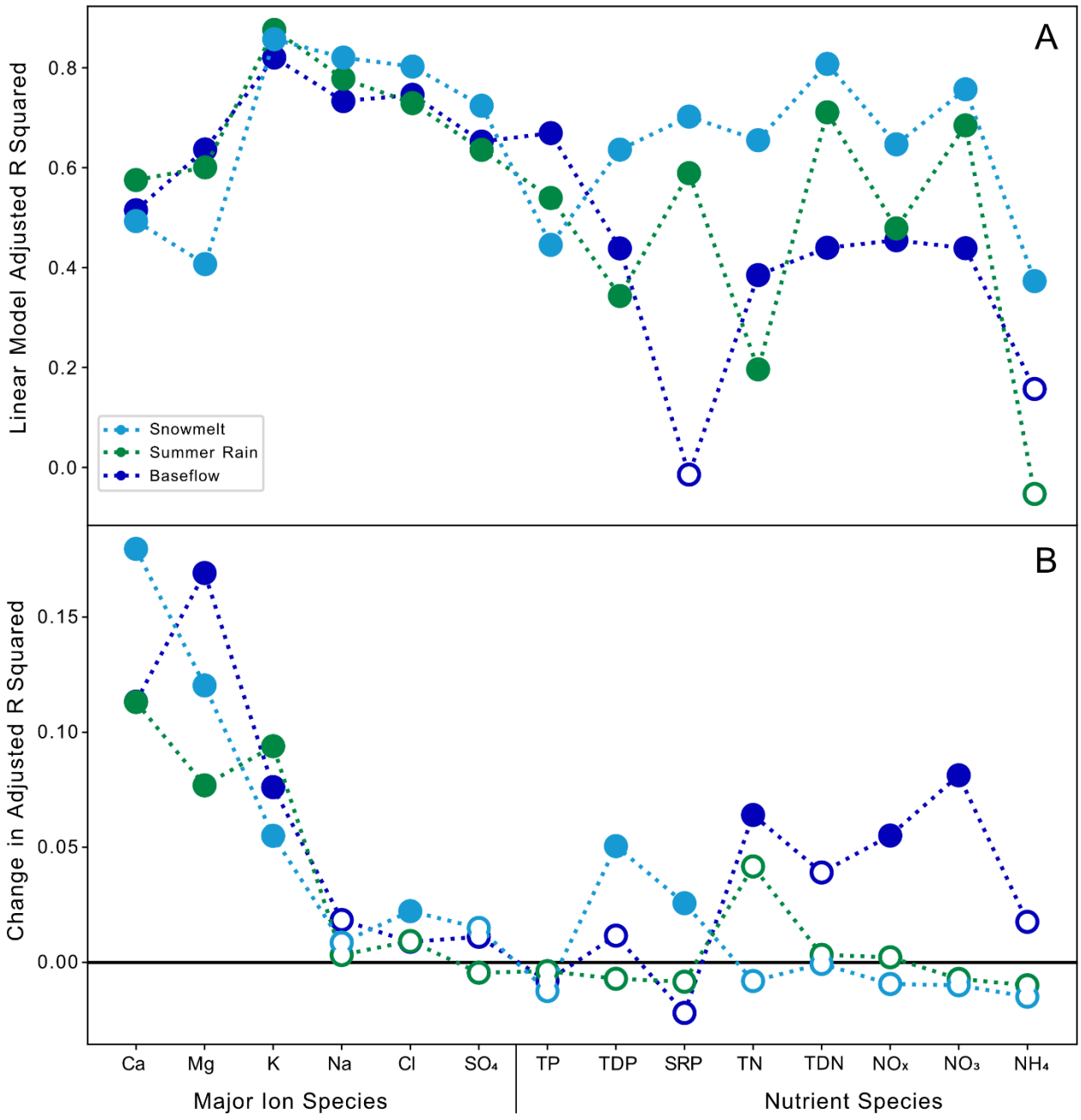

Figure 6: Combined Land Cover and Hydrogeology Linear Model. Adjusted R^2 for the *hydrogeology model* (A), and change in adjusted R^2 compared to the *land cover model* (B) when hydrogeologic characteristics of mean soil K, mean recharge, and mean groundwater travel time were included in the land cover proportion model shown in Figure 5. Including hydrogeologic parameters increased model performance for Ca and Mg, conservative elements often associated with water-rock interactions in groundwater. Moderate improvements were also observed for some N species during baseflow, and P species during snowmelt. Open circles represent model results with a p-value ≥ 0.05 for the chi-squared test on the Likelihood Ratio statistic, indicating no significant difference between the two models.

3.4 Variation in Hydrologic Process across Seasons

Given the observed degradation in linear model performance during summer rainfall and baseflow, log baseflow-normalized concentration (Cn) values were quantified to investigate the role of seasonally variable hydrologic processes on this unexplained variation in nutrient loads. Specifically, Cn values are used to assess the influence that changing flowpaths, and the nutrient availability along these flowpaths, have on seasonal nutrient fluxes.

Changes in event concentration relative to baseflow are observed for TP and TN during both snowmelt and summer rainfall streamflow events in watersheds across the study region (Figure 7). During snowmelt, both TN and TP were enriched relative to baseflow, with average Cn values of 0.61 and 1.1 respectively (values greater than 0 indicate enrichment on a log10 scale). TP enrichment was similar across the gradient of percent watershed development, while TN enrichment increased with increased developed area (Figure 7A). During summer rainfall TP enrichment responses were weaker, and dilution responses were more common leading to a lower average Cn of 0.31, and no trend in the responses with respect to developed area was observed. TN responses during summer rainfall were also lower on average relative to snowmelt (Cn = 0.31). Interestingly, the opposite trend in TN enrichment with respect to land cover was observed, with weak enrichment responses in minimally developed watersheds and strengthening dilution responses in watersheds with greater than ~40% developed area (Figure 7B).

Near zero log baseflow-normalized concentration (Cn) values would suggest seasonally uniform nutrient source concentrations and transport processes. For example, work by Basu et al., (2010) and Thompson et al. (2011) suggest that in watersheds with significant nutrient inputs, storage increases until the amount of nutrients available for mobilization is nearly uniform across space and through time, leading to chemostatic responses. Average TN and TP Cn values show enrichment of both species on average across the study region during the snowmelt and summer rainfall events. This enrichment relative to baseflow indicates that nutrient concentrations along the overland flow and shallow subsurface pathways active during event flows are distinct from, and generally increased relative to, the saturated subsurface flowpaths that dominate during baseflow conditions. Higher enrichment during snowmelt relative to summer rainfall suggests mobilization of landscape-stored nutrients not available during summer rainfall events. However, increased in-stream uptake may also play a role.

The opposing trends in Cn values for TN with respect to development intensity between

the two event flows suggest that although flow conditions during snowmelt were similar to those during summer rainfall, a different set of sources and flowpaths were active. During snowmelt, agricultural and urban watersheds were enriched relative to baseflow, while during summer rainfall these same watersheds were somewhat diluted on average. This indicates that nutrients stored in those watersheds were less available or mobile during summer rainfall, but also suggests that in-stream uptake may have been substantially higher during this period, producing lower Cn values.

Enrichment and dilution of TN and TP during the event flows suggest distinct hydrologic processes and nutrient availability across all three sampled hydrologic conditions. This interpretation is supported by previous studies linking variation in event nutrient concentrations to changes in nutrient availability and streamflow sources throughout the year (e.g., Blaen et al., 2020, Gorski and Zimmer, 2021, Jones et al., 2017, Knapp et al., 2020, Knapp et al., 2022, Lin et al., 2019, Van Meter et al., 2020, Zimmer et al., 2019). For example, Blaen et al., (2020) linked variation in event nutrient concentrations to the activation of different nutrient source zones across 29 storm events in a single catchment in the United Kingdom. Lin et al. (2019) demonstrated both a switch from agricultural to urban-sourced nitrate and a shift from high nitrate groundwater to low nitrate groundwater across seasons in the Illinois River Basin using N isotope data.

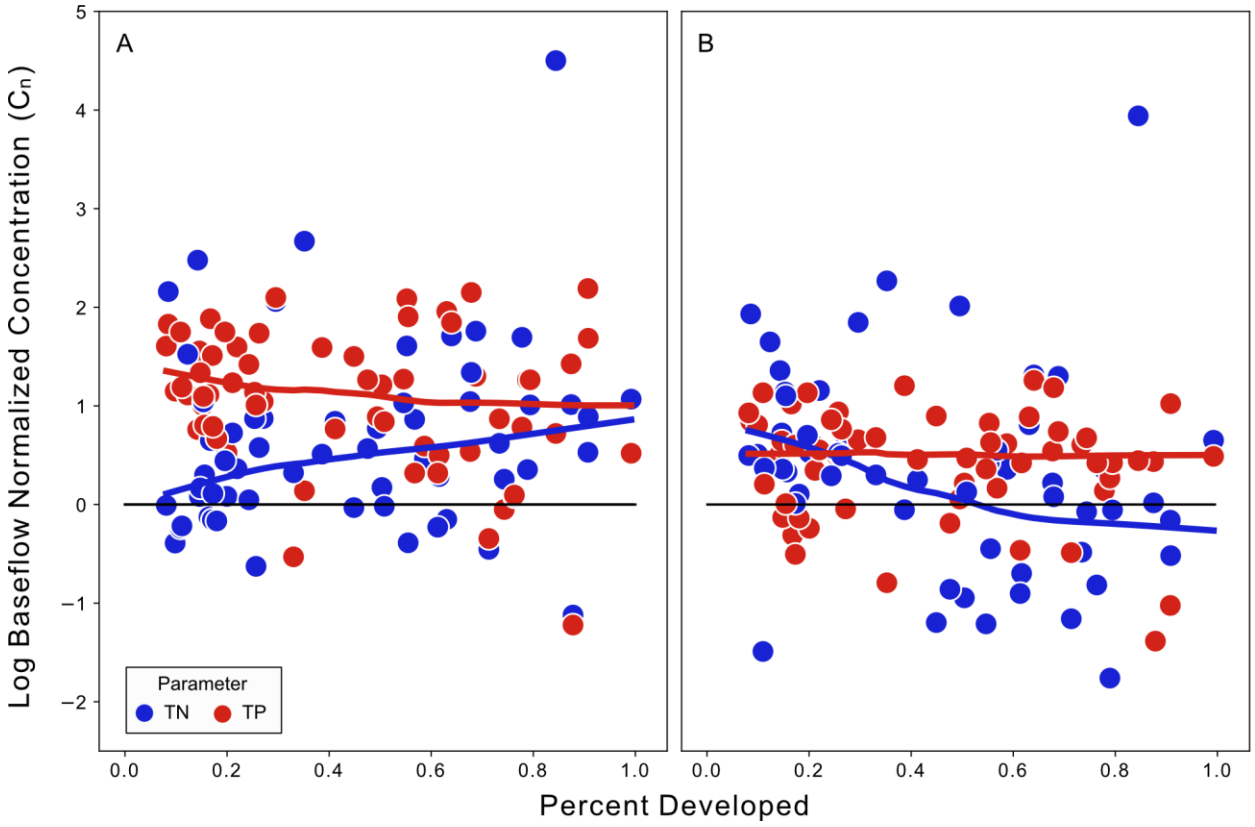

Figure 7: Relationship Baseflow Normalized Concentrations to Developed Land Cover. Variation in TN and TP Cn with percent developed (sum of urban and agricultural land uses) area in the sample point watershed for A) snowmelt and B) summer rainfall events, with solid lines from LOWESS smoothing. During snowmelt, both TN and TP were generally enriched across the sites, with greater enrichment for TP. During summer rainfall, enrichment weakens and dilution responses become more common with more developed land cover in the sample watershed.

3.5 Conceptual Model

Based on observations made during the analysis presented here, and by the findings of previous studies of nutrient transport and hydrologic processes that affect stream chemistry, a conceptual model (Figure 8) was developed to illustrate the complex factors controlling the observed variability of seasonal nutrient concentrations. This conceptual model is underpinned by three assumptions about how hydrologic processes change across seasons in this region, which are supported by previous work linking seasons to different dominant runoff processes: 1) *Snowmelt*: overland flow, shallow subsurface and deep groundwater flowpaths are all active, with overland and shallow subsurface flow dominating (Stottlemyer and Toczydlowski, 1991), 2) *Summer Rainfall:* overland flow is important, while shallow subsurface and groundwater discharge decreases compared to snowmelt (Freeze, 1974), and 3) *Baseflow*: overland flow is essentially

inactive, and saturated groundwater flowpaths dominate (Freeze, 1974) except in urban watersheds where low flows may be augmented by WWTP's and other municipal outflows (Carey and Migliaccio, 2009, Ledford et al., 2021).

During snowmelt, increased transport along all flowpaths (Stottlemyer and Toczydlowski, 1991) should flush stored N and P from the landscape, creating a strong, direct connection between landscape conditions and instream nutrient concentrations. Also during this time, cold temperatures limit in-stream nutrient uptake (e.g., Comer-Warner et al, 2020). Agricultural watersheds have the highest concentrations due to the direct landscape connectivity, while urban watersheds experience lower concentrations due to the dilution of WWTP effluent by urban runoff.

For summer rain events, recent applications of fertilizers combined with active surface and agricultural drainage pathways lead to elevated nutrient concentrations in regions with agricultural influence, particularly for P species. N species tend to be more strongly sourced from shallow subsurface pathways than P species (Gentry et al., 1998, Gentry et al., 2007, Lin et al., 2019, Wan et al., 2023). Increased instream cycling due to warmer temperatures during the summer should reduce nutrient concentrations relative to snowmelt (e.g., Comer-Warner et al., 2020). Urban watersheds respond similarly to snowmelt, with urban runoff low in nutrients diluting WWTP effluent.

At baseflow, nutrient concentrations are lowest in all watersheds, except those dominated by urban land cover. Such watersheds should have the highest concentrations during baseflow due to enriched WWTP effluent accounting for a larger portion of total flow during these conditions (Carey and Migliaccio, 2009, Ledford et al., 2021). Reduced nutrient input and active instream cycling further disconnect the landscape from concentrations (e.g., Comer-Warner et al., 2020).

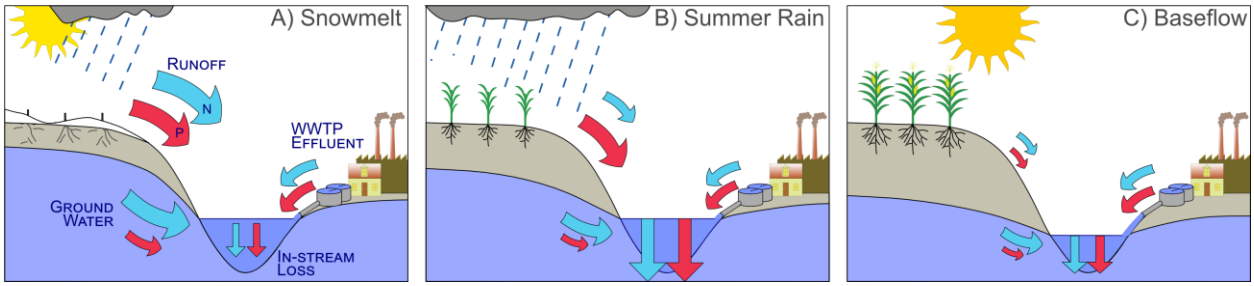

Figure 8: Seasonal Nutrient Export Conceptual Model. Conceptual model of changing streamflow sources and nutrient inputs across the three seasons with: A) significant runoff, high groundwater elevations and limited instream processing during snowmelt, B) P enriched runoff and moderate groundwater contribution, along with significant instream processing during summer rainfall, and C) limited surface runoff, moderate instream processing and low groundwater contributions resulting in low nutrient exports during baseflow. The absolute contribution of WWTP effluent is expected to be consistent across seasons but result in relative differences due to changes in streamflow, where loading from WWTP effluent will be diluted during high flows and most influential during low flow conditions.

4. Conclusions

Stream chemistry, including major ions and nutrient species, was sampled across 64 Michigan watersheds draining the majority of its Lower Peninsula. The field sample collection effort included three synoptic sampling events, specifically designed to capture distinct hydrologic and nutrient conditions within the study watersheds. Average stream nutrient concentrations across Michigan's Lower Peninsula were highest during snowmelt, elevated during summer rainfall, and lowest during baseflow, supporting our initial hypothesis. Concentrations were also generally higher in watersheds with significant proportions of agricultural or urban land use. Seasonal patterns in TN and TP concentrations were variable across dominant land cover types: they were highest in predominantly agricultural watersheds during snowmelt and peaked during baseflow in urban watersheds.

Linear regression models with catchment landscape characteristics as predictor variables explained most of the variability in major ion concentrations across seasons but performed variably for nutrients. The relationships between landscape characteristics were strongest during snowmelt, moderate but highly variable during summer rainfall, and weakest during baseflow. This progressive weakening of the landscape influence on river nutrient fluxes as the seasons progress is attributed to a shift from overland flow and shallow (short) subsurface flowpaths during snowmelt, to regional groundwater discharge-dominated flows during baseflow, and to increased aquatic biogeochemical cycling during summer.

TN and TP concentrations are responsive to event flows (resulting in enrichment or dilution with respect to baseflow) across the study region, suggesting distinct hydrologic processes and nutrient sources between event flows and baseflow conditions. Furthermore, differences in the magnitude and direction of trends in baseflow-normalized concentrations with respect to developed land cover between snowmelt and summer rainfall suggest that streamflow sources and nutrient availability were different between these two high flow event types. Specifically, they indicate increased nutrient availability or increased ability to transport the available nutrients during snowmelt as compared to summer rainfall, especially in highly developed watersheds. These results, along with a large body of previous work (referenced in section 3.4), support the interpretation that at least some of the observed variation in stream nutrient concentrations not currently explained by the linear model is related to seasonal changes to nutrient storage and dominant runoff pathways.

To further understand the role that shifting hydrologic flowpaths have on seasonal surface water nutrient fluxes in the Great Lakes region, more complex and intensive methods (such as hydrologic modeling, additional field data collection, and remote sensing) are required. While long term nutrient monitoring programs exist, repeated observations of stream nutrient concentrations collected by state and federal agencies (such as Michigan Environment Great Lakes and Energy or the U.S. Geological Survey) generally occur in larger, developed watersheds. Continued collection of seasonal stream data in watersheds representing a range of size and impact would be useful to confirm the observations and conceptual model presented here. Further context can be added to these observations using modeled and remotely sensed products including the location of tile drainage, and the contribution of surface vs. subsurface flowpaths to streamflow and nutrient transport. For example, Wan et al. (2023) used a statistical transport model SENSEFlux to demonstrate the importance of tile drainage pathways in delivering nutrients from the landscape to the coastline of the Great Lakes basin. Finally, the use of statistical (i.e., SENSEFlux) and process-based (i.e., MODFLOW, MODPATH, and MT3D) models of nutrient transport can improve understanding of the underlying processes that affect seasonal variation in stream chemistry, by further interrogating relationships between nutrient sources, hydrologic processes and observed stream chemistry.

Acknowledgments

I would first like to acknowledge my co-authors on the version of this chapter being prepared for

submission to a journal: Anthony Kendall, Sherry Martin and David Hyndman. The authors would like to thank Mark Verhougstraete, Emily Luscz and Steve Hamilton for their help in data collection and sample analysis. We would also like to thank Dr. Daniel Hayes for his technical help in refining the statistical modeling and analysis approach. This work was funded in part by the Michigan State University (MSU) Clifford Humphrys Fellowship for Preservation of Water Quality in The Great Lakes, the MSU Department of Earth and Environmental Science, and the NASA OCEAN Grant 80NSSC21K1652.

REFERENCES

Abbott, B.W., Gruau, G., Zarnetske, J.P., Moatar, F., Barbe, L., Thomas, Z., Fovet, O., Kolbe, T., Gu, S., Pierson-Wickmann, A., Davy, P., Pinay, G., 2018. Unexpected spatial stability of water chemistry in headwater stream networks. Ecol. Lett. 21, 296–308. https://doi.org/10.1111/ele.12897

Allan, J.D., 2004. Landscapes and Riverscapes: The Influence of Land Use on Stream Ecosystems. Annu Rev Ecol Evol Syst 35, 257–284.

Basu, N.B., Dony, J., Meter, K.J., Johnston, S.J., Layton, A.T., 2023. A Random Forest in the Great Lakes: Stream Nutrient Concentrations Across the Transboundary Great Lakes Basin. Earth's Futur. 11. https://doi.org/10.1029/2021ef002571

Blaen, P.J., Khamis, K., Lloyd, C., Comer-Warner, S., Ciocca, F., Thomas, R.M., MacKenzie, A.R., Krause, S., 2017. High-frequency monitoring of catchment nutrient exports reveals highly variable storm event responses and dynamic source zone activation. J Geophys Res Biogeosciences 122, 2265–2281. https://doi.org/10.1002/2017jg003904

Boesch, D.F., Brinsfield, R.B., Magnien, R.E., 2001. Chesapeake Bay Eutrophication: Scientific Understanding, Ecosystem Restoration, and Challenges for Agriculture. J. Environ. Qual. 30, 303–320. https://doi.org/10.2134/jeq2001.302303x

Bowes, M.J., Read, D.S., Joshi, H., Sinha, R., Ansari, A., Hazra, M., Simon, M., Vishwakarma, R., Armstrong, L.K., Nicholls, D.J.E., Wickham, H.D., Ward, J., Carvalho, L.R., Rees, H.G., 2020. Nutrient and microbial water quality of the upper Ganga River, India: identification of pollution sources. Environ. Monit. Assess. 192, 533. https://doi.org/10.1007/s10661-020-08456-2

Byrnes, D.K., Meter, K.J.V., Basu, N.B., 2020. Long-Term Shifts in U.S. Nitrogen Sources and Sinks Revealed by the New TREND-Nitrogen Data Set (1930–2017). Global Biogeochem Cy 34. https://doi.org/10.1029/2020gb006626

Cain, M. R., D. K. Woo, P. Kumar, L. Keefer, and A. S. Ward. 2022. Antecedent Conditions Control Thresholds of Tile-Runoff Generation and Nitrogen Export in Intensively Managed Landscapes. *Water Resources Research* 58, no. 2, https://doi.org/10.1029/2021wr030507.

Carey, R.O., Migliaccio, K.W., 2009. Contribution of Wastewater Treatment Plant Effluents to Nutrient Dynamics in Aquatic Systems: A Review. Environ Manage 44, 205–217. https://doi.org/10.1007/s00267-009-9309-5

Comer-Warner, S.A., Gooddy, D.C., Ullah, S., Glover, L., Kettridge, N., Wexler, S.K., Kaiser, J., Krause, S., 2020. Seasonal variability of sediment controls of nitrogen cycling in an agricultural stream. Biogeochemistry 148, 31–48. https://doi.org/10.1007/s10533-020-00644-z

Dewitz, J., and U.S. Geological Survey, 2021, National Land Cover Database (NLCD) 2019 Products (ver. 3.0, February 2024): U.S. Geological Survey data release, https://doi.org/10.5066/P9KZCM54.

Ebeling, P., Dupas R., Abbott B., Kumar R., Ehrhardt S., Fleckenstein J. H. and Musolff A. (2021) Long-Term Nitrate Trajectories Vary by Season in Western European Catchments. *Global Biogeochem. Cycles* **35**, 1–19.

Ford, C.M., Kendall, A.D., Hyndman, D.W., 2020. Effects of shifting snowmelt regimes on the hydrology of non-alpine temperate landscapes. J Hydrol 590, 125517. https://doi.org/10.1016/j.jhydrol.2020.125517

Fraterrigo, J. M. and Downing J. A. (2008) The influence of land use on lake nutrients varies with watershed transport capacity. *Ecosystems* **11**, 1021–1034.

Figueiredo, R. de O., Cak, A., Markewitz, D., 2020. Agricultural Impacts on Hydrobiogeochemical Cycling in the Amazon: Is There Any Solution? Water 12, 763. https://doi.org/10.3390/w12030763

Freeze, R.A., 1974. Streamflow generation. Rev Geophys 12, 627–647. https://doi.org/10.1029/rg012i004p00627

Fry, J.A., Xian, G., Jin, S.M., Homer, C.G., Yang, L.M., Barnes, C.A., Herold, N.D., Wickham, J.D., 2011. Completion of the 2006 National Land Cover Database for the conterminous United States. Photogrammetric Engineering & Remote Sensing **77**, 858–864.

Foster, D., Swanson, F., Aber, J., Burke, I., Brokaw, N., Tilman, D., Knapp, A., 2003. The Importance of Land-Use Legacies to Ecology and Conservation. Bioscience 53, 77–88. https://doi.org/10.1641/0006-3568(2003)053[0077:tiolul]2.0.co;2

Gorski, G. and Zimmer M. A. (2021) Hydrologic regimes drive nitrate export behavior in human-impacted watersheds. *Hydrol. Earth Syst. Sci.* **25**, 1333–1345.

Green, C. T., Liao L., Nolan B. T., Juckem P. F., Shope C. L., Tesoriero A. J. and Jurgens B. C. (2018) Regional Variability of Nitrate Fluxes in the Unsaturated Zone and Groundwater, Wisconsin, USA. *Water Resour. Res.* **54**, 301–322.

Hamlin, Q.F., Kendall, A.D., Martin, S.L., Whitenack, H.D., Roush, J.A., Hannah, B.A., Hyndman, D.W., 2020. Quantifying Landscape Nutrient Inputs With Spatially Explicit Nutrient Source Estimate Maps. J. Geophys. Res. Biogeosciences 125, 1–24. https://doi.org/10.1029/2019JG005134

Hamlin, Q.F., Martin, S.L., Kendall, A.D., Hyndman, D.W., 2022. Examining Relationships Between Groundwater Nitrate Concentrations in Drinking Water and Landscape Characteristics to Understand Health Risks. Geohealth 6, e2021GH000524. https://doi.org/10.1029/2021gh000524

Hannah, B. A., Kendall A. D., Martin S. L. and Hyndman D. W. (2020) Quantifying linkages between watershed factors and coastal wetland plant invasion in the US Great Lakes. *Landsc. Ecol.* **35**, 2843–2861. Available at: https://doi.org/10.1007/s10980-020-01124-3.

Hansen, A. T., Dolph C. L., Foufoula-Georgiou E. and Finlay J. C. (2018) Contribution of wetlands to nitrate removal at the watershed scale. *Nat. Geosci.* **11**, 127–132.

Harris, C.R., Millman, K.J., Walt, S.J. van der, Gommers, R., Virtanen, P., Cournapeau, D., Wieser, E., Taylor, J., Berg, S., Smith, N.J., Kern, R., Picus, M., Hoyer, S., Kerkwijk, M.H. van, Brett, M., Haldane, A., Río, J.F. del, Wiebe, M., Peterson, P., Gérard-Marchant, P., Sheppard, K., Reddy, T., Weckesser, W., Abbasi, H., Gohlke, C., Oliphant, T.E., 2020. Array programming with NumPy. Nature 585, 357–362. https://doi.org/10.1038/s41586-020-2649-2

Haygarth, P. M., Jarvie H. P., Powers S. M., Sharpley A. N., Elser J. J., Shen J., Peterson H. M., Chan N. I., Howden N. J. K., Burt T., Worrall F., Zhang F. and Liu X. (2014) Sustainable phosphorus management and the need for a long-term perspective: The legacy hypothesis. *Environ. Sci. Technol.* **48**, 8417–8419.

Hensley, R.T., Spangler, M.J., DeVito, L.F., Decker, P.H., Cohen, M.J., Gooseff, M.N., 2020. Evaluating spatiotemporal variation in water chemistry of the upper Colorado River using longitudinal profiling. Hydrol. Process. 34, 1782–1793. https://doi.org/10.1002/hyp.13690

Ho, J. C. and Michalak A. M. (2015) Challenges in tracking harmful algal blooms: A synthesis of evidence from Lake Erie. *J. Great Lakes Res.* **41**, 317–325. Available at: http://dx.doi.org/10.1016/j.jglr.2015.01.001.

Hunter, T.S., Clites, A.H., Campbell, K.B., Gronewold, A.D., 2015. Development and application of a North American Great Lakes hydrometeorological database — Part I: Precipitation, evaporation, runoff, and air temperature. J Great Lakes Res 41, 65–77. https://doi.org/10.1016/j.jglr.2014.12.006

Hyndman, D. W., Kendall A. D. and Welty N. R. H. (2007) Evaluating temporal and spatial variations in recharge and streamflow using the integrated landscape hydrology model (ILHM). *Geophys. Monogr. Ser.* **171**, 121–141.

Jarvie, H.P., Withers, P.J.A., Hodgkinson, R., Bates, A., Neal, M., Wickham, H.D., Harman, S.A., Armstrong, L., 2008. Influence of rural land use on streamwater nutrients and their ecological significance. J. Hydrol. 350, 166–186. https://doi.org/10.1016/j.jhydrol.2007.10.042

Jones, C. S., Wang, B., Schilling, K. E. & Chan, K. Nitrate transport and supply limitations quantified using high-frequency stream monitoring and turning point analysis. *J Hydrol* **549**, 581–591 (2017).

Kendall A.D., 2009. Predicting the impacts of land use and climate on regional-scale hydrologic fluxes. Doctoral dissertation, Michigan State University. https://doi.org/doi:10.25335/M5ZC7RZ6R

Kincaid, D.W., Seybold, E.C., Adair, E.C., Bowden, W.B., Perdrial, J.N., Vaughan, M.C.H., Schroth, A.W., 2020. Land Use and Season Influence Event-Scale Nitrate and Soluble Reactive Phosphorus Exports and Export Stoichiometry from Headwater Catchments. Water Resour Res 56. https://doi.org/10.1029/2020wr02736

King, K. W., M. R. Williams, M. L. Macrae, N. R. Fausey, J. Frankenberger, D. R. Smith, P. J. A. Kleinman, and L. C. Brown. 2015. Phosphorus Transport in Agricultural Subsurface Drainage: A Review. *Journal of Environmental Quality* 44, no. 2: 467–85, https://doi.org/10.2134/jeq2014.04.0163.

Knapp, J.L.A., Von Freyberg, J., Studer, B., Kiewiet, L., Kirchner, J.W., 2020. Concentration-discharge relationships vary among hydrological events, reflecting differences in event characteristics. Hydrol. Earth Syst. Sci. 24, 2561–2576.

Knapp, J.L.A., Li, L., Musolff, A., 2022. Hydrologic connectivity and source heterogeneity control concentration–discharge relationships. Hydrol. Process. 36. https://doi.org/10.1002/hyp.14683

Knoll, L., Breuer, L., Bach, M., 2019. Large scale prediction of groundwater nitrate concentrations from spatial data using machine learning. Sci. Total Environ. 668, 1317–1327. https://doi.org/10.1016/j.scitotenv.2019.03.045

Langmuir, D. (1997). *Aqueous environmental geochemistry*. New Jersey.

Lin, J., Böhlke, J.K., Huang, S., Gonzalez-Meler, M., Sturchio, N.C., 2019. Seasonality of nitrate sources and isotopic composition in the Upper Illinois River. J Hydrol 568, 849–861. https://doi.org/10.1016/j.jhydrol.2018.11.043

Ledford, S. H., Diamond J. S. and Toran L. (2021) Large spatiotemporal variability in metabolic regimes for an urban stream draining four wastewater treatment plants with implications for dissolved oxygen monitoring. *PLoS One* **16**, 1–21.

Lee, M. S., Lee K. K., Hyun Y., Clement T. P. and Hamilton D. (2006) Nitrogen transformation and transport modeling in groundwater aquifers. *Ecol. Modell.* **192**, 143–159.

Lewis, F., Butler, A., Gilbert, L., 2011. A unified approach to model selection using the likelihood ratio test. Methods Ecol Evol 2, 155–162. https://doi.org/10.1111/j.2041-210x.2010.00063.x

Marinos, R. E., Van Meter K. J. and Basu N. B. (2020) Is the River a Chemostat?: Scale Versus Land Use Controls on Nitrate Concentration-Discharge Dynamics in the Upper

Mississippi River Basin. *Geophys. Res. Lett.* **47**, 1–11. Available at: https://doi.org/10.1029/2020GL087051.

Malin, J.T., Kaushal, S.S., Mayer, P.M., Maas, C.M., Hohman, S.P., Rippy, M.A., 2024. Longitudinal stream synoptic (LSS) monitoring to evaluate water quality in restored streams. Environ. Monit. Assess. 196, 437. https://doi.org/10.1007/s10661-024-12570-w

Mararakanye, N., Roux, J.J.L., Franke, A.C., 2022. Long-term water quality assessments under changing land use in a large semi-arid catchment in South Africa. Sci. Total Environ. 818, 151670. https://doi.org/10.1016/j.scitotenv.2021.151670

Martin, S.L., D.B. Hayes, D.T. Rutledge, and D.W. Hyndman, 2011, The land-use legacy effect: Adding temporal context to lake chemistry. Limnology and Oceanography 56(6) 2362-2370, https://doi.org/10.4319/lo.2011.56.6.2362.

Martin, S.L., Hayes, D.B., Kendall, A.D., Hyndman, D.W., 2017. The land-use legacy effect: Towards a mechanistic understanding of time-lagged water quality responses to land use/cover. Sci Total Environ 579, 1794–1803. https://doi.org/10.1016/j.scitotenv.2016.11.158

Martin, S. L., Hamlin Q. F., Kendall A. D., Wan L. and Hyndman D. W. (2021) The land use legacy effect: Looking back to see a path forward to improve management. *Environ. Res. Lett.* **16**.

McKinney, W. Data structures for statistical computing in Python. In *Proc. 9th Python in Science Conf*. (eds van der Walt, S. & Millman, K. J.) 56–61 (2010).

Messer, J.J., Ariss, C.W., Baker, J.R., Drousé, S.K., Eshleman, K.N., Kinney, A.J., Overton, W.S., Sale, M.J., Schonbrod, R.D., 1988. STREAM CHEMISTRY IN THE SOUTHERN BLUE RIDGE: FEASIBILITY OF A REGIONAL SYNOPTIC SAMPLING APPROACH1. JAWRA J. Am. Water Resour. Assoc. 24, 821–829. https://doi.org/10.1111/j.1752-1688.1988.tb00933.x

Milstein, Randall L. (compiler), 1987, Bedrock geology of southern Michigan: Geological Survey Division, Michigan Dept. of Natural Resources. https://ngmdb.usgs.gov/Prodesc/proddesc_71887.htm

Mooney, R.J., Stanley, E.H., Rosenthal, W.C., Esselman, P.C., Kendall, A.D., McIntyre, P.B., 2020. Outsized nutrient contributions from small tributaries to a Great Lake. Proc National Acad Sci 117, 28175–28182. https://doi.org/10.1073/pnas.2001376117

Neff, B.P., Day, S.M., Piggott, A.R., Fuller, L.M., 2005. Base flow in the Great Lakes Basin, Scientific Investigations Report 2005-5217. U.S. Geological Suvey, Reston, VA.

Nolan, B.T., Ruddy, B.C., Hitt, K.J., Helsel, D.R., 1997. Risk of Nitrate in Groundwaters of the United StatesA National Perspective. Environ. Sci. Technol. 31, 2229–2236. https://doi.org/10.1021/es960818d

Olive, D.J., 2017. Linear Regression. https://doi.org/10.1007/978-3-319-55252-1

Paerl, H.W., Fulton, R.S., Moisander, P.H., Dyble, J., 2001. Harmful Freshwater Algal Blooms, With an Emphasis on Cyanobacteria. Sci. World J. 1, 76–113. https://doi.org/10.1100/tsw.2001.16

Pennino, M. J., Compton J. E. and Leibowitz S. G. (2017) Trends in Drinking Water Nitrate Violations Across the United States. *Environ. Sci. Technol.* **51**, 13450–13460.

Poor C. J. and McDonnell J. J. (2007) The effects of land use on stream nitrate dynamics. *J. Hydrol.* **332**, 54–68.

Power, J.F., Schepers, J.S., 1989. Nitrate contamination of groundwater in North America. Agric., Ecosyst. Environ. 26, 165–187. https://doi.org/10.1016/0167-8809(89)90012-1

PRISM Climate Group, Oregon State University, https://prism.oregonstate.edu, (2020) accessed 31 Oct 2022.

Robertson, D. M. and Saad D. A. (2011) Nutrient Inputs to the Laurentian Great Lakes by Source and Watershed Estimated Using SPARROW Watershed Models. *J. Am. Water Resour. Assoc.* **47**, 1011–1033.

Rogers, K.M., Raaij, R. van der, Phillips, A., Stewart, M., 2023. A national isotope survey to define the sources of nitrate contamination in New Zealand freshwaters. J. Hydrol. 617, 129131. https://doi.org/10.1016/j.jhydrol.2023.129131

Runkel, R.L., Verplanck, P.L., Walton-Day, K., McCleskey, R.B., Byrne, P., 2023. The truth is in the stream: Use of tracer techniques and synoptic sampling to evaluate metal loading and remedial options in a hydrologically complex setting. Sci. Total Environ. 876, 162458. https://doi.org/10.1016/j.scitotenv.2023.162458

Runkel, R.L., Walton-Day, K., Kimball, B.A., Verplanck, P.L., Nimick, D.A., 2013. Estimating instream constituent loads using replicate synoptic sampling, Peru Creek, Colorado. J. Hydrol. 489, 26–41. https://doi.org/10.1016/j.jhydrol.2013.02.031

Runkel, R.L., Verplanck, P.L., Walton-Day, K., McCleskey, R.B., Byrne, P., 2023. The truth is in the stream: Use of tracer techniques and synoptic sampling to evaluate metal loading and remedial options in a hydrologically complex setting. Sci. Total Environ. 876, 162458. https://doi.org/10.1016/j.scitotenv.2023.162458

Schaap, M.G., Leij, F.J., Genuchten, M.Th. van, 2001. rosetta: a computer program for estimating soil hydraulic parameters with hierarchical pedotransfer functions. J. Hydrol. 251, 163–176. https://doi.org/10.1016/s0022-1694(01)00466-8

Seabold, S., Perktold, J., 2010. Statsmodels: Econometric and Statistical Modeling with Python, in: Proceedings of the 9th Python in Science Conference. pp. 92–96. https://doi.org/10.25080/majora-92bf1922-011

Smerdon, B.D., Gardner, W.P., 2022. Characterizing groundwater flow paths in an undeveloped region through synoptic river sampling for environmental tracers. Hydrol. Process. 36. https://doi.org/10.1002/hyp.14464

Smith, V.H., 2003. Eutrophication of freshwater and coastal marine ecosystems a global problem. Environ. Sci. Pollut. Res. 10, 126–139. https://doi.org/10.1065/espr2002.12.142

Soller, D.R., and Garrity, C.P., 2018, Quaternary sediment thickness and bedrock topography of the glaciated United States east of the Rocky Mountains: U.S. Geological Survey Scientific Investigations Map 3392, 2 sheets, scale 1:5,000,000. https://doi.org/10.3133/sim3392.

Stottlemyer, R. and Toczydlowski D. (1991) Stream chemistry and hydrologic pathways during snowmelt in a small watershed adjacent Lake Superior. *Biogeochemistry* **13**, 177–197.

Thompson, S.E., Basu, N.B., Lascurain, J., Aubeneau, A., Rao, P.S.C., 2011. Relative dominance of hydrologic versus biogeochemical factors on solute export across impact gradients. Water Resour Res 47. https://doi.org/10.1029/2010wr009605

Treuer, G., Kirchhoff, C., Lemos, M.C., McGrath, F., 2021. Challenges of managing harmful algal blooms in US drinking water systems. Nat. Sustain. 4, 958–964. https://doi.org/10.1038/s41893-021-00770-y

U.S. Environmental Protection Agency (2015) *Connectivity of Streams and Wetlands to Downstream Waters: A Review and Synthesis of the Scientific Evidence*., Washington, D.C.

Van Meter, K. J. and Basu N. B. (2017) Time lags in watershed-scale nutrient transport: An exploration of dominant controls. *Environ. Res. Lett.* **12**.

Van Meter, K. J., Van Cappellen P. and Basu N. B. (2018) Legacy nitrogen may prevent achievement of water quality goals in the Gulf of Mexico. *Science (80-.).* **360**, 427–430. Available at: https://www.sciencemag.org/lookup/doi/10.1126/science.aar4462.

Van Meter, K.J., Chowdhury, S., Byrnes, D.K., Basu, N.B., 2020. Biogeochemical asynchrony: Ecosystem drivers of seasonal concentration regimes across the Great Lakes Basin. Limnol. Oceanogr. 65, 848–862. https://doi.org/10.1002/lno.11353

Virtanen, P., Gommers, R., Oliphant, T.E., Haberland, M., Reddy, T., Cournapeau, D., Burovski, E., Peterson, P., Weckesser, W., Bright, J., Walt, S.J. van der, Brett, M., Wilson, J., Millman, K.J., Mayorov, N., Nelson, A.R.J., Jones, E., Kern, R., Larson, E., Carey, C.J., Polat, İ., Feng, Y., Moore, E.W., VanderPlas, J., Laxalde, D., Perktold, J., Cimrman, R., Henriksen, I., Quintero, E.A., Harris, C.R., Archibald, A.M., Ribeiro, A.H., Pedregosa, F., Mulbregt, P. van, Contributors, S. 1 0, Vijaykumar, A., Bardelli, A.P., Rothberg, A., Hilboll, A., Kloeckner, A., Scopatz, A., Lee, A., Rokem, A., Woods, C.N., Fulton, C., Masson, C., Häggström, C., Fitzgerald, C., Nicholson, D.A., Hagen, D.R., Pasechnik, D.V., Olivetti, E., Martin, E., Wieser, E., Silva, F., Lenders, F., Wilhelm, F., Young, G., Price, G.A., Ingold, G.-L., Allen, G.E., Lee, G.R., Audren, H., Probst, I., Dietrich, J.P., Silterra, J., Webber, J.T., Slavič, J., Nothman, J., Buchner, J., Kulick, J., Schönberger, J.L., Cardoso, J.V. de M., Reimer, J., Harrington, J., Rodríguez, J.L.C., Nunez-Iglesias, J., Kuczynski, J., Tritz, K., Thoma, M., Newville, M., Kümmerer, M., Bolingbroke, M., Tartre, M., Pak, M., Smith, N.J., Nowaczyk, N., Shebanov, N., Pavlyk, O., Brodtkorb, P.A., Lee, P., McGibbon, R.T., Feldbauer, R., Lewis, S., Tygier, S., Sievert, S., Vigna, S., Peterson, S., More, S., Pudlik, T., Oshima, T., Pingel, T.J., Robitaille, T.P., Spura, T., Jones, T.R., Cera, T., Leslie, T., Zito, T., Krauss, T., Upadhyay, U., Halchenko, Y.O., Vázquez-Baeza, Y., 2020. SciPy 1.0: fundamental algorithms for scientific computing in Python. Nat. Methods 17, 261–272. https://doi.org/10.1038/s41592-019-0686-2

Vitousek, P.M., Naylor, R., Crews, T., David, M.B., Drinkwater, L.E., Holland, E., Johnes, P.J., Katzenberger, J., Martinelli, L.A., Matson, P.A., Nziguheba, G., Ojima, D., Palm, C.A., Robertson, G.P., Sanchez, P.A., Townsend, A.R., Zhang, F.S., 2009. Nutrient Imbalances in Agricultural Development. Science 324, 1519–1520. https://doi.org/10.1126/science.1170261

Verhougstraete, M.P., Martin, S.L., Kendall, A.D., Hyndman, D.W., Rose, J.B., 2015. Linking fecal bacteria in rivers to landscape, geochemical, and hydrologic factors and sources at the basin scale. Proc. Natl. Acad. Sci. U. S. A. 112, 10419–10424. https://doi.org/10.1073/pnas.1415836112

Vidon, P. G. F. and Hill A. R. (2004) Landscape controls on nitrate removal in stream riparian zones. *Water Resour. Res.* **40**, 1–14.

Vörösmarty, C.J., McIntyre, P.B., Gessner, M.O., Dudgeon, D., Prusevich, A., Green, P., Glidden, S., Bunn, S.E., Sullivan, C.A., Liermann, C.R., Davies, P.M., 2010. Global threats to human water security and river biodiversity. Nature 467, 555–561. https://doi.org/10.1038/nature09440

Wan, L., Kendall, A.D., Martin, S.L., Hamlin, Q.F., Hyndman, D.W., 2023. Important Role of Overland Flows and Tile Field Pathways in Nutrient Transport. Environ. Sci. Technol. 57, 17061–17075. https://doi.org/10.1021/acs.est.3c03741

Ward, M. H., Jones R. R., Brender J. D., de Kok T. M., Weyer P. J., Nolan B. T., Villanueva C. M. and van Breda S. G. (2018) Drinking water nitrate and human health: An updated review. *Int. J. Environ. Res. Public Health* **15**, 1–31.

Watson, S.B., Miller, C., Arhonditsis, G., Boyer, G.L., Carmichael, W., Charlton, M.N., Confesor, R., Depew, D.C., Höök, T.O., Ludsin, S.A., Matisoff, G., McElmurry, S.P., Murray, M.W., Richards, R.P., Rao, Y.R., Steffen, M.M., Wilhelm, S.W., 2016. The re-eutrophication of Lake Erie: Harmful algal blooms and hypoxia. Harmful Algae 56, 44–66. https://doi.org/10.1016/j.hal.2016.04.010

Wayland, K.G., Long, D.T., Hyndman, D.W., Pijanowski, B.C., Woodhams, S.M., Haack, S.K., 2003. Identifying Relationships between Baseflow Geochemistry and Land Use with Synoptic Sampling and R-Mode Factor Analysis. J Environ Qual 32, 180–190. https://doi.org/10.2134/jeq2003.1800

Westjohn, D.B., Weaver, T.L., 1998. Hydrogeologic framework of the Michigan Basin regional aquifer system, Professional Paper 1418. U.S. Geological Survey, Denver, CO.

Williams, E.L., Szramek, K.J., Jin, L., Ku, T.C.W., Walter, L.M., 2007. The carbonate system geochemistry of shallow groundwater–surface water systems in temperate glaciated watersheds (Michigan, USA): Significance of open-system dolomite weathering. GSA Bull. 119, 515–528. https://doi.org/10.1130/b25967.1

Wilson, H. F., Casson N. J., Glenn A. J., Badiou P. and Boychuk L. (2019) Landscape Controls on Nutrient Export during Snowmelt and an Extreme Rainfall Runoff Event in Northern Agricultural Watersheds. J. Environ. Qual. 48, 841–849.

Wilson, A.M., Martin, S.L., Verhougstraete, M.P., Kendall, A.D., Zimmer-Faust, A.G., Rose, J.B., Bell, M.L., Hyndman, D.W., 2022. Detangling Seasonal Relationships of Fecal Contamination Sources and Correlates with Indicators in Michigan Watersheds. Microbiol. Spectr. 10, e00415-22. https://doi.org/10.1128/spectrum.00415-22

Yin, P., Fan, X., 2001. Estimating R 2 Shrinkage in Multiple Regression: A Comparison of Different Analytical Methods. J Exp Educ 69, 203–224. https://doi.org/10.1080/00220970109600656

Zhang, W., Li H., Kendall A. D., Hyndman D. W., Diao Y., Geng J. and Pang J. (2019) Nitrogen transport and retention in a headwater catchment with dense distributions of lowland ponds. *Sci. Total Environ.* **683**, 37–48.

Zimmer, M. A., Pellerin B., Burns D. A. and Petrochenkov G. (2019) Temporal variability in nitrate-discharge relationships in large rivers as revealed by high-frequency data. *Water Resour. Res.* Available at: https://doi.org/10.1029/2018WR023478.

CHAPTER 3: BASIN GROUNDWATER STORAGE DYNAMICS DURING RECORD-SETTING WATER LEVEL CHANGES IN THE LAURENTIAN GREAT LAKES

Abstract

North America's Laurentian Great Lakes hold ~23,000 km^3 of freshwater, including ~4,000 km^3 of groundwater, containing ~21% of the world's available freshwater. Previous field and modeling work has demonstrated a dynamic hydrologic connection between the Great Lakes and the adjacent groundwater aquifers. The combined surface water and groundwater of the Great Lakes support drinking water needs, agriculture, manufacturing, maritime shipping, recreation, and power generation for the surrounding region. Record-setting changes in Great Lakes elevations occurred between 2002-2020 due to shifting regional climate patterns, including variability in the ENSO and polar air currents. The resulting shifts in precipitation, evaporation, and temperature simultaneously affect the terrestrial water balance of the Great Lakes Basin. While changes to the lake levels are highly visible and widely documented, little is known about how groundwater storage and discharge may have changed during this time period. To investigate these groundwater dynamics, a coupled surface and groundwater model for the state of Michigan was developed using the Landscape Hydrology Model (LHM) for the 2000-2023 period. LHM is a gridded, process-based water balance model which is coupled to the USGS MODFLOW code to simulate saturated groundwater flow. Results from this simulation show changes in groundwater elevations closely mirror but are lagged 2-4 years behind changes in lake levels. Average heads across the model domain were lowest in September 2013 and highest in December 2020, corresponding to an average groundwater storage increase of 0.2 m. This change is about one-tenth the average increase in lake elevations of 1.46 m during the same period, but an order of magnitude larger than the average seasonal change in groundwater storage of 0.028 m. Surface model estimates of the terrestrial water balance suggest changing groundwater storage was the result of coincident increases in precipitation and decreases in evapotranspiration which occurred between 2008 and 2018. This effort provides the first estimates of modeled groundwater storage change across a large portion of the Great Lakes region for the recent period of record-setting lake level variability. Continued development of groundwater simulations in the Great Lakes Basin, and their integration into decision-making frameworks, will be necessary to address the impacts of changing climate and increased demand for freshwater resources across the region.

1. Introduction

The Laurentian Great Lakes represent the largest unfrozen freshwater resource in the world, containing approximately 23,000 km^3 of surface and groundwater. Surface water elevations in the Great Lakes have historically fluctuated, with both seasonal and interannual variations observed since data collection began in 1918 (Figure 9, Panel 1). This record, maintained by the National Oceanic and Atmospheric Administration (NOAA), shows seasonal variations of 0.35-0.67 m, and maximum interannual variations of ~1-2 m across the five lakes. In the past 20 years, the lake elevations have swung between record lows and highs, driven by changes in regional climate (Gronewold et al., 2014, Gronewold et al., 2016, Gronewold et al., 2021). Little is known to date, however, about how these changes have affected inland groundwater storage and discharge across the Great Lakes region.

Water levels in the Great Lakes are controlled by a combination of direct precipitation and evaporation over the lake surface, surface runoff from rivers (which are in turn controlled by the terrestrial water balance), interlake flows through the connecting channels (St. Mary's, St. Clare, Detroit, and Niagara Rivers), and outflow through the St. Lawrence River (Neff and Nicholas, 2005). Changes to local climate conditions can alter both the terrestrial water balance and the direct-to-lake fluxes, however, these changes are not always consistent between the landscape and lake (Gronewold et al., 2021). In addition to changes driven by shifts in the basin's water balance, glacial isostatic rebound and thermal expansion can also change lake levels. Estimated rates of glacial isostatic adjustment in the Great Lakes are small relative to the observed change in lake level, on the order of millimeters per year (Argus et al., 2020) but are always increasing. Thermal induced changes of ~0.4 m occur cyclically, and should not change the year over year trends in lake elevation (Meredith, 1975). Due to their large water volume and thermal capacity, the lakes also exert a significant effect on regional climate. The lakes store heat during the summer and release it during the winter, increasing wintertime evaporation and precipitation, leading to significant increases in snowfall on the lee sides of the lakes (Notaro et al., 2013, Shi and Xue 2019). Inclusion of lake surface temperature dynamics into a Weather Research and Forecasting (WRF) simulation of the Great Lakes region increased mean snow water equivalent between 3-15% in the Great Lakes region (Shi and Xue 2019).

While the lake levels have historically fluctuated, more distinct shifts in the lake levels have been observed over the last thirty-five years. Starting in the 1990's, an El Niño event brought

on a period of sustained increase in surface water temperatures and low winter ice cover, increasing over-lake evaporation (Assel et al., 2004, Gronewold et al., 2016). During this period, over-land precipitation was well above historical averages, increasing runoff to the Great Lakes; however, the increased evaporative flux was enough to offset this increased input. As a result, lake levels fell precipitously from the mid 1990's into the early 2000's, with historical or near-historical low lake levels recorded between 2007 and 2013 in all five lakes (Gronewold et al., 2021). Simulations of future lake levels during this time period predicted continued declines due to increased over-lake evaporation under a warming climate (Lofgren et al., 2011).

In 2013, Lakes Superior and Michigan-Huron started the fastest two-year average rate of water level rise ever recorded across the lakes. Destabilization of polar air currents resulted in a polar vortex; extremely cold air from the arctic descended into the Great Lakes region, significantly decreasing average lake surface temperature. This resulted in widespread ice cover, lowering over-lake evaporation to a point where this flux was overwhelmed by the continued elevated input of precipitation to the basin (Gronewold et al., 2016, Gronewold et al., 2021). Lake levels continued to rise through the end of the decade until by spring of 2020, all the lakes had neared or exceeded their absolute maximum water levels (Figure 9, Panel 2). Specifically, Lake Erie had exceeded its previous historical maximum, while Lakes Superior, Michigan and Huron were within 0.03 m and 0.04 m of their record levels respectively. These record high levels were the result of continued increases in over-land and over-lake precipitation, and near long term average landscape ET and lake evaporation (Gronewold et al., 2021). These sustained high lake levels impacted both natural systems and human communities through coastal habitat loss (Theuerakauf and Braun 2021) and damage to infrastructure, including roads and structures (Reynolds, 2020).

The mismatch between lake level projections during the early 2000's and the changes observed between ~2010 and 2020 is the result of an overprediction in potential evapotranspiration (PET), as identified by Lofgren et al. (2011). Recent advancements in predicting Great Lakes water levels have focused on improving climate simulations including the downscaling of global circulation models (GCM's) through the use of regional climate models (RCMs) and their online coupling to land surface models (Notaro et al., 2015) and three dimensional lake models (Kayastha et al., 2018). These improved models predict continued interannual variations and increasing extremes in water levels, and significant variability in the direction of change based on the specific

approach and climate scenarios used (Kayastha et al., 2018, Notaro et al., 2015). Continued efforts are underway to create more dynamically coupled land-lake-atmosphere models, to further resolve local-regional climate feedbacks between the land surface, lake surface and atmosphere (Sharma et al., 2018).

Compared to the links between the climate, land surface, and lakes, much less is known about the groundwater of the Great Lakes region. There is significant, but largely indirect evidence, that the Great Lakes are hydrologically connected to the adjacent groundwater system within the basin (Feinstein et al., 2010, Grannemann et al. 2000, Xu et al., 2021). Groundwater provides water to the Great Lakes both indirectly through streamflow (Grannemann et al., 2000), and directly through discharge to the near shore and lake bed regions (Feinstein et al., 2010, Xu et al., 2021). Xu et al. (2021) used a coupled surface and groundwater model to estimate the direct fluxes between groundwater and the Great Lakes. This model indicates that both direct groundwater recharge and discharge occur across all five Great Lakes. Their results suggest that most of this exchange occurs in the near-shore region, and that this flux is primarily from the groundwater into the lake. In addition to being a source and sink for water in the Great Lakes, the basin's groundwater system plays a critical role in sustaining streams, rivers, and wetlands, as well as being an important source of drinking water.

While the recent swings in lake levels are highly visible, little is known about how groundwater storage and discharge to surface waters has changed over this same period. The same climate factors that drive changes in lake levels also affect terrestrial hydrology. These factors include shifts in precipitation, temperature, and evapotranspiration, all of which have changed significantly over both the lakes and land surface within the Great Lakes basin within the last 30 years (Costa et al., 2021, Ford, 2020, Gronewold et al., 2016). Here, a coupled surface and groundwater model is developed to understand how the climate forces that drove the rapid lake level changes in the Great Lakes have affected groundwater over the state of Michigan region. The Landscape Hydrology Model (LHM) is used to quantify how groundwater storage, evapotranspiration, recharge and groundwater discharge, have changed between 2000-2023. Specifically, the following research questions are addressed: 1) What is the seasonal cycle of groundwater storage relative to seasonal changes in lake levels?; 2) How has groundwater storage changed during the recent interannual swings in lake levels?; 3) What is the timing of changes in groundwater storage relative to changes in lake levels?; and 4) What changes to the

surface water balance are observed, and how do these relate to changes in groundwater storage.

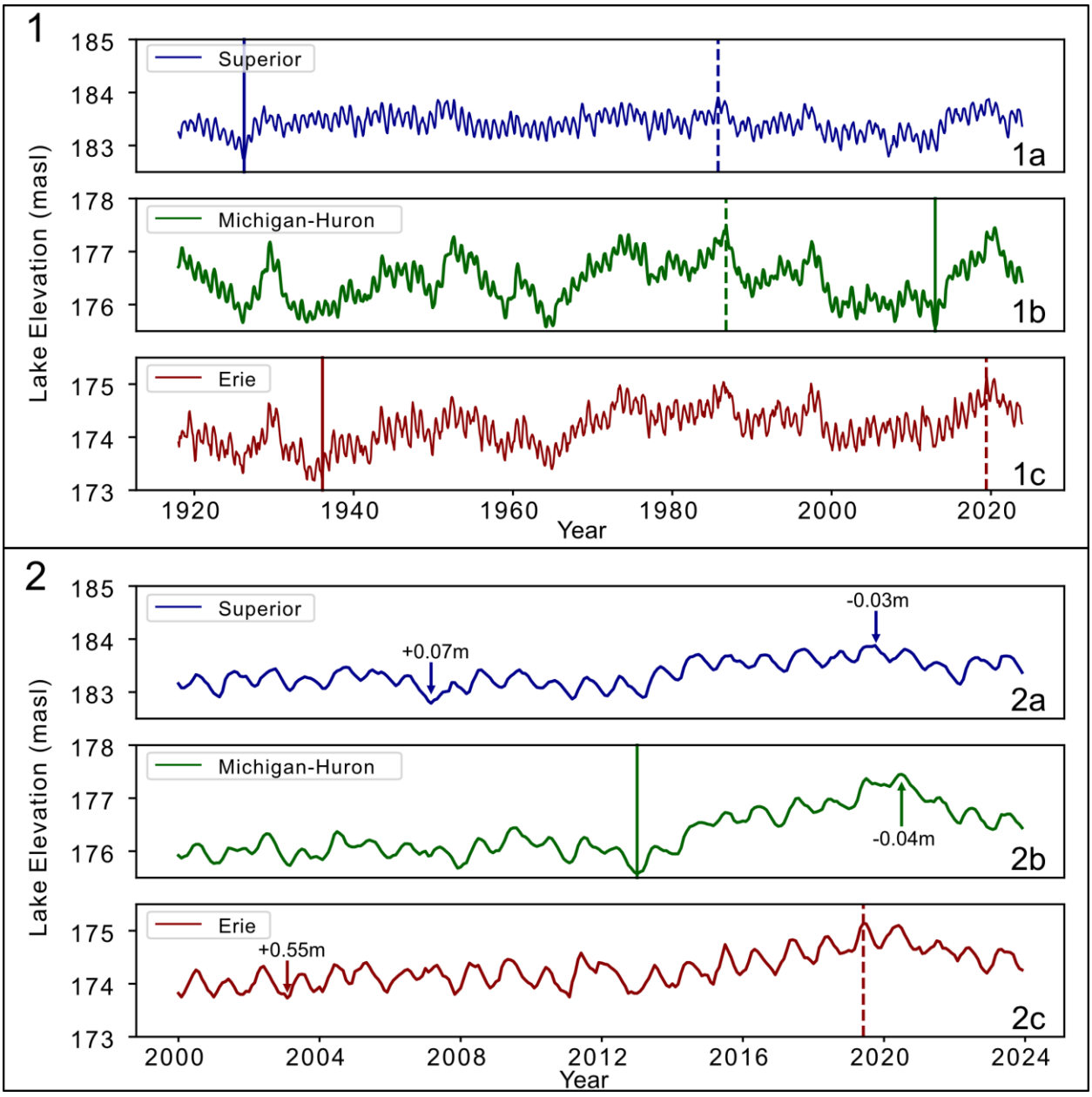

Figure 9: Great Lakes Lake Elevations 1918-2023. Elevations of lakes Superior (a), Michigan-Huron (b), and Erie (c) for the periods of 1918-2023 (Panel 1) and 2000-2023 (Panel 2).The minimum and maximum historical lake level are shown by the solid and dashed lines respectively. The colored arrows Panel 2 indicate the recent minimums (for Superior and Erie) and maximums (for Michigan-Huron and Superior), while the accompanying text indicates how much higher (or lower) this recent extreme was from the all time record conditions (NOAA Great Lakes Monitoring Network).

2. Methods

2.1 Study Region and Model Boundary

The area of interest for this modeling investigation was defined as all the U.S. Geological Survey Hydrologic Unit Code 8-digit (HUC8) sub-basins that intersect the state of Michigan. The model domain was defined using separate criteria for the inland (terrestrial) and lake portions of the domain. In the terrestrial portion of the model, the boundary was defined as an adjacent major hydrologic divide beyond the area of interest. Where possible, this terrestrial boundary follows higher order river channels within these adjacent watersheds, and is conceptualized as a no-flow boundary within the groundwater model. For the portion of the domain that intersects the Great Lakes, the model boundary follows the coastline. In the surface model, the boundary follows the coastline directly. In the groundwater model, the boundary is extended 10km into the lakes using a buffer around the coastline, to allow the model simulate direct exchange of water between the Great Lakes and groundwater system though the lake bed. Hereafter, this domain is referred to as the "LHM Michigan Model" or "Michigan Model".

This domain consists of two primary geographic regions centered around Michigan's Upper and Lower Peninsulas. The upper portion of the domain consists of the north-eastern portion of Wisconsin and the Upper Peninsula (Figure 10). The lower portion of the domain consists of the Lower Peninsula and portions of Illinois, Indiana, and Ohio. This domain also covers portions of the surface drainage basins for Lakes Superior, Huron, Michigan and Erie. It is important to note that Lakes Michigan and Huron are connected by the Straits of Mackinac, and as a result their levels are the same. Thus, this water body is referred to as Lake Michigan-Huron in the rest of this manuscript, and land surface draining to this water body is treated as a single drainage basin.

Two primary geologic settings are present within the modeling domain. The western half of the upper domain is characterized by Precambrian to Cambrian era metamorphic bedrock, primarily basaltic lavas and metamorphosed sedimentary rocks (Dietrich, 1983). These units are either overlain by thin soils and glacial sediments (Larson and Schaetzl, 2001), or exposed at the surface, particularly within the Porcupine Mountains. The eastern half of the upper domain and the lower domain are characterized by Pleistocene-era glacial deposits overlying bedrock units of the Michigan Basin (Dietrich, 1983, Milstein, 1987, Reed and Daniels, 1987, Westjohn and Weaver 1998). Glacial deposits consist of till, outwash and lacustrine sediments (Soller and Garrity 2018, Westjohn and Weaver 1998). Thick sand, outwash, and coarse to medium till deposits create

a topographically high region in the northern Lower Peninsula, the thickest portion of the glacial aquifer within the model domain. Lacustrine sediments and fine tills dominate along the lake shores, particularly within the Saginaw Bay watershed and Lake Erie basin (Farrand et al., 1984, Fullerton et al., 1991, Gobel et al., 1983, Lineback et al., 1983, Sado et al., 1993). The underlying units of the upper Michigan Basin are thick sedimentary sequences of sandstone, limestone, shale, and dolomite units from the Ordovician through Jurassic periods. Deeper units of the Michigan Basin include Precambrian and Cambrian sandstones overlying Precambrian crystalline rock units. (Dietrich, 1983, Reed and Daniels, 1987, Milstein, 1987, Westjohn and Weaver 1998). Primary aquifers within the modeling domain consist of the glacial sediments, and the more permeable units of the Michigan basin (Westjohn and Weaver 1998). Groundwater is a significant contributor to surface water and streamflow in this region. A USGS study of streamflow in the Great Lakes basin shows that baseflow contributes between ~40% to > 90% of total flow across most of the modeling domain (Neff et al., 2005).

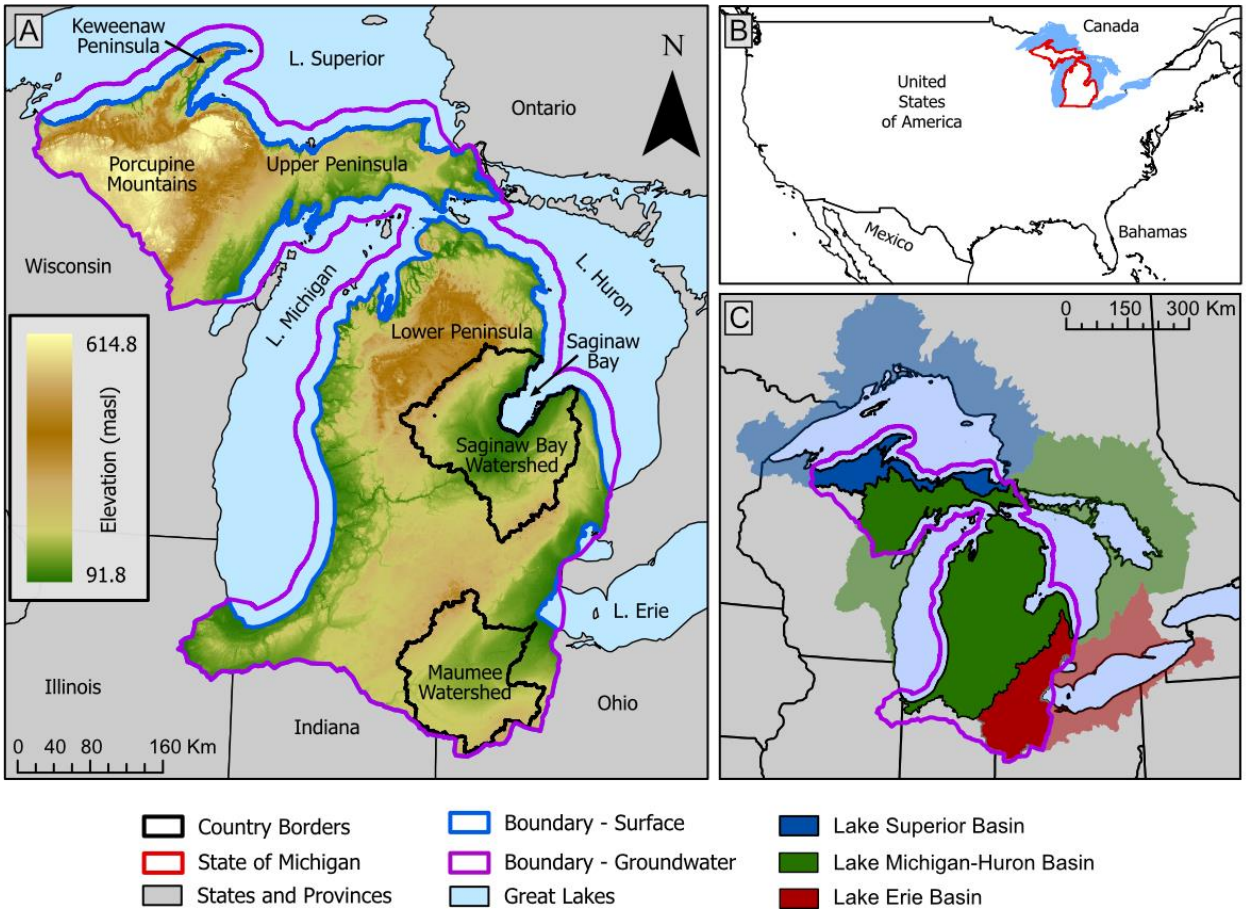

Figure 10: Study Region, Model Domain and Surface Elevations. Domains for the surface (blue outline) and groundwater (purple outline) models (A) shown with surface elevations form the USGS 3D Elevation Program (USGS, 2023) and common names of places referenced throughout the manuscript. The model domain contains every HUC8 subbasin in the state of Michigan, and includes portions of the coastline of lakes Superior, Huron, Michigan and Erie. Panel (B) shows the relative location of the state of Michigan and the Great Lakes in North America. Model outputs are summarized across the model domain, and within the portions of the Great Lakes surface drainage basins contained within the model, shown in Panel C. The lightly shaded regions of corresponding color show the extent of each lake basin outside the model domain.

2.2 The Landscape Hydrology Model

The Landscape Hydrology Model and its functionality are described in detail in Kendall (2009) and Hyndman et al. (2007). Briefly, LHM is a distributed, process-based surface and subsurface water and energy balance model. LHM consists of three modules which each simulate the relevant processes in one of three hydrologic zones: the landscape surface and root zone, the unsaturated zone, and the saturated zone. The landscape module is a gridded 2-dimensional model simulating water and energy fluxes from the canopy through the root zone. The generalized form of the water balance equation solved by the surface module is given in Equation 1 as:

[1] $$\Delta Sm = P - E - T - Ss - R - Ex - Pd$$

Where ΔSm is the change in root zone soil moisture, P is precipitation, E is evaporation, T is transpiration, Ss is surface storage (combination of canopy, depression, snowpack and ice storage), R is runoff, Ex is exfiltration from (water leaving) the root zone and Pd is deep percolation (water reaching the water table after transport through the unsaturated zone). The landscape surface has one layer, while the root zone is in general multi-layered.

The unsaturated zone module takes deep percolation from the surface model, removes throughflow created by resistive deeper layers, then simulates the vertical propagation of water through the unsaturated zone until its delivery to the saturated water table as recharge. Here, throughflow is defined as water that moves laterally through the unsaturated zone before discharging to a surface feature. Throughflow occurs when deep percolation exceeds the vertical conductivity of the unsaturated zone material beneath the root zone, and is governed by Equation 2:

[2] $$Tf = max((Pd - Kv),0)$$

Where throughflow Tf is the maximum of 0 and the difference between deep percolation Pd and unsaturated zone vertical saturated hydraulic conductivity Kv. Recharge Rch is calculated as the difference between deep percolation Pd and throughflow Tf convoluted with a time delay function as show in Equation 3:

[3] $$Rch = (Pd - Tf) * Df$$

This time delay function was derived empirically from the 1-dimensional Richards Equation (Richards, 1931) and uses soil hydrologic properties to simulate the delay in transport between water leaving the bottom of the soil zone and reaching the top of the water table. It is important to note that this computed transit time is that of the pressure wave pushing soil moisture downward, not the hydrologic transit time of water particles.

The saturated zone module is based primarily around the modular 3-dimensional finite difference groundwater flow model MODFLOW (Harbaugh, 2005). Recharge from the unsaturated zone module and unsatisfied evapotranspiration demand from the surface model are passed to MODFLOW which then computes the change in groundwater storage ΔS_G , groundwater supplied evapotranspiration ET_G, and groundwater discharge Q as shown in Equation 4:

[4] $$\Delta S_G = R - ET_G - Q$$

Groundwater elevations and fluxes in MODFLOW are governed by a variety of optional

'packages' used to represent boundary conditions such as groundwater evapotranspiration, groundwater discharge to streams and constant heads. Details on the MODFLOW packages used in this work are provided in Section 2.8. Hereafter we will refer to the combination of the landscape surface, root zone, and unsaturated zone as the "surface model" and to MODFLOW as the "groundwater model".

Currently the surface and groundwater models are coupled offline using the following approach. First the surface model is run for the full simulation period, and the outputs are saved. Second, deep percolation and unsatisfied ET demand are passed to MODFLOW which is run for the full simulation period to compute groundwater elevations and discharge to surface features. Finally, post-processing combines the surface runoff fluxes and groundwater discharge to compute streamflows. More details on the calculation of streamflows and their comparison to observed streamflow data are provided in Section 2.10.

Five major changes have been made to the basic structure of the LHM since its description in Hyndman et al. (2007) and Kendall (2009), which are important to its function as applied in this paper.

1. A snowpack thickness calculation has been added to the snow model, including the addition of terms for snowpack liquid water holding capacity and ice/water fraction. Snowmelt at the surface is now retained in the snowpack, and melt only occurs after the holding capacity has been reached (Ford, 2022).
2. Infiltration capacity, previously static and defined as the saturated infiltration capacity provided in the SSURGO database (USDA, 2016), is now calculated using the Green and Ampt method (Green and Ampt, 1911).
3. The user can now select from two different methods for calculating root zone soil moisture in the land surface module: 1) a linearized 1-dimensional Richards equation approach described in Kendall (2009) or 2) a hybrid bucket model computes fluxes from one layer of the soil zone to the layer below it using the unsaturated hydraulic conductivity, which is computed using the soil moisture in that layer with the Van Genuchten equation (Van Genuchten 1980)
4. A mechanism has been implemented using MODFLOW's Drain Package to simulate discharge from the groundwater aquifer through lateral discontinuities caused by rapid changes in elevation, hereafter referred to as vertical seepage faces. A detailed

description of these vertical seepage faces and their governing equations are provided in Section 2.7.

5. The groundwater coupling and model preparation infrastructure have been updated to allow LHM to run newer versions of MODFLOW, including MODFLOW-NWT (Niswonger et al., 2011).

2.3 Model Data Sources

LMH instances are built and driven using a variety of existing regional to national scale datasets describing the climate and landscape. Climate forcing data including precipitation, windspeed, air temperature, humidity, and incoming solar radiation are sourced from the North American Land Data Assimilation System (NLDAS-2A) reanalysis product (Mitchell et al., 2004, Xia et al., 2012a, Xia et al., 2012b). Leaf area index (LAI) data used in calculating ET in the model come from the MODIS MCD15A2H LAI product (Myneni et al., 2015). Land cover and impervious surface area are taken from the USGS National Land Cover Database (NLCD) 2001, 2006, 2011, 2016, 2019 and 2021 data products (Dewitz, 2023, Yang et al., 2018). Municipal boundaries are defined using the Topologically Integrated Geographic Encoding and Referencing (TIGER) dataset (U.S. Census Bureau, 2012). LHM uses two main hydrography datasets, the National Hydrography Dataset (NHD) (USGS, 2020) and wetland data from the National Wetlands Inventory (NWI) (USFWS, 2018). Surface elevation data come from the USGS 3D Elevation Program (3DEP) 1/3rd arc second digital elevation model (DEM) (USGS, 2023) and Great Lakes bathymetry comes from the NOAA Great Lakes Bathymetry dataset (National Geophysical Data Center, 1999a,1999b, 1999c, 1999d, 1999e). Soil type and soil property data are taken from the Gridded Soil Survey Geographic (gSSURGO) Database (USDA, 2016), with soil hydrologic properties computed using the ROSETTA model (Schaap et al., 2001).

Well data were accessed from the Michigan Department of Environment, Great Lakes, and Energy (EGLE) Wellogic database, which provides the locations and characteristics of public and private water wells across the state. This database includes information compiled from driller logs including depth to water, well depth, aquifer type and aquifer thickness. Also included are estimates of hydraulic conductivity based on lithology (EGLE, 2020). Drinking water wells for Wisconsin, Illinois, Indiana, and Ohio were compiled from their respective state agencies which oversee well records (IDNR, 2015, ISGS, 2015, ODNR, 2015, WDNR, 2015) , which compiles well data from state agencies across the United States.

To ensure cross scale consistency, the location and extent of Quaternary geology units were compiled from a series of 4x6 degree Quaternary geologic maps from the U.S Geology Survey for the Chicago (Lineback et al., 1983), Lake Erie (Fullerton et al., 1991), Lake Superior (Farrand et al., 1984), Minneapolis (Goebel et al., 1983) and Sudbury (Sado et al., 1989) quadrangles. Data for Quaternary deposit thickness and bedrock topography came from maps by Soller and Garrity (2018). Bedrock geology unit locations and extents were specified using the Geologic Map of North America (Garrity and Soller, 2009). Additional information on bedrock unit formations was taken from the Michigan Bedrock Geology maps (Milstein, 1987, Reed and Daniels, 1987). Lakebed material units were specified using the lakebed substrate material product provided in the Great Lakes Aquatic Habitat Framework (GLAHF) (Wang et al., 2015).

2.4 Model Layering and Discretization

For the Michigan Model, LHM's surface model contains one land surface layer and seven root-zone soil layers, and is discretized with 1000 m cells and hourly time steps. The groundwater model uses 500 m cells, daily time steps and weekly stress periods. To initialize the groundwater model, a steady state stress period is run at the beginning of the simulation period using average recharge and evaporative demand from LHM's surface model. During the transient simulation period, recharge and evaporative demand are updated at the beginning of each week-long stress period, but remain constant during each time step within a given stress period.

Land surface elevations are specified using the 3DEP DEM (USGS 2023), and the soil thickness is defined using the gSSURGO database (USDA, 2016), with a minimum thickness of 0.5m and a maximum thickness of 2.5m. The groundwater model has three layers, two in the Quaternary glacial materials and one representing the bedrock material. Land surface elevations in the groundwater model are defined using a combination of the NED DEM and Great Lakes Bathymetry data (Described in Section 2.4). Specifically, top elevation in the first layer is set to the land surface elevation in the terrestrial portion of the model and the lakebed elevation in the portion of the model domain covered by the Great Lakes. The top elevation in layer 2 is set to half the distance between the starting head elevation and the bedrock surface, and the top of layer 3 is set to the bedrock surface. A map of the surface aquifer thickness, calculated as the difference between the DEM and bedrock elevations is shown in Figure A22. Layer 3, representing the bedrock units, was set to a fixed depth of 100m, and was included primarily to provide stability to the heads in layers 1 and 2. Although units of the Michigan Basin can include highly saline water,

movement of groundwater due to density dependent flow is not considered in this model.

2.5 Surface and Bedrock Elevations and Starting Heads

Model top elevations were created by combining the 3DEP DEM (USGS, 2023) with the NOAA Great Lakes bathymetry dataset (National Geophysical Data Center, 1999a,1999b, 1999c, 1999d, 1999e) to create a continuous elevation map representing the land surface and lake bottom elevations. The 3DEP DEM includes lake surface elevations, representative of the lake level at the time of data collection. To convert these lake surface elevations to lake bottom elevations, the NOAA bathymetry data were first combined from their individual lake basins to a single raster, then only the cells with negative elevation (measurable lake depth) were selected. This resulting lake depth raster was then subtracted from the DEM, to yield a combined elevation product spanning the land surface and lakebed. Bedrock elevations, which define the contact between Quaternary glacial and bedrock aquifers in the groundwater model, were created by smoothing the Soller and Garrity (2018) bedrock elevation product using a 3x3 focal mean implemented using the Focal Statistics tool in ArcPy (ESRI, 2023).

Starting heads were created using an input layer consisting of groundwater well elevations compiled from data from the agencies responsible for permitting and/or tracking private water wells in each state in the model domain (EGLE, ODNR 2015, ISGS 2015, IDNR 2015, WDNR 2015) located within the model boundary and screened in the Quaternary aquifer. First an initial gridded estimate of static water table elevations is created by randomly selecting a subset of the wells, then interpolating the static water levels reported in the database using the Empirical Bayesian Kriging function in ArcPy (ESRI, 2023). Second, this initial water table elevation is used to select areas where the water table is above the land surface. Third, elevations (taken from the DEM) for surface water features (taken from the hydrography datasets) in areas where the initial water table is above the land surface are converted to points. Finally, a combined dataset of the water well subset, and points representing surface hydrologic features are combined, and interpolated using the same kriging routine. The result is a gridded estimate of water table elevations which considers surface hydrologic features, considered to be expressions of the water table.

2.6 Quaternary and Bedrock Geology Maps

A unified Quaternary geology map (Figure A23A) was created by combining the five quadrangle Quaternary geology maps and clipping it to the model boundary. The Quaternary

material classes reported in the original datasets were then re-classified into a simplified list of geology classes (Table A1). Polygons within this reclassified map were then dissolved using the summary Quaternary geology classes to combine polygons of the same material type adjacent to one another. All of these initial processing steps were performed in Python (version 3.9.18) using the Geopandas (Jordahl et al., 2021) and ArcPy packages (ESRI, 2023). Some linear features bisecting Quaternary unit polygons were present from the compositing of the individual maps. These features not removed by the dissolve were manually removed in the ArcGIS Pro desktop interface.

A bedrock geology unit map (Figure A23B) was created by first clipping the bedrock geology polygon product from the Geologic Map of North America (Garrity and Soller, 2009) to the model domain. This map has coarse spatial resolution, but was uniform and nearly continuous across our model domain. There were, however, some missing data in a thin band along the coastline of the Great Lakes. To fill in this missing data, polygons of the same age and material type on either side of these missing data were connected by manually editing the polygon vertices in the ArcGIS Pro desktop application (ESRI, 2023). Because this data was uniform across the model region, the unit names and rock type information were not re-classified. However, attributes from the Michigan Bedrock Geology product were combined with those of the Geologic Map of North America, as the Michigan bedrock product had more descriptive geologic unit names helpful in specifying aquifer property estimates (described in detail in the next section).

2.7 Initial Aquifer Property Estimates (Quaternary, Bedrock and Lakebed Substrate)

Hydraulic conductivity (HK) estimates in the Quaternary material (Figure A24 A) were derived by combining the Wellogic conductivity information with the merged and refined bedrock and Quaternary geology maps described in Section 2.3. The Wellogic data were cleaned to remove all wells with no data for HK and to remove all wells with whole number HK values (i.e. 0, 50,100,200,300) which were repeated more often than other values and assumed to be spurious data. Subsets of this dataset representing wells in sedimentary and bedrock aquifers were then created. For the Quaternary geology units, the formatted Quaternary geology map and cleaned Quaternary well data were combined using their spatial locations using the spatial join function in the Python package Geopandas (Jordahl et al., 2021). One of two methods was used to assign HK values to the individual Quaternary unit map polygons. In polygons with more than five wells, the geometric mean of the reported hydraulic conductivities for all the wells within that polygon was

calculated. The arithmetic mean was then taken for all of the polygons of a given class with more than five wells to create type-average HK values. The unit average HK values were then assigned to polygons with less than five wells based on the unit type, and are reported in Table A10. Two Quaternary geology summary classes had no polygons with wells in them, bedrock and artificial fill. The bedrock units were assigned an HK value based on that of the corresponding location bedrock HK map, and artificial fill was assigned the same HK value as coarse textured till. HK values for the lake bed were computed by relating the six substrate classes listed in the GLAHF dataset (clay, silt, sand, mud, hard, rock) to the existing Quaternary geologic classes using Table S11. HK values for the substrate classes were then assigned as the average HK in the corresponding Quaternary geologic material. For bedrock HK estimates (Figure A24 B), a similar procedure was used. First, the Geologic Map of North America polygons were edited to fill in gaps around the lake shore present in the original shapefiles. Second, the bedrock unit polygons were merged with the cleaned bedrock wells, and the geometric mean of the reported HK values was calculated for each polygon.

Estimates of specific yield from the Quaternary aquifer materials were derived from the gSSURGO soil data for the lowest soil layer in LHM's surface model. Specific yield, or the ratio of water that can drain from an aquifer to the total value of the aquifer, was calculated by taking the difference between the soil saturated water content (Θ_{sat}) and soil field capacity (Θ_{fc}), as shown in Equation 5.

[5] $$Sy = \Theta_{sat} - \Theta_{fc}$$

The calculated specific yield raster was then resampled to the Quaternary geology polygons by taking the mean across each polygon. Geologic unit information from both the Geologic Map of North America and the Michigan Bedrock Geology maps were used to assign specific yield values from the literature to the bedrock geology polygons. Assigned specific yield values were taken from published estimates for different geologic materials compiled in Anderson, Woessner, and Hunt (2015) and Woessner and Poeter (2020). Porosity estimates were derived as the difference in the specific yield estimates (Sy, described above) and the residual water content (Θ_{res}) reported for the lowest soil layer reported in the gSSURGO database (USDA. 2016) as shown in Equation and range from 0.139 to 0.382 across the model domain.

[6] $$\phi = Sy + \Theta_{res}$$

Specific yield estimates for the bedrock units were taken from published values for bedrock

units of different lithologies (Anderson et al., 2015, Woessner and Poeter, 2020).

2.8 Groundwater Model Boundary Conditions

Six internal boundary condition types are included in the groundwater model, implemented using one of three MODFLOW head-dependent flux boundary packages: Drain (DRN), Evapotranspiration (EVT) or General-Head Boundary (GHB) (Harbaugh, 2005).

A two-way head-dependent flux boundary condition is specified from the coastline 10 km into the lakes using the GHB package. This package is used to represent exchange of water between the Great Lakes and the terrestrial groundwater system. Heads for this boundary condition are specified using the monthly observed lake elevation data from the NOAA Great Lakes Monitoring Network. The direction of the flux is computed in MODFLOW as the difference between the head h and the lake elevation E_L. The total flux across this boundary is the product of this difference in head multiplied by the conductance of the lakebed sediments (C_{LB}) as shown in as shown in Equation 7:

[7] $$Q = (h - E_L) * C_{LB}$$

Here, lakebed conductance is defined as the hydraulic conductivity K multiplied by the cell area A_L divided by resistive sediment thickness T here assumed to be 1 m everywhere as shown in Equation 8.

[8] $$C_{lb} = K * A_L/T$$

Four types of one-way head dependent fluxes, which allow water to drain from the aquifer, are represented in the model as "drains" using the DRN package: rivers, lakes/wetlands, horizontal seepage faces (surface drains) and vertical seepage faces. Every cell in the first layer of the model is specified as a river, lake/wetland or horizontal seepage face, while vertical seepage faces are specified in layers 2 and 3 where lateral discontinuities in the layers occur. MODFLOW computes flux across these boundaries as the difference in calculated head h and drain feature elevation E_d, multiplied by a conductance term C as shown in Equation 9.

[9] $$Q = (h - E_d) * C$$

A unique conductance term is defined for each of the four drain types. For all four drain types, water can only leave the aquifer, so in the case that $(h - E) \leq 0$, Q is zero.

The locations and geometry of rivers are defined using the National Hydrography Dataset (USGS, 2020), and streambed elevations are derived from the 3DEP DEM (USGS, 2023). River conductance is defined in Equation 10 as:

[10] $$C_r = K * L * W / T_{sed}$$

Where C_r is riverbed conductance, K is horizontal hydraulic conductivity, L is the length of the stream feature in each cell, T_{sed} is the thickness of the river bottom sediment, assumed to be 1m in all locations and W is stream width. Here, W is estimated as a spatially-variable relationship between stream width and streamflow as given in Equation 11:

[11] $$W = a * Q^{b}$$

Where a and b are spatially variable constants and Q is discharge inferred from the USGS stream gauging network stations within the model domain. Values of these constants are set by fitting stream cross-sectional measurement data collected by the USGS during site visits (USGS, 2019) using the at-many-stations hydraulic geometry method (Gleason and Wang, 2015). Because these constants reflect underlying geologic, climatologic, and other hydrologic conditions, they vary across space, and at different flow levels (e.g. low, medium, and high flow) and spatial scales. However, the spatial distribution of stream geometry measurements is uneven, and sparse in regions with lower populations, such as Michigan's Upper Peninsula. To address this, we iteratively fit the constants in Equation 11 to best describe stream width at a given discharge percentile for all of the gauges within a given watershed. This process was repeated across successively decreasing watershed sizes, starting with 2-digit HUC code watersheds, followed by HUC 4, 6 and finally HUC 8. If a watershed at a certain scale did not contain sufficient points for an accurate fit (10 gauges was selected as the threshold), that watershed then inherited constants fit at the next coarsest scale. For stream velocity and geometry calculations here, constants fit to median flow geometry data were used.

Wetland and inland lake locations are defined using the NHD dataset (USFWS, 2018), and elevations are defined using the 3DEP DEM (USGS, 2023). Conductance (C_{wl}) in these features is defined in Equation 12 as:

[12] $$C_{wl} = K * A_f / T_{sed}$$

Where K is the hydraulic conductivity of the bed sediments, A_f is the area of the feature within the cell, and T_{sed} the thickness of the sediments along the bottom of the feature, assumed to be 1 m in all locations.

Horizontal seepage faces (surface drains) are specified in every cell without a river or lake/wetland drain. Elevations for these surface drains are set equal to the land surface elevations specified by the DEM (USGS, 2023). Surface drain conductance C_{surf} is defined in Equation 13

as:

[13] $$C_{surf} = K * A_c / T_{soil}$$

Where K is the hydraulic conductivity, A_c is the area of the cell and T_{soil} is assumed to be a unit thickness of soil closest to the surface.

Vertical seepage faces are defined as a special case in the model, allowing water to drain from cells in any layer where a lateral discontinuity in the model layers occurs. This condition simulates the lateral drainage of water from topographic faces in areas of high relief, such as in the Porcupine Mountains in the north-western portion of the model region. Vertical seepage faces are allowed to occur in layers 2 and 3 anywhere that the layer bottom is above the layer top of an adjacent model cell, such that the cell is exposed to the surface on one of its four lateral faces. No vertical seepage faces were specified in layer 1, as all layer 1 cells contained either a river, lake/wetland or horizontal seepage face boundary.

A seepage face conductance term is derived to describe the discharge across the wetted area of the seepage face, as shown in Equation 14 such that:

[14] $$C_{sf} = K * (E_{top} - E_{seep}) \frac{3}{4}$$

Where C_{sf} is the seepage face conductance, K is hydraulic conductivity in the given layer, E_{top} is the top elevation in the cell, and E_{seep} is the elevation of the bottom of the seepage face (equal to the model top of the adjacent cell where the lateral discontinuity occurs). Using Darcy's equation and the Dupuit-Forchheimer, we estimate that the height of the wetted area of the seepage face is ¾ the total seepage face height, here given by $(E_{top} - E_{seep})$. The derivation of this seepage face conductance, including the simplifying assumptions used therein, is described in the Appendix B. And accompanying figure showing a conceptual diagram of head within the seepage face cell is included in figure A21.

When insufficient soil moisture exists to meet evaporative demand in areas with shallow water tables, plants can access saturated groundwater to meet this unsatisfied evaporative demand (Lowry et al., 2010, Zipper et al., 2015). In LHM, groundwater evapotranspiration is allowed in wetland areas, where water tables are within 3 m of the land surface. Wetland evapotranspiration from groundwater is represented using the EVT package, and is specified by three parameters: an ET rate, surface elevation and extinction depth (here set to 3 m). ET occurs at the specified rate when the simulated head is equal to or greater than the ET surface; when head is below the

extinction depth no ET occurs. At head elevations below the ET surface and extinction depth, the ET rates vary linearly with head. Here, ET rates are specified as the unsatisfied ET demand, or the difference between potential evapotranspiration (PET) and the ET supplied by surface fluxes as computed by LHM's surface model.

In addition to the internal boundary conditions described above, a no-flow boundary condition is specified along the margins of the model boundary. In the terrestrial portion of the model domain, this no flow boundary follows major river systems outside the area of interest, and in the lakes this boundary follows a 10km buffer out from the shoreline.

2.9 Observational Data

Both observed groundwater head elevation and streamflow records are used for comparison with model outputs. Head observations are compiled from the same static water level measurements reported by state agencies in their municipal and drinking water well databases that were used to create starting heads for the model. Static water level measurements are filtered to select only those from within the model period (01-01-2000 to 12-31-2023). During a transient run, heads are written out using the MODFLOW Head Observation Package at the same date and location as the observed water level. During a steady state run, all observed heads are compared to the modeled head at the end of the single steady state stress period. Model performance for heads is assessed using the root mean square error, calculated using the Python package NumPy (Harris et al., 2020) as shown in Equation 15:

[15] $$RMSE = \sqrt{\Sigma(H_S - H_O)\hat{}\,2/N}$$

Where H_S is the simulated head elevation in the cell containing the observation well, H_O is the head elevation in the observation well, and N is the total number of observations.

Streamflow observations are downloaded from the USGS NWIS system for every gage active during the model period within the model domain. An observation watershed is automatically delineated for the contributing area to each streamflow observation location. Groundwater discharge fluxes from MODFLOW along with surface runoff and throughflow from the surface model are summarized within the observation gage basins to create simulated daily streamflow at the observation gage. Model performance for streamflow is assessed by comparing the monthly mean of simulated and observed streamflows at each site using the Normalized Nash-Sutcliffe Efficiency ($NNSE$) in Equation 16 as:

[16] $$NNSE = 1 / (1 + \frac{\Sigma((S_O - S_S) \wedge 2)}{\Sigma((S_O - S_M) \wedge 2)})$$

Where: S_O is the observed streamflow, S_S is the simulated streamflow and S_M is the mean of the observed streamflow. Streamflow simulation performance across the whole model domain is computed as the average of the $NNSE$. Values of $NNSE$ = 1 indicates perfect summation, 0.5 indicates the simulation is no better than the mean of observations, 0 indicates no predictive power.

2.10 Model Calibration

Model calibration was performed in two primary phases: 1) steady state calibration to head observations, and 2) transient calibration to both heads and flows. In the first phase, HK values were iteratively updated by scaling HK values based on the head residuals from the previous run summarized within the Quaternary geologic units. The scaling factor (SF) used to update HK for the next run is shown in Equation [17]:

[17] $$SF = a^{R / Rmax - Rmin}$$

Where a is a constant, R is the residual within the given geologic unit, $Rmax$ is the maximum residual across the geologic units, and $Rmin$ is the minimum residual across the geologic units. The constant was varied between 3 and 8 to control the degree to which HK values could be changed within each iteration. Higher values of a (Between 8 and 5) were used in early calibration runs to allow larger adjustments to HK values, while a smaller a of 3 was used in later runs to make smaller adjustments to HK values.

2.11 Data Analysis

To reduce dimensionality in the model outputs for interpretation, spatial and temporal summaries were computed. First, time series of spatial averages were created by computing the mean of each gridded output across the entire model domain and within individual lake drainage basins at each timestep. Second, cross year averages for each month were created to quantify changes within a year on average across the simulation period. For groundwater (and observed lake) elevations, mean monthly anomalies were computed by computing the mean elevation within each year, then subtracting each year's mean from its monthly values, and finally taking an average of this mean-removed monthly value across all years. For surface fluxes (e.g. ET, deep percolation), mean fluxes in each month across all years were computed. Groundwater storage is computed as meters of water in the aquifer at a given time point, calculated as the MODFLOW estimated head time porosity. Hereafter “head” or “groundwater elevation” refers to the

MODFLOW estimated groundwater elevation in meters above sea level, while "storage" or "groundwater storage" refers the computed aquifer storage in meters of water (MODFLOW estimated head times porosity). Changes in groundwater storage are only assessed in the surficial aquifer. Groundwater flow across the Great Lakes region is primarily in the shallow flow system, which for most of the model region is dominated by glaciofluvial material. These aquifers are also the most productive; however significant storage and drinking water withdrawals occur from the deeper bedrock aquifers, including from units of the Michigan Basin (Grannemann et al., 2000, Feinstein et al., 2010). These deeper bedrock aquifers are not fully simulated in this model.

These time series of the spatially averaged model outputs were then used to inform creation of spatially explicit maps of change in groundwater storage across the model period. In the first case, the difference in head in each cell was taken between the domain average minimum and maximum head conditions. Second, a maximum seasonal groundwater storage change map was created by: 1) identifying the months with the maximum and minimum average groundwater elevation anomaly (December and September respectively), 2) computing the average head in each cell during these two months across the simulation period, and 3) computing the difference in head mean September from the mean December groundwater elevation in each cell.

Segmented linear regression is employed to identify when distinct changes in trends of lake elevation and groundwater storage occurred. For this analysis, the data records are truncated to the period of 2006-2021 and after initial analysis of the model output data, 2012-2021 for groundwater elevations. The approach implemented search for the single most significant breakpoint in the time series. Restricting these date ranges for the analysis assured that the inflection point between extreme low and high water levels in each series were captured. The dates of these inflection points are then compared for the lake elevations and groundwater storage in their respective basins to assess to what degree there is a lag between these two signals. This analysis is implemented using the Python package piecewise-regression (Pilgrim, 2021, Pilgrim, 2023), which is based on the methods of Muggeo (2003).

Breakpoint analysis was used to investigate the relationships between changes in groundwater elevation and surface fluxes. Breakpoints in the domain average time series of each model output were selected using the Python package Ruptures (Turong et al., 2018). Specifically, a bottom-up segmentation approach was used with a least squared deviation cost function to select two breakpoints in each time series. These two breakpoints were then used to segment the time

series into three periods, representing changes in the long-term mean of the given model output. Mean head and surface fluxes in each model cell were computed within the three periods created by the breakpoint analysis, and compared to understand the spatial variability in changes to the surface water balance and groundwater elevations.

3. Results and Discussion

3.1 Model Calibration

The initial, uncalibrated model performance values for the first fully transient model run were an RMSE of 8.03m for head and an average NNSE of 0.435 for streamflows. A steady state only version of this same run yielded an RMSE of 7.96. A total of eight subsequent steady state model runs were completed where HK values were scaled based on RMSE values from the previous runs summarized in the geologic unit polygons (Equation 17). The last of these eight runs yielded an RMSE of 6.56, and the corresponding transient run had an RMSE of 6.60 and an average NNSE of 0.41. There is no obvious bias toward over or underprediction in the model in the simulated-vs-observed plot shown in Figure A25A. Figure A25C shows the spatial distribution of head errors, with clusters of underprediction occurring in the northern Lower Peninsula where Quaternary sediments are thick, and along the northern shore of the Upper Peninsula and into the Keweenaw Peninsula, where bedrock exists near the surface adjacent to the lakeshore. Clusters of overprediction occur along the shoreline of the northern Lower Peninsula, and along the south-eastern portion of the model domain including the Maumee Watershed. No trend in residuals though time is observed, indicating that the model is not accumulating error or bias toward any particular period of the observational data (Figure A25B). Model performance for streamflow is highest in the central and eastern Upper Peninsula, and is weakest in watersheds of the northern Lower Peninsula, in the same regions with the largest underprediction in groundwater heads (Figure A26).

3.2 Average Conditions

On average, the study region receives 894 mm of precipitation per year, 541 mm of which is returned to the atmosphere as ET, and 260 mm of which passes below the root zone as deep percolation. Overland runoff averages 93 mm per year. Annual average precipitation, ET, and deep percolation across the model regions are shown in Figure A27. Precipitation in the region is strongly influenced by the lake effect, especially along the Lake Superior and Lake Michigan shorelines. Lake effect precipitation also affects deep percolation, while the ET pattern is

considerably more heterogeneous across the model region. Average water table elevations (Figure A28A) closely follow trends in topography and are influenced by the presence of discharge points (rivers, lakes and wetlands), while depth to water (A28B) is considerably more variable, even across areas of similar relief, due to variations in soil and aquifer properties and the locations and elevations of groundwater drainage boundary conditions. Depth to water in roughly 45% of the model region is within 5m of the surface, and is especially shallow in the central Upper Peninsula, Saginaw Bay watershed, in the Thumb of Michigan and in the Maumee River Basin. The largest depths to water occur in the northern Lower Peninsula in areas of deep, sandy surficial aquifers.

3.2 Seasonal Changes in Groundwater Storage

Seasonal cycles of groundwater heads and lake elevations are out of phase, with peak groundwater heads occurring three to four months after peak lake elevations (Figure 11). Lake elevations are highest during mid-summer, with peak elevations occurring in August in Lake Superior (Figure 11A), July in Lake Michigan-Huron (Figure 11B), and in June in Lake Erie (Figure 11C). Maximum average groundwater heads within the lake basins occur in November in the Lake Superior basin, December in the Michigan-Huron basin and October in the Lake Erie Basin. Conversely minimum average heads occur during late summer; in September for the Lake Superior and Michigan-Huron basins, and August for the Lake Erie Basin. Average seasonal changes in heads across the lake basins range from 0.34 m in the Lake Superior basin to 0.13 m in the Michigan-Huron basin and 0.06 m in the Lake Erie basin. These seasonal changes in head are similar in magnitude to those of lake elevation for Lake Superior (0.29 m), much lower than those in Lakes Michigan-Huron (0.29 m) and Erie (0.37 m). These changes in head correspond to changes in groundwater storage of 0.08 m, 0.03 m and 0.01 m for the Superior, Michigan-Huron and Erie Basins. The same seasonal pattern of groundwater heads which peak during winter and are lowest during the summer are observed in the model of Xu et al. (2021). Their model also shows groundwater discharge to the Great Lakes is highest during winter, when heads are highest and lake levels are lowest.

Argus et al. (2020) estimate changes to groundwater storage across the Great Lakes Basin using GRACE and GPS data along with modeled soil moisture (NLDAS/Noah) and snow cover (SNODAS). They estimate seasonal changes of ~0.12 m in groundwater storage, or about four times the LHM derived estimate of 0.03 m across the domain. Their results also suggest that both terrestrial water storage and groundwater storage peak during March, 3-5 months before peak lake

levels and 7-9 months before (or several months after) the maximum seasonal groundwater elevations simulated by LHM. The timing of peak groundwater storage suggested by Argus et al. (2020) also contrasts with those simulated using a coupled surface and groundwater model for the Great Lakes Basin (Xu et al., 2021). Differences in the magnitude and timing of inferred groundwater storage change may be due to coarse resolution of the GRACE mass concentration solution used, ~350 km: two to three orders of magnitude larger than the resolutions of the models presented here. Additionally, the method used by Argus et al. (20200 lumps together changes in soil moisture (unsaturated zone water storage) and saturated groundwater, while the storage changes reported here from LHM are only those in saturated groundwater. Other complicating factors include coarse resolution of soil moisture estimates from the NLDAS/Noah model, and that their analysis ignores changes to surface water storage in other non-Great Lake reservoirs such as inland lakes and wetlands.

Spatial patterns in the timing (Figure A29) and magnitude (Figure 11D) of seasonal head minimums and maximums are significantly more complex than these spatial averages. Minimum heads generally occur between April and October in most of the upper domain and northern lower domain (Figure A29A). In the southern domain, minimum heads can occur year round, with significant portions of the Lake Erie basin having minimum head elevations in winter (December to February). Timing of maximum heads (Figure A29B) is slightly more consistent across the domain occurring between November and February however large portions of the southern half of the lower domain have maximum heads which occur in spring (April-May). Seasonal increases in head between September and December are widespread across the Upper Peninsula and northern Lower Peninsula and Upper Peninsula, and are strongest in the north-western portion of the Upper Peninsula and eastern Wisconsin. Areas of decreased head between September and December occur in the lower-lying regions of the model, such as in the Saginaw Bay watershed and Lake Erie basin and are most prevalent in the Maumee River basin. These observed seasonal head decreases are due to the variation in timing of minimum and maximum heads across the domain.

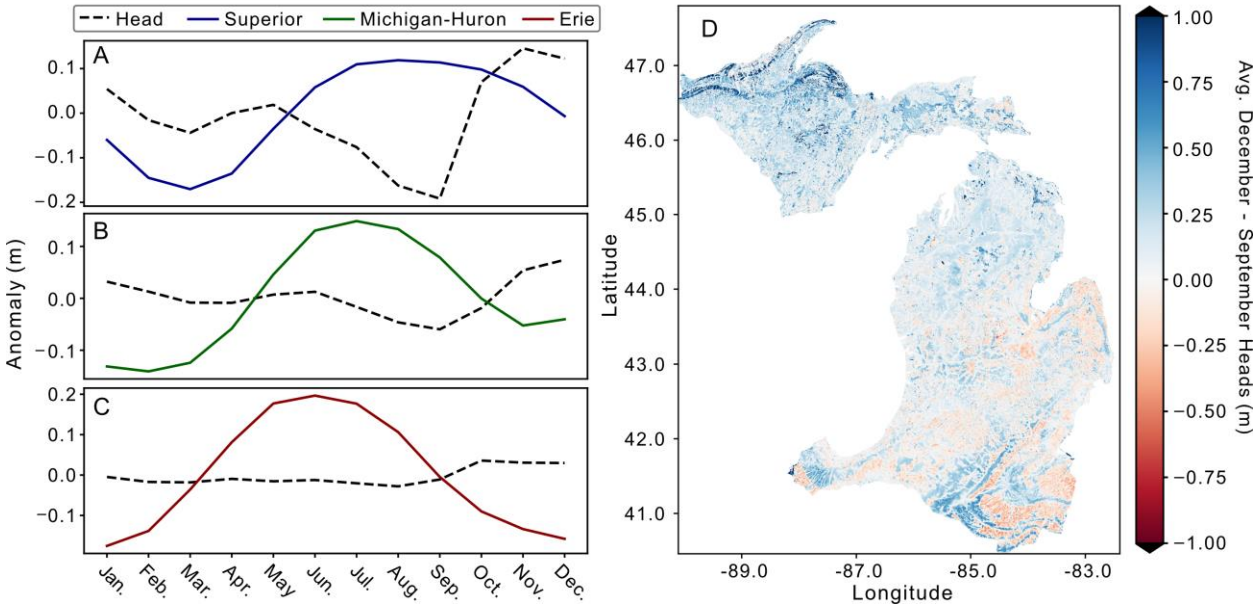

Figure 11: Seasonality in Lake Levels and Groundwater Elevations. Monthly anomalies in lake levels and lake basin groundwater elevations (heads) for lakes Superior (A), Michigan-Huron (B) and Erie (C). Elevation across the three lakes (solid line) peak during summer (June-July), while groundwater elevations (dashed line) peak in fall or early winter (October-December). Differences in the average September and December groundwater elevation (D) are greatest in the western Upper Peninsula and Northern Lower Michigan. Portions of the Lower Peninsula and Maumee Watershed have lower groundwater in December than in September, indicating seasonal cycles in groundwater storage vary across the model domain.

The observed seasonal changes in simulated groundwater heads across the domain are driven by seasonal shifts in the surface water balance (Figure 12). Precipitation and terrestrial ET both increase during spring, peak during summer and decrease though fall to minimums in winter. Precipitation is elevated from April through November, while peaks in ET are sharper but shorter lived, increasing rapidly from April to July before falling steadily through November. Deep percolation rises from February to its peak in April and May, then declines to its minimum in September, before increasing slightly during November and December. Domain average groundwater heads are highest in December, decline though March when a brief increase occurs, then continue to decline to minimums in August and September.

The relationship between seasonal changes in the surface water balance and those in groundwater heads is the result of complex processing including simultaneous changes to opposing fluxes (P and ET) and time it takes for changes in the water balance to propagate across different hydrologic (e.g. the surface, root and vadose) zones. Starting in early spring, deep percolation begins to rise as snowmelt and early spring rains increase infiltration. As the growing season begins

in spring and early summer, increased ET rates reduce the fraction of precipitation which percolates below the root zone. Deep percolation rates remain low until ET rates decrease during plant senescence and harvest in fall, after which continued precipitation causes a slight rise in deep percolation from November to January.

The seven month delay (April to December) between peak deep percolation and peak groundwater elevations highlights the significant lags between when changes to the surface water balance are expressed in groundwater. For changes in groundwater to occur, first alterations to the surface water balance must affect the root zone and subsequent deep percolation. Second, this change in deep percolation must propagate through the unsaturated zone, before reaching the water table as recharge. Unsaturated zone travel times can be especially long in areas where the unsaturated zone is thick, such as in portions of the central and northern Lower Peninsula (Hunt et al., 2008). Furthermore, the observed offset between seasonal peak lake elevations and heads is likely driven by differences in the water balance of the landscape and lake surfaces. Precipitation over the lakes and land surface follows a similar pattern, however over-lake evaporation peaks during the winter (Xu et al., 2021).

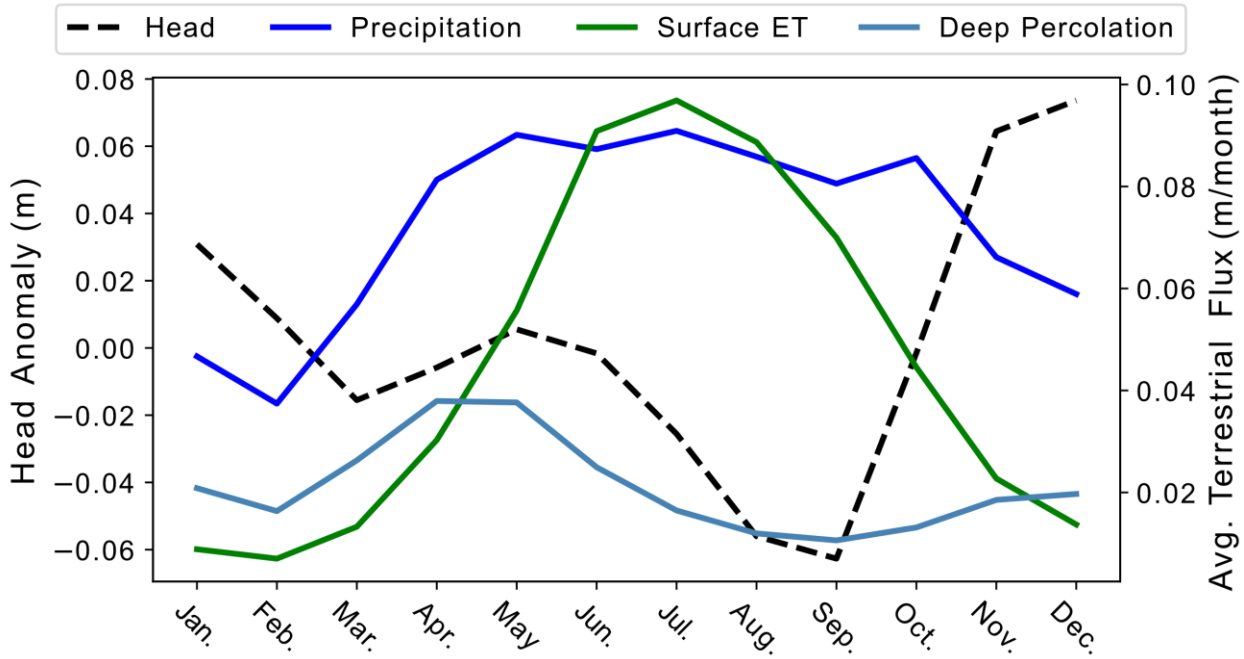

Figure 12: Seasonality of Head Elevation and Surface Fluxes. Average monthly groundwater elevation (head) anomaly (dashed line, left axis) plotted against average monthly surface fluxes (solid lines, right axis) from 2000-2023. Increases in groundwater elevation occur from March-May and follow increases in both precipitation and deep percolation. Groundwater elevations then fall from May-September as terrestrial ET increases, and deep percolation decreases. Groundwater elevations increase rapidly from their minimum in September to their maximum in December, corresponding with decreases in ET, increases in deep percolation and sustained precipitation.

3.3 Groundwater Storage Changes 2000-2023

Accompanying the record-setting increases in lake elevation which have occurred since 2007, rapid increases in groundwater storage occurred in all three simulated Great Lakes basins between 2013 and 2020 (Figure 13). Average groundwater storage in the Lake Superior and Michigan-Huron basins increased 0.47 m and 0.22 m respectively, from minimums in August and September of 2013 to maximums in October and December of 2020. Lake Erie's groundwater storage trends are considerably different from those of the other two lake basins. Maximum and minimum groundwater storage in Lake Erie occurred in November 2009 and December 2015, respectively. In addition to the groundwater storage increases in the Lake Erie basin between 2015-2020 of 0.14 m, storage increases of comparable magnitude occur between 2007-2011 and in 2013. Estimates of groundwater storage change derived from GRACE, GPS and land surface models across the Great Lakes basin between 2013 and 2019 by Argus et al. (2020) indicate approximately half the increase in groundwater storage (~0.1 m) as is simulated on average across the Michigan

Model domain between 2013 and 2020 (0.2 m). The difference in these estimates may be due to the much larger area in the Argus et al. (2020) study, their reliance on land surface model-derived estimates of subsurface hydrology, the slightly shorter period of record used during their study, and their inclusion of soil moisture in groundwater storage change.

The increases in groundwater storage lagged behind the changes in lake elevation between two and five years across the domain. This lag is most clearly observed in Lake Michigan-Huron (Figure 13B). Breakpoints identified by segmented linear regression indicate this delay is smallest in Lake Superior and largest in Lake Erie (Figure A30). Specifically, these inflection points occur for each lake and its lake basin in: October 2011 and January 2013 for Lake Superior, February 2013 and August 2016 for Lake Michigan-Huron and October 2013 and February 2017 for Lake Erie. The trends in storage closely follow those in lake level for Lakes Michigan-Huron, but are starkly different for Lake Erie.

Changes in groundwater storage between the between September of 2013 and December of 2020 as shown in Figure 13D, with a median change of 0.12 m. Groundwater storage increases over a majority of the domain, with a median increase of 0.16 m, with the largest head increases in the western Upper Peninsula to 9 m near the northern shore of Lake Superior. Increases in the Lower Peninsula are largest in the northern and western portions of the peninsula. Decreases in head (median of -0.02 m, maximum of -5.9 m) during this period are observed in part of the eastern Upper Peninsula, and across the lower two-thirds of the Lower Peninsula. While seasonal fluctuations in the surface water balance and groundwater storage are part of the normal hydrological cycle in the Great Lakes, year-over-year changes have the potential to impact aquatic systems. Changes to groundwater elevations and storage may affect streamflows, inland lake levels, evapotranspiration and wetland connectivity, especially in areas with shallow water tables (Condon and Maxwell 2019, Winter, 1999). As with seasonal groundwater cycles, the timing of minimum and maximum heads (and thus storage) have a spatially complex pattern across the model domain. The year in which minimum heads occur (Figure A31) is considerably more variable than the year in which maximum heads occur. Minimum heads occur across the entire range of the simulation period, with some regionally consistent patterns. Maximum heads generally occur latest in the far north western portions of the domain (~2023), and earliest in the far southern portions of the domain (~2009).

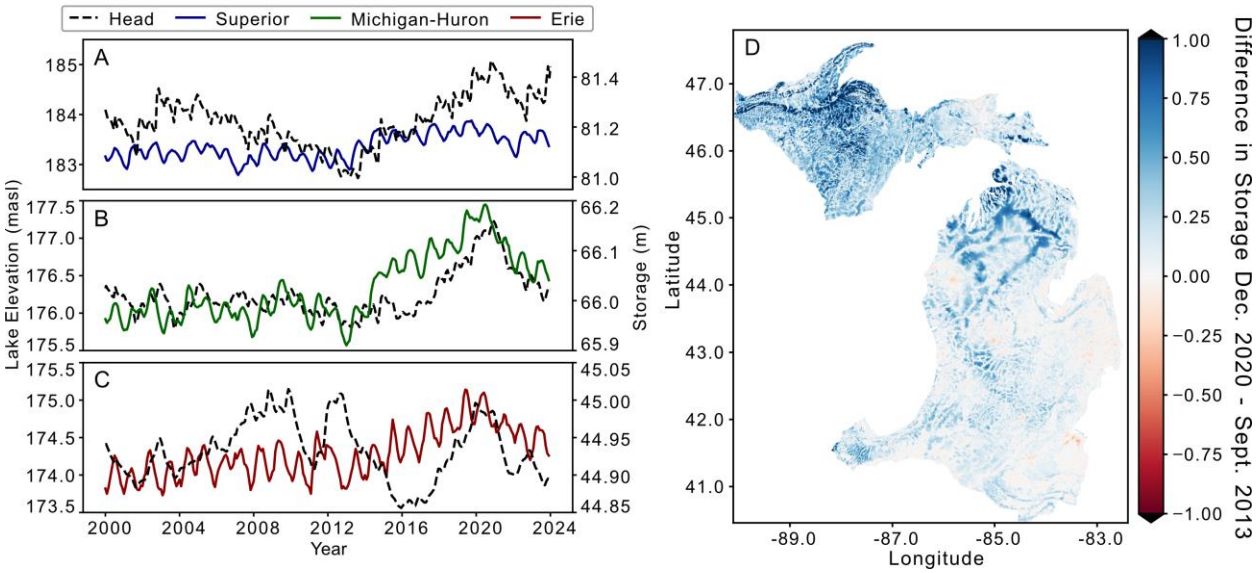

Figure 13: Changes in Lakes Levels and Groundwater Storage 2000-2023. Changes in lake elevation (solid line), and average groundwater storage (dashed line) across the lake basin for (A) Superior, (B) Michigan-Huron and (C) Erie between 2000 and 2023. Considerable increases in both lake elevations and groundwater storage occur between the early 2010's and the 2020's. Changes in groundwater storage start later (between two and four years) but peak at near the same time as those in lake levels. Changes in groundwater storage across the domain from September 2013 to December 2020 (D) show widespread increases in groundwater storage across the basin, especially in the western Upper Peninsula and northern Lower Peninsula.

3.4 Drivers of Groundwater Storage Change 2000-2023

The observed recent increases in groundwater storage are preceded by changes to the surface water balance, specifically an increase in precipitation and decrease in ET (Figure 14A and B). These changes to precipitation and ET also result in increased deep percolation and streamflow across the region (Figure 14B and C). Breakpoints analysis (Figure 14D-H) suggest that, preceding the circa 2020 peaks in groundwater elevation, a period of low groundwater storage occurs between June 2010 and December 2017. This coincides with a period of increased ET relative to the model period beginning in July 2010. Precipitation rates increase starting in July 2016 and remain elevated through 2021, while average ET rates drop in January 2018. Increases in deep percolation, groundwater storage and streamflow all occur beginning in December 2017 or January 2018, only after ET has decreased but precipitation remains elevated. Periods of increased deep percolation and streamflow both occur between January 2018 and January 2021, and coincide with peaks in groundwater storage. The fastest rate of lake level rise occurred during 2013-2014. Gronewold et al. (2016) identified the causes for this change as: 1) increased runoff and over-lake precipitation in 2013 and 2) continued elevated runoff combined with decreased over-lake

evaporation. Our results suggest the same forcings of increased precipitation and decreased ET, lagged by ~2 years from changes to the lake water balance, caused the rapid rise in groundwater storage between 2016-2020. In both the lakes and the groundwater system, a change in precipitation alone was not enough to cause the recent storage increases; both systems required a shift in precipitation and ET for this change to occur.

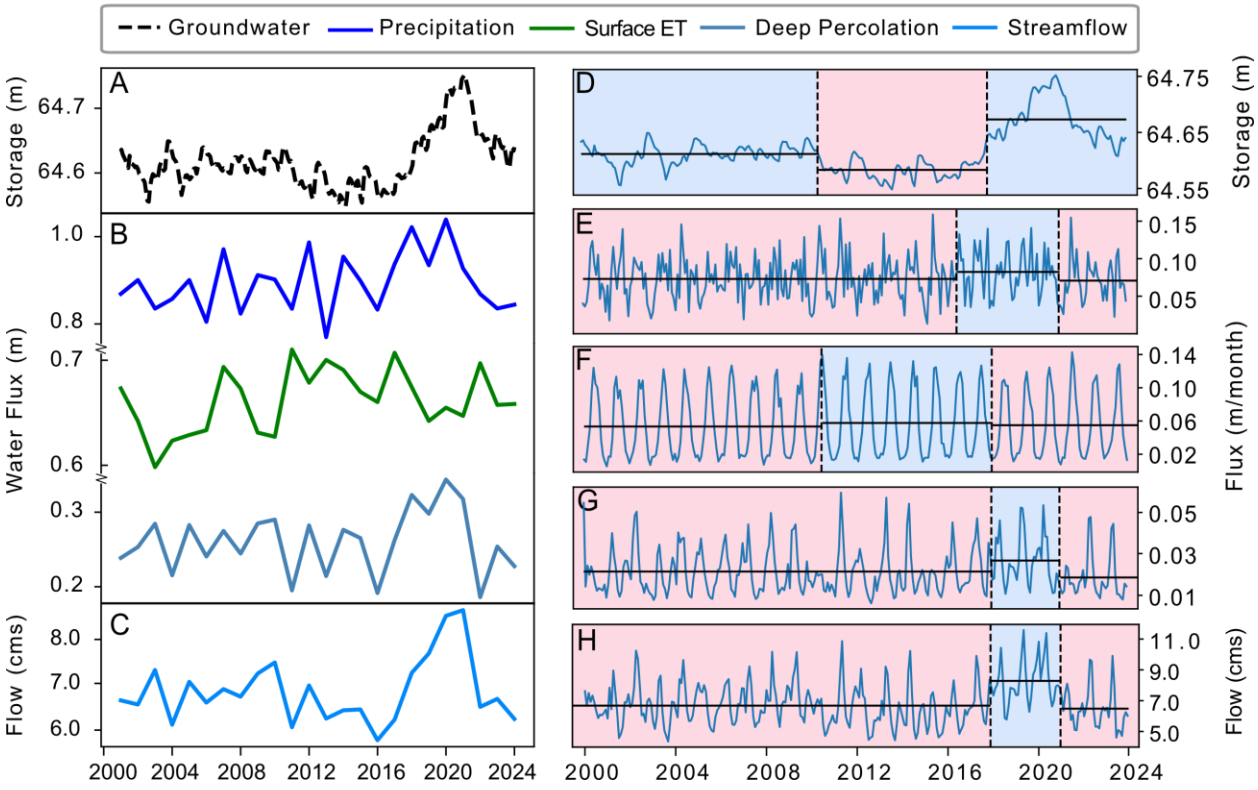

Figure 14: Changes in Surface Fluxes 2000-2023 as Drivers of Groundwater Storage Change. Changes in monthly (a) groundwater storage (product of saturated thickness and porosity) and (B) annual total precipitation (rain + snow), surface evapotranspiration, and deep percolation averaged across the model domain for the period of 2000-2023. Panels D through H show breakpoints for groundwater storage and the three surface fluxes. Breakpoints, shown by vertical dashed lines, in all four quantities occur in 2017-2018, corresponding to increased precipitation, decreased ET, increased deep percolation and increased head. Means for the three segments created by the breakpoints are shown in horizontal black lines, and shading indicates the change in mean, with red shaded regions having lower means than blue shaded regions.

Changes to the surface water balance and groundwater storage within the windows identified by the breakpoints analysis (Figure 15) were largest in the western Upper Peninsula where precipitation increased, while ET decreased and deep percolation increased. In the northern Lower Peninsula changes in both precipitation and ET were more moderate, however deep

percolation and groundwater storage both increased. This region is characterized by high permeability glacial deposits of considerable thickness. Changes in southern Lower Peninsula and the Maumee Basin are much more mixed, with both increases and decreases in storage and all three surface fluxes observed. Generally, regions with decreased precipitation saw increased ET, decreased deep percolation and decreased storage. This southern portion of the domain includes large areas of lower permeability soil, and has distinctly different weather and climate patterns to that of the northern Lower Peninsula and Upper Peninsula.

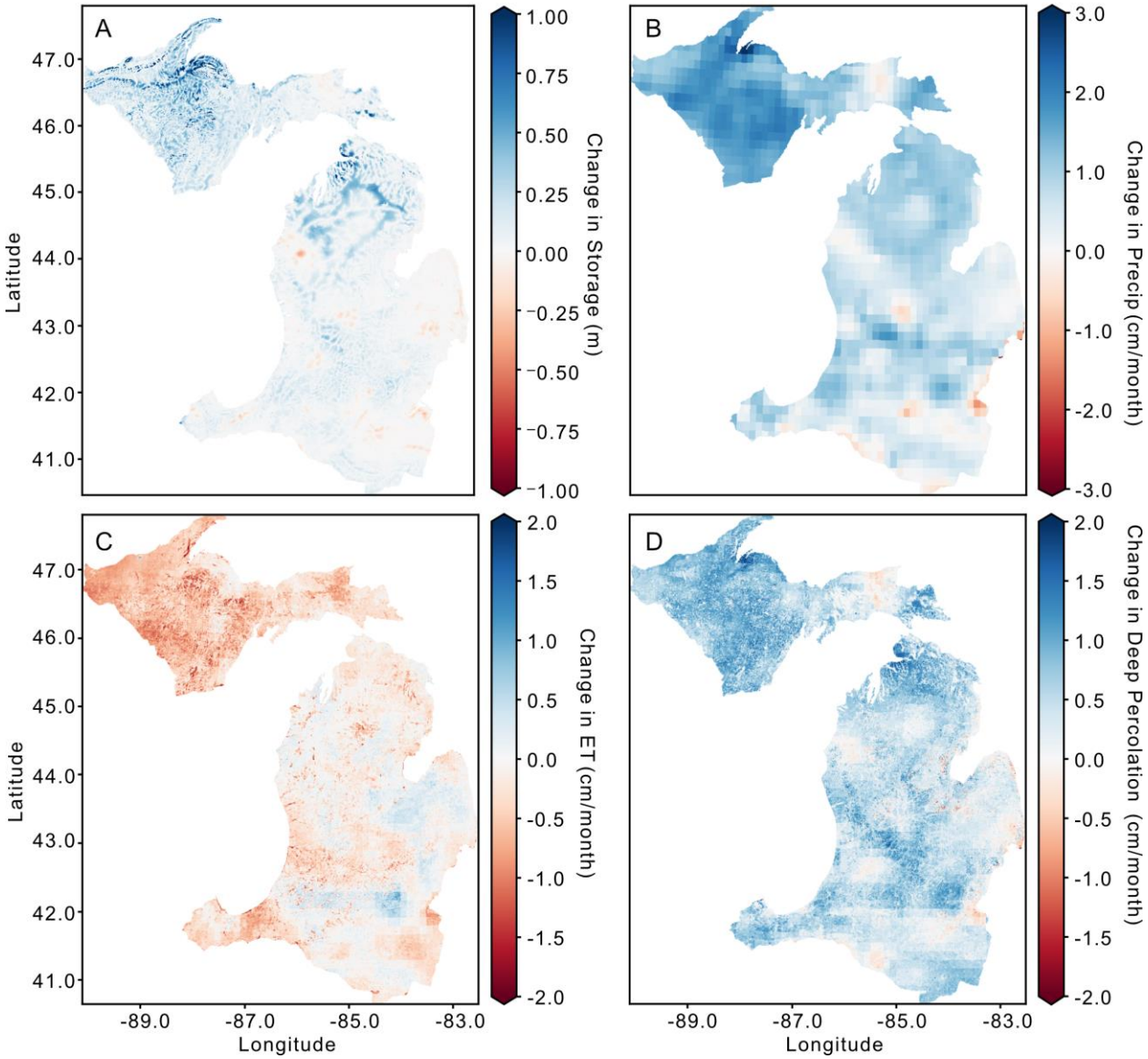

Figure 15: Maps of Average Surface Fluxes in Breakpoint Windows. Differences in mean (A) groundwater storage (B), precipitation, (C) ET and (D) deep percolation for the breakpoint window that includes the 2020 peak in groundwater elevations and the means across the previous window. Increases in precipitation and decreases in ET were strongest in the western Upper Peninsula, where groundwater storage increases were also strongest. Shifts in the surface water balance are more heterogeneous in the Lower Peninsula and Maumee River Basin (see Figure 10), with both increases (decreases) in precipitation and ET observed respectively.

3.5 Other Modeling Studies in the Region

A considerable amount of hydrologic modeling, for both research and operational purposes, has been done within the Great Lakes basin. A large portion of this work has focused on using a variety of rainfall-runoff models to simulate streamflow across the region (e.g. Fry et al., 2014, Mai et al., 2022). These streamflow estimates are used for a variety of water resource

management applications, including to supply the streamflow component of net basin supply to the lake level models used for operational forecasting of the Great Lakes (Fry et al., 2020). The Large Basin Runoff model, a lumped parameter rainfall-runoff mode, is commonly used across the Great Lakes basin to supply estimates of tributary flow to the lake models (Fry, 2014). More recent efforts have included applying the processed based Weather Research and Forecasting hydrologic model (WRF-Hydro) as an operational model for the Great Lakes Basin, as an extension of the National Water Model (Mason et al., 2019). These models are often assessed solely on their ability to reproduce streamflow, and as such have underrepresented other hydrologic processes including groundwater. Both WRF-Hydro and LBRM use simple bucket models to represent groundwater, which "fill" with excess soil water and "spill" into streams as baseflow (Gochis et al., 2020, Shin et al., 2024). As a result, these models often struggle to simulate streamflows in areas with significant groundwater contribution, such as the Great Lakes region (Mai, 2023). They are also unable to quantify changes in the broader groundwater system including those in direct groundwater contributions to the Great Lakes or those in groundwater storage (Shin et al., 2024).

While a number of site- to watershed-scale groundwater models (Costa et al., 2021, Curtis et al., 2019, Holtschlag et al., 1998, Hunt et al., 2013, Kang et al., 2021, Kendall, 2009, Luukkonen et al., 2004) have been developed for the region, only two previous works have developed regional (e.g. state or lake basin) scale hydrologic models with explicit, physically based representations of groundwater: a MODFLOW model for the Lake Michigan Basin (LMB) (Fienstein et al., 2010), and a coupled surface and groundwater model for the Great Lakes Basin in modeling program HydroGeoSphere (HGS) (Xu et al., 2021). The LMB model was developed to quantify the impacts of pumping on local and regional groundwater flow systems in the Lake Michigan Basin from the mid 1800's to 2005. This study finds limited local reductions in streamflow from the surficial aquifer, while significant groundwater flow changes have occurred in the bedrock aquifers around large urban areas including in the Chicago IL., Milwaukee WI., and Lansing MI. regions (Feinstein et al., 2010). The Great Lakes basin HGS model was developed primarily to investigate groundwater as a source and sink of water to the Great Lakes. It shows direct groundwater discharge supplies between 0.6-1.3% of total water supply for the Great Lakes, and that this contribution is greatest during the winter (Xu et al., 2021). While these models, and the aforementioned large body of rainfall-runoff/land surface modeling has provided insight into both

surface and groundwater processes within the Great Lakes Basin, the Michigan Model developed is the first coupled, process-based surface and groundwater model developed to study storage changes at the regional scale within the Great Lakes Basin.

3.6 Recent Changes and Future Projections

After reaching their peak elevations in 2012-2022, both groundwater and lake levels began to drop in 2022-2023. Since the end of the model period in December of 2023, lake elevations have continued to fall, with a lake-wide average annual elevation 0.14 m lower than in 2023. As of the most recent measurement in February of 2025 average lake elevations are lower than they have been at any time since 2013 (GLERL, 2025). A recent effort by Kayastha et al. (2022) predicted lake levels using coupled regional climate and 3D lake model to downscale CMIP5 climate projections for 2030-2049 under the RCP 8.5 scenario. This model predicts increases in annual average water levels between 0.19 m (Superior) and 0.44 m (Michigan-Huron), due to increases in both over-lake precipitation (27-66 mm/year) and stream discharge (31-80 mm/year) to the lakes which outpace increases to over-lake evaporation (8-38 mm/year).

Streamflow, over-lake precipitation, and over-lake evaporation are approximately equal components of net basin supply in the Great Lakes (Gronewold et al., 2016, Hunter et al., 2015). Given the underrepresentation of groundwater in the models used to supply runoff estimates to lake forecasting models (Mai, 2022, 2023; Shin et al., 2024), and importance of baseflow in large portions of the Great Lakes Basin (Neff et al., 2005), current projections may misrepresent the runoff component of net basin supply and therefore lake levels. To better constrain future projections of streamflow and lake elevations, and to understand the potential impacts of climate change on groundwater storage, continued development and integration of models which more explicitly represent groundwater processes is needed.

4. Conclusions

Across the state of Michigan region, groundwater storage has increased by an average of 0.2 m from minima in September 2013 to maxima in December 2020. This increase is seven times that of the seasonal fluctuation of 0.028 m in groundwater storage across the region, and about one tenth the average change in lake elevation of 1.46 m across lakes Superior, Michigan-Huron and Erie. The recent increases in groundwater storage mirror, but are delayed between 2 and 4 years behind associated increases to lake levels. These changes to groundwater storage are greatest within the Lake Superior basin and least in the Lake Erie basin. Specifically, storage changes are

greatest in areas with high precipitation and thick permeable aquifers able to accept increased recharge, such as in the Western Upper Peninsula and Northern Lower Peninsula. Changes to storage are smallest in regions with lower permeability aquifers and thin unsaturated zones, and which have experienced much more heterogeneous changes to precipitation and other components of the surface water balance, such as the Saginaw Bay and Maumee River Watersheds. Similar to the drivers for change in lake elevation identified by Gronewoeld et al. (2016) the recent changes to groundwater storage were likely driven by a combination of increased precipitation and decreased ET; change in one component of the water balance alone was not enough to cause the precipitous changes in both surface and groundwater storage across the central Great Lakes region.

While this model has provided the first regional-scale estimates of groundwater storage changes within the Great Lakes basin, three major changes are necessary to fully assess how shifting climate patterns will affect water resources within the basin. First, groundwater pumping and other water use data should be added to this model, to assess their impact on groundwater storage and discharge. While the results of the Lake Michigan Basin model did not suggest regional scale changes to the surficial aquifer due to pumping, they indicated local effects can be significant in areas of concentrated withdrawal (Feinstein et al., 2010). Second, is an effort currently underway to develop a similar model for the entire Great Lakes Basin, which will require significant effort to pull together datasets from the eight US states and two Canadian provinces within the basin. Third, more explicit representations of groundwater storage and its effects of streamflow should be incorporated into the operations models used to forecast hydrologic changes within the Great Lakes basin, including lake levels. While groundwater supplies only a small portion of the Lakes water budget directly (Xu et al., 2021) it supplies a significant amount of water though stream baseflow (Gronewold et al., 2016, Hunter et al., 2015, Neff et al., 2005). In addition, considering changes to the groundwater system itself will be critical to understand how future extremes in climate and lake levels may impact water resources, human communities and aquatic ecosystems across the world's largest system of connected freshwater lakes.

Acknowledgements

I would first like to acknowledge Anthony Kendall for his co-development of the LHM Michigan Model, and Dave Hyndman for his input doing the model development process. I would like to acknowledge Chanse Ford for his contributions to an early version of this model, and Howard Reeves for sharing his technical expertise of MODFLOW and FloPy, and his experiences in

modeling groundwater across the Great Lakes region. I would like to acknowledge the National Science Foundation (NSF) Frontier Research in Earth Science (FRES) Grant #2218028 for funding support, and the research team of this grant provided valuable feedback at various stages of this work. I would also like to acknowledge Travis Dahl for his parallel work in developing an LHM model for a subset of the state of Michigan region, as his efforts advanced this model as well. Finally I would like to acknowledge Erin Haacker and Alex Kuhl who provided feedback on an early version of this chapter.

REFERENCES

Allen, T.R., Crawford, T., Montz, B., Whitehead, J., Lovelace, S., Hanks, A.D., Christensen, A.R., Kearney, G.D., 2019. Linking Water Infrastructure, Public Health, and Sea Level Rise: Integrated Assessment of Flood Resilience in Coastal Cities. Public Work. Manag. Polic. 24, 110–139. https://doi.org/10.1177/1087724x18798380

Anderson, M. P., Woessner, W. W., & Hunt, R. J. 2015. Applied groundwater modeling: Simulation of flow and advective transport (3rd ed.). Academic Press.

Argus, D.F., Ratliff, B., DeMets, C., Borsa, A.A., Wiese, D.N., Blewitt, G., Crowley, J.W., Martens, H.R., Kreemer, C., Landerer, F.W., 2020. Rise of Great Lakes Surface Water, Sinking of the Upper Midwest of the United States, and Viscous Collapse of the Forebulge of the Former Laurentide Ice Sheet. J. Geophys. Res. Solid Earth 125. https://doi.org/10.1029/2020jb019739

Assel, R.A., Quinn, F.H., Sellinger, C.E., 2004. Hydroclimatic Factors of the Recent Record Drop in Laurentian Great Lakes Water Levels. Bull. Am. Meteorol. Soc. 85, 1143–1151. https://doi.org/10.1175/bams-85-8-1143

Befus, K.M., Barnard, P.L., Hoover, D.J., Hart, J.A.F., Voss, C.I., 2020. Increasing threat of coastal groundwater hazards from sea-level rise in California. Nat. Clim. Chang. 10, 946–952. https://doi.org/10.1038/s41558-020-0874-1

Bjerklie, D.M., Mullaney, J.R., Stone, J.R., Skinner, B.J., Ramlow, M.A., 2012. Preliminary investigation of the effects of sea-level rise on groundwater levels in New Haven, Connecticut, Open-File Report 2012–1025.

Condon, L.E., Maxwell, R.M., 2019. Simulating the sensitivity of evapotranspiration and streamflow to large-scale groundwater depletion. Sci. Adv. 5, eaav4574. https://doi.org/10.1126/sciadv.aav4574

Costa, D., Zhang, H., Levison, J., 2021. Impacts of climate change on groundwater in the Great Lakes Basin: A review. J. Gt. Lakes Res. 47, 1613–1625. https://doi.org/10.1016/j.jglr.2021.10.011

Curtis, Z.K., Liao, H., Li, S., Sampath, P.V., Lusch, D.P., 2019. A Multiscale Assessment of Shallow Groundwater Salinization in Michigan. Groundwater 57, 784–806. https://doi.org/10.1111/gwat.12873

Dewitz, J., 2023, National Land Cover Database (NLCD) 2021 Products: U.S. Geological Survey data release, https://doi.org/10.5066/P9JZ7AO3

Dietrich, R.V., 1983. The Geology of Michigan. Rocks Miner. 58, 99–106. https://doi.org/10.1080/00357529.1983.11767127

Egan, D., 2021. A battle between a great city and a great lake. *New York Times*. https://www.nytimes.com/interactive/2021/07/07/climate/chicago-river-lake-michigan.html

EGLE. 2020. Michigan Environment, Great Lakes and Energy. Wellogic System. Accessed 2020-03-05. https://www.egle.state.mi.us/wellogic

ESRI. 2023. ArcGIS Pro (3.1.4). Environmental Systems Research Institute. https://www.esri.com/en-us/arcgis/products/arcgis-pro

Farrand, W.R., Mickelson, D.M., Cowan, W.R., Goebel, J.E., Richmond, G.M., and Fullerton, D.S., 1984. Quaternary geologic map of the Lake Superior 4 degrees x 6 degrees quadrangle, United States and Canada. U.S. Geological Survey Miscellaneous Investigations Series Map I-1420(NL-16). https://doi.org/10.3133/i1420(NL16)

Feinstein, D.T., Hunt, R.J., and Reeves, H.W., 2010, Regional groundwater-flow model of the Lake Michigan Basin in support of Great Lakes Basin water availability and use studies. U.S. Geological Survey Scientific Investigations Report 2010–5109. https://doi.org/10.3133/sir20105109

Fry, L.M., Apps, D., Gronewold, A.D., 2020. Operational Seasonal Water Supply and Water Level Forecasting for the Laurentian Great Lakes. J. Water Resour. Plan. Manag. 146. https://doi.org/10.1061/(asce)wr.1943-5452.0001214

Fry, L.M., Gronewold, A.D., Fortin, V., Buan, S., Clites, A.H., Luukkonen, C., Holtschlag, D., Diamond, L., Hunter, T., Seglenieks, F., Durnford, D., Dimitrijevic, M., Subich, C., Klyszejko, E., Kea, K., Restrepo, P., 2014. The Great Lakes Runoff Intercomparison Project Phase 1: Lake Michigan (GRIP-M). J. Hydrol. 519, 3448–3465. https://doi.org/10.1016/j.jhydrol.2014.07.021

Fullerton, D.S., Cowan, W.R., Savon, W.D., Goldthwait, R.P., Ferrand, W.R., Muller, E.H., Bahling, R.E., Stravers, J.A., and Richmond, G.M., 1991. Quaternary geologic map of the Lake Erie 4 degrees x 6 degrees quadrangle, United States and Canada. u.S. Geological Survey Miscellaneous Investigations Series Map I-1420(NK-17). https://doi.org/10.3133/i1420(NK17)

Ford, C.M. 2022. Hydrologic Variations Owing to Snowmelt Changes in the Mid Latitudes, Michigan State University.

Garrity, C.P., and D.R. Soller. 2009. Database of the GeologicMap of North America; Adapted from the Map by J.C. Reed, Jr. et al. (2005): U.S. Geological Survey Data Series 424. Reston, Virginia: USGS. https://doi.org/10.3133/ds424

Gleason, C.J., Wang, J., 2015. Theoretical basis for at-many-stations hydraulic geometry. Geophys. Res. Lett. 42, 7107–7114. https://doi.org/10.1002/2015gl064935

Green, W.H., Ampt, G.A., 1911. Studies on Soil Physics. J. Agric. Sci. 4, 1–24. https://doi.org/10.1017/s0021859600001441

Great Lakes Environmental Research Laboratory, 2025. The Great Lakes Water Level Dashboard. NOAA. https://www.glerl.noaa.gov/data/wlevels/dashboard/

Goebel, J.E., Mickelson, D.M., Ferrand, W.R., Clayton, Lee, Knox, J.C., Cahow, Adam, Hobbs, H.C., Walton, M.S., Richmond, G.M., and Fullerton, D.S., 1983. Quaternary geologic map of the Minneapolis 4 degrees x 6 degrees quadrangle, United States. U.S. Geological Survey Miscellaneous Investigations Series Map I-1420(NL-15). https://doi.org/10.3133/i1420(NL15)

Grannemann, N.G., Hunt, R.J., Nicholas, J.R., Reilly, T.E., Winter, T.C., 2000. The Importance of Ground Water in the Great Lakes Region, Water-Resources Investigations Report 2000-4008. U.S. Geological Survey. https://doi.org/10.3133/wri004008

Gronewold, A.D., Bruxer, J., Durnford, D., Smith, J.P., Clites, A.H., Seglenieks, F., Qian, S.S., Hunter, T.S., Fortin, V., 2016. Hydrological drivers of record-setting water level rise on Earth's largest lake system. Water Resour Res 52, 4026–4042. https://doi.org/10.1002/2015wr018209

Gronewold, A.D., Do, H.X., Mei, Y., Stow, C.A., 2021. A Tug-of-War Within the Hydrologic Cycle of a Continental Freshwater Basin. Geophys Res Lett 48. https://doi.org/10.1029/2020gl090374

Gochis, D.J., M. Barlage, R. Cabell, M. Casali, A. Dugger, K. FitzGerald, M. McAllister, J. McCreight, A. RafieeiNasab, L. Read, K. Sampson, D. Yates, Y. Zhang (2020). The WRF-Hydro® modeling system technical description, (Version 5.1.1). NCAR Technical Note. 108 pages. Available online at: https://ral.ucar.edu/sites/default/files/public/WRFHydroV511TechnicalDescription.pdf

Harbaugh, A.W., 2005. MODFLOW-2005: the U.S. Geological Survey modular ground-water model--the ground-water flow process, Techniques and Methods 6-A16. U.S. Geological Survey, Reston, Va. https://doi.org/10.3133/tm6A16

Harris, C.R., Millman, K.J., Walt, S.J. van der, Gommers, R., Virtanen, P., Cournapeau, D., Wieser, E., Taylor, J., Berg, S., Smith, N.J., Kern, R., Picus, M., Hoyer, S., Kerkwijk, M.H. van, Brett, M., Haldane, A., Río, J.F. del, Wiebe, M., Peterson, P., Gérard-Marchant, P., Sheppard, K., Reddy, T., Weckesser, W., Abbasi, H., Gohlke, C., Oliphant, T.E., 2020. Array programming with NumPy. Nature 585, 357–362. https://doi.org/10.1038/s41586-020-2649-2

Holtschlag, D.J., Luukkonen, C.L., Nicholas, J.R., 1996. Simulation of ground-water flow in the Saginaw Aquifer, Clinton, Eaton, and Ingham counties, Michigan, Water Supply Paper 2480. U.S. Geological Survey, Washington, D.C.

Hunt, R.J., Walker, J.F., Selbig, W.R., Westenbroek, S.M., Regan, R.S., 2013. Simulation of Climate-Change Effects on Streamflow, Lake Water Budgets, and Stream Temperature Using GSFLOW and SNTEMP, Trout Lake Watershed, Wisconsin, U.S. Geological Survey Scientific Investigations Report 2013–5159. U.S. Geological Survey, Reston, Virginia.

Hunter, T.S., Clites, A.H., Campbell, K.B., Gronewold, A.D., 2015. Development and application of a North American Great Lakes hydrometeorological database — Part I: Precipitation, evaporation, runoff, and air temperature. J Great Lakes Res 41, 65–77. https://doi.org/10.1016/j.jglr.2014.12.006

Hyndman, D.W., Kendall, A.D., Welty, N.R.H., 2007. Evaluating Temporal and Spatial Variations in Recharge and Streamflow Using the Integrated Landscape Hydrology Model (ILHM). GEOPHYSICAL MONOGRAPH-AMERICAN GEOPHYSICAL UNION. https://doi.org/10.1029/171gm11

llinois State Water Survey (ISWS). (2015). Groundwater Data [Dataset]. Retrieved May, 2015, from https://www.isws.illinois.edu/data/gwdb/

Indiana Department of Natural Resources (IDNR), Division of Water. (2015). Water Well Record Database [Dataset]. May, 2015 from https://www.in.gov/dnr/water/ground-water-wells/water-well-record-database/

Jordahl, K., den Bossche, J. V, .Fleischmann, M., McBride, J., Wasserman, J., Badaracco, A.G., Gerard, J., Snow, A.D., Tratner, J., Perry, M., Farmer, C., Hjelle, G. A., Cochran, M., Gillies, S., Culbertson, L., Bartos, Ward, B., Caria, G., Taves, M., Eubank, N., Flavin, J., Richards, M., Rey, S., Albert, M., Bilogur, A., Ren, C., Arribas-Bel, D., Meseho-Leon, D., Wasser, L. 2021. geopandas/geopandas: v0.10.1, Zenodo https://doi.org/10.5281/zenodo.5573592

Kang, G., Luo, L., Pokhrel, Y., Lusch, D., Phanikumar, M.S., 2021. Quantifying the spatiotemporal dynamics of recharge in a composite Great Lakes watershed using a high-resolution hydrology model and multi-source data. J. Hydrol. 601, 126594. https://doi.org/10.1016/j.jhydrol.2021.126594

Kayastha, M.B., Ye, X., Huang, C., Xue, P., 2022. Future rise of the Great Lakes water levels under climate change. J Hydrol 612, 128205. https://doi.org/10.1016/j.jhydrol.2022.128205

Kendall, Anthony D. 2009. Predicting the Impacts of Land use and Climate on Regional-Scale Hydrologic Fluxes, Michigan State University

Lin, C.-Y., Miller, A., Waqar, M., Marston, L.T., 2024. A database of groundwater wells in the United States. Sci. Data 11, 335. https://doi.org/10.1038/s41597-024-03186-3

Lineback, J.A., Bleuer, N.K., Mickelson, D.M., Ferrand, W.R., Goldthwait, R.P., Richmond, G.M., and Fullerton, D.S, 1983. Quaternary geologic map of the Chicago 4 degrees x 6 degrees quadrangle, United States. U.S. Geological Survey Miscellaneous Investigations Series Map I-1420(NK-16). https://doi.org/10.3133/i1420(NK16)

Lofgren, B.M., Quinn, F.H., Clites, A.H., Assel, R.A., Eberhardt, A.J., Luukkonen, C.L., 2002. Evaluation of Potential Impacts on Great Lakes Water Resources Based on Climate Scenarios of Two GCMs. J Great Lakes Res 28, 537–554. https://doi.org/10.1016/s0380-1330(02)70604-7

Lowry, C.S., Loheide, S.P., 2010. Groundwater-dependent vegetation: Quantifying the groundwater subsidy. Water Resour. Res. 46. https://doi.org/10.1029/2009wr008874

Luukkonen, C.L., Blumer, S.P., Weaver, T.L., Jean, J., 2004. Simulation of the ground-water-flow system in the Kalamazoo County area, Michigan, U.S. Geological Survey Scientific Investigations Report 2004-5054. U.S. Geological Survey, Reston, VA.

Mai, J., 2023. Ten strategies towards successful calibration of environmental models. J. Hydrol. 620, 129414. https://doi.org/10.1016/j.jhydrol.2023.129414

Mai, J., Shen, H., Tolson, B.A., Gaborit, É., Arsenault, R., Craig, J.R., Fortin, V., Fry, L.M., Gauch, M., Klotz, D., Kratzert, F., O'Brien, N., Princz, D.G., Koya, S.R., Roy, T., Seglenieks, F., Shrestha, N.K., Temgoua, A.G.T., Vionnet, V., Waddell, J.W., 2022. The Great Lakes Runoff Intercomparison Project Phase 4: the Great Lakes (GRIP-GL). Hydrol. Earth Syst. Sci. 26, 3537–3572. https://doi.org/10.5194/hess-26-3537-2022

Mason, L.A., Gronewold, A.D., Laitta, M., Gochis, D., Sampson, K., Read, L., Klyszejko, E., Kwan, J., Fry, L., Jones, K., Steeves, P., Pietroniro, A., Major, M., 2019. New Transboundary Hydrographic Data Set for Advancing Regional Hydrological Modeling and Water Resources Management. J. Water Resour. Plan. Manag. 145, 06019004. https://doi.org/10.1061/(asce)wr.1943-5452.0001073

Mathney, K. 2020. Record-high Michigan water levels are a nightmare for homeowners, state. Detroit Free Press. https://www.freep.com/story/news/local/michigan/2020/07/17/great-lakes-water-levels-records-erosion-damage/5450910002/

Meredith, D.D., 1975. Temperature Effects On Great Lakes Water Balance Studies. JAWRA J. Am. Water Resour. Assoc. 11, 60–68. https://doi.org/10.1111/j.1752-1688.1975.tb00660.x

McKinney, W. Data structures for statistical computing in Python. In Proc. 9th Python in Science Conf. (eds van der Walt, S. & Millman, K. J.) 56–61 (2010).

Milstein, R.L., 1987, Bedrock geology of southern Michigan: Michigan Department of Natural Resources, Geological Survey Division, Geological Publication BG-01. https://ngmdb.usgs.gov/Prodesc/proddesc_71887.htm

Mitchell, K.E., Lohmann, D., Houser, P.R., Wood, E.F., Schaake, J.C., Robock, A., Cosgrove, B.A., Sheffield, J., Duan, Q., Luo, L., Higgins, R.W., Pinker, R.T., Tarpley, J.D., Lettenmaier, D.P., Marshall, C.H., Entin, J.K., Pan, M., Shi, W., Koren, V., Meng, J., Ramsay, B.H., Bailey, A.A., 2004. The multi-institution North American Land Data Assimilation System (NLDAS): Utilizing multiple GCIP products and partners in a continental distributed hydrological modeling system. J. Geophys. Res.: Atmos. 109. https://doi.org/10.1029/2003jd003823

Muggeo, V.M.R., 2003. Estimating regression models with unknown break-points. Stat. Med. 22, 3055–3071. https://doi.org/10.1002/sim.1545

Myneni, R., Knyazikhin, Y., Park, T. (2015). MCD15A2H MODIS/Terra+Aqua Leaf Area Index/FPAR 8-day L4 Global 500m SIN Grid V006. NASA EOSDIS Land Processes DAAC.http://doi.org/10.5067/MODIS/MCD15A2H.006

National Geophysical Data Center, 1999a. Bathymetry of Lake Huron. National Geophysical Data Center, NOAA. doi:10.7289/V5G15XS5. Accessed 2023-08-23

National Geophysical Data Center, 1999b. Bathymetry of Lake Erie and Lake St. Clair. National Geophysical Data Center, NOAA. doi:10.7289/V5KS6PHK Accessed 2023-08-23

National Geophysical Data Center, 1996c. Bathymetry of Lake Michigan. National Geophysical Data Center, NOAA. doi:10.7289/V5B85627 Accessed 2023-08-23

National Geophysical Data Center, 1999d. Bathymetry of Lake Ontario. National Geophysical Data Center, NOAA. doi:10.7289/V56H4FBH Accessed 2023-08-23

National Geophysical Data Center, 1999e. Bathymetry of Lake Superior. National Geophysical Data Center, NOAA. Accessed from https://www.ncei.noaa.gov/products/great-lakes-bathymetry Accessed 2023-08-23

Neff, B.P., Nicholas, J.R., 2005. Uncertainty in the Great Lakes Water Balance, Scientific Investigations Report 2004-5100. U.S. Geological Survey, Reston, Virginia.https://doi.org/10.3133/sir20045100

Nicholls, R.J., Cazenave, A., 2010. Sea-Level Rise and Its Impact on Coastal Zones. Science 328, 1517–1520. https://doi.org/10.1126/science.1185782

Niswonger, R.G., Panday, S., Ibaraki, M., 2011. MODFLOW-NWT, a Newton formulation for MODFLOW-2005, Techniques and Methods 6-A37. https://doi.org/10.3133/tm6A37

Notaro, M., Holman, K., Zarrin, A., Fluck, E., Vavrus, S., Bennington, V., 2013. Influence of the Laurentian Great Lakes on Regional Climate*. J. Clim. 26, 789–804. https://doi.org/10.1175/jcli-d-12-00140.1

Neumann, B., Vafeidis, A.T., Zimmermann, J., Nicholls, R.J., 2015. Future Coastal Population Growth and Exposure to Sea-Level Rise and Coastal Flooding - A Global Assessment. PLoS ONE 10, e0118571. https://doi.org/10.1371/journal.pone.0118571

Ohio Department of Natural Resources, Division of Water Resources. (2016). Water Wells of Ohio. [Dataset] Retrieved May, 2015, from https://waterwells.ohiodnr.gov/search

Oppenheimer, M., B.C. Glavovic , J. Hinkel, R. van de Wal, A.K. Magnan, A. Abd-Elgawad, R. Cai, M. Cifuentes-Jara, R.M.DeConto, T. Ghosh, J. Hay, F. Isla, B. Marzeion, B. Meyssignac, and Z. Sebesvari, 2019: Sea Level Rise and Implications for Low-Lying Islands, Coasts and Communities. In: IPCC Special Report on the Ocean and Cryosphere in a Changing Climate [H.-O. Pörtner, D.C. Roberts, V. Masson-Delmotte, P. Zhai, M. Tignor, E. Poloczanska, K. Mintenbeck, A. Alegría, M. Nicolai, A. Okem, J. Petzold, B.

Rama, N.M. Weyer (eds.)]. Cambridge University Press, Cambridge, UK and New York, NY, USA, pp. 321–445. https://doi.org/10.1017/9781009157964.006

Pilgrim, C., 2021. piecewise-regression (aka segmented regression) in Python. J. Open Source Softw. 6, 3859. https://doi.org/10.21105/joss.03859

Pilgrim, C.. 2023. Piecewise-regression. Version 1.5.0 https://github.com/chasmani/piecewise-regression

Python Software Foundation. 2023. Python (version 3.9.18) Python Software Foundation. https://www.python.org/downloads/release/python-3918/

Ranga Myneni, Knyazikhin, Yuri, Taejin Park - Boston University and MODAPS SIPS - NASA. (2015). MOD15A2H MODIS/Combined Terra+Aqua Leaf Area Index/FPAR Daily L4 Global 500m SIN Grid. NASA LP DAAC. http://doi.org/10.5067/MODIS/MOD15A2H.006

Reed, R.C., and Daniels, Jennifer, 1987, Bedrock geology of northern Michigan: Michigan Department of Natural Resources, Geological Survey Division, Geological Publication BG-01. https://ngmdb.usgs.gov/Prodesc/proddesc_71888.htm

Reynolds, Dean (2020) Great Lakes Erosion Destroying Beachfront Homes, CBS News, https://www.cbsnews.com/news/rising-great-lakes-water-levels-threatening-homes-2020-02-06/

Richards, L.A., 1931. Capillary Conduction Of Liquids Through Porous Mediums. Physics 1, 318–333. https://doi.org/10.1063/1.1745010

Rotzoll, K., Fletcher, C.H., 2013. Assessment of groundwater inundation as a consequence of sea-level rise. Nat. Clim. Chang. 3, 477–481. https://doi.org/10.1038/nclimate1725

Sado, E.V., Fullerton, D.S., Baker, C.L., and Farrand, W.R., 1993. Quaternary geologic map of the Sudbury 4 degrees x 6 degrees quadrangle, United States and Canada (revised, 2002). U.S. Geological Survey Miscellaneous Investigations Series Map I-1420(NL-17). https://doi.org/10.3133/i1420(NL17)

Schuerch, M., Spencer, T., Temmerman, S., Kirwan, M.L., Wolff, C., Lincke, D., McOwen, C.J., Pickering, M.D., Reef, R., Vafeidis, A.T., Hinkel, J., Nicholls, R.J., Brown, S., 2018. Future response of global coastal wetlands to sea-level rise. Nature 561, 231–234. https://doi.org/10.1038/s41586-018-0476-5

Sharma, A., Hamlet, A.F., Fernando, H.J.S., Catlett, C.E., Horton, D.E., Kotamarthi, V.R., Kristovich, D.A.R., Packman, A.I., Tank, J.L., Wuebbles, D.J., 2018. The Need for an Integrated Land-Lake-Atmosphere Modeling System, Exemplified by North America's Great Lakes Region. Earth's Futur 6, 1366–1379. https://doi.org/10.1029/2018ef000870

Shi, Q., Xue, P., 2019. Impact of Lake Surface Temperature Variations on Lake Effect Snow Over the Great Lakes Region. J. Geophys. Res.: Atmos. 124, 12553–12567. https://doi.org/10.1029/2019jd031261

Shin, S., Gronewold, A.D., Fry, L.M., Dugger, A., Kessler, J., 2024. Evaluating surface and subsurface fluxes in hydrological models to advance basin-scale operational water supply forecasting. Hydrol. Sci. J. 69, 1539–1556. https://doi.org/10.1080/02626667.2024.2378100

Soller, D.R, and Garrity, C.P., 2018. Quaternary sediment thickness and bedrock topography of the glaciated United States east of the Rocky Mountains. U.S. Geological Survey Scientific Investigations Map 3392. Reston, Verginia. https://doi.org/10.3133/sim3392

Theuerkauf, E.J., Braun, K.N., 2021. Rapid water level rise drives unprecedented coastal habitat loss along the Great Lakes of North America. J Great Lakes Res 47, 945–954. https://doi.org/10.1016/j.jglr.2021.05.004

Truong, C., Oudre, L., & Vayatis, N. (2018). ruptures: change point detection in Python. ArXiv https://doi.org/10.48550/arXiv.1801.00826

United States Census Bureau. 2012. Topologically Integrated Geographic Encoding and Referencing TIGER/Line Shapefiles: 2012. https://www.census.gov/geographies/mapping-files/time-series/geo/tiger-line-file.html Accessed 2016-10-16

United States Geological Survey (USGS). 2020. National Hydrography Dataset (ver. USGS National Hydrography in FileGDB 10.1 format (published 20201127)) Accessed 2020-12-19

United States Geological Survey (USGS). 2023. 1/3rd arc-second Digital Elevation Models (DEMs) - USGS National Map 3DEP Downloadable Data Collection. U.S. Geological Survey. https://apps.nationalmap.gov/downloader/ Accessed 2023-04-19

United States Geological Survey (USGS). 2019. National Water Information System (NWIS): Site visit data, including stream width measurements. November 24, 2019, from https://waterdata.usgs.gov/nwis/

United States Fish & Wildlife Service (USFWS) (2018). National Wetlands Inventory. U.S. Fish & Wildlife Service. https://data.nal.usda.gov/dataset/national-wetlands-inventory. Accessed 2023-10-4.

United States Department of Agriculture (USDA) Soil Survey Staff, 2016. Gridded Soil Survey Geographic (gSSURGO) Database for the Conterminous United States. United States Department of Agriculture, Natural Resources Conservation Service. Available online at https://gdg.sc.egov.usda.gov/. Accessed 2023-10-8

van Genuchten, M.Th., 1980. A Closed-form Equation for Predicting the Hydraulic Conductivity of Unsaturated Soils. Soil Sci. Soc. Am. J. 44, 892–898. https://doi.org/10.2136/sssaj1980.03615995004400050002x

Wang, L., Riseng, C.M., Mason, L.A., Wehrly, K.E., Rutherford, E.S., McKenna, J.E., Castiglione, C., Johnson, L.B., Infante, D.M., Sowa, S., Robertson, M., Schaeffer, J., Khoury, M., Gaiot, J., Hollenhorst, T., Brooks, C., Coscarelli, M., 2015. A spatial classification and database for management, research, and policy making: The Great Lakes aquatic habitat framework. J. Gt. Lakes Res. 41, 584–596. https://doi.org/10.1016/j.jglr.2015.03.017

Westjohn, D.B., Weaver, T.L., 1998. Hydrogeologic framework of the Michigan Basin regional aquifer system (USGS Numbered Series), Professional Paper 1418. U.S. Geological Survey, Denver, CO. https://doi.org/10.3133/pp1418

Winter, T.C., 1999. Relation of streams, lakes, and wetlands to groundwater flow systems. Hydrogeol. J. 7, 28–45. https://doi.org/10.1007/s10040005017

Wisconsin Department of Natural Resources. Well Construction Information System. Accessed May, 2015 from https://apps.dnr.wi.gov/wellconstructionpub/#!/PublicSearch/Index

Woessner, W.W. and Poeter, E.P. 2020. Hydrogeologic Properties of Earth Materials and Principles of Groundwater Flow. The Groundwater Project. https://gw-project.org/

Xia, Y., Mitchell, K., Ek, M., Cosgrove, B., Sheffield, J., Luo, L., Alonge, C., Wei, H., Meng, J., Livneh, B., Duan, Q., Lohmann, D., 2012a. Continental-scale water and energy flux analysis and validation for North American Land Data Assimilation System project phase 2 (NLDAS-2): 2. Validation of model-simulated streamflow. J. Geophys. Res.: Atmos. 117, n/a-n/a. https://doi.org/10.1029/2011jd016051

Xia, Y., Mitchell, K., Ek, M., Sheffield, J., Cosgrove, B., Wood, E., Luo, L., Alonge, C., Wei, H., Meng, J., Livneh, B., Lettenmaier, D., Koren, V., Duan, Q., Mo, K., Fan, Y., Mocko, D., 2012b. Continental-scale water and energy flux analysis and validation for the North American Land Data Assimilation System project phase 2 (NLDAS-2): 1. Intercomparison and application of model products. J. Geophys. Res.: Atmos. 117, n/a-n/a. https://doi.org/10.1029/2011jd016048

Xu, S., Frey, S.K., Erler, A.R., Khader, O., Berg, S.J., Hwang, H.T., Callaghan, M.V., Davison, J.H., Sudicky, E.A., 2021. Investigating groundwater-lake interactions in the Laurentian Great Lakes with a fully-integrated surface water-groundwater model. J Hydrol 594, 125911. https://doi.org/10.1016/j.jhydrol.2020.125911

Zipper, S.C., Soylu, M.E., Booth, E.G., Loheide, S.P., 2015. Untangling the effects of shallow groundwater and soil texture as drivers of subfield-scale yield variability. Water Resour. Res. 51, 6338–6358. https://doi.org/10.1002/2015wr017522

CHAPTER 4: IMPACTS OF EXTREME LAKE LEVEL CHANGES ON GROUND AND SURFACE WATER CONNECTIVITY TO GREAT LAKES COASTAL WETLANDS

Abstract

The Laurentian Great Lakes contain ~21% of the worlds available freshwater and have the most coastline of any region in the contiguous United States. Between the early 2000's and 2020, water levels in the Great Lakes rose from historic lows to historic highs, driven by shifts in regional climate patterns. Coastal wetlands are widely distributed along the Great Lakes coastline and have a direct hydraulic connection to the lakes. They are an important component of the Great Lakes ecosystem, providing habitat for a range of species and serving as hotspots of nutrient cycling. While changing lake elevations have direct, observable impacts on coastal wetlands, they may also be affected by associated changes in groundwater elevations. While previous modeling efforts have simulated groundwater discharge to, and recharge from, the lakes, little is known about how changes to lake elevations may affect groundwater elevations. An existing surface and groundwater model developed for the state of Michigan region using the Landscape Hydrology Model (LHM) is applied to investigate the relationships between lake levels, groundwater and coastal wetlands within the Great Lakes Region. Four groundwater model scenarios with different lake level boundary conditions are used to first simulate the direct effects of changing lake levels on coastal groundwater elevations, and second to assess changes in groundwater connectivity to coastal wetlands. Model derived estimates of groundwater connectivity are then compared to estimates of surface water inundation to compute total changes in wetland connectivity as the lakes and groundwater elevations rise from their lowest to highest conditions. Model results suggest groundwater is discharged to the Great Lakes during the entire simulation period, and that lake levels have the potential to alter coastal groundwater elevations up to 1.9 m. They reveal however, that climate variability between 2000 and 2023 caused groundwater elevation changes which nearly matched the potential impact of direct feedbacks from the lakes. When lake levels and groundwater elevations rise from their lowest to highest conditions, total wetland connectivity increases by ~2,323 km^2. Surface water inundation is responsible for ~77.4% of this change, while rising groundwater elevations account for 18.3% of the increase in connected area. These changes to coastal wetland connectivity are concentrated along the Lake Michigan and Huron shoreline in Michigan's Upper Peninsula, and along the Lake Huron Shoreline in the Lower Peninsula.

1. Introduction

The Laurentian Great Lakes, the world's largest system of interconnected freshwater lakes, have experienced record variability in lake levels over the last 20 years. Between 2007 and 2020 all five lakes approached or exceeded the minimum and maximum elevation recorded by the National Oceanic and Atmospheric Administration (NOAA) since 1918 (Figure 16A). These extreme swings in lake surface elevation have had significant and highly visible effects on the coastline of the Great Lakes (Figure 16B-F). Extreme low water levels between 2003-2013 impeded navigation, affecting the region's recreational and industrial economies (Gronewold and Stow, 2014). The high water levels between 2019 and 2022 eroded habitat (Theuerkauf and Braun, 2021), damaged infrastructure (Matheny, 2020), and caused flooding in urban areas (Egan, 2021) along the Great Lakes coastline. As Lake Michigan reached its near maximum elevation in 2020, it rose above the flood stage of the Chicago River, rendering a primary water management tool for the city useless. The combination of extreme lake levels and heavy rain in May of 2020 lead to historic flooding around the city of Chicago (Egan, 2021). Along less developed parts of the coastline, what had been coastal wetland or upland habitat in the mid 2000's to early 2010's became inundated wetlands and open water by 2020 (Figure 16B-F). This historic swing between near minimum and maximum lake levels was driven by shifts in regional climate, which affected both the lake water balance and terrestrial water balance over the lakes drainage basin (Gronewold et al., 2016, Gronewold et al., 2019). While the effects of changing surface water levels on the coastal region are highly visible, associated changes in the adjacent groundwater system during this period of lake level extremes are largely unknown.

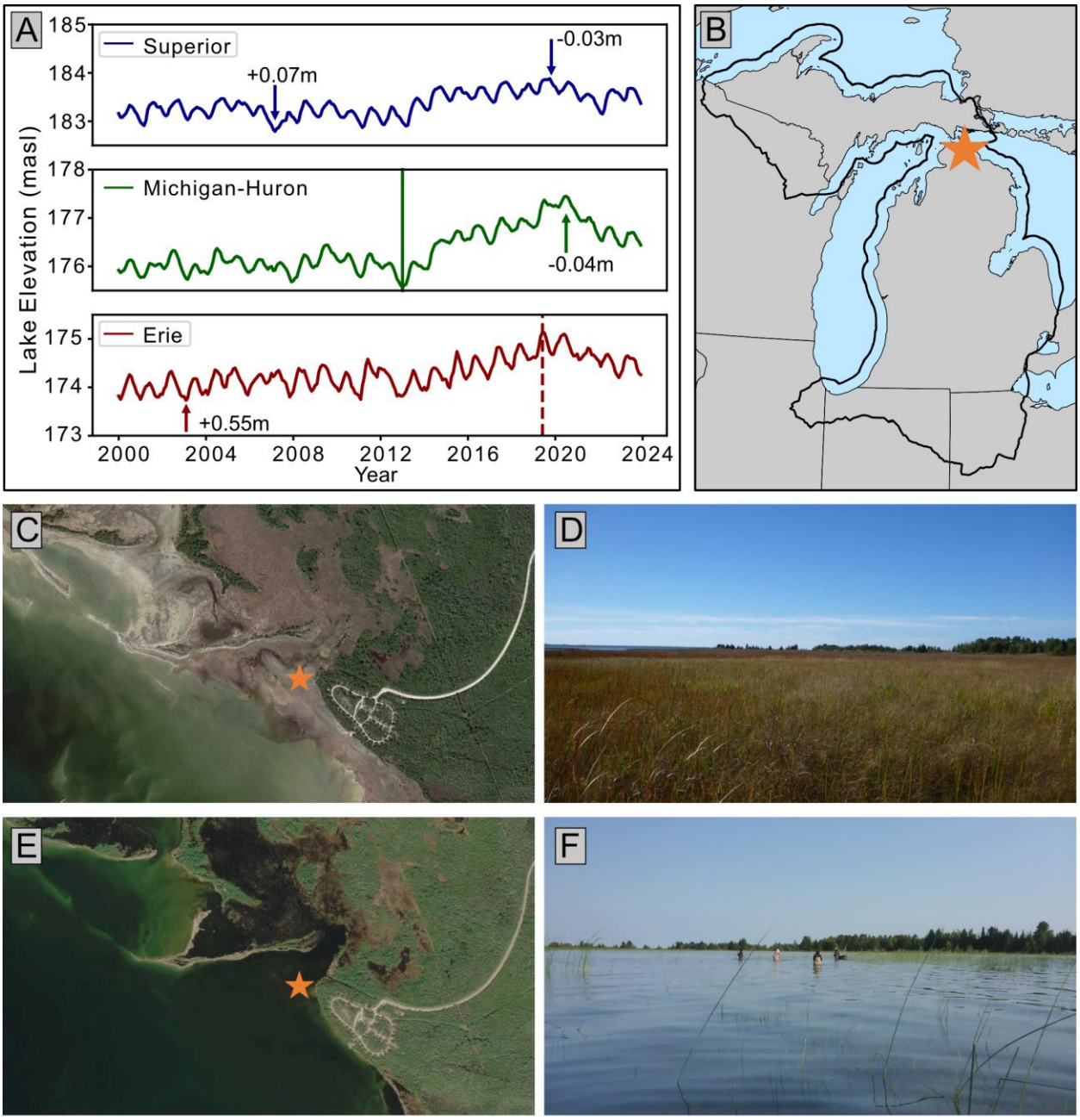

Figure 16: Lake Level Changes 2020-2023 and the Impact on Coastlines. Changes to Great Lakes water levels between 2003-2020 (Panel A) resulted in significant changes to the Great Lakes coastline. All four of the lakes within the study domain neared or reduced their historical extreme levels between 2000-2021. Solid lines indicate a historic low lake level, dashed lines indicate histoirc high lake levels, and arrows with annotations indicate how close recent extremes came to those over the period of record starting in 1918. An example of coastal change is shown for a coastal wetland monitoring site near Cheboygan, Michigan along the Lake Huron Coast (Panel B). Panels C and E show Google Earth satellite images of the site in 2013 and 2020. A groundwater monitoring well was installed at this site (location shown by the orange star). Field photos show that in 2013 (Panel D) this site monitored shallow groundwater in a wet meadow adjacent to the lake, and by 2020 (Panel F) the site was inundated with approximately 1 meter of water.

The Great Lakes hold roughly 23,000 km^3 of freshwater, and have over 4,500 miles of coastline, more than either the U.S. Atlantic or Gulf Coasts (Gronweold et al., 2013). The structure of the Great Lakes coastline varies from sand beaches to rocky shorelines, sand dunes and steep bedrock cliffs. Land cover and use within a 10 km buffer around the shoreline of the Great Lakes varies from heavily agricultural and urban in southern Lake Michigan and Huron, to forested and wetland dominated in northern Lake Michigan-Huron and along most of Lake Superior (Bourgeau-Chavez et al., 2015). Coastal wetlands are a prominent feature of the Great Lakes coastline providing important ecosystem services including habitat for fish, birds, amphibians and invertebrates. They also play a significant role in regulating local water quality, as they can trap sediment and are hotspots of nutrient cycling (Sierszen et al., 2012). Coastal wetlands are located between permanently upland and permanently open water areas of the coastline (Mynard and Wilcox, 1997), and are defined as those "under substantial hydrologic influence from Great Lakes waters" (Keough et al., 1999). Thus the physical structure and ecosystem function of coastal wetlands is closely related to variations in Great Lakes water levels.

Fluctuations of 10-40 cm in lake levels, which occur regularly over hourly to annual time scales, maintain the natural function of Great Lakes coastal wetlands. High waters keep woody, upland plants from encroaching on wetland species while low waters expose seeds stored in wetland sediment and allow for new growth of wetland species (Anderson et al., 2023, Keddy and Reznicek, 1986). Inter-annual variations in lake levels however can cause the migration of coastal wetlands either toward the upland at high water levels or toward the lake at low water levels. If these changes occur too quickly, or the physical structure of the coastal zone prevents migration, the loss of coastal wetlands can occur (Anderson et al., 2023, Theuerkauf and Braun, 2021). Using a combination of field data and Bayesian hierarchical modeling, Anderson et al. (2023) studied the position and relative length of coastal wetlands around the Great Lakes from 2011-2019, as lake levels were rising toward their recent maximum. They demonstrated a contraction of wetland area due to rising lake levels; this loss of wetland habitat was most severe for wet meadows (e.g. Albert et al., 2005) which have plant species intolerant of sustained inundation.

In addition to the effects of changing surface water elevation, groundwater conditions can also affect coastal wetlands. Previous studies using both field data and numerical models suggest that across the Great Lakes region, groundwater is an important component of coastal wetland hydrology and water quality. In a review of coastal wetland-groundwater interactions in the Great

Lakes, Crowe and Shikaze (2004) suggest that all of the region's coastal wetlands are connected to groundwater. The nature of this connection however, is dependent on wetland morphology. In wetlands which are directly connected to the lake, regional groundwater flows through the wetland, imparting little control on wetland level, but significant impacts on wetland water chemistry. In wetlands partially or fully protected from the open lake by beach deposits (spits and barrier bars) regional water from the uplands discharges to the wetlands, while groundwater in the spits and barriers may flow toward either the wetland or lake (Doss, 1993). The water levels in such wetlands are controlled by a combination of lake levels and groundwater elevations. For coastal wetlands further removed from the open lake, such as those behind beach ridges or dunes, groundwater is a primary control of wetland elevations. Groundwater flow systems around these wetlands can be highly complex, and are influenced by localized recharge and ET, as well as boundary conditions effects of the lake. The works summarized by Crowe and Shikaze (2004) however focus exclusively on the very local scale, and do not consider how groundwater connectivity to wetlands may change further inland.

In addition to the localized linkages described above, the Great Lakes surface waters are hydrologically connected to the adjacent terrestrial groundwater system at the regional scale. The Great Lakes receive groundwater both directly through discharge along the coasts, and previous regional modeling studies of the Lake Michigan basin by Feinstein et al. (2010) and the Great Lakes basin by Xu et al. (2021) both suggest that the lakes act as a discharge point for local and regional flowpaths, primarily through the surficial aquifer system. The model developed by Xu et al. (2021) suggests that groundwater from the surficial aquifer continuously discharges through the nearshore zone throughout the year. This contribution of groundwater discharge to the lakes is greatest during winter, when groundwater elevations are at their seasonal high and lake levels are at their seasonal low. Much less is known however about how changes in lake level, and thus the discharge point for terrestrial groundwater, may propagate upgradient within the surficial groundwater system.

In coastal ocean regions, recent work has suggested that increased coastal groundwater elevations increase the effect of sea level rise far beyond areas inundated by rising surface waters alone (Befus et al., 2020, Bjerklie et al., 2012, Rotzoll and Fletcher, 2013). A study of groundwater inundation caused by rising sea levels in Oahu, Hawaii indicated that considering groundwater elevation changes increased the area flooded by sea level rise by more than double the direct effect

of surface water inundation alone (Rotzoll and Fletcher, 2013). A recent study by Befus et al. (2020) modeled groundwater table elevation responses to sea level rise in a 1 km buffer along California's coastline. Their results indicate that 1 m of sea level rise would extend inundated areas between 50-150 m inland from current conditions. Groundwater discharge though topographic lows (existing or emergent drainage networks) can offset this groundwater inundation and should not be ignored in calculating the impact of sea level rise on groundwater conditions (Befus et al., 2020, Bjerklie et al., 2012). Based on these observations from ocean coastal regions, it is likely that the extreme changes in lake levels may affect groundwater conditions at larger scales than previously identified in the Great Lakes.

A more holistic assessment of the relationships between lake levels, groundwater elevations, and coastal wetland connectivity is required to understand the impacts of historical and future interannual variation in the Great Lakes. In this study, a coupled surface and groundwater model for the state of Michigan region (Figure 17) is combined with remotely sensed estimates of coastal wetland inundation to study interactions between Great Lakes lake levels, groundwater elevations and coastal wetland connectivity during the recent period of extreme lake level changes from 2000-2023. The groundwater flow model is used to quantify the amount of groundwater discharging along the coastline, how changing lake levels affect groundwater elevations, and how changes in coastal groundwater elevations affect wetland connectivity. These estimates of groundwater connectivity change are then compared to estimates of surface water connectivity change derived from remotely sensed coastal wetland inundation at high and low lake levels. Given the importance of coastal wetlands to the Great Lakes ecosystem, and predictions of continued interannual variability in lake levels (Kayastha et al., 2022), it is critical to understand how the lakes are interacting with terrestrial groundwater in the near shore region, and how these changes may affect coastal wetlands along the Great Lakes.

2. Hypothesis and Conceptual Framework

This study seeks to assess changes in coastal hydrology and groundwater-wetland connectivity at a regional scale, along the Great Lakes coastline within the state of Michigan. Great Lakes coastal wetlands are historically considered to be those directly affected by the surface water hydrology of the lakes (Keough et al., 1999, Mynard and Wilcox, 1997). Previous considerations of coastal wetland-groundwater interactions have been limited to investigations of very localized conditions, and to seasonal variations of lake and groundwater elevations (Crowe and Shikaze

(2004)). Based on the observations of groundwater-sea level interactions along ocean coastlines (Befus et al., 2020, Bjerklie et al., 2012, Rotzoll and Fletcher, 2013), it is possible that more extreme lake level variations may affect groundwater elevations, and thus their connectivity to wetland features much farther inland than previously considered.

Palustrine wetlands are those that lie outside of coastal, inland lake or river systems; they are commonly described as marshes, bogs, swamps and wetlands (Cowardin et al., 1979, Federal Geographic Data Committee, 2013). As shown in the high resolution coastal land cover dataset by Bourgeau-Chavez et al. (2015) there are significant palustrine (e.g. emergent, shrub, and forested) wetlands along the coastal region in the state of Michigan. To more fully assess the extent of groundwater-driven coastal change, the groundwater connectivity to both traditionally defined coastal wetlands (Keough et al., 1999, Mynard and Wilcox, 1997) as well as low lying palustrine wetlands near the Great Lakes coastline is assessed. We hypothesized that there are palustrine wetlands along the Great Lakes where connectivity to groundwater is determined by the lake levels. Additionally, we hypothesize that there are wetlands that become disconnected from the lakes during low level conditions, but remain groundwater connected. Changes in groundwater connectivity to near-shore palustrine and coastal wetlands have not been directly quantified in previous works, and the degree of groundwater influence may be important to understanding how lake level variability affects wetland habitat along the Great Lakes coastline.

Here, we define groundwater-coastal wetland hydraulic connectivity as any case where the groundwater head reaches or exceeds the elevation of the estimated wetland bottom. Under this condition, groundwater actively affects wetland water levels (Crowe and Shikaze 2004). Groundwater is important to not only wetland hydrologic function, but to wetland chemistry and plant distribution (Crowe and Shikaze 2004, Goslee et al., 1997). Although not captured in this analysis, groundwater may also be important to wetland ecology by sustaining wetland plants during periods where the water table falls below the wetland bottom elevation. Groundwater has been previously shown to provide a subsidy to soil moisture and plant transpiration in upland and riparian habitats (Zipper et al., 2015, Lowry and Loheide, 2010). This subsidy is the result of both plants accessing saturated groundwater directly, and capillary action pulling water from the saturated zone into the vadose zone. In this way, groundwater below the wetland bottom elevation may still be ecologically important to wetland ecosystems. The shallow rooting depth of plants in saturated soils (Fan et al., 2017), however, may limit the depth to which groundwater can fall

before it becomes inaccessible by wetland plants.

Figure 17 illustrates a conceptual framework which guided development of the hypothesis about lake-groundwater-coastal wetland interactions. Specifically, this conceptual model describes changes to connectivity to one coastal and one palustrine wetland at three lake and groundwater level conditions: low, moderate and high. At low lake levels, coastal wetlands are disconnected from surface water and both coastal and palustrine wetlands are disconnected from groundwater. At median conditions, rising groundwater elevations connected coastal wetlands and may cause intermittent wetting of palustrine wetlands. At high water levels, coastal wetlands are directly connected to (or inundated by) surface waters while palustrine wetlands become groundwater connected.

It is important to note that this is a highly generalized conceptual model of Great Lakes coastal hydrology. Changes in wetland connectivity and position may happen across a range of water levels based on shoreline morphology and topography. In addition to changes in wetland connectivity, changing surface water levels may cause the migration of coastal wetlands toward the lake at low levels and toward the upland at high lake levels. Furthermore, coastal wetlands which exist at the most lakeward extent at low water may be converted to open water habitat at high lake levels.

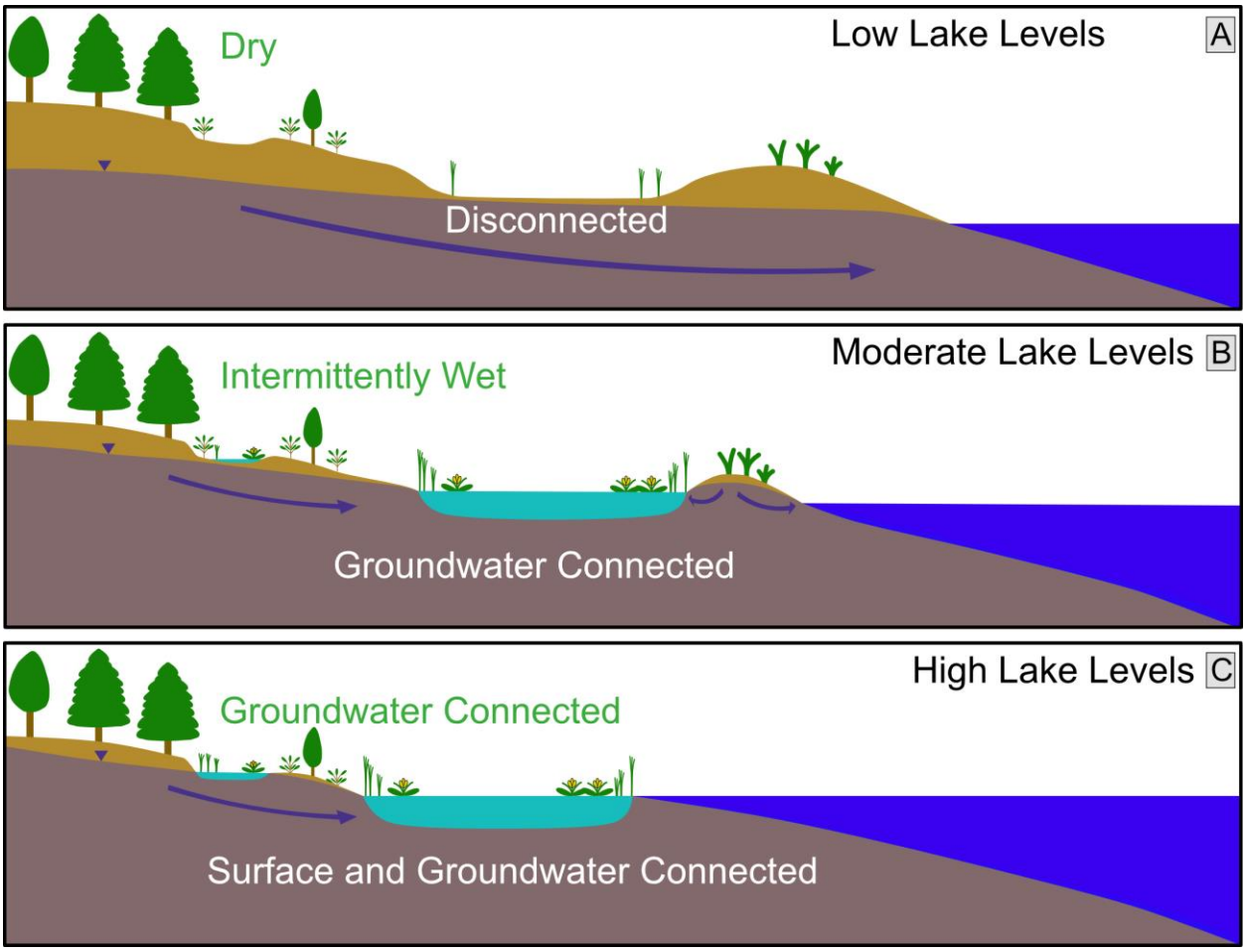

Figure 17: Coastal Wetland Connectivity Conceptual Diagram. A conceptual model of interactions between lake levels, groundwater, and wetlands along the Great Lakes coastline. At low water levels (A), both coastal and palustrine wetlands are disconnected. At moderate water levels (B), rising groundwater elevations connect coastal wetlands and may cause intermittent wetting in palustrine wetlands. At high water levels (C), coastal wetlands are connected to both surface and groundwater, and palustrine wetlands become connected to groundwater. While groundwater-lake-coastal wetland linkages have been established at the very local scale, it is hypothesized that the influence of lake levels on coastal groundwater, and of groundwater on wetland connectivity, may extend much further inland than previously documented.

3. Methods

3.1 Study Region

The state of Michigan (Figure 18) lies in the central portion of the Great Lakes drainage basin, and is composed of two peninsulas: The Upper Peninsula (UP), which borders Lake Superior to the north, and Lakes Michigan and Huron to the south; and the Lower Peninsula (LP), which lies directly between Lake Michigan to the west and Lakes Huron and Erie to the east. It is important to note that Lakes Michigan and Huron are connected by the Straits of Mackinac, and

function as one hydrologic system sharing the same lake elevation. They are, therefore, sometimes referred to as Lake Michigan-Huron. The boundary of the hydrologic model used in this study was defined by selecting all of the U.S. Geological Survey 8-digit hydrologic unit code (HUC) watersheds that intersect the state of Michigan. This boundary was then extended to a nearby hydrologic divide; where possible this divide was specified as the river channel of the adjacent river system away from the area of interest. The resulting ~251,000 km^2 area includes all of the state of Michigan as well as parts of Illinois, Indian, Ohio and Wisconsin.

Michigan has over 3,224 miles of coastline, the most of any Great Lakes state (NOAA, 2025). The Lake Michigan shoreline in the LP is characterized by sandy beaches and extensive high relief dune structures, including Sleeping Bear Dunes National Lakeshore. The Lake Huron shoreline in the LP is similarly characterized by sand beaches, but is generally of lower relief. The southern shoreline of the UP is generally sandy or rocky and of mixed relief, while the Lake Superior shoreline varies from sandy and pebble beaches to sand dunes and exposed bedrock cliffs. Coastal land cover in the LP varies from heavily urban and agricultural in the south to a mix of forest, wetland and agriculture in the north. Forest and wetland land covers dominant most of the Huron-Michigan and Superior coastlines in the UP (Bourgeau-Chavez et al., 2015).

Michigan's climate is temperate and strongly seasonal, with significant influence from the Great Lakes, resulting in concentrated lake effect precipitation along the Lake Superior and Lake Michigan shorelines (Anderson, 2012, Notaro et al., 2013). The hydrogeology of this region is strongly influenced by Pleistocene glaciation (Milstein, 1987, Reed and Daniels, 1987, Westjohn and Weaver 1998). In the central Upper Peninsula, northern LP, and along the Lake Michigan shoreline in the southern LP, surficial geology is characterized by deposits of high conductivity glacial outwash, sand, and coarse till. The eastern UP and Lake Huron shoreline in the LP are characterized by lower conductivity lacustrine and finer grained till deposits (Farrand et al., 1984, Fullerton et al., 1991, Gobel et al., 1983, Lineback et al., 1983, Sado et al., 1993). In the western UP, thin glacial sediments overlie Precambrian to Cambrian bedrock units which are exposed at the surface in a number of locations, inducing along the Lake Superior coastline (Dietrich, 1983, Larson and Schaetzl, 2001).

To highlight the results at relevant scales, each map in the following sections include an inset of three regions; Grand Traverse Bay, the Eastern Upper Peninsula, and the Lower Saginaw River. These areas represent unique coastline conditions representative of other portions of the

modeling domain. The Grand Traverse Bay region (Figure 18B) has sandy beaches and generally higher relief away from the coastline. In the eastern Upper Peninsula (Figure 18C), especially along the Huron shoreline, extensive coastal wetlands exist at both high and low water conditions, with generally low relief away from the coastline. In the Lower Saginaw River region (Figure 18D), low relief and the large river channel allow changes in lake level to propagate a significant distance inland, farther than anywhere else in the model domain.

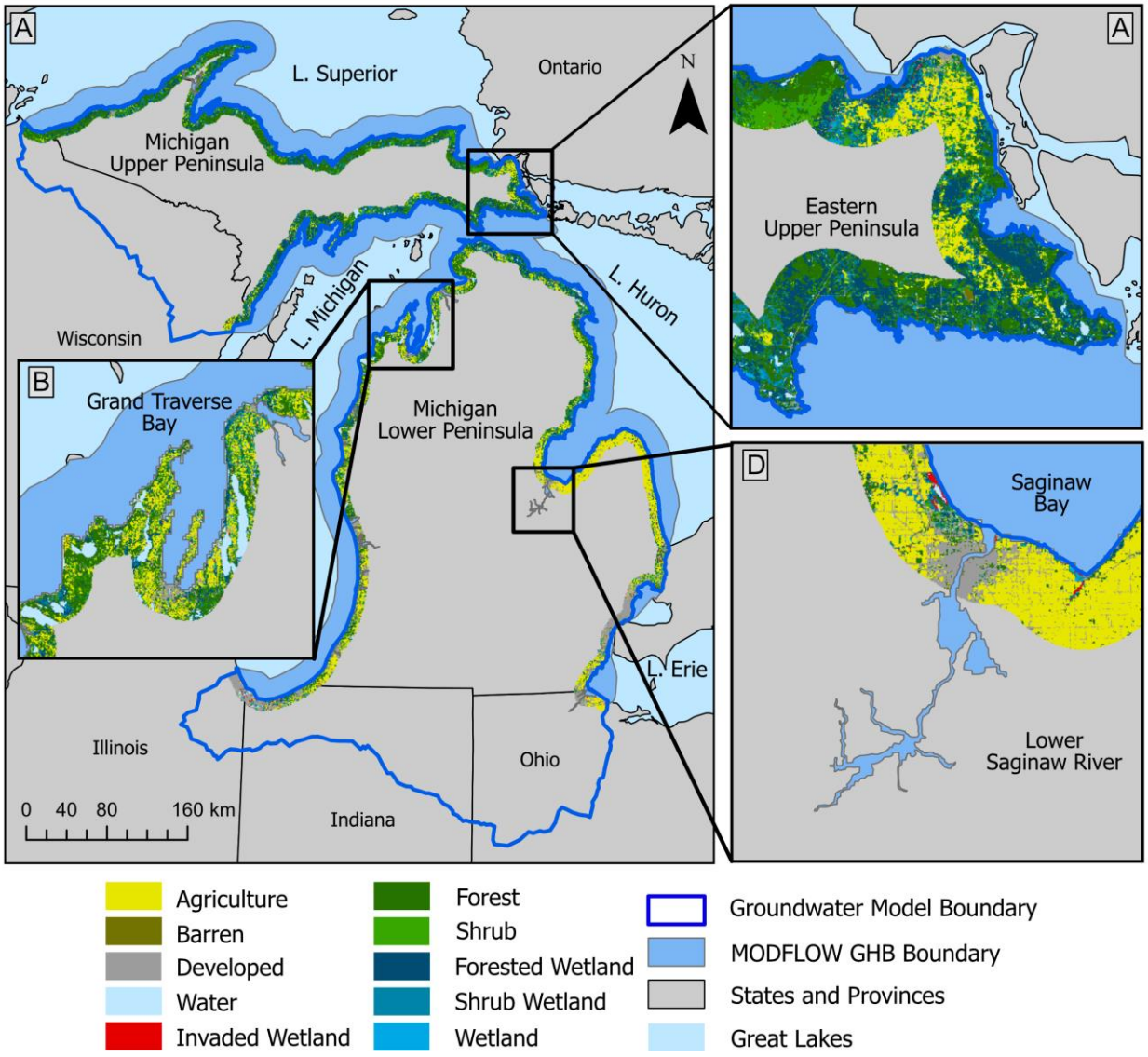

Figure 18: Study Region, Groundwater Model Boundary and Coastal Land Cover. The state of Michigan (A) lies south of Lake Superior, and between Lakes Michigan and Huron in the central Great Lakes Basin. High resolution coastal land cover data (Bourgeau-Chavez et al., 2015) shows Michigan's coastline includes significant wetland area, especially in the northern Lower Peninsula (C) and Upper Peninsula (B). Highlihgted in read in this dataset are wetlands where invasie plants such as *Thypha* and *Phgragmites* have becoem established. In the central and southern Lower Peninsula (D), considerable portions of the coastline have been converted to urban or agricultural areas. The model extent is shown with the dark blue line, while the MODLFOW General head boundary, used to simulate the effects of changing lake levels, is shown in a lighter blue. This boundary extends from the coastline, 10km into the lakes, and inland in areas where the surface elevation of hydrographic features (e.g. lakes and river mouths) is at or below the mean lake elevation, such as in the Saginaw Bay region (Panel D).

3.2 Landscape Hydrology Model

The Landscape Hydrology Model (LHM) is a process-based, coupled surface and

subsurface hydrology model capable of simulating water and energy fluxes from the canopy through deep groundwater. The development of LHM is described in Kendall (2009) and recent updates to the model's structure and function are described in detail in Chapter 2. Briefly, LHM consists of a land surface hydrology model and a vadose zone model, which then pass fluxes of recharge and groundwater evaporative demand to the three-dimensional saturated groundwater flow model MODFLOW (Harbaugh, 2005). This surface model simulates all of the major surface fluxes including evaporation, transpiration, infiltration, and runoff, while MODFLOW is used to simulate groundwater elevations and discharge across three drainage boundary condition types using the drain package: streams and wetlands, and horizontal and vertical seepage faces. In addition to these drains, two other boundary condition fluxes are represented: groundwater evapotranspiration using the EVT package, and two-way head dependent fluxes to the Great Lakes using the General Head Boundary (GHB) package.

Using LHM, a transient 24-year simulation has been developed for the state of Michigan Region, shown in Figure 18, and hereafter referred to as the Michigan Model. The model boundary was developed as described in Section 3.1 and is shown in the blue line on Figure 18. The landscape within the model defined using the 3-D Elevation Program (3DEP) 1/3rd arc-second DEM (USGS 2023) for surface elevations, National Hydrography Dataset (USGS, 2020) and the National Wetlands Inventory (USFWS, 2018) for hydrography, the National Land Cover Database (NLCD) data for land use, land cover and imperviousness, the MODIS MCD15A2H product (Myneni et al., 2015) for LAI and the Gridded Soil Survey Geographic (gSSURGO) Database (USDA, 2016) for soils data. Climate data used to force the model surface fluxes, including precipitation, temperature and incoming solar radiation are taken from the North American Land Data Assimilation System (NLDAS-2A) (Mitchell et al., 2004, Xia et al., 2012a, Xia et al., 2012b). Surficial geology in the groundwater model is defined using USGS 4x6 degree quadrangle Quaternary geologic maps, while bedrock geology is defined using the Geologic Map of North America (Garrity and Soller, 2009). Estimates of horizontal hydraulic conductivity (HK) for the surgical and bedrock geology units are derived from estimates included in the Michigan Department of Environment, Great Lakes, and Energy (EGLE) Wellogic database (EGLE, 2020). A detailed description of the preparation of these data for use in the Michigan Model is provided in Chapter 2.

Particularly relevant to this investigation is the use of the MODFLOW GHB package to

simulate direct time varying interactions between the Great Lakes and adjacent coastal groundwater. The GHB package is used to simulate head dependent fluxes, where the direction of the flux (i.e. into our out of the aquifer) is controlled by comparing a user specified (observed) head elevation to the head computed by MODFLOW, as shown in Equation 1:

[1] $$q = (h_b - h_s) * C$$

Where q is flow into (positive) or out of (negative) the aquifer, h_b is the specified head in a GHB cell, h_s is the simulated head in that cell and C is a conductance term describing the ability of water to move across the boundary. When simulated heads are above the specified head elevation, water discharges from the aquifer, while when the simulated head is below the specified head water recharges the aquifer from the boundary condition. Here, this flux occurs across the top of the model cell, and is controlled by a conductance parameter C, the basic form of which is shown in Equation 2:

[2] $$C = \mathrm{K} * A/T$$

Where K is hydraulic conductivity of the material at the boundary between the aquifer and the boundary condition, A is the area across which the flux occurs and T is the thickness of the material separating the aquifer and the boundary condition.

In the Michigan Model, the GHB package is used to represent two key processes: the movement of water between the lakes and the underlying aquifer, and the effect of lake levels on adjacent terrestrial groundwater. The GHB boundary extends 10 km into the lakes from the coastline and also includes inland waterways affected by changes in lake levels. Lake level-affected inland waters include lakes that have been directly connected to the Great Lakes (e.g Muskegon Lake, Lake Macatawa, and Lake Charlevoix) and low-lying river systems including the Saginaw River. These inland waterways were identified by selecting all of the model domain where the 3DEP DEM surface elevation was below the maximum elevation of the adjacent Great Lake from the NOAA Great Lakes Monitoring Network monthly lake level observations between 2000-2023. Movement of water between the Great Lakes and the underlying aquifer system occurs across the lake bed sediment. Aquifer top elevations within the GHB cells representing the Great Lakes are specified as the lake bottom elevation using a combination of the DEM and the NOAA Great Lakes Bathymetry dataset (National Geophysical Data Center, 1999a,1999b, 1999c, 1999d, 1999e). The lakebed conductance C_{lb} is computed as the hydraulic conductivity of the lakebed sediments (K_{sed}) times the cell area divided by the thickness of the lakebed sediments (T_{sed},

assumed to be 1 everywhere), as shown in Equation 3:

[3] $$C_{lb} = K_{sed} * A_{cell} / T_{sed}$$

Lakebed sediment types and their distribution are taken from the Great Lakes Aquatic Habitat Framework (GLAHF) (Wang et al., 2015) lakebed substrate map. As direct observations of conductivity in these lakebed sediments are extremely limited, HK estimates from the surficial aquifer material were used to define HK for the GLAHF substrate types. First, the GLAHF substrates were reclassified to match the Quaternary geologic material classes. Second, an average HK was computed for each material by taking the mean of estimated HK across all polygons of a given material. Third, HK values for the subtract classes were specified as the mean in the corresponding Quaternary geologic material. The relationship between the GLAHF substrate and Quaternary geology classes, and the average HK for these units is shown in Table A12.

To separate the effects of direct lake interactions on groundwater dynamics, four groundwater model scenarios are assessed, each with the GHB boundary specified at different lake levels. In the first scenario, hereafter referred to as the 'BASE' scenario, time variant boundary conditions are specified using the NOAA Great Lakes Monitoring Network monthly lake level observations from 2000-2023. In the other three scenarios, referred to as "MIN", "MED" and "MAX" respectively, lake boundary conditions are fixed in time at the minimum, median, or maximum lake level observed between 2000 and 2023. The same NLDAS-2A time-variant climate forcing data is used for all four scenarios.

3.3 MODFLOW Output Processing

MODFLOW-derived estimates of groundwater head (elevation) and fluxes across the GHB were used to characterize the lake-groundwater-coastal wetland interactions across the model region. Prior to this analysis these gridded outputs were processed using a combination of MATLAB (MathWorks Inc., 2021) and the python packages Numpy (Harris et al., 2020) and Xarray (Hoyer and Hamman, 2017). The general workflow was as follows: 1) read the binary MODFLOW outputs, 2) format the data as arrays, 3) spatially and temporally resample as needed. Head outputs from MODFLOW are saved at the end of every month, while GHB fluxes are saved at the end of every time step (daily).

Binary head arrays were initially read by MATLAB, saved as single ASCII arrays for each month, then read using Numpy and combined into a single 3D array using Xarray. Time series of average heads were generated by taking the average head in each month across the model domain.

Temporal summaries including the minimum and maximum heads were then created by summarizing values in each cell through time. The arrays of head elevation at each month, as well as the temporal summaries (such as maximum and minimum head elevations in each cell) were compared to estimates of wetland bottom elevations to quantify changes in connectivity (described in detail in section 3.3.3).

Boundary condition fluxes were read using FloPy (Bakker et al., 2016), then spatially and temporally aggregated. GHB fluxes were characterized in two ways. First, an average time series was created by taking the average flux from all GHB cells across the model domain for each monthly total flux. Second, the average of the GHB flux in each month across the 24 years was computed, to characterize the seasonal cycle of groundwater exchange with the lakes.

3.4 Wetland Locations, Depths and Inundation

Palustrine wetland locations were selected from National Wetlands Inventory (NWI) polygon data (USFWS, 2018), which were downloaded for the states in the model region, then clipped to the modeling domain. Palustrine wetland depths were assigned based on the NWI Wetland Water Regime classifier for palustrine wetlands. These water regimes describe the frequency with which a palustrine wetland is inundated or saturated, and is illustrated on page 18 of the Federal Geographic Data Committee (2013) Classification of Wetlands and Deepwater Habitats of the United States report. Permanently flooded wetlands were assumed to be the deepest and were assigned a depth of 2.5m (the maximum palustrine wetland depth as defined by the NWI), while those with only seasonal saturation were assumed to be the most shallow and were assigned a depth of 0. Water regimes between permanently flooded and seasonally saturated were assigned depths based on their degree of inundation and/or saturation. The depths assigned to each wetland water regime are included in Table A11. This palustrine depth polygon feature was then converted to a raster at the 3DEP DEM resolution (~30m) using ArcPy (ESRI, 2023). A copy of the 3DEP DEM was also created and masked to the palustrine wetland area, to create a raster of wetland elevations.

These derived palustrine wetland elevation and depth rasters were then aggregated to the MODFLOW grid resolution of 500m for comparison with model output. This aggregation was performed using the ArcPy Spatial Analyst Aggregate function (ESRI, 2023), taking the mean elevation or depth value in the high resolution grids within each MODFLOW cell. Finally, wetland bottom elevation was computed by subtracting the wetland depth from wetland elevation at the

MODFLOW grid resolution.

Surface water inundated coastal wetland areas were identified by GIS analysis in a dataset developed by Michigan Technological Research Institute (Miller et al., in prep). Areas inundated by Great Lakes surface water were identified by comparing high resolution LIDAR based surface elevation data along the coastlines to lake levels at their average, low and high conditions. These data were downloaded from the MTRI data server (https://webserver.mtri.org/pub/MDEQ_conn), then compiled into a single map for Lakes Superior, Michigan, Huron and Erie, and clipped to the model domain. This was then converted to a raster at the resolution of the 3DEP DEM for the model region, then aggregated to the MODFLOW grid resolution using the same method as the palustrine wetland depth and elevation products.

3.5 Wetland Connectivity Analysis

A "coastal groundwater zone" was defined as any area where the difference between mean head elevations for the "MIN" and "MAX" scenarios was greater than 1 cm. This represents the zone where lake level fluctuations of the magnitude observed between 2000-2023 can directly affect groundwater levels. This coastal groundwater zone was then combined with the maximum surface water wetland inundation extent to create a "coastal wetland zone" specific to this study, shown in Figure A32. This combined 'coastal wetland zone' was assumed to represent the area in which groundwater elevations and wetland connectivity could be affected by the recent changes in lake levels.

For the purposes of this study, both traditionally defined coastal wetlands and palustrine wetlands within this coastal wetland zone are considered "coastal wetlands". Surface and groundwater connectivity are subsequently quantified for all wetlands within this coastal wetland zone. Any changes to groundwater-wetland connectivity outside of this zone were considered to be the result of climate drivers alone, and not the primary focus of this study.

Wetlands are considered groundwater connected (GC) if the head elevation within a model cell (h_i) is greater than or equal to the wetland bottom elevation (WB_i) in that cell, as shown in Equation 4:

[4] $$GC_i = h_i \geq WB_i$$

Groundwater wetland connectivity (GWC) is defined as the total number of groundwater model cells containing wetlands that are groundwater connected (GC_i) as shown in Equation 5:

[5] $$GWC = \Sigma\, GC_i$$

GWC was assessed for all four scenarios ("BASE","MIN","MED","MAX") at three groundwater conditions: 1) the maximum and 2) the minimum head elevation during the simulation period in each model cell, and 3) groundwater head elevations at the 15th of every month during the simulation period. The minimum and maximum conditions were compared to estimate the total potential change in GWC during the model period. Monthly heads were used to assess how the amount of GWC changed through time over the model period. Changes in GWC are expressed as a percent difference with respect to the theoretical minimum connectivity (GWC at absolute minimum heads). Estimates of groundwater connected wetland (GWC) area were computed by multiplying GWC by the cell area, or 0.25 km^2.

Surface water connectivity (SWC) was defined as the total number of cells where surface water inundated wetlands were present in the 500 m resolution rasters derived from the MTRI inundation dataset (described in Section 3.3.2). SWC was calculated for the low and high lake level conditions reported by MTRI, and change in SWC was reported as a percent of SWC at low lake levels. To keep estimates of SWC wetlands consistent with GWC estimates, surface water connected area is computed as SWC multiplied by the cell area (0.25 km^2). Combined surface and groundwater wetland connectivity (CWC) is defined as cells where both the GWC and SWC conditions are met. The number of these cells at high and low water levels is then multiplied by the cell area (0.25 km^2) to estimate CWC area.

GWC was compared between the different model scenarios to assess how much influence lake levels have on groundwater connectivity, through direct influence on coastal groundwater elevations. Connectivity at maximum and minimum groundwater head elevations were compared between the BASE and MED scenarios to assess the effects of including time variant lake levels on wetland connectivity. Maximum connectivity was compared for the BASE and MAX scenarios, while minimum connectivity was compared for the BASE and MIN scenarios, to assess how much more or less connectivity could have occurred if the lakes maintained their extreme levels. Finally, connectivity was computed for each time step in the MIN, MED, and MAX scenarios, then compared to the time series of connectivity from the BASE scenario to assess how close the observed conditions came to the theoretical impact of the lakes equilibrating at their extreme conditions.

3.6 Sensitivity Analysis

Due to the use of an absolute elevation to determine groundwater wetland connectivity,

GWC may be very sensitive to simulated head elevations. As all models have some degree of uncertainty, assessing the sensitivity of this GWC approach to absolute head elevation provides content for interpretation of the results presented above. Sensitivity of GWC to simulated groundwater elevations was assessed by varying minimum, maximum and monthly head elevations in the "base" scenario by +/- 0.5m, +/- 0.3m and +/- 0.1m. A seventh case was also assessed where heads were adjusted by the median error, defined as the difference between modeled and observed head elevations. This error was calculated by first by taking the mean of the simulated vs observed heads for all observation points within the coastal wetland zone. The impact of adjusting head elevations was calculated as the amount of wetland area connected to groundwater in each time step for the seven sensitivity cases, expressed as a percentage of absolute maximum BASE scenario connectivity.

The effect of data resolution on wetland connectivity estimates was assessed by resampling the groundwater model outputs to the 3DEP DEM resolution, then comparing groundwater elevations and wetland bottom elevations at this resolution. Groundwater model heads were resampled with a nearest neighbor approach using the Rasterio python package (Gillies et al, 2024). The result was a groundwater head grid at the DEM where each cell in the higher resolution grid inherited the value of the nearest cell in the native groundwater model output resolution grid. While this method does not account for sub-grid variation in groundwater elevation, it does allow for smaller scale variability in wetland elevation and depth to be considered. It also more accurately represents the amount of wetland area within the domain.

4. Results and Discussion

4.1 Direct Groundwater-Lake Exchange

Groundwater discharges to the Great Lakes through the nearshore lakebed at a rate of between 0.01 and 0.12 m/month between 2000-2023 (Figure 19A). Seasonally, groundwater discharge peaks in April and is lowest in September (Figure A33), closely following the seasonal patterns in simulated deep percolation from the surface model, shown in Figure 14. Groundwater discharge to the lakes is similar at the beginning and end of the model period, and is lowest between ~2009-2013 (Figure 19E), when both the lakes and the groundwater are at their lowest point. Groundwater discharge is very consistent within the lakebed region (Figure 19A), however significant variability is observed along the coastline (Figure 19B), and within inland features directly connected to the Great Lakes (Figure 19C).

This consistent discharge of groundwater through the near-shore lakebed regions was also observed by Xu et al. (2021) who modeled groundwater and lake elevations across the Great Lakes basin using the HydroGeoSphere hydrologic model. Their results estimate a seasonal pattern of groundwater discharge similar to this work, but shifted one month earlier, with maximum discharge in March and minimum discharge in August. Xu et al. (2021) estimated annual average discharge to the lakes to range between 29.0, 38.6 and 24.5 m^3/s for lakes Superior, Michigan and Huron respectively, while a modeling study of the Lake Michigan Basin by Feinstein et al (2020) estimated direct discharge to Lake Michigan of 9.6 m^3/s. While not directly comparable to either study, as we only simulate portions of each lake, annual average discharge through the combined GHB in this model ranged from 246-673 m^3/s. This is considerably more discharge than the combined discharge of Lakes Superior, Michigan and Huron of 92.1 m^3/s estimated by the Xu et al. (2021) model. Higher simulated direct groundwater discharge rates in this study relative to the Xu et al. (2021) model may be due to the significantly smaller cell size used in this study (500 m vs 2-10 km) or the much higher conductivity value used for the GHB cells (4.5-18.3 m/day in this study versus 0.0864 m/day (Xu et al., 2021)).

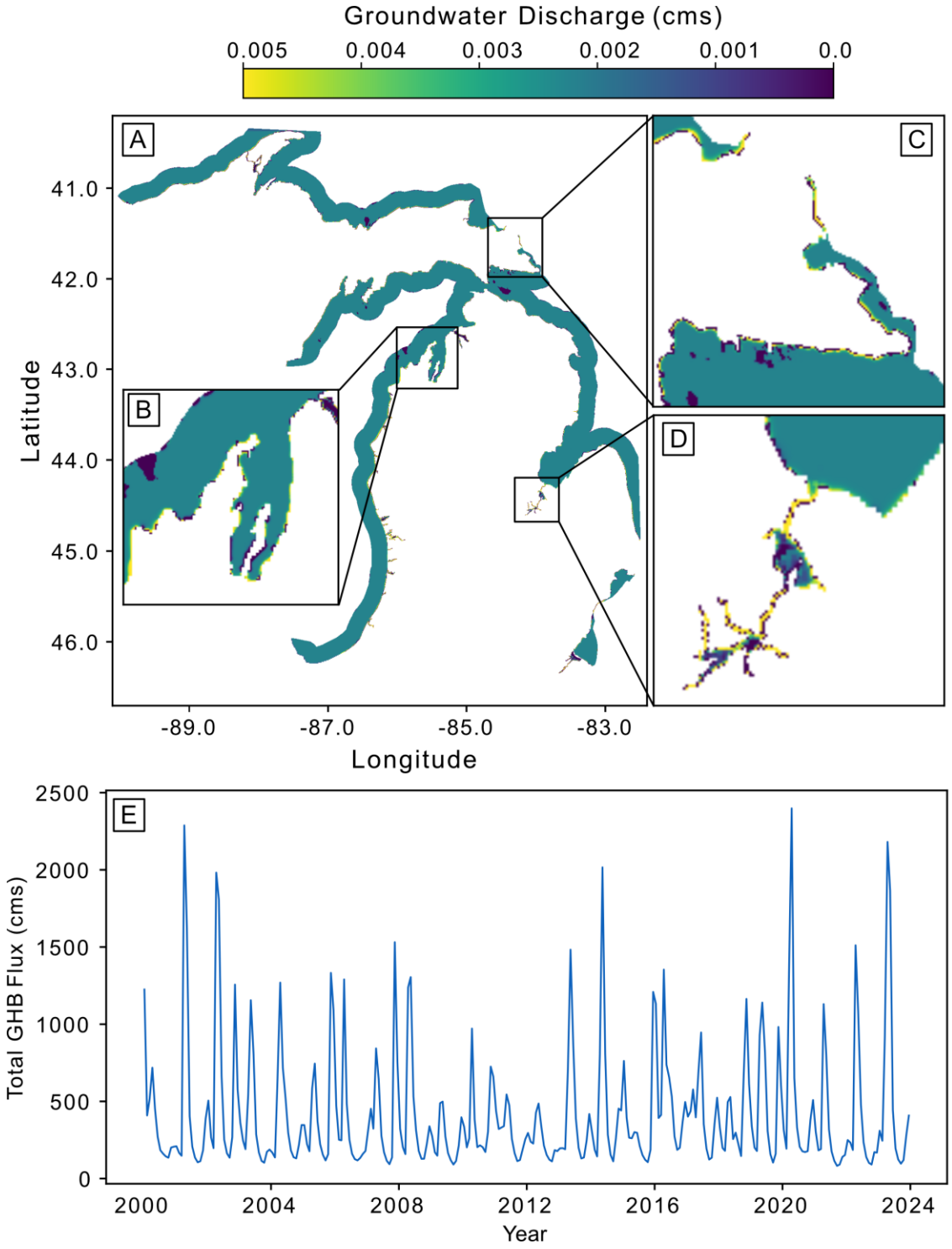

Figure 19: Groundwater Discharge to the Great Lakes. Average direct groundwater discharge to the lakes during the model period is very consistent though the lakebed (A), but concentrated along the coastline (B and C) and in inland waterway connected to the Great Lakes (D). Groundwater continuously discharges to the lakes during the simulation period, but is lowest between 2009-2011 when both lake and groundwater elevations were near their lowest (E).

4.2 Influence of Lake Levels on Coastal Groundwater

Comparison of the MIN and MAX scenario heads indicate lake levels changes ranging from 1.1-1.9m across the three lakes have the potential to directly influence groundwater elevations by at least 1 cm in a zone extending from the shoreline up to ~17. 5km inland (Figure 20A). Change in groundwater elevations over this region averages 21.2 cm, with a maximum of 1.93 m. This potential effect of lake levels on groundwater is highest along the inland waters included in the GHB boundary, and in areas surrounded by the lake, such as the two peninsulas in the Grand Traverse Bay region (Figure 20B). The difference between these two scenarios represents the maximum difference in groundwater head that could be directly caused by lake levels, if the lakes had equilibrated with the groundwater system at their observed minimum and maximum levels.

The observed lake level variation between 2000-2023 resulted in coastal groundwater elevation changes which nearly equaled the maximum potential effect (Figure 20E). At their extremes, coastal groundwater elevations in the base run were 5.2 cm higher than the theoretical minimum, and 4.4 cm lower than the theoretical maximum. On average, heads in this coastal groundwater zone varied by 124 cm during the BASE scenario (Figure 20E). Coastal groundwater heads in the MED lake level scenario varied by 113 cm over this same period. These results suggest that of the observed variation in coastal groundwater elevations, approximately 91% is due to variations in the surface water balance, while ~9% is due to direct effects of the lakes. The difference in coastal groundwater head between the BASE and MED lake level scenarios is shown in Figure A34. Together, results of this modeling study suggest the observed dynamic climate and lake level variations between 2000-2023 resulted in changes to coastal groundwater elevations approximately equal to the effect of changing the lake level by 2 meters. Further, these results indicate most of this variability is due to the observed changes in climate, which alter the surface water balance and ultimately groundwater elevations.

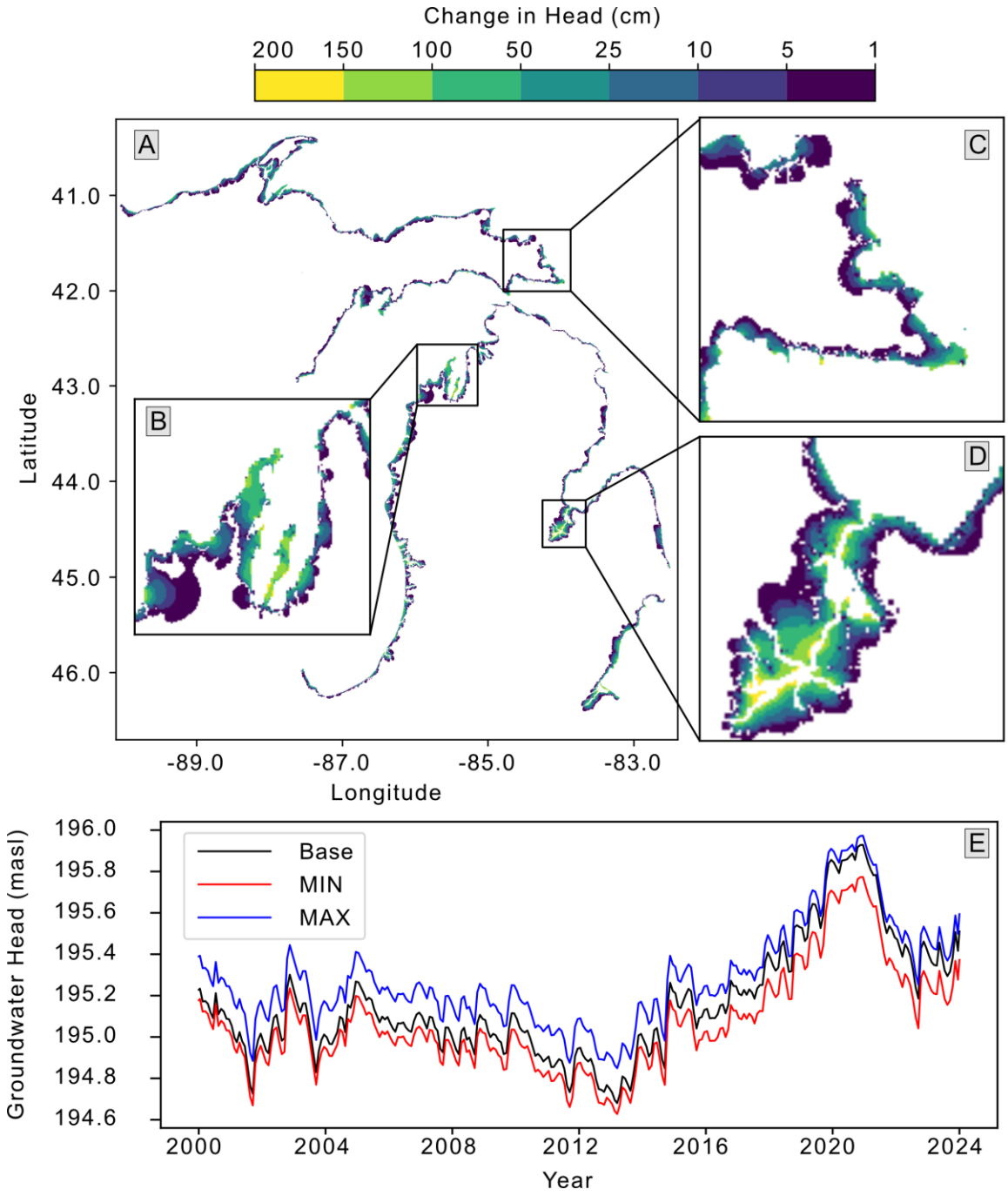

Figure 20: Groundwater Model Scenario Comparison. Average difference in heads between the "MIN" and "MAX" scenarios, showing the potential impact of lake levels on groundwater elevation. Direct lake level impacts are generally greater along the Lake Michigan coastline (Panel A), in peninsulas such as those in Grand Traverse Bay (Panel B), and in low lying inland waterways such as the Lower Saginaw River Watershed (Panel D). Differences between the BASE scenario (black line) and the two extreme scenarios (MIN, red line, and MAX, blue line) shown in Panel E suggest that between 2000-2023, coastal groundwater elevations nearly reached the theoretical impact that would be observed if the lakes had been fixed at their extremes.

4.3 Changes to Coastal Wetland Connectivity

Coastal wetland surface water connectivity (SWC) increases by a factor of 2.9 when the lakes rise from extreme low to high water levels, as they did between 2007 and 2021 (Figure A35). This ~3,716 km^2 increase in SWC area is concentrated along the Lake Michigan-Huron shoreline in the UP, and along the Lake Michigan Shoreline in the LP. Of the 5,488 km^2 of surface water connected coastal wetlands at high water levels, 67.7% is newly inundated while 32.3% was also inundated at low water levels. This newly connected area at high lake levels may be the result of rising water levels inundating existing but previously surface water-disconnected wetlands, or the result of wetland migration. Increased lake levels cause both the expansion of coastal wetland area landward, and the loss of wetland habitat near the low water level coastline (Anderson et al., 2023, Theuerkauf and Braun, 2021). When the lake levels rise to their maximum, about 6% of the SWC area at low water is lost, as rising waters convert some of the low water SWC area to open water.

GWC in the coastal wetland zone increased by 120.9% when heads rose from their minimum to maximum between 2000-2023 (Figure A36). This represents an increase from ~526 km^2 of coastal GWC area at minimum heads, to ~1,161 km^2 at maximum heads. All of the GWC at minimum head elevations remains connected at maximum head elevations. Due to the structure of the groundwater model, the location of the lake-land interface is fixed across the model runs. Thus, changes to wetland connectivity due to the expansion or contraction of the coastal zone with changing lake levels cannot be assessed. Groundwater wetland connectivity changes between 2000-2023 are not limited to coastal wetlands. GWC in palustrine wetlands outside the coastal wetland zone increased by 103.9% increase at the maximum groundwater heads when compared to minimums (Figure A36). These changes occur throughout the model domain, but areas of wetland connectivity increases are concentrated in the central LP, Saginaw Bay watershed and in the southern half of the UP.

The combined wetland connectivity (CWC) area at minimum lake and groundwater elevations totals approximately 2,323 km^2. Of this total connected area, 77.4% is connected by surface water, 18.3% is connected to groundwater, and 4.3% is connected to both. At the maximum lake and groundwater conditions, CWC increases by 160% to approximately 6,047 km^2. At high water conditions, 80.8% of coastal wetlands are connected to surface water, 9.2% to groundwater, and 10.0% to both surface and groundwater. Of the additional coastal wetland area that becomes connected at high water levels, shown in Figure 21, 84% is connected to surface water, 10.1% to

groundwater and 5.2% to both. Including groundwater connectivity change with the estimate of surface water connectivity change increased the estimated amount of coastal wetland area gained when lake levels rise by 18.2%. In addition to extending the amount of increased wetland connectivity at high water levels, including groundwater in this analysis of wetland connectivity also indicates that ~6.1% of the coastal wetland area connected to the lakes at high lake levels, remains groundwater connected at low lake levels. These areas may remain wetland habitat through a groundwater subsidy even during a loss of surface water connectivity.

The minimum and maximum in lake levels and groundwater elevations used to assess connectivity changes do not occur at the same time. Minimum head elevations occurred between 2000-2017, while minimum lake elevations occurred between 2003-2013. Similarly maximum head conditions occurred between 2008 and 2020, while maximum lake elevations occurred between 2019 and 2020. Quantifying this total connectivity, and its change as the lakes and groundwater reach their maximum conditions is however useful to summarize the effects of changing hydraulic conditions on wetland connectivity between 2000-2023. While the MTRI dataset only includes a single layer each for high and low inundation, simulated groundwater head elevations were saved at monthly intervals. Over the model period, the amount of groundwater connectivity ranges from 55% to 89.6% of maximum GWC, as shown by the solid blue line in Figure 22. Trends in GWC over the model period generally follow those in lake level and groundwater elevations; CWC is lowest in 2004-2013 and highest in 2019-2021.

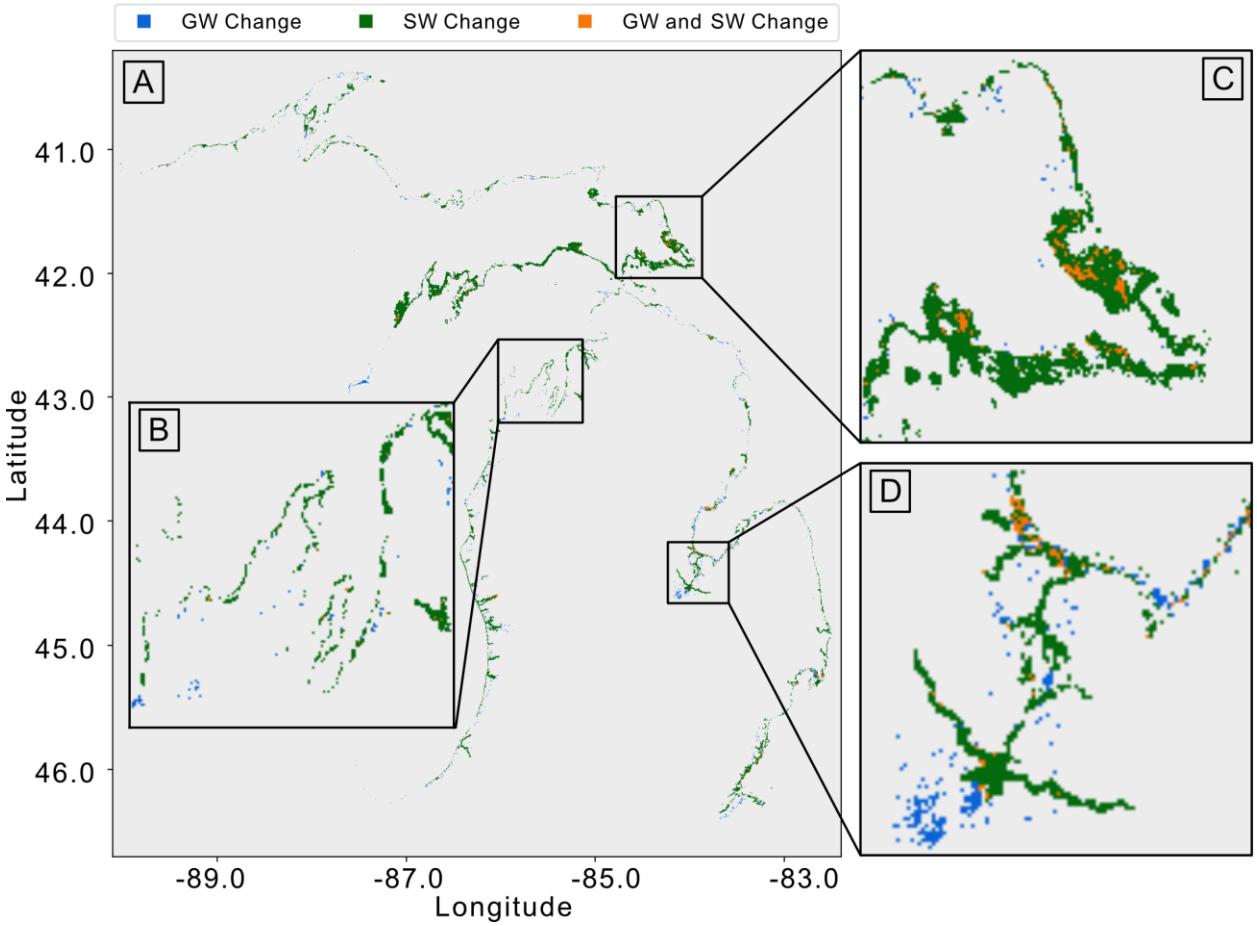

Figure 21: Ground and Surface Water Connectivity Change in Coastal Wetlands. Change in combined wetland connectivity within the coastal zone due to changes in surface water connectivity (SWC, green), groundwater elevations (GWC, blue) or both (CWC, orange) between minimum and maximum lake level scenarios are shown in Panel A. The increase in connected wetland area is primarily due to an increase in SWC, as is the case in the Eastern Upper Peninsula (Panel C). Rising groundwater elevations alone account for approximately 10.1% of the increased wetland area, and can extend the impact of rising surface and groundwater conditions a considerable distance inland. This effect is most strongly observed in low lying conductivity areas such as in the Lower Saginaw River (Panel D).

4.4 Drivers of Coastal Wetland Connectivity Change

GWC estimates from the MED scenario are 2.1% lower at maximum connectivity, and 1.6% higher at minimum connectivity when compared to the BASE scenario. Wetland connectivity in the base scenario was ~5.5% higher at minimum conditions and about 1.4% lower at maximum conditions when compared to the extreme scenarios (MAX and MIN). Together, comparing these scenarios to the BASE scenario indicate that direct feedback between lake levels and groundwater elevations had minimal impact on groundwater connectivity to coastal wetlands

between 2000-2023. As such, climate forcings appear to control most of the variability in groundwater elevation and GWC change over the simulation period.

There is considerable difference between the potential impact of lake level variation on groundwater elevations, and its simulated effect on GWC between 2000-2023. This minimal feedback from the lakes, through groundwater heads to coastal wetlands is attributed to two factors. First, groundwater head and surface elevation gradients along the coastline limit the impact of changing groundwater elevations on wetland connectivity. This is illustrated by the Grand Traverse Bay region, where potential changes in groundwater elevation due to lake level are large (Figure 20B), but groundwater-wetland connectivity across all conditions is limited due to high relief (Figure 21B, Figure A36B). Second is the significant coupling between lake elevations and terrestrial hydrology through regional climate processes. The Great Lakes are closely linked to the basin climate; changes to precipitation and ET are a strong control on lake levels, while moisture from the lakes provides a significant amount of precipitation over the basin's land area (Gronewold et al., 2016, Notaro et al., 2013). The results of Chapter 3 suggests that groundwater elevations and lake levels co-evolved during the simulation period. Thus, the impact of climate forcings on groundwater elevations and thus wetland connectivity cannot be completely separated from those directly controlled by the lakes. Further counterfactual model runs, such as those with varying lake levels but fixed climate, would be needed to fully attribute the changes in groundwater elevation and wetland connectivity to climate forcings and direct boundary condition effects of the lakes.

4.5 Sensitivity Analysis and Uncertainty

The uncertainty in groundwater elevations, inherited from uncertainty in the groundwater model structure, parameters, and forcing data affects estimates of GWC, as the absolute elevation of the head and wetland bottom are used to quantify connectivity. The median difference between simulated and observed heads within the coastal groundwater zone (Shown in Figure A37) is -0.81 m, indicating that on average, simulated groundwater elevations are below those observed within the coastal groundwater zone. Groundwater head elevations have a significant impact on the total amount of groundwater connected-wetland across the model period when varied. During the base model run, GWC within each month varied from ~55-90% of maximum connectivity (the amount of connected area if each model cells were at its maximum elevation). Varying the monthly head grids from the base scenario by +/- 0.5 m, 0.3 m and 0.1 m, and the median simulated-observed head difference of 0.81 resulted in GWC which ranged between ~40-140% of maximum GWC

during the base run, shown in Figure 22. In addition to changing absolute area connected, changing heads also altered the amount of variability during the model simulation. Relative to GWC at maximum heads in the base run, the proportion of GWC varied by 21.5% when heads were decreased by 0. 5m, and 50.4% when heads were increased by 0.5 m. Increasing the minimum and maximum heads by the median simulated-observed head difference in the coastal zone increases GWC by 78.1% at minimum head and 62.4% at maximum. These differences are greatest where groundwater head elevations are near the surface, such as along the Lake Huron coastline in the LP and the Michigan-Huron coastline in the UP, as shown in Figure A38.

This approach gives some indication of the sensitivity of wetland connectivity to heads, however it oversimplifies the model error in heads in two ways. First, while the median error in heads is -0.81 m, this error is not evenly distributed across the coastal region. Some areas have a bias toward underprediction, such as along much of the Lake Michigan coastline, while other areas are generally overpredicted, such as in Saginaw Bay and Lake St. Clair and Erie shorelines (Figure A38). Second, addressing this error in the groundwater model would require, at minimum, adjusting model parameters such as hydraulic conductivity. Applying such changes to the model would result in a significantly more complex response in head than raising or lowering elevations uniformly across the grid. Continued refinement of the groundwater model, and a model based sensitivity analysis, would improve estimates of groundwater connectivity to wetlands and better constrain uncertainty.

Assessing surface and groundwater connectivity change at the 3DEP DEM scale changed both estimates of connected area and the relative amount of connectivity change. Table A13 compares the GWC and SWC area at minimum and maximum water levels, as well as the change in GWC and SWC area, when assessed at the groundwater model resolution (500 m) and the DEM resolution (24.6 m). Analysis at the 500 m resolution shows an increase from low to high lake levels in SWC of 2.9 times totaling ~3,716 km^2, while analysis at the 24.6 m resolution indicates an increase of 3.8 times totaling 1462 km^2. For GWC, analysis at the 500 m resolution suggests an increase of 121% totaling 635 km^2, while analysis at the 24.6 m resolution showed an increase of 60.8% totaling 216 km^2. Both analyses however support increases in GWC areas beyond those connected to surface waters when lake levels and groundwater elevations increase between 2000-2023. The differences in area are the result of the considerable scale differences between the groundwater model resolution and that of the wetland and DEM products. The coarser cell

resolution therefore overestimates both the amount of area connected, and the amount of change in connected area that occurs due to changing groundwater levels. The considerably larger size of the high resolution datasets however require more time and computational resources to process, especially for the analysis of the change in connectivity through time and sensitivity analysis. The overestimation of wetland area and connectivity when assed at the groundwater model resolution could be addressed in three ways. First, estimates of connected wetland area could be scaled by the fraction of wetland area within each groundwater model cell. Second, the workflow for analyzing wetland connectivity at the DEM resolution could be refined to improve efficiency in processing and analyzing the high resolution datasets through the use of parallel processing tools for python such as Dask (Dask Development Team, 2016). Third, a smaller portion of the model domain could be selected, either for post-processing and analysis at higher resolution, or for the construction of a higher resolution inset model.

In addition to the uncertainty in modeled heads, and those introduced by the scale of this analysis, the wetland location and depths are also uncertain. Wetland locations and types from the NWI are the highest quality wetland data available across the United States. Both coastal wetland and the included palustrine wetlands are connected to either surface water, groundwater or both (Cowardin et al., 1979, Crowe and Shikaze, 2004). When and how often these wetlands are inundated by surface or groundwater, and their detailed morphology (e.g. depth) are largely unknown however. A combination of increased field data collection and novel remote sensing analysis, however, can constrain these attributes. For example, the Great Lakes Coastal Wetland Monitoring Program has, since the early 2010's, taken physical measurements of wetland morphology and ecology at over 1000 coastal wetland locations across the Great Lakes Basin (Uzarski et al., 2019). Incorporation of this data, and collection of similar data for coastal palustrine wetlands, would bridge the gap between highly localized (e.g. within wetland) investigations (Crowe and Shikaze, 2004) and those derived from the regional groundwater modeling insights such as are presented here. Remotely sensed estimates of surface water extent, derived through a combination of optical and infrared radar data, have the potential to map the presence and temporal occurrence of surface water in wetlands. For example, the Observational Products for End-Users from Remote Sensing Analysis (OPERA) project lead by the NASA Jet Propulsion Laboratory (JPL) has developed maps of surface water inundation extent at 30m resolution using Sentinel-1, NISAR, and Harmonized Landsat Sentinel-2 (HLS) data (OPERA, 2024). This product could be

used to identify the presence of surface water inundation in the NWI wetlands, which would indicate connectivity to surface water and/or groundwater, and used as validation data for the groundwater model derived estimates of connectivity presented here.

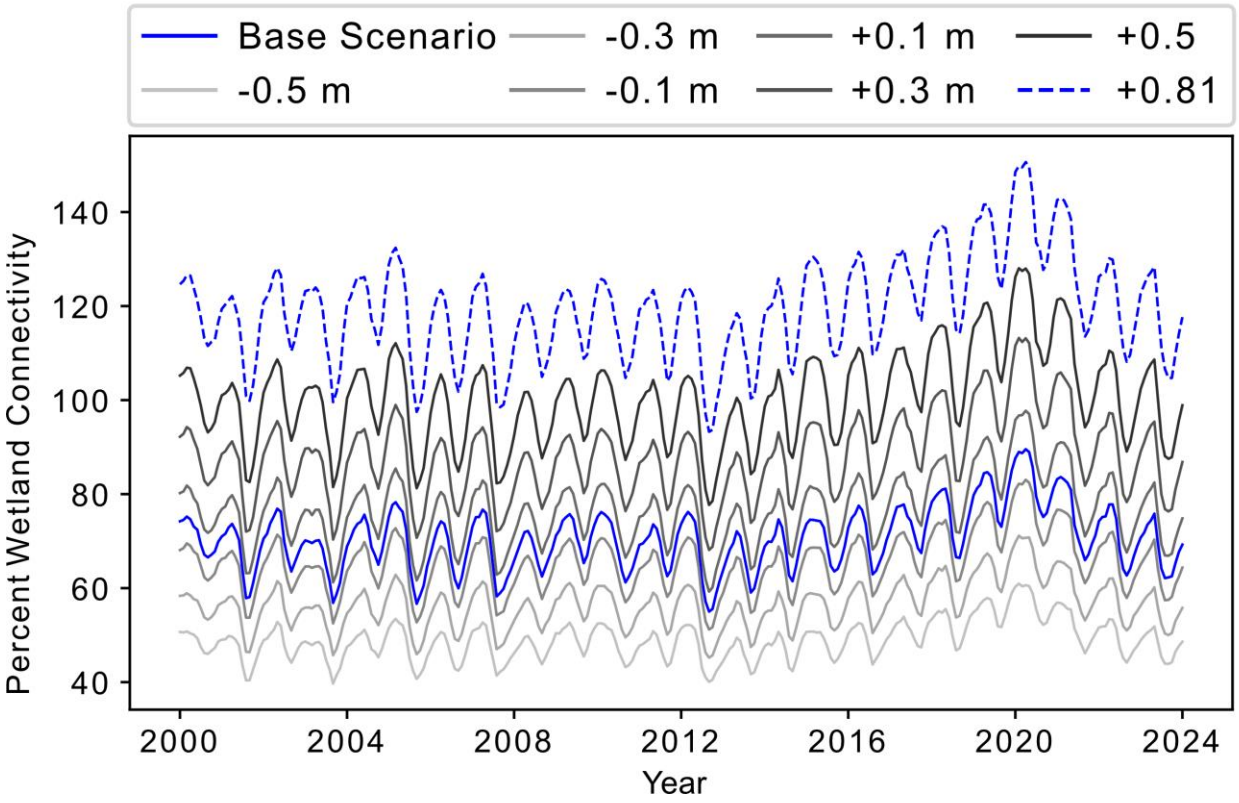

Figure 22: Sensitivity of Groundwater-Coastal Wetland Connectivity to Simulated Head Elevation. Head elevation is a strong control on the absolute amount of wetland area connected to groundwater. Sensitivity of wetland connectivity to head elevations, shown as a percent of the area connected to groundwater at maximum heads in the base scenario (shown in the solid blue line), for a range of adjustments in head (shown in the grey lines). These values, ranging from -0.5m to +0.5m were added uniformly to the base scenario head grids, before computing connectivity with the adjusted head for each time step. The dashed blue line represents connectivity when heads are adjusted by the median error in the coastal groundwater, where heads were a median of 0.81m lower than observed heads. Head elevations also affected the degree of variability over the model period; connectivity varied by 34.6% in the base run, 21.5% when heads were decreased by 0.5 m and 50.4% when heads were increased by 0.5

5. Conclusions

This groundwater modeling analysis indicates a dynamic and direct connection between the Great Lakes and the associated groundwater system. This direct connection is evident by the simulated discharge of groundwater into the lakes, and the effects and the boundary condition

effects of lake levels on coastal zone groundwater elevations. Groundwater is directly discharged into the lakes though a 10 km buffer around the shoreline over the entire model period at rates ranging from 82.1 to 2,398 m^3/s, however this discharge is primarily concentrated alone the shoreline. The observed lake elevation changes have the potential to alter groundwater elevations between 1 cm to 1.9 m in a zone of "coastal groundwater" ranging between 500 m and ~20 km inland. Within this zone, groundwater connectivity to coastal wetlands increased by 120.9% when heads rose from their minima to maxima between 2000 and 2023.

When combined with estimates of surface water connectivity between low and high lake elevations over the same period, a total of ~2,323 km^2 became connected to ground or surface water with 18.2% of this increase in connected area due to groundwater alone. These results highlight the close connection between groundwater elevation and lake levels, and the potential effects of groundwater elevations on connectivity in Great Lakes coastal wetlands. Improved and refined modeling approaches, continued field data collection and integration of remoting sensing data are required to better understand the connectivity of groundwater to Great Lakes coastal wetlands. This improved understanding is critical to protect the important ecosystem services provide by Great Lakes coastal wetlands given projections of continued climate and lake level variability within the Great Lakes (Kayastha et al., 2022).

Acknowledgements

I would first like to acknowledge Anthony Kendall for his co-development of the LHM Michigan Model, and Dave Hyndman for his input doing the model development process. I would like to acknowledge Laura Bourgeau-Chavez, Mary Ellen Miller, Michael Battaglia for sharing the MTRI Wetland Inundation Product and for their discussions about coastal wetland interactions with the Great Lakes. I would like to acknowledge the National Science Foundation (NSF) Frontier Research in Earth Science (FRES) Grant #2218028 for funding support. Finally I would like to acknowledge Alex Kuhl who provided feedback on an early version of this chapter.

REFERENCES

Albert, D.A., Wilcox, D.A., Ingram, J.W., Thompson, T.A., 2005. Hydrogeomorphic Classification for Great Lakes Coastal Wetlands. J. Gt. Lakes Res. 31, 129–146. https://doi.org/10.1016/s0380-1330(05)70294-x

Andresen, J.A., 2012. Historical Climate Trends in Michigan and the Great Lakes Region, in: Dietz, T., Bidwell, D. (Eds.), Climate Change in the Great Lakes Region: Navigating an Uncertain Future. Michigan State University Press, East Lansing, Michigan, pp. 17–34.

Anderson, O., Harrison, A., Heumann, B., Godwin, C., Uzarski, D., 2023. The influence of extreme water levels on coastal wetland extent across the Laurentian Great Lakes. Sci. Total Environ. 885, 163755. https://doi.org/10.1016/j.scitotenv.2023.163755

Armstrong, W., Brandle, R., Jackson, M.B., 1994. Mechanisms of flood tolerance in plants. Acta Bot. Neerlandica 43, 307–358. https://doi.org/10.1111/j.1438-8677.1994.tb00756.x

Bakker, M., Post, V., Langevin, C.D., Hughes, J.D., White, J.T., Starn, J.J., Fienen, M.N., 2016. Scripting MODFLOW Model Development Using Python and FloPy. Groundwater 54, 733–739. https://doi.org/10.1111/gwat.12413

Befus, K.M., Barnard, P.L., Hoover, D.J., Hart, J.A.F., Voss, C.I., 2020. Increasing threat of coastal groundwater hazards from sea-level rise in California. Nat. Clim. Chang. 10, 946–952. https://doi.org/10.1038/s41558-020-0874-1

Bjerklie, D.M., Mullaney, J.R., Stone, J.R., Skinner, B.J., Ramlow, M.A., 2012. Preliminary investigation of the effects of sea-level rise on groundwater levels in New Haven, Connecticut, Open-File Report 2012–1025.

Bourgeau-Chavez, L., Endres, S., Battaglia, M., Miller, M.E., Banda, E., Laubach, Z., Higman, P., Chow-Fraser, P., Marcaccio, J., 2015. Development of a Bi-National Great Lakes Coastal Wetland and Land Use Map Using Three-Season PALSAR and Landsat Imagery. Remote Sens. 7, 8655–8682. https://doi.org/10.3390/rs70708655

Cowardin, L. M., V. Carter, F. C. Golet, and E. T. LaRoe. 1979. Classification of wetlands and deepwater habitats of the United States. U.S. Fish and Wildlife Service. FWS/OBS-79/31. Washington, DC

Crowe, A.S., Shikaze, S.G., 2004. Linkages between groundwater and coastal wetlands of the Laurentian Great Lakes. Aquat. Ecosyst. Heal. Manag. 7, 199–213. https://doi.org/10.1080/14634980490461560

Dask Development Team (2016). Dask: Library for dynamic task scheduling http://dask.pydata.org

Dietrich, R.V., 1983. The Geology of Michigan. Rocks Miner. 58, 99–106. https://doi.org/10.1080/00357529.1983.11767127

Doss, P.K., 1993. The nature of a dynamic water table in a system of non-tidal, freshwater coastal wetlands. J. Hydrol. 141, 107–126. https://doi.org/10.1016/0022-1694(93)90046-c

Egan, D., 2021. A battle between a great city and a great lake. *New York Times*. https://www.nytimes.com/interactive/2021/07/07/climate/chicago-river-lake-michigan.html

ESRI. 2023. ArcGIS Pro (3.1.4). Environmental Systems Research Institute. https://www.esri.com/en-us/arcgis/products/arcgis-pro

Fan, Y., Miguez-Macho, G., Jobbágy, E.G., Jackson, R.B., Otero-Casal, C., 2017. Hydrologic regulation of plant rooting depth. Proc. Natl. Acad. Sci. 114, 10572–10577. https://doi.org/10.1073/pnas.1712381114

Farrand, W.R., Mickelson, D.M., Cowan, W.R., Goebel, J.E., Richmond, G.M., and Fullerton, D.S., 1984. Quaternary geologic map of the Lake Superior 4 degrees x 6 degrees quadrangle, United States and Canada. U.S. Geological Survey Miscellaneous Investigations Series Map I-1420(NL-16). https://doi.org/10.3133/i1420(NL16)

Federal Geographic Data Committee. 2013. Classification of wetlands and deepwater habitats of the United States. FGDC-STD-004-2013. Second Edition. Wetlands Subcommittee, Federal Geographic Data Committee and U.S. Fish and Wildlife Service, Washington, DC.

Fullerton, D.S., Cowan, W.R., Savon, W.D., Goldthwait, R.P., Ferrand, W.R., Muller, E.H., Bahling, R.E., Stravers, J.A., and Richmond, G.M., 1991. Quaternary geologic map of the Lake Erie 4 degrees x 6 degrees quadrangle, United States and Canada. u.S. Geological Survey Miscellaneous Investigations Series Map I-1420(NK-17). https://doi.org/10.3133/i1420(NK17)

Feinstein, D.T., Hunt, R.J., Reeves, H.W., 2010. Regional groundwater-flow model of the Lake Michigan Basin in support of Great Lakes Basin water availability and use studies, Scientific Investigations Report 2010-5109. U.S. Geological Survey.

Gillies and others, 2019. Rasterio: geospatial raster I/O for Python programmers. https://github.com/rasterio/rasterio

Goebel, J.E., Mickelson, D.M., Ferrand, W.R., Clayton, Lee, Knox, J.C., Cahow, Adam, Hobbs, H.C., Walton, M.S., Richmond, G.M., and Fullerton, D.S., 1983. Quaternary geologic map of the Minneapolis 4 degrees x 6 degrees quadrangle, United States. U.S. Geological Survey Miscellaneous Investigations Series Map I-1420(NL-15). https://doi.org/10.3133/i1420(NL15)

Goslee, S.C., Brooks, R.P., Cole, C.A., 1997. Plants as indicators of wetland water source. Plant Ecol. 131, 199–206. https://doi.org/10.1023/a:1009731904915

Gronewold, A.D., Bruxer, J., Durnford, D., Smith, J.P., Clites, A.H., Seglenieks, F., Qian, S.S., Hunter, T.S., Fortin, V., 2016. Hydrological drivers of record-setting water level rise on Earth's largest lake system. Water Resour Res 52, 4026–4042. https://doi.org/10.1002/2015wr018209

Gronewold, A.D., Fortin, V., Lofgren, B., Clites, A., Stow, C.A., Quinn, F., 2013. Coasts, water levels, and climate change: A Great Lakes perspective. Climatic Change 120, 697–711. https://doi.org/10.1007/s10584-013-0840-2

Gronewold, A.D., Rood, R.B., 2019. Recent water level changes across Earth's largest lake system and implications for future variability. J Great Lakes Res 45, 1–3. https://doi.org/10.1016/j.jglr.2018.10.012

Gronewold, A.D., Stow, C.A., 2014. Unprecedented Seasonal Water Level Dynamics on One of the Earth's Largest Lakes. Bull. Am. Meteorol. Soc. 95, 15–17. https://doi.org/10.1175/bams-d-12-00194.1

Harbaugh, A.W., 2005. MODFLOW-2005: the U.S. Geological Survey modular ground-water model--the ground-water flow process, Techniques and Methods 6-A16. U.S. Geological Survey, Reston, Va. https://doi.org/10.3133/tm6A16

Harris, C.R., Millman, K.J., Walt, S.J. van der, Gommers, R., Virtanen, P., Cournapeau, D., Wieser, E., Taylor, J., Berg, S., Smith, N.J., Kern, R., Picus, M., Hoyer, S., Kerkwijk, M.H. van, Brett, M., Haldane, A., Río, J.F. del, Wiebe, M., Peterson, P., Gérard-Marchant, P., Sheppard, K., Reddy, T., Weckesser, W., Abbasi, H., Gohlke, C., Oliphant, T.E., 2020. Array programming with NumPy. Nature 585, 357–362. https://doi.org/10.1038/s41586-020-2649-2

Hoyer, S., Hamman, J., 2016. xarray: N-D labeled Arrays and Datasets in Python. J. Open Res. Softw. 5, 10. https://doi.org/10.5334/jors.148

Kayastha, M.B., Ye, X., Huang, C., Xue, P., 2022. Future rise of the Great Lakes water levels under climate change. J Hydrol 612, 128205. https://doi.org/10.1016/j.jhydrol.2022.128205

Keddy, P.A., Reznicek, A.A., 1986. Great Lakes Vegetation Dynamics: The Role of Fluctuating Water Levels and Buried Seeds. J. Gt. Lakes Res. 12, 25–36. https://doi.org/10.1016/s0380-1330(86)71697-3

Keough, J.R., Thompson, T.A., Guntenspergen, G.R., Wilcox, D.A., 1999. Hydrogeomorphic factors and ecosystem responses in coastal wetlands of the Great Lakes. Wetlands 19, 821–834. https://doi.org/10.1007/bf03161786

Larson, G., Schaetzl, R., 2001. Origin and Evolution of the Great Lakes. J Great Lakes Res 27, 518–546. https://doi.org/10.1016/s0380-1330(01)70665-x

Lineback, J.A., Bleuer, N.K., Mickelson, D.M., Ferrand, W.R., Goldthwait, R.P., Richmond, G.M., and Fullerton, D.S, 1983. Quaternary geologic map of the Chicago 4 degrees x 6

degrees quadrangle, United States. U.S. Geological Survey Miscellaneous Investigations Series Map I-1420(NK-16). https://doi.org/10.3133/i1420(NK16)

Lowry, C.S., Loheide, S.P., 2010. Groundwater-dependent vegetation: Quantifying the groundwater subsidy. Water Resour. Res. 46. https://doi.org/10.1029/2009wr008874

Mathney, K. 2020. Record-high Michigan water levels are a nightmare for homeowners, state. Detroit Free Press. https://www.freep.com/story/news/local/michigan/2020/07/17/great-lakes-water-levels-records-erosion-damage/5450910002/

MathWorks Inc. (2021). MATLAB version: 9.11.0 (R2021b), Natick, Massachusetts: The MathWorks Inc. https://www.mathworks.com

Maynard, L., Wilcox, D.A., 1997. Coastal Wetlands, State of the Lakes Ecosystem Conference.

Miller, M.E.,Bourgeau-Chavez, L.L., Battaglia,M. Colin, B. and Meadows, G. *in prep.* Modeling hydrological connectivity in coastal wetlands of the Laurentian Great Lakes. *Journal of Great Lakes Research.*

Milstein, R.L., 1987, Bedrock geology of southern Michigan: Michigan Department of Natural Resources, Geological Survey Division, Geological Publication BG-01. https://ngmdb.usgs.gov/Prodesc/proddesc_71887.htm

National Oceanographic and Atmospheric Administration (NOAA), 2025. Shoreline Mileage Of the United States https://coast.noaa.gov/data/docs/states/shorelines.pdf

Notaro, M., Holman, K., Zarrin, A., Fluck, E., Vavrus, S., Bennington, V., 2013. Influence of the Laurentian Great Lakes on Regional Climate*. J. Clim. 26, 789–804. https://doi.org/10.1175/jcli-d-12-00140.1

OPERA. (2024). OPERA dynamic surface water extent from harmonized Landsat Sentinel-2 provisional product (version 0). Ver. 1.0 [Dataset]. DPO.DAAC, CA, USA. https://doi.org/10.5067/OPDSW-PL3V0

Reed, R.C., and Daniels, Jennifer, 1987, Bedrock geology of northern Michigan: Michigan Department of Natural Resources, Geological Survey Division, Geological Publication BG-01. https://ngmdb.usgs.gov/Prodesc/proddesc_71888.htm

Restif, O., Hayman, D.T.S., Pulliam, J.R.C., Plowright, R.K., George, D.B., Luis, A.D., Cunningham, A.A., Bowen, R.A., Fooks, A.R., O'Shea, T.J., Wood, J.L.N., Webb, C.T., 2012. Model-guided fieldwork: practical guidelines for multidisciplinary research on wildlife ecological and epidemiological dynamics. Ecol. Lett. 15, 1083–1094. https://doi.org/10.1111/j.1461-0248.2012.01836.x

Rotzoll, K., Fletcher, C.H., 2013. Assessment of groundwater inundation as a consequence of sea-level rise. Nat. Clim. Chang. 3, 477–481. https://doi.org/10.1038/nclimate1725

Sado, E.V., Fullerton, D.S., Baker, C.L., and Farrand, W.R., 1993. Quaternary geologic map of the Sudbury 4 degrees x 6 degrees quadrangle, United States and Canada (revised, 2002). U.S. Geological Survey Miscellaneous Investigations Series Map I-1420(NL-17). https://doi.org/10.3133/i1420(NL17)

Sierszen, M.E., Morrice, J.A., Trebitz, A.S., Hoffman, J.C., 2012. A review of selected ecosystem services provided by coastal wetlands of the Laurentian Great Lakes. Aquat. Ecosyst. Heal. Manag. 15, 92–106. https://doi.org/10.1080/14634988.2011.624970

Theuerkauf, E.J., Braun, K.N., 2021. Rapid water level rise drives unprecedented coastal habitat loss along the Great Lakes of North America. J Great Lakes Res 47, 945–954. https://doi.org/10.1016/j.jglr.2021.05.004

United States Geological Survey (USGS). 2020. National Hydrography Dataset (ver. USGS National Hydrography in FileGDB 10.1 format (published 20201127)) Accessed 2020-12-19

United States Geological Survey (USGS). 2023. 1/3rd arc-second Digital Elevation Models (DEMs) - USGS National Map 3DEP Downloadable Data Collection. U.S. Geological Survey. https://apps.nationalmap.gov/downloader/ Accessed 2023-04-19

United States Fish & Wildlife Service (USFWS) (2018). National Wetlands Inventory. U.S. Fish & Wildlife Service. https://data.nal.usda.gov/dataset/national-wetlands-inventory. Accessed 2023-10-4.

United States Department of Agriculture (USDA) Soil Survey Staff, 2016. Gridded Soil Survey Geographic (gSSURGO) Database for the Conterminous United States. United States Department of Agriculture, Natural Resources Conservation Service. Available online at https://gdg.sc.egov.usda.gov/. Accessed 2023-10-8

Uzarski, D.G., Wilcox, D.A., Brady, V.J., Cooper, M.J., Albert, D.A., Ciborowski, J.J.H., Danz, N.P., Garwood, A., Gathman, J.P., Gehring, T.M., Grabas, G.P., Howe, R.W., Johnson, L.B., Lamberti, G.A., Moerke, A.H., Niemi, G.J., Redder, T., III, C.R.R., Steinman, A.D., Tozer, D.C., O'Donnell, T.K., 2019. Leveraging a Landscape-Level Monitoring and Assessment Program for Developing Resilient Shorelines throughout the Laurentian Great Lakes. Wetlands 39, 1357–1366. https://doi.org/10.1007/s13157-019-01139-w

Westjohn, D.B., Weaver, T.L., 1998. Hydrogeologic framework of the Michigan Basin regional aquifer system (USGS Numbered Series), Professional Paper 1418. U.S. Geological Survey, Denver, CO.

Xu, S., Frey, S.K., Erler, A.R., Khader, O., Berg, S.J., Hwang, H.T., Callaghan, M.V., Davison, J.H., Sudicky, E.A., 2021. Investigating groundwater-lake interactions in the Laurentian Great Lakes with a fully-integrated surface water-groundwater model. J Hydrol 594, 125911. https://doi.org/10.1016/j.jhydrol.2020.125911

Zipper, S.C., Soylu, M.E., Booth, E.G., Loheide, S.P., 2015. Untangling the effects of shallow groundwater and soil texture as drivers of subfield-scale yield variability. Water Resour. Res. 51, 6338–6358. https://doi.org/10.1002/2015wr017522

CHAPTER 5: SUMMARY AND FUTURE WORK

5.1 Conclusions

This dissertation seeks to integrate field data and hydrologic models to better understand water quality and water resources across and within the Great Lakes Basin, focusing specifically on the state of Michigan region. Both the field study presented in Chapter 2, and the modeling analysis presented in Chapters 3 and 4, indicate the importance of groundwater and its interactions with surface water for water resources within the Great Lakes. While groundwater has been long considered an important resource for the region, the works presented herein advance our knowledge of surface and groundwaters coupling in the state of Michigan.

In Chapter 2, a straightforward linear modeling analysis of water quality data collected across Michigan's Lower Peninsula demonstrates seasonal variability in both stream nutrient concentrations and their relationships to landscape conditions. Stream nutrient concentrations were most strongly correlated to land use and land cover during spring snowmelt, moderately correlated during summer rainfall and least correlated during fall baseflows. The degradation in model performance across the sampling events suggests progressive decoupling of stream chemistry from landscape conditions as the seasons progress. This decoupling is attributed to changes in runoff processes, nutrient availability, and nutrient cycling throughout the year. Baseflow-normalized concentrations show distinct responses of nutrient concentrations to high flows during spring snowmelt versus summer rainfall. These results suggest different nutrient availability and streamflow sources, or a combination of both, during the two high flow events. Collectively, the results of this study demonstrate the considerable seasonality of nutrient concentrations in streams across Michigan's Lower Peninsula, and that static landscape characteristics alone are insufficient to explain this variability.

Chapter 3 describes the development of a coupled surface and groundwater hydrologic model for the state of Michigan region between 2000-2023, and its use to characterize changes in groundwater elevation during a period where the Great Lakes rose from record low to record high lake elevations. Development of this model required the addition of new physical processes in the Landscape Hydrology Model in order to simulate the highly variable hydrogeologic landscape within the model region. Model results indicate groundwater storage increases which mirror, but lag 2-4 years behind, increases in lake elevation. These changes in groundwater storage were shown to be the result of increased precipitation and decreased evaporation, the onset of which

occurred between 2015-2017.

This modeling framework was then used in Chapter 4 to investigate relationships between lake levels, groundwater elevations and coastal wetland connectivity. Modeling results show that groundwater is continually discharged to the lake through the near shore region, and changes to lake elevation have the potential to significantly alter coastal groundwater elevations. Comparing simulated heads to estimated coastal wetland bottom elevations suggest the amount of coastal wetland area connected to groundwater increases by approximately 120% when heads rise from their minimum to maximum conditions. Estimates of coastal wetland connectivity change between low and high water levels are 18% greater when groundwater is considered, compared to estimates of this change derived from remotely sensed surface water connectivity alone. The amount of groundwater-connected wetland area however, is sensitive to the groundwater elevations, which are underestimated relative to observations by a median of 0.81 m within the coastal region.

Water resources in the Great Lakes Basin are threatened by changing climate, landscape and water use demands. In order to properly manage the region's water resources, models capable of predicting how these changes will propagate through the hydrologic system are necessary. Such models are also needed to predict how these changes will impact important ecosystem services such as coldwater fish habitat provided by groundwater-fed streams, and nutrient cycling within groundwater-connected wetlands. Field data are an important component of model construction, calibration and validation. Close integration of existing and newly collected field data with hydrologic models is a critical step toward developing the tools needed to protect water resources in the Great Lakes region.

5.2 Limitations

While the works presented in Chapters 2-4 have advanced the understanding of processes driving water quality and groundwater connectivity across the Michigan Region, each has its own inherent limitations. In Chapter 2, the long delay between data collection (2011-2012) and data analysis (2020-2023) presented challenges in properly analyzing and interpreting the data. While this dataset was a unique look at seasonal water quality at a regional scale, there were likely subtle details overlooked due to this long delay. The patterns observed in Chapter 2 should also be compared, to the extent possible, with similar analysis done on long term discrete or continuous water quality samples. The same analysis used in Chapter 2 should be applied to data from the USGS WQX portal or state agencies. Finally, while the hydrologic interpretation of the data in

Chapter 2 is sound, it is largely circumstantial, and based on a first principals understanding of regional groundwater and streamflow processes. To constrain the influence of streamflow generation processes on water quality, additional field data and/or model derived processes representations are required. The addition of tracers such as isotopes or age tracers could help constrain the sources of streamflow in future synoptic water quality datasets. Estimates of streamflow processes from a calibrated surface and groundwater model could also provide greater context for how seasonally variable runoff process affect water chemistry.

Chapters 3 and 4 both rely on the coupled surface and groundwater model developed for the state of Michigan region. The development of a process-based, coupled surface and groundwater model for the regional is novel, especially given its use to investigate changes to groundwater storage and wetland connectivity. Improvements to the existing model however could provide significant value in improving both model performance and system interpretation. An improved unsaturated zone model, either between LHM's surface model and MODLFOW or through the use of the MODFLOW UZF package, would likely improve estimates of recharge or soil moisture. The current unsaturated zone representation is a simple linear time delay function, and likely oversimplifies the timing of moisture pulses though the unsaturated zone and of their delivery to the water table as recharge. Because the surface and groundwater model are offline coupled, and vadose zone simulation occurs before MODLFOW, the model is not currently capable of representing saturation excess overland flow. This process may be important for properly simulating peak streamflows, especially in areas with shallow water tables. A more robust, systematic, and automated calibration approach is also needed. The current calibration approach presented in Chapter 2 was sufficient for an initial analysis. Significant improvements are needed however, to better match observed streamflows and groundwater heads across the region. In certain areas, a more powerful calibration routine may not be enough. For example in the thick glaciated sediments of the northern Lower Peninsula where underestimation in heads in currently greatest, the subsurface geology conceptual model may need to be updated. This could include the addition of one or two layers to the model, which could be used to represent discontinuous confining units within the glacial sediments.

Specific to Chapter 4, uncertainty in simulated groundwater elevations and the prescribed wetlands depths complicate the ability to make accurate assessments of wetland connectivity to groundwaters. As is discussed above, a more robust calibration is needed to improve estimates of

groundwater elevation. This is a primary control on its connectivity with surface waters, along with the permeability of the sediments within the bed of the surface water feature. While spatially explicit maps of wetland location exist, the estimates of wetland depth are rudimentary at best. A combination of fieldwork and novel remote sensing to constrain wetland depths and inundation would aid in improving repetition of coastal and palustrine wetlands at the regional scale. Collection of novel field data, integration of new remotely sensed datasets, refinement of model process representation and more robust calibration of the hydrologic model would help to address limitations across all three research chapters presented in this dissertation.

5.3 Future Work

Building off of the work presented in Chapters 2, 3 and 4, there is an opportunity to leverage a Model-Experiment (ModEx) framework to enhance both our understanding of the controls on stream water quality, and the performance of regional scale hydrologic models. The ModEx framework (illustrated in Figure 23) consists of using existing field data to help construct, parameterize and calibrate a model, and then using the model to help design new field data collection efforts or experiments (e.g. Restif et al., 2012). Using models to help inform field data collection has also been implemented though the data worth approach (e.g. Neuman et al., 2012) where model parameter estimation can be used to identify where additional field data would provide the greatest value to improving model calibration. While the data worth approach is focused on improving model performance, the ModEx approach can be used to design experiments which also improve conceptual models or address specific hypotheses. Bridging the themes presented in Chapter 2 with those presented in Chapters 3 and 4, there is an exciting opportunity to apply the regional modeling framework presented here studying changes to stream chemistry within the Great Lakes region using a ModEx approach. Specifically, though the use of additional modeling tools and water chemistry observations, this approach can be applied to better understanding the role of legacy nutrients transported by groundwater to determine current stream nutrient concentrations.

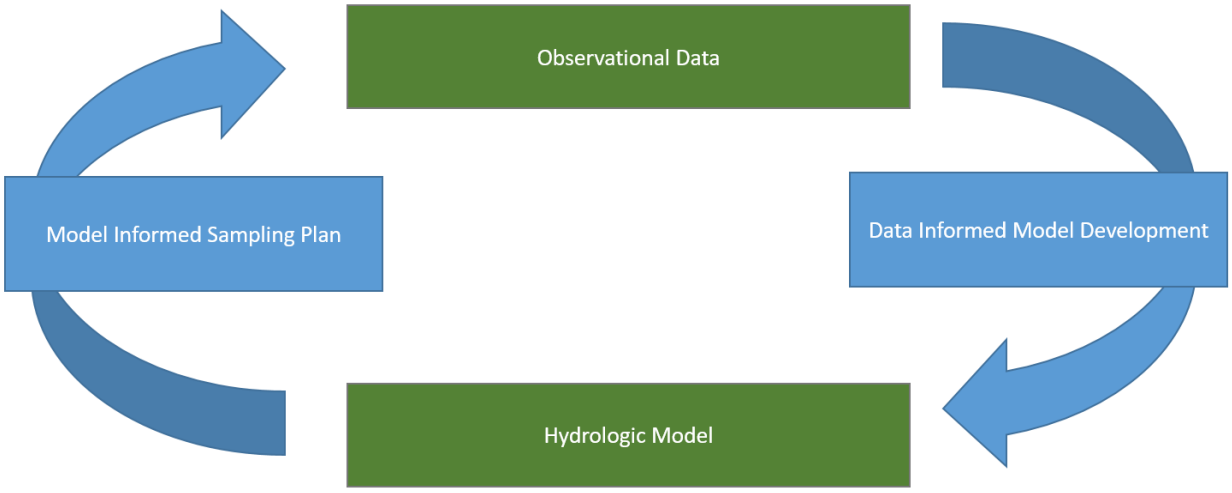

Figure 23: ModEx Framework for Hydrologic Model-Field Data Integration. Illustration of the model-experiment framework for field data collection: a model is developed using existing observation data for parameterization, calibration and validation. The model is then used to assess potential locations for future sample collection efforts that will either increase process knowledge, model performance or both.

Human activates have released nitrogen and phosphorus into the environment far in excess of natural conditions (Byrnes et al., 2020, Hamlin et al., 2020), overwhelming natural nutrient cycles (Vitousek et al., 2009), and contaminating water resources globally (Vörösmarty et al., 2010). The primary sources of these anthropogenic nutrients are agricultural fertilizers and wastewater management (Byrnes et al., 2020, Hamlin et al., 2020). The buildup of anthropogenic nutrients has resulted in eutrophication and harmful algal blooms (Ho and Michalak, 2015, Rabalais et al., 2002); contributed to the spread of invasive species (Hannah et al., 2020); and threatened drinking water resources (Hamlin et al., 2022). Once released to the environment, nutrients can be can be taken up by plants, stored in the soil zone, transported by runoff to surface waters or transported through the subsurface via soil moisture and groundwater (Wan et al., 2023). Nutrients can be transported from the uplands to streams and inland lakes by surface processes or tile drainage over the course of hours to months after their application. Delays between application and delivery are considerably longer for nutrients stored in the soil zone or transported via subsurface pathways, ranging from days to decades (Figure 24) (Ilampooranan et al., 2019, Martin et al., 2021). The delivery of these legacy nutrient can keep surface water nutrient concentrations high long after inputs to the land surface had decreased, impeding effective management (Van Meter et al., 2018, Van Meter et al., 2017).

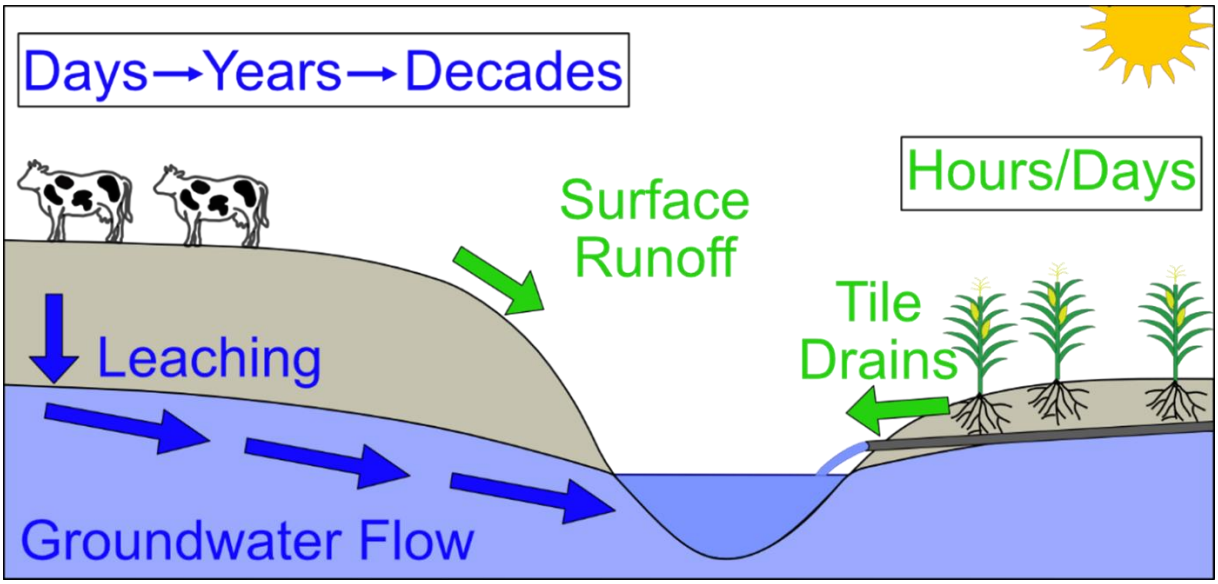

Figure 24: Groundwater Legacy Nuterint Conceptual Figure. A conceptual diagram showing the differences in resonance time for nutrients transported via surface/tile drainage and groundwater flow pathways. Nutrients transported via overland flow or tile drainage can reach surface waters within hours or days after their application or release from storage. Those transported by groundwater flowpaths can have significant delays of days to decades between release and delivery.

Most of the applied phosphorus not taken up by plants is transported via surface runoff, discharged to surface waters via tile drainage, or stored in the soil zone (Gentry et al., 2007 King et al., 2015). While nitrogen can also be transported by surface and tile drainage, large amounts, primarily in the form of nitrate, can be leached below the root zone and transported via subsurface flowpaths (Lin et al., 2019, Gentry et al., 1998, Wan et al., 2023). As such, nitrate transport via groundwater flow paths plays a considerable role in determining legacy nutrient additions to surface waters (Van Meter et al., 2016, Van Meter et al., 2017). While some denitrification can occur in oxic groundwater and in the hyporheic zone of streams (Lin et al., 2019, Juckem et al., 2024), nitrate is generally conservative during groundwater transport due to low dissolved organic carbon levels needed for microbial metabolism. Therefore, groundwater travel times are a strong control on the delivery of legacy nitrate to surface waters. Using a particle tracking model such as MODPATH, both the pathways by which water moves, and the time it takes to travel along these pathways can be simulated (Fienen et al., 2018, Juckem and Starn, 2021). MODPATH tracks groundwater flowpaths and transit times from the outputs of a MODFLOW groundwater flow model (Pollock, 2016). It has been previously used to simulate groundwater travel times at regional scales (Fienen et al., 2018), estimate nitrate delivery to wells (Juckem et al., 2024) and streams

(Moore et al., 2023).

By combining MODPATH with the existing MODFLOW model in a ModEx framework, hypotheses about groundwater nutrient transport can be tested while also improving the performance of groundwater flow and transport models. Due to the limited number of observations, aquifer properties such as hydraulic conductivity are often lumped into zones (i.e. geologic units) or distributed across the domain (i.e. interpolated) often using multiple realizations (Fienen et al., 2009). In either case, due to the relatively small number of parameter observations, significant calibration is required to produce simulations with performance fit to the models' purpose (Konikow and Mercer, 1988). Observations of groundwater elevations and stream baseflows are used to parameterize groundwater model inputs; modern parameter estimation tools like PEST have increased the power of these observational data (Doherty and Hunt, 2010, Hunt et al., 2020). When simulating solute transport or particle tracking in groundwater flow systems, additional subsurface characteristics including porosity are required (Pollock, 2016). This introduces another dimension of uncertainty into the modeling framework, but allows for calibration to water chemistry and age tracer data (Juckem and Starn, 2021). All field data are inherently uncertain, as are all environmental models (Bevin, 2005). The nature of groundwater modeling is especially uncertain, as widespread direct observations of the subsurface are impossible. While bore logs and pumping tests provide valuable information, these characterize only a very small portion of the subsurface (Anderson, Woessner and Hunt, 2015).

To achieve the goals of improving both numerical models and qualitative conceptualizations of the subsurface, a model-experiment framework based on the addition of a MODPATH simulation to the existing groundwater model described in Chapters 2 and 3 is proposed to study the effect of legacy nutrients on observed stream water chemistry in the Maumee and St. Joseph Watersheds (Figure 25). Such a framework can advanced the understanding of legacy nutrients in the southern Great Lakes region in two primary ways. First, existing water quality data can be combined with historical nitrogen application estimates and estimates of groundwater contributing areas and travel times from MODPATH. Second, the MODPATH modeling framework can be used to identify new sites for potential data collection that would capture a broader range of groundwater contributing areas and travel time distributions than existing data alone. This approach will allow us to learn what we can from existing data and increase the value of future data collection efforts. The Maumee and St. Joseph watersheds have

similar current land use and landscape nutrient input histories (Figure 25). However the hydrogeologic setting of these two watersheds is quite different. The St. Joseph is characterized by high permeability glacial materials such as outwash and sand, while the Maumee is dominated by much finer textured till and lacustrine deposits. As a result, hydraulic conductivity values estimated from well data are generally higher across watersheds within the St. Joseph than they are the Maumee (Figure 25). Performing the data analysis and model-experiment across these two watersheds will allow for the effects of subsurface conditions on groundwater nutrient legacies.

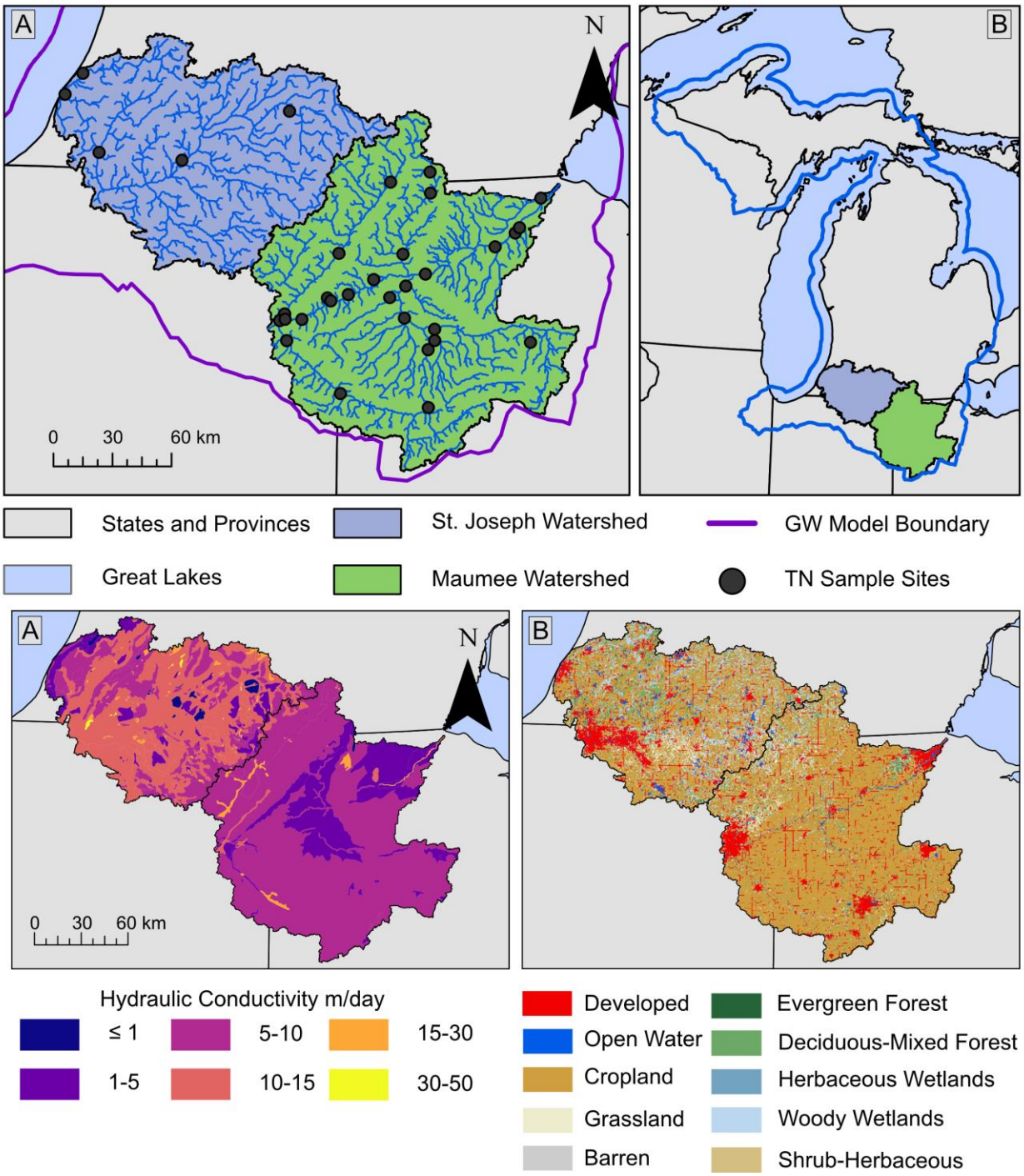

Figure 25: Model Informed Sampling Study Region. The Maumee and St. Joseph Watersheds (A) span southern Michigan, norther Indiana and Ohio, and are located at the southern extent of the Michigan Model domain. These two watersheds have similar land use (C), but the Maumee has generally lower hydraulic conductivity (D). Across the two watersheds there are 34 sites in the Water Quality Portal where TN has been sampled more than ten times. Nutrient data from these sites can serve as the basis for initial investigations into the relationships between historical N inputs, modeled groundwater travel times and observed stream chemistry.

In the first phase, existing water quality data will be collected from published databases of surface water chemistry, including the Water Quality Portal (https://www.waterqualitydata.us/) and the National Center for Water Quality Research Heidelberg Tributary Loading Program (HTLP) Dataset (NCWQR, 2022). These data will then be filtered to select sites with repeated data for nutrient data, specifically nitrate. At every sample point with sufficient data (e.g. greater than 10 samples), a groundwater contributing area will be delineated using MODPATH. First a surface watershed for the point will be generated, then the sample point surface watershed will be buffered and intersected with the groundwater model grid, and MDOPATH will with a particle in every cell within the buffered watershed. After particle tracking is performed with MODAPTH, the cells which terminate within the un-buffered surface watershed will be selected, and their starting points will be used to delineate a groundwatershed. Groundwater travel time distributions and historical nitrogen inputs from the TREND-Nitrogen dataset (Byrnes et al., 2020) within this groundwatershed will then be compared to observed surface water nitrate species concentrations to investigate relationships between historical inputs, groundwater travel time and observed stream chemistry. Optionally at this step, an inset of the existing groundwater model for the area of interest at higher spatial resolution could be developed.

In the second phase, the modeling-experiment framework can be applied to select new sample locations within the study watersheds which represent a large range of groundwater contributing areas, nutrient input histories and groundwater travel time distributions. First, possible sampling locations can be developed by identifying where streams can be accessed for sample collection, such as at road crossings (bridges), hiking trails, public easements, and established research sites which currently lack surface water nitrogen data. Existing sample points identified in phase one would be removed at this step. Second, the same approach for the established sites described above would be used to estimate groundwater contributing areas and travel times for all potential sites. Third, the list of potential new sample locations would be assessed to select a set of approximately 30 sites each in the St. Joseph and Maumee watersheds which would strengthen the data analysis described in Phase 1. A synoptic sampling approach will then be used to collect water chemistry data including ions and nitrogen species, along with groundwater and nitrogen age tracers across the selected sample location. Specifically, the collection of established groundwater age tracer tritium will be combined with the novel age tracer MESA (McCarty et al., 2014). Tritium is a radioisotope with a known release history in the atmosphere from nuclear

testing, which can be used to date relatively young groundwater (Beyer et al., 2014). MESA is an environmental degradation product of the herbicide Metolachlor, which is widely applied to agricultural fields around the same time as fertilizer. Importantly, a known shift in the ratios of the two Metolachlor isomers occurred in 1999 (Plummer et al., 2020). MESA also has similar conservative transport to nitrate in groundwater. As a result, MESA can be used to both indicate the presence of agricultural (vs. wastewater or other source) nitrogen, and to constrain the age of any observed agricultural nitrogen (Rice et al., 2016). While groundwater age tracers are traditionally sampled from groundwater wells, recent works have demonstrated that the sampling of groundwater age tracers from streams at low flow, does characterize the age of groundwater contributions to streamflow (Gilmore et al., 2016). Together the water chemistry data, isotope tracers and MESA data can be used to strengthen the performance and of the groundwater flow and particle tracking models. While this approach proposes a synoptic sampling event, the same model-experiment framework could be used to established new long term nutrient monitoring locations where legacy nitrogen is likely to affect future water quality.

The resulting dataset would provide valuable information on how groundwater legacy nitrate contributes to observed surface water nutrient concentrations. First, using the newly connected groundwater age tracers can help to further constrain modeled groundwater travel times. This should thus improve further analysis which incorporates groundwater travel times in assessing legacy nutrients. For example, comparing the observed water chemistry with historical landscape nutrient inputs (i.e. TREND-Nitrogen) and simulated groundwater travel time can help to reveal how legacy inputs are affecting current water quality. Specifically, this approach would allow for a better understanding of where in a given system legacy inputs where highest, where legacy nutrients have already been discharged from the system though quick flowpaths, and where slower flowpaths may continue to contribute legacy nitrogen. Better understanding both the current and historical contribution of anthropogenic nutrients to current water quality can aid in the development, selection and application of nutrient and water quality management practices.

In addition to the work proposed above, there are numerous other ways a model-experiment framework using the Michigan Model could be applied to advance our knowledge of the processed controlling groundwater/surface water interactions and increase model performance. Such a coupled surface and groundwater model could be used to explicitly simulate different streamflow generation processes including overland flow, throughflow, shallow groundwater flow and deep

groundwater flow. These model simulations could then be used to select sites where additional streamflow and water chemistry observations could be collected. These new streamflow estimates could then be used to identify which flowpaths contribute most to streamflow, and to the seasonal changes in water chemistry observed in Chapter 2. A similar approach could be used to study how inland lakes are responding to the same climate forcings which have driven the observed changed to Great Lakes levels and groundwater storage observed in Chapter 3.

The disciplines of water quality and hydrogeology are moving more and more toward bigger data and larger modeling domains. Continental to global scale models are becoming more and more common in hydrology, as so is the use of both unsupervised and physics-informed machine learning approaches. Such large scale models have been notoriously poor at simulating regional processes that can be critically import to the systems which they seek to represent. Continental models, for example, have struggled to represent both the lake-atmosphere feedbacks and importance of groundwater to regional hydrology within the Great Lakes region. These models do however provide a uniform basis for model development and interpretation across large areas. Developing approaches which more closely integrate insights from field observations to large scale physical and machine learning models may help to address the current shortcomings in these large scale models. Specifically, a diligent combination of process-based models developed at tractable scales, with field observation data which can improve and refine process representation, is required to develop the solutions to water resources and water quality challenges.

Acknowledgements

I would like to thank Anthony Kendall, Sherry Martin and Kimberly Van Meter for sharing their ideas with me on the approaches presented in the future work section of this chapter.

REFERENCES

Anderson, M. P., Woessner, W. W., & Hunt, R. J. (2015). Applied groundwater modeling: simulation of flow and advective transport. Academic press.

Beven, K., 2005. On the concept of model structural error. Water Sci. Technol. 52, 167–175. https://doi.org/10.2166/wst.2005.0165

Beyer, M., Morgenstern, U., Jackson, B., 2014. Review of techniques for dating young groundwater (<100 years) in New Zealand. J Hydrol 6, 226. https://doi.org/10.1016/0022-1694(68)90175-3

Byrnes, D.K., Meter, K.J.V., Basu, N.B., 2020. Long-Term Shifts in U.S. Nitrogen Sources and Sinks Revealed by the New TREND-Nitrogen Data Set (1930–2017). Global Biogeochem Cy 34. https://doi.org/10.1029/2020gb006626

Doherty, J.E., Hunt, R.J., 2010. Approaches to highly parameterized inversion-A guide to using PEST for groundwater-model calibration, Scientific Investigations Report 2010-5169. U.S. Geological Survey, Reston, Virginia.

Fienen, M.N., Muffels, C.T., Hunt, R.J., 2009. On Constraining Pilot Point Calibration with Regularization in PEST. Groundwater 47, 835–844. https://doi.org/10.1111/j.1745-6584.2009.00579.x

Fienen, M.N., Nolan, B.T., Kauffman, L.J., Feinstein, D.T., 2018. Metamodeling for Groundwater Age Forecasting in the Lake Michigan Basin. Water Resour Res 54, 4750–4766. https://doi.org/10.1029/2017wr022387

Gentry, L.E., David, M.B., Royer, T.V., Mitchell, C.A., Starks, K.M., 2007. Phosphorus Transport Pathways to Streams in Tile-Drained Agricultural Watersheds. J Environ Qual 36, 408–415. https://doi.org/10.2134/jeq2006.0098

Gentry, L.E., David, M.B., Smith, K.M., Kovacic, D.A., 1998. Nitrogen cycling and tile drainage nitrate loss in a corn/soybean watershed. Agric Ecosyst Environ 68, 85–97. https://doi.org/10.1016/s0167-8809(97)00139-4

Gilmore, T.E., Genereux, D.P., Solomon, D.K., Solder, J.E., 2016. Groundwater transit time distribution and mean from streambed sampling in an agricultural coastal plain watershed, North Carolina, USA. Water Resour Res 52, 2025–2044. https://doi.org/10.1002/2015wr017600

Hamlin, Q.F., Kendall, A.D., Martin, S.L., Whitenack, H.D., Roush, J.A., Hannah, B.A., Hyndman, D.W., 2020. Quantifying Landscape Nutrient Inputs With Spatially Explicit Nutrient Source Estimate Maps. J Geophys Res Biogeosciences 125. https://doi.org/10.1029/2019jg005134

Hamlin, Q.F., Martin, S.L., Kendall, A.D., Hyndman, D.W., 2022. Examining Relationships Between Groundwater Nitrate Concentrations in Drinking Water and Landscape

Characteristics to Understand Health Risks. Geohealth 6, e2021GH000524. https://doi.org/10.1029/2021gh000524

Hannah, B.A., Kendall, A.D., Martin, S.L., Hyndman, D.W., 2020. Quantifying linkages between watershed factors and coastal wetland plant invasion in the US Great Lakes. Landscape Ecol 35, 2843–2861. https://doi.org/10.1007/s10980-020-01124-3

Ho, J.C., Michalak, A.M., 2015. Challenges in tracking harmful algal blooms: A synthesis of evidence from Lake Erie. J Great Lakes Res 41, 317–325. https://doi.org/10.1016/j.jglr.2015.01.001

Hunt, R.J., Fienen, M.N., White, J.T., 2020. Revisiting "An Exercise in Groundwater Model Calibration and Prediction" After 30 Years: Insights and New Directions. Groundwater 58, 168–182. https://doi.org/10.1111/gwat.12907

Ilampooranan, I., Meter, K.J.V., Basu, N.B., 2019. A Race Against Time: Modeling Time Lags in Watershed Response. Water Resour Res 55, 3941–3959. https://doi.org/10.1029/2018wr023815

Juckem, P.F., Clark, B.R., Feinstein, D.T., 2017. Hydrogeology and simulation of ground-water flow in the Sandstone Aquifer, northeastern Wisconsin, Scientific Investigations Report 2017–5010. U.S. Geological Survey, Reston, Virginia.

Juckem, P.F., Corson-Dosch, N.T., Schachter, L.A., Green, C.T., Ferin, K.M., Booth, E.G., Kucharik, C.J., Austin, B.P., Kauffman, L.J., 2024. Design and calibration of a nitrate decision support tool for groundwater wells in Wisconsin, USA. Environ. Model. Softw. 176, 105999. https://doi.org/10.1016/j.envsoft.2024.105999

King, K.W., Williams, M.R., Macrae, M.L., Fausey, N.R., Frankenberger, J., Smith, D.R., Kleinman, P.J.A., Brown, L.C., 2015. Phosphorus Transport in Agricultural Subsurface Drainage: A Review. J Environ Qual 44, 467–485. https://doi.org/10.2134/jeq2014.04.0163

Konikow, L.F., Mercer, J.W., 1988. Groundwater flow and transport modeling. J. Hydrol. 100, 379–409. https://doi.org/10.1016/0022-1694(88)90193-x

Lin, J., Böhlke, J.K., Huang, S., Gonzalez-Meler, M., Sturchio, N.C., 2019. Seasonality of nitrate sources and isotopic composition in the Upper Illinois River. J Hydrol 568, 849–861. https://doi.org/10.1016/j.jhydrol.2018.11.043

Martin, S.L., Hamlin, Q.F., Kendall, A.D., Wan, L., Hyndman, D.W., 2021. The land use legacy effect: looking back to see a path forward to improve management. Environ Res Lett 16, 035005. https://doi.org/10.1088/1748-9326/abe14c

McCarty, G.W., Hapeman, C.J., Rice, C.P., Hively, W.D., McConnell, L.L., Sadeghi, A.M., Lang, M.W., Whitall, D.R., Bialek, K., Downey, P., 2014. Metolachlor metabolite (MESA) reveals agricultural nitrate-N fate and transport in Choptank River watershed. Sci Total Environ 473, 473–482. https://doi.org/10.1016/j.scitotenv.2013.12.017

Meter, K.J.V., Basu, N.B., 2017. Time lags in watershed-scale nutrient transport: an exploration of dominant controls. Environ Res Lett 12, 084017. https://doi.org/10.1088/1748-9326/aa7bf4

Meter, K.J.V., Basu, N.B., Veenstra, J.J., Burras, C.L., 2016. The nitrogen legacy: emerging evidence of nitrogen accumulation in anthropogenic landscapes. Environ Res Lett 11, 035014. https://doi.org/10.1088/1748-9326/11/3/035014

Meter, K.J.V., Cappellen, P.V., Basu, N.B., 2018. Legacy nitrogen may prevent achievement of water quality goals in the Gulf of Mexico. Science 360, 427–430. https://doi.org/10.1126/science.aar4462

Moore, E.M., Barclay, J.R., Haynes, A.B., Jackson, K.E., Bisson, A.M., Briggs, M.A., Helton, A.M., 2023. Where the past meets the present: connecting nitrogen from watersheds to streams through groundwater flowpaths. Environ. Res. Lett. 18, 124039. https://doi.org/10.1088/1748-9326/ad0c86

Neuman, S.P., Xue, L., Ye, M., Lu, D., 2012. Bayesian analysis of data-worth considering model and parameter uncertainties. Adv. Water Resour. 36, 75–85. https://doi.org/10.1016/j.advwatres.2011.02.007

NCWQR. 2022. Heidelberg Tributary Loading Program (HTLP) Dataset. Zenodo. https://doi.org/10.5281/zenodo.6606949

Plummer, R.E., Hapeman, C.J., Rice, C.P., McCarty, G.W., Schmidt, W.F., Downey, P.M., Moorman, T.B., Douglas, E.A., Strickland, T.C., Pisani, O., Bosch, D.D., Elkin, K.R., Buda, A.R., 2020. Method to Evaluate the Age of Groundwater Inputs to Surface Waters by Determining the Chirality Change of Metolachlor Ethanesulfonic Acid (MESA) Captured on a Polar Organic Chemical Integrative Sampler (POCIS). J. Agric. Food Chem. 68, 2297–2305. https://doi.org/10.1021/acs.jafc.9b06187

Pollock, D.W., 2016. User guide for MODPATH Version 7—A particle-tracking model for MODFLOW, Open-File Report 2016-1086. U.S. Geological Survey.

Rabalais, N.N., Turner, R.E., Jr., W.J.W., 2002. Gulf of Mexico Hypoxia, A.K.A. "The Dead Zone." Annu. Rev. Ecol. Syst. 33, 235–263. https://doi.org/10.1146/annurev.ecolsys.33.010802.150513

Rice, C.P., McCarty, G.W., Bialek-Kalinski, K., Zabetakis, K., Torrents, A., Hapeman, C.J., 2016. Analysis of metolachlor ethane sulfonic acid (MESA) chirality in groundwater: A tool for dating groundwater movement in agricultural settings. Sci. Total Environ. 560, 36–43. https://doi.org/10.1016/j.scitotenv.2016.04.007

Vitousek, P.M., Naylor, R., Crews, T., David, M.B., Drinkwater, L.E., Holland, E., Johnes, P.J., Katzenberger, J., Martinelli, L.A., Matson, P.A., Nziguheba, G., Ojima, D., Palm, C.A., Robertson, G.P., Sanchez, P.A., Townsend, A.R., Zhang, F.S., 2009. Nutrient Imbalances in Agricultural Development. Science 324, 1519–1520. https://doi.org/10.1126/science.1170261

Vörösmarty, C.J., McIntyre, P.B., Gessner, M.O., Dudgeon, D., Prusevich, A., Green, P., Glidden, S., Bunn, S.E., Sullivan, C.A., Liermann, C.R., Davies, P.M., 2010. Global threats to human water security and river biodiversity. Nature 467, 555–561. https://doi.org/10.1038/nature09440

Wan, L., Kendall, A.D., Martin, S.L., Hamlin, Q.F., Hyndman, D.W., 2023. Important Role of Overland Flows and Tile Field Pathways in Nutrient Transport. Environ. Sci. Technol. 57, 17061–17075. https://doi.org/10.1021/acs.est.3c03741

Williams, E.L., Szramek, K.J., Jin, L., Ku, T.C.W., Walter, L.M., 2007. The carbonate system geochemistry of shallow groundwater–surface water systems in temperate glaciated watersheds (Michigan, USA): Significance of open-system dolomite weathering. GSA Bull. 119, 515–528. https://doi.org/10.1130/b25967.1

APPENDIX A: SUPPLEMENTARY INFORMATION FOR CHAPTER 2

Table A1: Analytes and Analytical Methods for Stream Chemistry Parameters. Stream chemistry analytes used for this study. Note that for simplicity we use symbolic abbreviations for ions without valances. Analytical method information re-produced from Verhougstraete et al. 2014 Table S3.

Analyte (valence)	Method Description	Method Reference	Abbreviation
$Calcium^{2+}$	Flame atomic absorption spectrophotometry	Wetzel R, Likens G (2000) Limnological Analyses (Springer, New York), 3rd Ed.	Ca
$Magnesium^{2+}$	Flame atomic absorption spectrophotometry	Wetzel R, Likens G (2000) Limnological Analyses (Springer, New York), 3rd Ed.	Mg
$Potassium^{+}$	Flame atomic absorption spectrophotometry (0.5% HNO 3 preservative)	Hamilton SK, Bruesewitz DA, Horst GP, Weed DB, Sarnelle O (2009) Biogenic calcite–phosphorus precipitation as a negative feedback to lake eutrophication. Can J FishAquat Sci 66(2):343–350.	K
$Sodium^{+}$	Flame atomic absorption spectrophotometry (0.5% HNO 3 preservative)	Hamilton SK, Bruesewitz DA, Horst GP, Weed DB, Sarnelle O (2009) Biogenic calcite–phosphorus precipitation as a negative feedback to lake eutrophication. Can J FishAquat Sci 66(2):343–350.	Na
$Chloride^{-}$	Dionex membrane-suppression ion chromatography	Wetzel R, Likens G (2000) Limnological Analyses (Springer, New York), 3rd Ed. Hamilton SK, Bruesewitz DA, Horst GP, Weed DB, Sarnelle O (2009) Biogenic calcite–phosphorus precipitation as a negative feedback to lake eutrophication. Can J FishAquat Sci 66(2):343–350.	Cl

Table A1 (cont'd)

$Sulfate^{2-}$	Dionex membrane-suppression ion chromatography	Hamilton SK, Bruesewitz DA, Horst GP, Weed DB, Sarnelle O (2009) Biogenic calcite–phosphorus precipitation as a negative feedback to lake eutrophication. Can J FishAquat Sci 66(2):343–350.	SO_4
Total Phosphorus	Ascorbic acid method following persulfate digestion	Standard methods 4500-P.E and 4500-N.C	TP
Total Dissolved Phosphorus	Ascorbic acid method following persulfate digestion	Standard methods 4500-P.E and 4500-N.C	TDP
Soluble Reactive Phosphorus	Ascorbic acid method	Standard methods 4500-P.E.	SRP
Total Nitrogen	Second derivative spectroscopy following persulfate digestion	Crumpton W, Isenhart T, Mitchell P (1992) Nitrate and organic N analyses with sec-ond-derivative spectroscopy. Limnol Oceanogr 37(4):907–913.	TN
Total Dissolved Nitrogen	Second derivative spectroscopy following persulfate digestion	Crumpton W, Isenhart T, Mitchell P (1992) Nitrate and organic N analyses with sec-ond-derivative spectroscopy. Limnol Oceanogr 37(4):907–913.	TDN
$Nitrate^{2-}$/$Nitrite^{-}$	Cadmium reduction	Standard methods 4500-NO 3-E	NO_x
$Nitrate^{2-}$	Cadmium reduction	Standard methods 4500-NO 3-E	NO_3
$Ammonium^{4+}$	Phenate Method	Standard methods 4500-NH 3-G	NH_4

Table A2: NLCD Land Cover Summary Classes. Table showing the relationship between the original 2006 NLCD classes and our summary land cover classes used in the linear model analysis.

NLCD Class	NLCD Label	Updated Class	Updated Label
21	Developed, Open Space	1	Developed
22	Developed, Low Intensity	1	Developed
23	Developed, Medium Intensity	1	Developed
24	Developed, High Intensity	1	Developed
82	Cultivated Crops	2	Cropland
71	Grassland/Herbaceous	3	Grassland
81	Pasture/Hay	3	Pasture/Hay
41	Deciduous Forest	4	Deciduous to Mixed Forest
43	Mixed Forest	4	Deciduous to Mixed Forest
11	Open Water	5	Open Water
95	Emergent Herbaceous Wetlands	6	Herbaceous Wetlands
31	Barren Land	7	Barren
42	Evergreen Forest	8	Evergreen Forest
52	Shrub/Scrub	9	Shrub/Herbaceous
72	Sedge/Herbaceous	9	Shrub/Herbaceous
90	Woody Wetlands	10	Woody Wetlands

Table A3: Summary Statistics for Stream Chemistry in Each Season. Minimum (min), mean, median (med.), maximum (max.) and standard deviation (stdev.) in concentration (mg/L) of all nutrient species summarized across sites for each sampling event. The highest median concentration of the three seasons is highlighted in green. pH and NOPC values are also provided in this table for additional geochemical context.

	Max.	Mean	Med.	Min.	Stdev.
	Snowmelt				
TN	7.887	1.903	1.303	0.253	1.679
TP	0.513	0.097	0.076	0.009	0.076
TDP	0.359	0.055	0.038	0.005	0.053
SRP	0.336	0.027	0.009	0.003	0.051
NH_3	0.387	0.087	0.062	0.001	0.092
NO_X	6.870	1.518	0.860	0.002	1.630
TDN	11.009	1.923	1.218	0.284	1.967
NO_4	10.272	1.576	0.909	0.047	1.869
pH	8.237	7.959	7.970	7.510	0.159
NPOC	14.026	6.907	6.805	1.788	2.746
	Summer Rainfall				
TN	7.776	1.276	0.923	0.126	1.244
TP	0.112	0.048	0.036	0.011	0.029
TDP	0.098	0.027	0.022	0.001	0.019
SRP	0.036	0.011	0.006	0.002	0.011
NH_3	0.999	0.215	0.028	0.002	0.376
NO_X	5.682	0.872	0.568	0.004	1.075
TDN	6.449	1.506	1.130	0.252	1.312
NO_4	5.491	1.073	0.580	0.017	1.298
pH	8.546	8.116	8.112	7.826	0.157

Table A3 (cont'd)

NPOC	64.16	21.68	17.163	1.635	15.313
	Baseflow				
TN	5.583	1.082	0.686	0.082	1.120
TP	0.396	0.038	0.025	0.008	0.052
TDP	0.292	0.025	0.016	0.003	0.038
SRP	0.266	0.023	0.010	0.001	0.045
NH_3	0.280	0.024	0.005	0.000	0.045
NO_X	5.639	0.858	0.337	0.000	1.300
TDN	5.609	1.048	0.658	0.124	1.036
NO_4	5.503	0.749	0.258	0.000	1.083
pH	8.382	8.197	8.209	7.896	0.105
NPOC	26.777	6.140	5.011	1.600	4.193

Table A4: Significance in Difference between Seasons in Land Cover Linear Model. P values for significant difference in the median concentration between the three seasons, values of $p \geq 0.05$ highlighted in red.

	Snowmelt-Summer Rain	Summer Rain-Baseflow	Snowmelt-Baseflow
TN	0.030	0.070	0.001
TP	0.004	0.011	6.86E-09
TDP	7.12E-06	0.048	2.58E-08
SRP	0.106	0.007	1.000
NH_4	0.043	2.73E-4	5.33E-05
NOX	0.361	0.361	0.045
TDN	0.713	0.141	0.066
NO_3	0.269	0.269	0.066

Table A5: Linear Model Adjusted R Squared Values. Adjusted R squared values for the land cover only and combined land cover and hydrology models.

	Land Cover Only Model			Hydrology + Land Cover Model		
Analyte	**Snowmelt**	**Summer Rain**	**Baseflow**	**Snowmelt**	**Summer Rain**	**Baseflow**
Ca	0.35	0.45	0.39	0.49	0.58	0.51
Mg	0.41	0.52	0.48	0.41	0.60	0.64
K	0.80	0.78	0.74	0.86	0.88	0.82
Na	0.83	0.77	0.71	0.82	0.78	0.73
Cl	0.79	0.72	0.73	0.80	0.73	0.75
SO_4	0.72	0.63	0.63	0.72	0.64	0.65
TP	0.45	0.55	0.68	0.45	0.54	0.67
TDP	0.58	0.36	0.42	0.64	0.34	0.44
SRP	0.67	0.59	0.002	0.70	0.59	-0.01
TN	0.66	0.14	0.31	0.65	0.20	0.38
TDN	0.81	0.70	0.39	0.81	0.71	0.44
NO_X	0.66	0.47	0.39	0.65	0.48	0.45
NO_3	0.77	0.69	0.36	0.76	0.68	0.44
NH_4	0.38	0.02	0.12	0.37	-0.05	0.16

Table A6: Significant Parameters from the Combined Linear Model. All significant coefficients (driver variables) for each species and season in the combined hydrology and land cover linear model. The instances of significant correlation between the hydrologic predictor variables and the dependent chemical species is highlighted in light blue in this table.

Snowmelt			
Predictor	Coefficient	P-value	Species
Ag	0.1133	0.039	Ca
Ag	0.3527	0	Cl
Ag	0.3777	0	K
Ag	0.1209	0.022	Mg
Ag	0.3256	0.004	Na
Ag	0.7106	0.019	NH_3
Ag	0.7575	0	NO_3
Ag	0.8509	0	NO_x
Ag	0.4876	0	SO_4
Ag	0.4426	0	TND
Ag	0.2735	0.02	TN
Forest	0.1964	0.028	Ca
Forest	0.361	0.014	Cl
Forest	0.5071	0.006	Na
Forest	0.6274	0	SO4
Forest	-0.6242	0.008	SRP
Forest	-0.3774	0.011	TDP
GWTT	0.0015	0.005	Cl
GWTT	0.0013	0.003	K
GWTT	-0.0009	0.007	Mg

Table A6 (cont'd)

Open	-0.2614	0.003	K
Open	-0.3492	0.043	NO_3
Open	-0.2511	0.024	SO_4
Open	-0.6198	0	SRP
Open	-0.3328	0.002	TND
Open	-0.3001	0.003	TDP
Open	-0.3492	0.01	TN
Open	-0.338	0.01	TP
Recharge	-0.0044	0.003	Ca
Recharge	-0.0042	0.004	Mg
Recharge	-0.007	0.004	TDP
Soil K	0.441	0.003	K
Soil K	0.7272	0.01	SRP
Urban	0.28	0	Ca
Urban	0.7417	0	Cl
Urban	0.3153	0	K
Urban	0.1988	0.001	Mg
Urban	1.0821	0	Na
Urban	0.3879	0.024	NO_3
Urban	0.5789	0.027	NO_x
Urban	0.5929	0	SO_4
Urban	-0.5895	0	SRP
Urban	-0.2765	0.008	TDP
Wetland	-0.9763	0	SRP
Wetland	-0.5777	0	TDP

Table A6 (cont'd)

Summer Rainfall			
Ag	0.108	0.015	Ca
Ag	0.3058	0.004	Cl
Ag	0.3053	0	K
Ag	0.1162	0.005	Mg
Ag	0.3127	0.003	Na
Ag	0.9999	0	NO_3
Ag	0.8889	0.002	NOx
Ag	0.4322	0.001	SO_4
Ag	0.3963	0	TND
Ag	0.314	0.026	TDP
Ag	0.2479	0.015	TP
Forest	0.5055	0.015	SO_4
GWTT	0.002	0	K
GWTT	-0.0008	0.001	Mg
Open	-0.198	0.007	K
Open	-0.3074	0.031	SO_4
Open	-0.3667	0.021	SRP
Recharge	-0.0081	0.043	TN
Soil K	0.3094	0.016	K
Soil K	0.6367	0.032	TN
Urban	0.1702	0.002	Ca
Urban	0.6206	0	Cl
Urban	0.2482	0.001	K
Urban	0.099	0.04	Mg

Table A6 (cont'd)

Urban	0.799	0	Na
Urban	0.5203	0.033	NO_3
Urban	0.505	0.001	SO_4
Urban	0.265	0.031	TP
Wetland	-0.1309	0.022	Mg
Baseflow			
Ag	0.1151	0.025	Ca
Ag	0.4637	0	Cl
Ag	0.3505	0	K
Ag	0.1453	0.003	Mg
Ag	0.4552	0.001	Na
Ag	0.4774	0	SO_4
Forest	0.5218	0.014	Cl
Forest	0.5554	0.014	Na
Forest	0.7852	0.001	SO_4
Forest	-0.6336	0.014	TND
Forest	-0.7538	0.01	TN
GWTT	0.0021	0	K
GWTT	-0.0013	0	Mg
GWTT	-0.0056	0.005	NO_3
GWTT	-0.0019	0.024	TND
GWTT	-0.0029	0.006	TN
Open	-0.1219	0.022	Mg
Open	-0.2836	0.04	Na
Open	-0.3317	0.017	SO_4

Table A6 (cont'd)

Open	-0.2508	0.03	TP
Soil K	-0.2764	0.006	Ca
Urban	0.1396	0.024	Ca
Urban	0.8173	0	Cl
Urban	0.2968	0.004	K
Urban	0.7655	0	Na
Urban	0.7604	0.048	NO_3
Urban	0.502	0.001	SO_4
Urban	0.3956	0.001	TP

Table A7: Sample Watershed Area and Dominant Land Cover. Sample point watershed area and domiant land cover class. Individual land cover propirtions are shown in table A8.

River	Area km^2	Dominant Land Cover
St. Joseph	11061.02	Agricultural
Paw Paw River	1027.30	Agricultural
Kalamazoo	5001.87	Agricultural
Grand	12853.63	Agricultural
Muskegon	6417.96	Forested
White River	1048.77	Forested
Pere Marquette	1789.84	Forested
Big Sable River	476.26	Forested
Little Manistee	525.83	Forested
Manistee	3558.73	Forested
Bear Creek	349.96	Mixed
Betsie	617.85	Forested
Platte	470.82	Forested
Boardman	715.70	Forested
Elk-Torch	1307.78	Forested
Cheboygan	2316.79	Forested
Black	1508.96	Forested
Thunder Bay	2240.89	Forested
Au Sable	5287.16	Forested
Au Gres	986.79	Mixed

Table A7 (cont'd)

Rifle	858.08	Forested
Black River	1250.01	Agricultural
Pine River	440.14	Agricultural
Belle River	511.69	Agricultural
Clinton River	1879.91	Urban
River Rouge	1033.25	Urban
Huron	2298.21	Mixed
Raisin	2682.81	Agricultural
S. Branch Black River	313.36	Agricultural
N. Branch Black River	397.78	Agricultural
Macatawa River	292.30	Agricultural
Pine Creek	48.25	Urban
Pigeon River	101.56	Agricultural
Rush Creek	151.54	Urban
Buck Creek	2.88	Urban
Sand Creek	141.77	Agricultural
Bass River	127.05	Agricultural
Little Pigeon Creek	13.95	Forested
Black Creek	135.89	Mixed
Silver Creek	41.10	Forested
Flower Creek	78.57	Agricultural
Stony Lake Outlet	160.43	Mixed

Table A7 (cont'd)

Swan Creek	54.06	Agricultural
Lincoln River	214.87	Mixed
Crystal River	109.95	Forested
Belangers Creek	25.48	Mixed
Mitchell Creek	37.57	Mixed
Jordan River	174.08	Forested
Monroe Creek	27.24	Forested
Boyne River	199.32	Forested
Bear River	293.12	Forested
Carp River	119.22	Mixed
Ocqueoc River	369.13	Forested
Trout River	81.76	Mixed
Little Trout River	27.75	Mixed
Long Lake Creek	162.12	Mixed
Tawas River	403.270	Forested
Harrington Drain	53.194	Urban
Marsh Creek	77.948	Urban
Sandy Creek	81.779	Agricultural
Cass River	2174.009	Agricultural
Flint River	3206.087	Agricultural
Shiawassee River	1517.388	Agricultural
Tiltabawasee River	6211.324	Mixed

Table A8: Sample Watershed Land Cover Proportions. Relative propirtion of the summary land cover classes in each sample point watershed. These values were used toe compute the domiant land cover class reported in Table A7.

	Land Cover Proportions						
River	**Urban**	**Ag**	**Open**	**Forest**	**Water**	**Wetland**	**Barren**
St. Joseph	0.143	0.595	0.011	0.104	0.024	0.122	0.002
Paw Paw River	0.115	0.475	0.026	0.211	0.014	0.156	0.003
Kalamazoo	0.141	0.478	0.018	0.215	0.021	0.124	0.004
Grand	0.127	0.553	0.010	0.166	0.015	0.127	0.003
Muskegon	0.076	0.196	0.096	0.405	0.039	0.186	0.001
White River	0.052	0.203	0.097	0.497	0.007	0.143	0.001
Pere Marquette	0.050	0.093	0.083	0.616	0.012	0.145	0.001
Big Sable River	0.053	0.115	0.080	0.524	0.050	0.170	0.008
Little Manistee	0.047	0.039	0.125	0.686	0.007	0.096	0.001
Manistee	0.057	0.096	0.159	0.564	0.014	0.109	0.001
Bear Creek	0.063	0.138	0.201	0.376	0.023	0.197	0.001
Betsie	0.081	0.076	0.131	0.462	0.099	0.150	0.001
Platte	0.066	0.099	0.134	0.562	0.075	0.061	0.002
Boardman	0.108	0.104	0.188	0.467	0.021	0.109	0.002
Elk-Torch	0.076	0.144	0.136	0.454	0.113	0.074	0.002
Cheboygan	0.064	0.082	0.116	0.510	0.081	0.145	0.002
Black	0.055	0.044	0.121	0.471	0.039	0.270	0.001
Thunder Bay	0.063	0.110	0.088	0.402	0.027	0.310	0.001
Au Sable	0.084	0.032	0.145	0.589	0.020	0.128	0.001

Table A8 (cont'd)

Au Gres	0.064	0.233	0.076	0.377	0.022	0.220	0.007
Rifle	0.093	0.165	0.089	0.442	0.016	0.194	0.001
Black River	0.062	0.742	0.012	0.106	0.001	0.075	0.001
Pine River	0.090	0.465	0.032	0.333	0.003	0.075	0.001
Belle River	0.095	0.597	0.017	0.190	0.003	0.097	0.002
Clinton River	0.515	0.202	0.013	0.149	0.028	0.086	0.007
River Rouge	0.829	0.054	0.005	0.072	0.007	0.029	0.003
Huron	0.325	0.245	0.012	0.218	0.042	0.151	0.006
Raisin	0.108	0.674	0.008	0.111	0.014	0.083	0.002
S. Branch Black River	0.091	0.458	0.044	0.228	0.012	0.165	0.002
N. Branch Black River	0.070	0.436	0.056	0.248	0.017	0.171	0.002
Macatawa River	0.235	0.678	0.007	0.040	0.002	0.031	0.009
Pine Creek	0.484	0.309	0.011	0.121	0.003	0.061	0.011
Pigeon River	0.110	0.660	0.020	0.153	0.001	0.051	0.005
Rush Creek	0.564	0.315	0.004	0.076	0.011	0.023	0.006
Buck Creek	0.913	0.000	0.006	0.014	0.009	0.058	0.000
Sand Creek	0.191	0.608	0.008	0.113	0.002	0.076	0.003
Bass River	0.111	0.636	0.021	0.160	0.002	0.066	0.005
Little Pigeon Creek	0.189	0.164	0.062	0.419	0.000	0.163	0.003
Black Creek	0.149	0.348	0.053	0.299	0.048	0.101	0.002
Silver Creek	0.117	0.006	0.152	0.637	0.042	0.044	0.002
Flower Creek	0.102	0.456	0.107	0.277	0.006	0.034	0.018

Table A8 (cont'd)

Stony Lake Outlet	0.101	0.377	0.117	0.351	0.010	0.041	0.003
Swan Creek	0.055	0.579	0.082	0.155	0.013	0.115	0.000
Lincoln River	0.056	0.332	0.118	0.306	0.021	0.165	0.002
Crystal River	0.047	0.034	0.087	0.537	0.237	0.033	0.024
Belangers Creek	0.067	0.384	0.127	0.308	0.015	0.099	0.000
Mitchell Creek	0.283	0.228	0.163	0.194	0.002	0.130	0.001
Jordan River	0.032	0.078	0.065	0.707	0.000	0.118	0.001
Monroe Creek	0.042	0.223	0.088	0.445	0.022	0.181	0.000
Boyne River	0.083	0.161	0.108	0.545	0.006	0.094	0.002
Bear River	0.064	0.133	0.070	0.485	0.066	0.181	0.002
Carp River	0.062	0.086	0.077	0.220	0.070	0.483	0.001
Ocqueoc River	0.047	0.065	0.115	0.434	0.022	0.314	0.003
Trout River	0.046	0.135	0.095	0.288	0.001	0.431	0.003
Little Trout River	0.054	0.278	0.075	0.143	0.001	0.446	0.003
Long Lake Creek	0.057	0.117	0.071	0.207	0.157	0.391	0.001
Tawas River	0.084	0.071	0.069	0.516	0.020	0.240	0.000
Harrington Drain	0.997	0.000	0.000	0.002	0.000	0.001	0.000
Marsh Creek	0.720	0.047	0.017	0.154	0.000	0.059	0.002
Sandy Creek	0.262	0.587	0.013	0.106	0.000	0.027	0.004
Cass River	0.069	0.574	0.022	0.197	0.002	0.135	0.001
Flint River	0.210	0.406	0.020	0.241	0.016	0.104	0.003
Shiawassee River	0.157	0.525	0.007	0.170	0.022	0.114	0.004

Table A8 (cont'd)

Tiltabawasee River	0.086	0.328	0.073	0.306	0.015	0.191	0.002

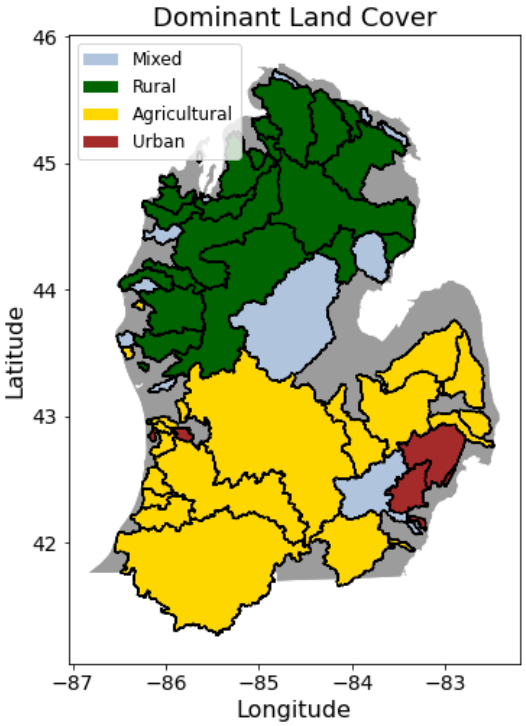

Figure A1: Dominant Land Cover in Each Sample Point Watershed. Dominant land cover in each sample point watershed. A dominant land cover class was assigned only if the watershed contained greater than 50% of agricultural, urban or forested land covers. Watersheds with no dominant land cover are considered mixed and shown in pale blue.

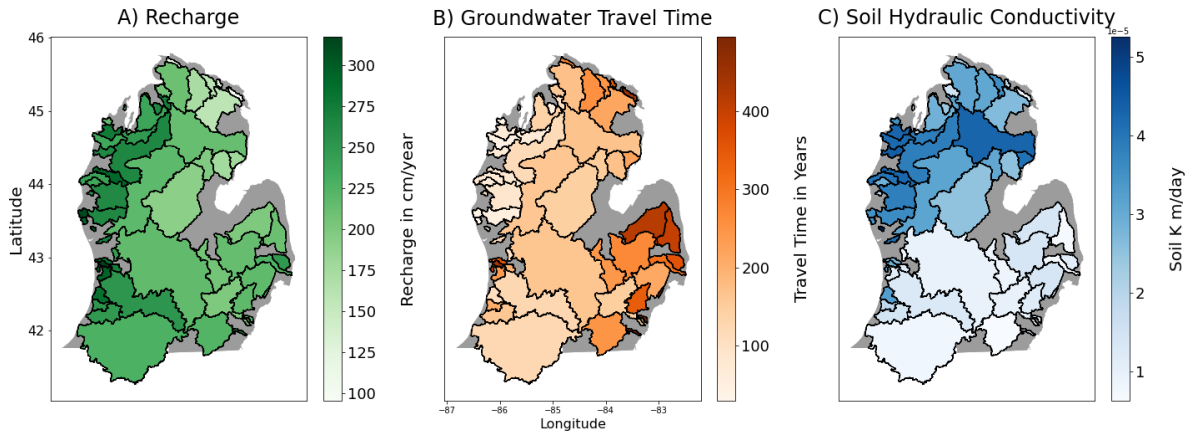

Figure A2: Recharge, Groundwater Travel Time and Soil Hydraulic Conductivity in the Study Region. Mean annual recharge in cm/year, groundwater travel time in years and soil hydraulic conductivity in m/day for sample watersheds.

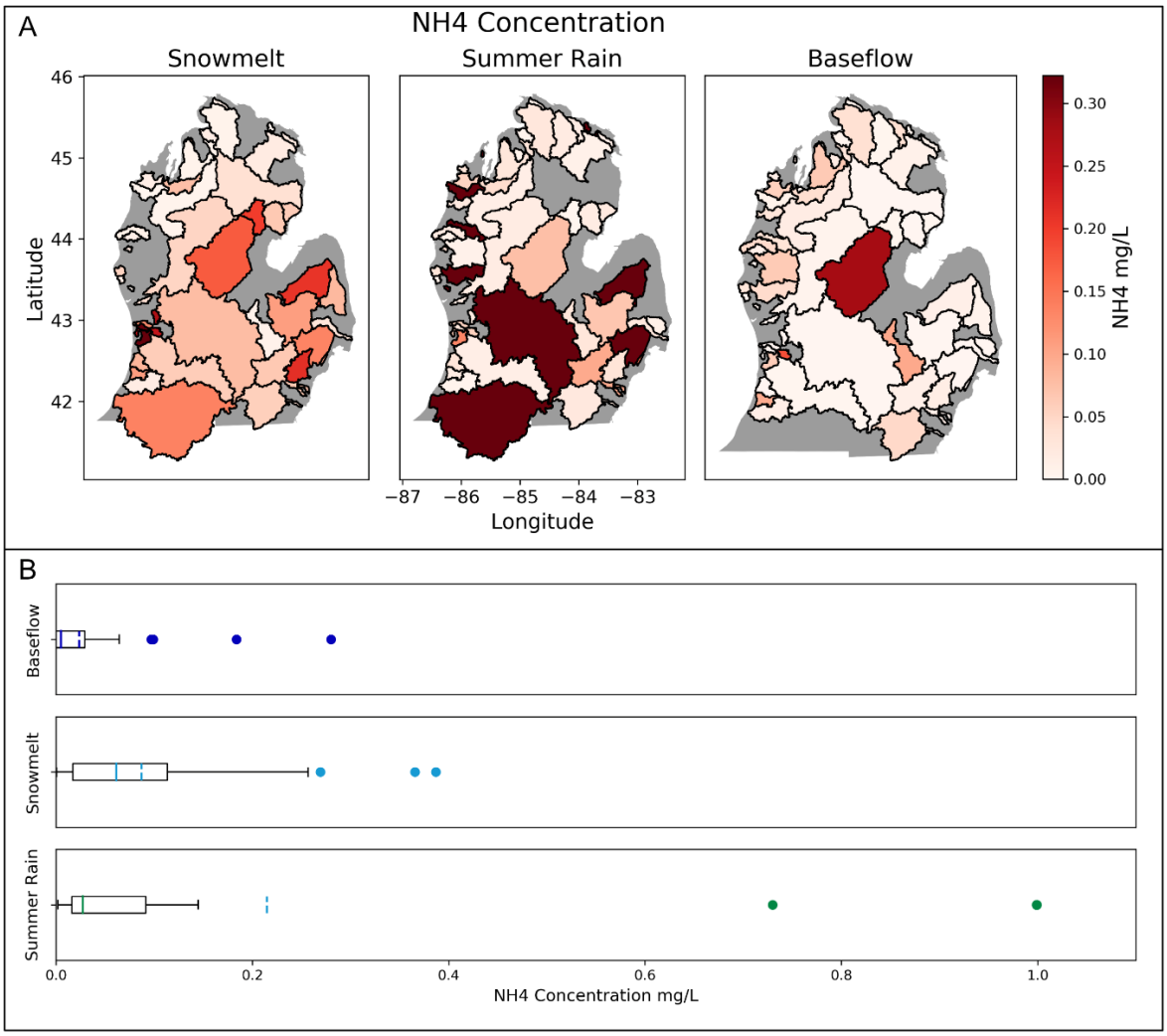

Figure A3: NH_4 Concentrations during the Three Sampling Events. NH_4 concentrations during the three sampling events with A) concentrations mapped to sample point watersheds and B) box plots showing distribution of observed concentrations across sample locations; solid lines representing the median and dashed lines representing the mean of observed concentrations.

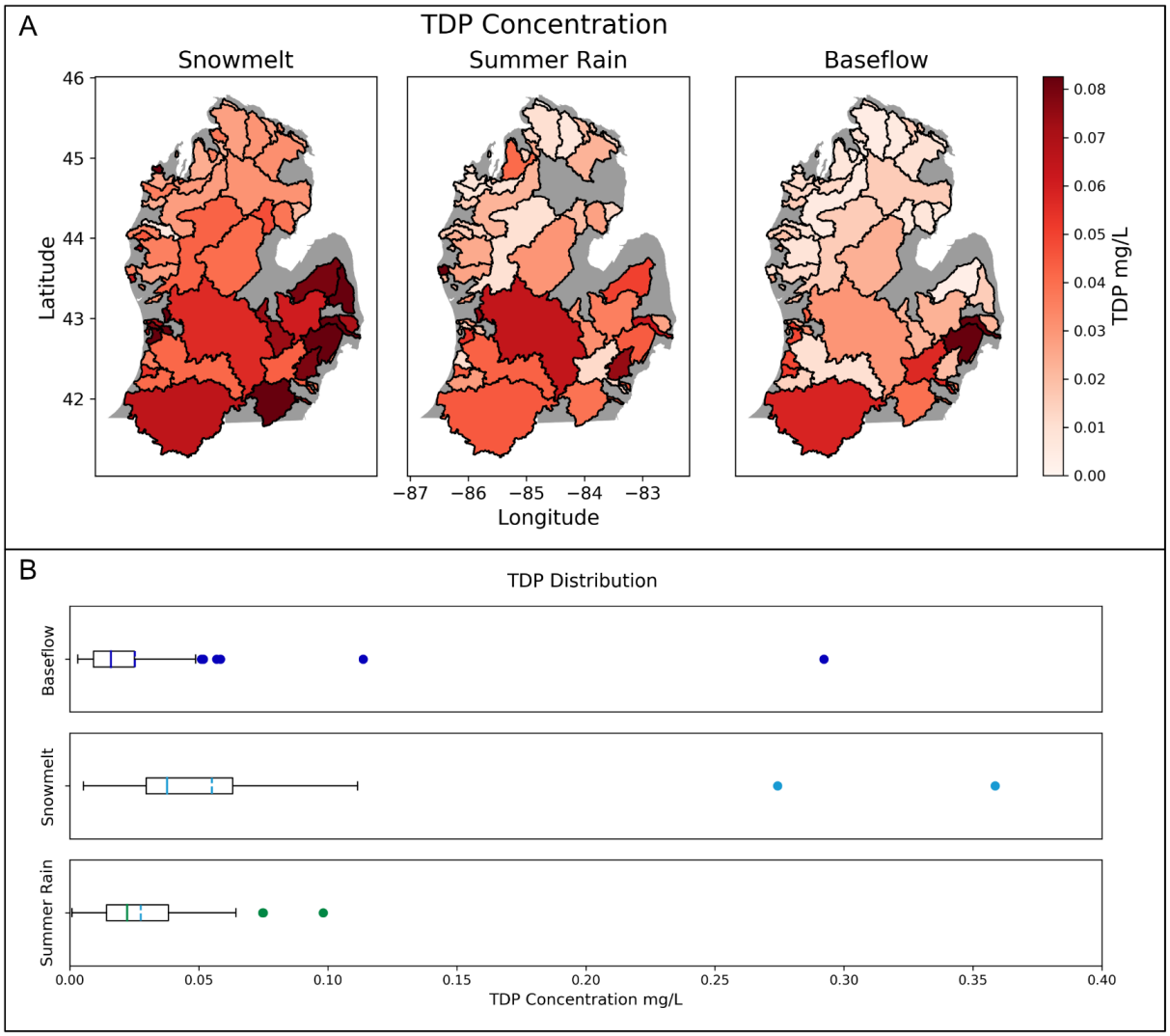

Figure A4: TDP Concentrations during the Three Sampling Events. TDP concentrations during the three sampling events with A) concentrations mapped to sample point watersheds and B) box plots showing distribution of observed concentrations across sample locations; solid lines representing the median and dashed lines representing the mean of observed concentrations.

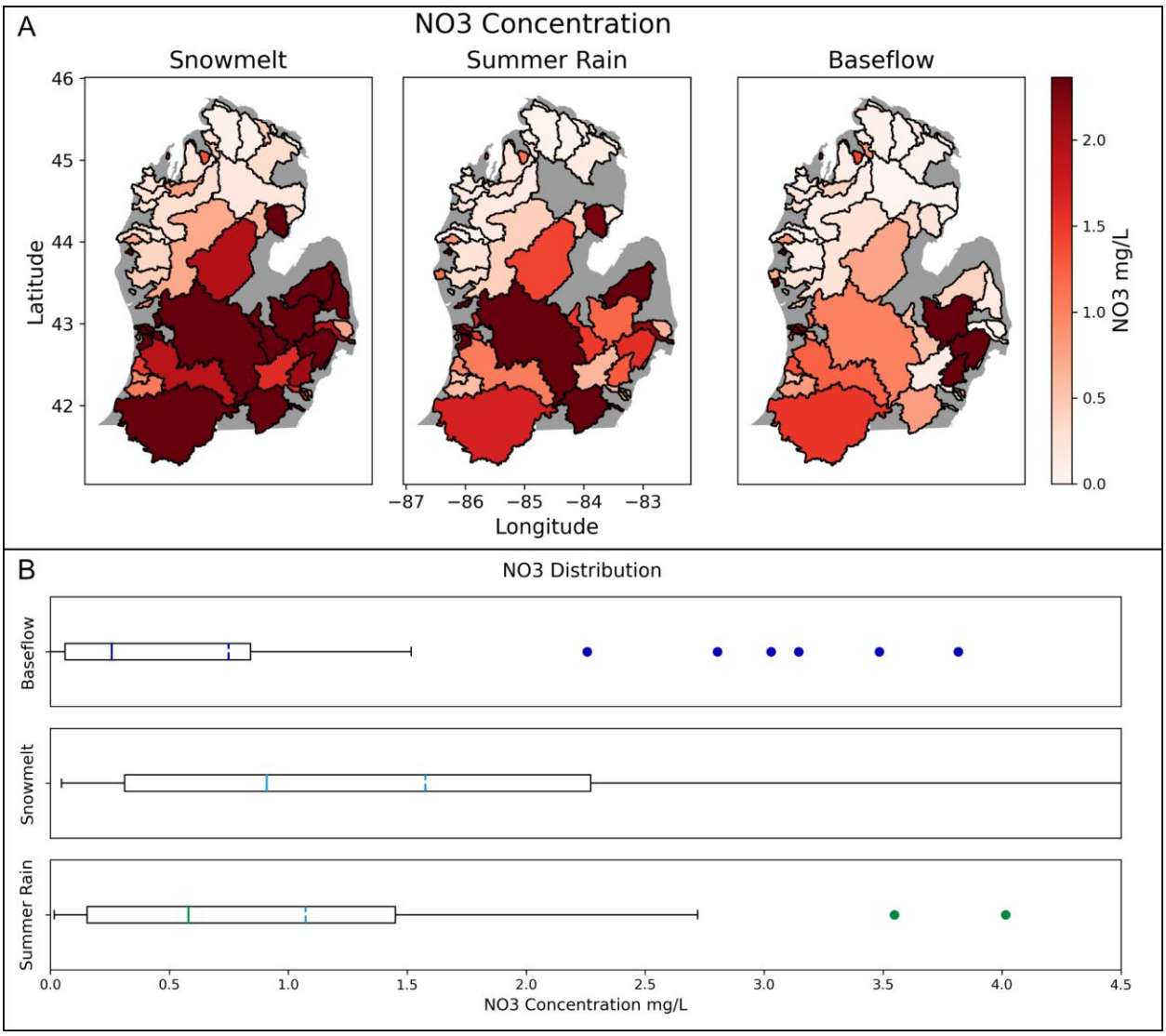

Figure A5: NO_3 Concentration during the Three Sampling Events. NO_3 concentrations during the three sampling events with A) concentrations mapped to sample point watersheds and B) box plots showing distribution of observed concentrations across sample locations; solid lines representing the median and dashed lines representing the mean of observed concentrations.

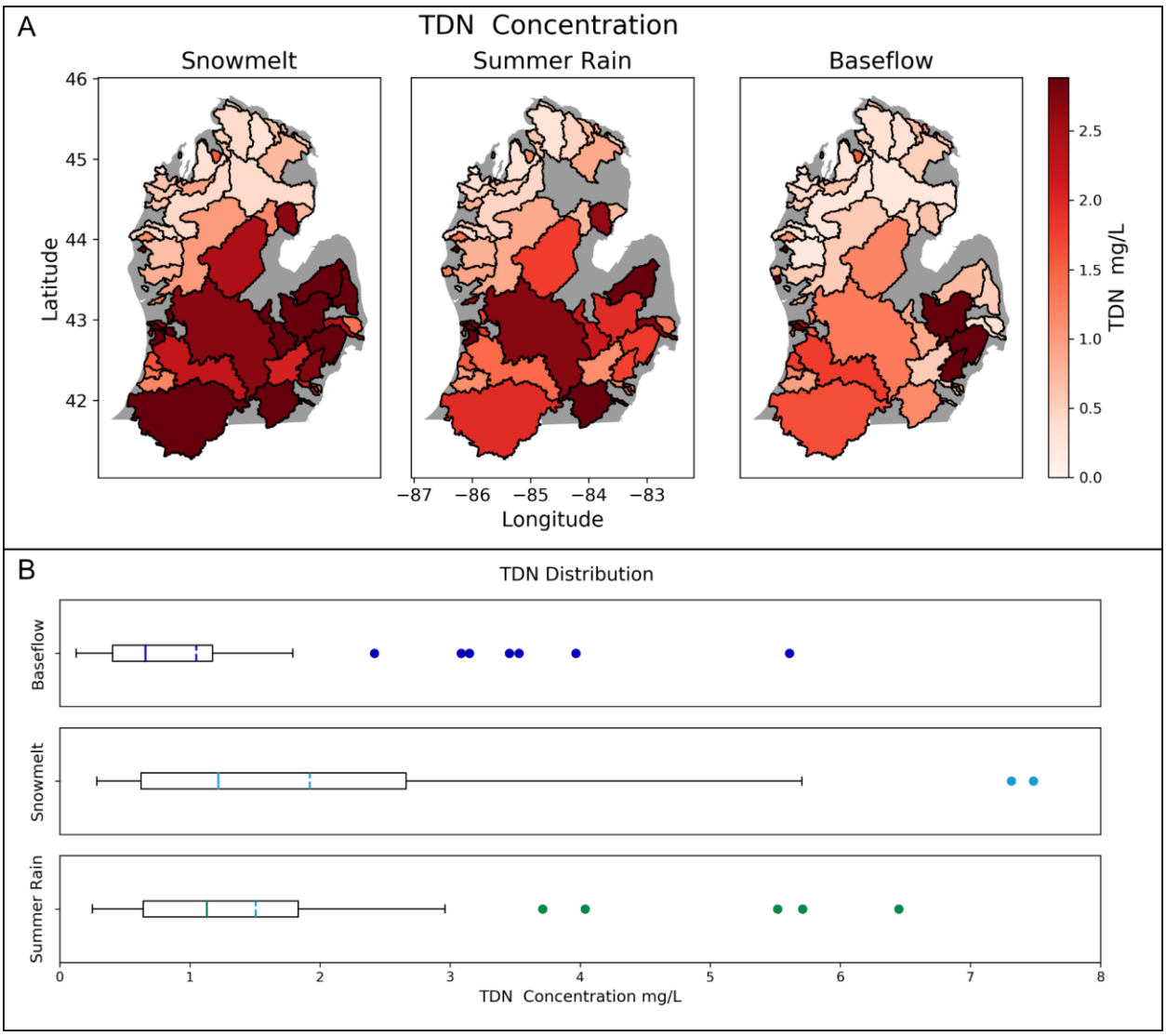

Figure A6: TDN Concentrations during the Three Sampling Events. TDN concentrations during the three sampling events with A) concentrations mapped to sample point watersheds and B) box plots showing distribution of observed concentrations across sample locations; solid lines representing the median and dashed lines representing the mean of observed concentrations.

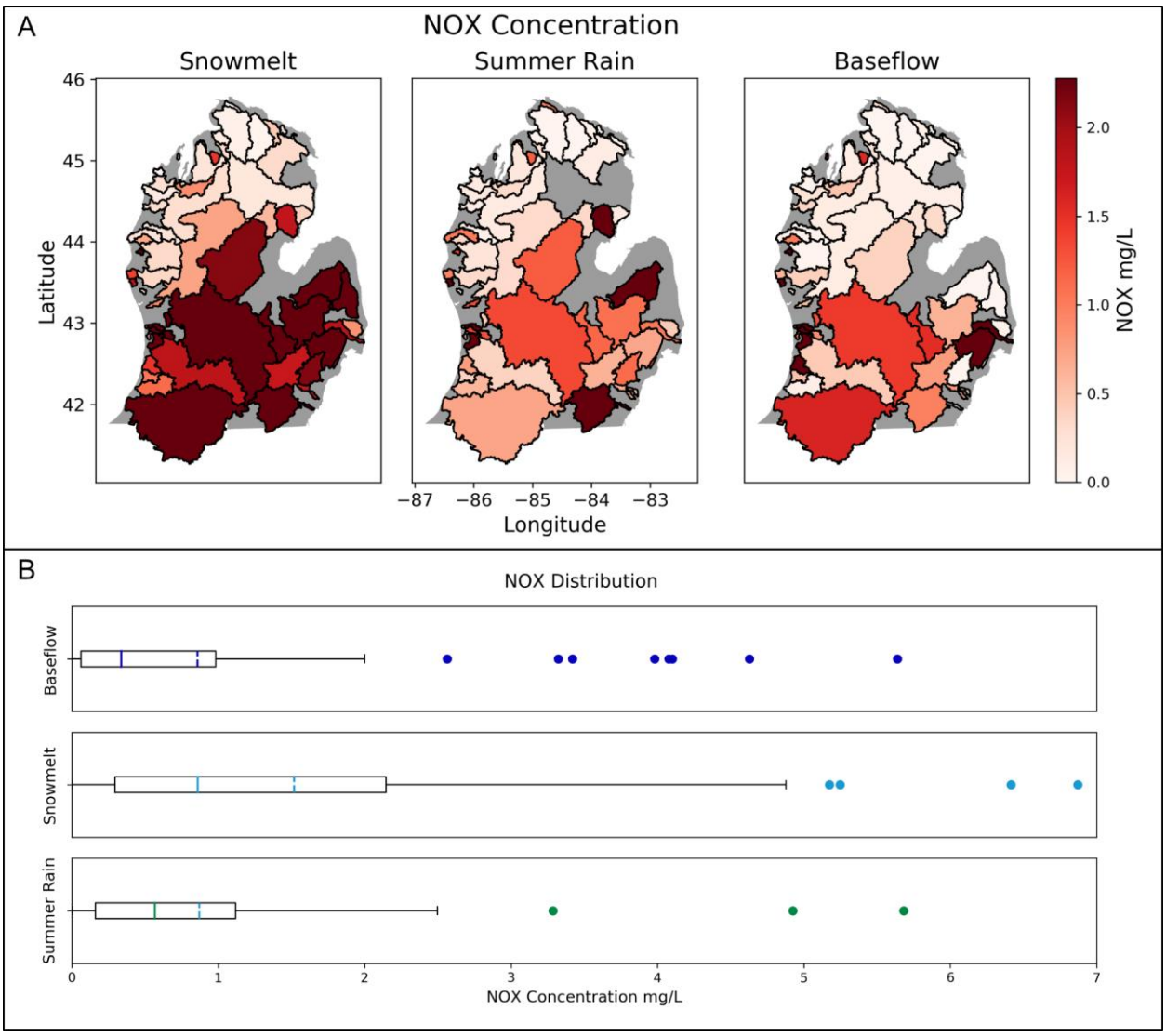

Figure A7: NO_x Concentrations during the Three Sampling Events. NO_x concentrations during the three sampling events with A) concentrations mapped to sample point watersheds and B) box plots showing distribution of observed concentrations across sample locations; solid lines representing the median and dashed lines representing the mean of observed concentrations.

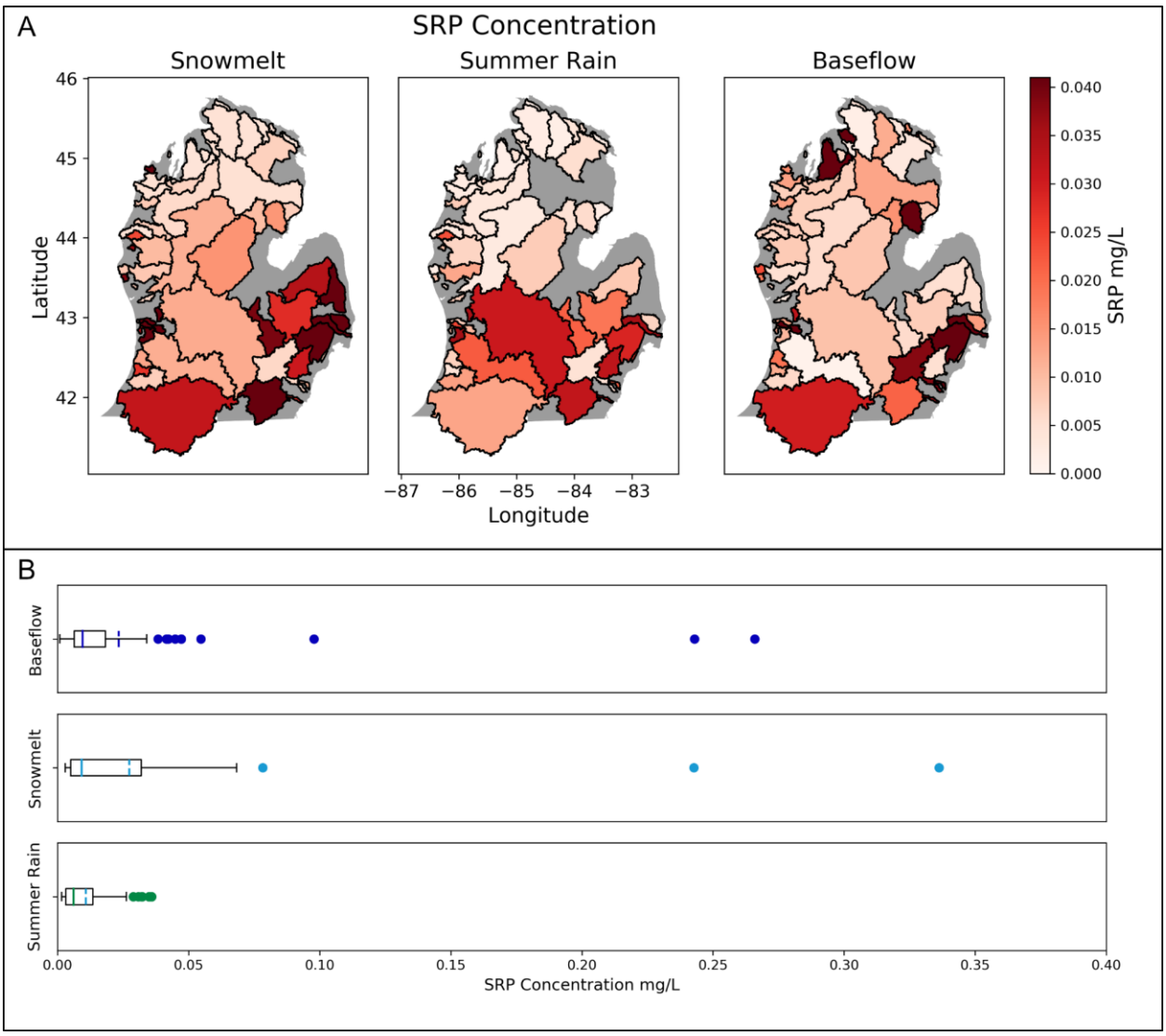

Figure A8: SRP Concentrations during Three Sampling Events. SRP concentrations during the three sampling events with A) concentrations mapped to sample point watersheds and B) box plots showing distribution of observed concentrations across sample locations; solid lines representing the median and dashed lines representing the mean of observed concentrations.

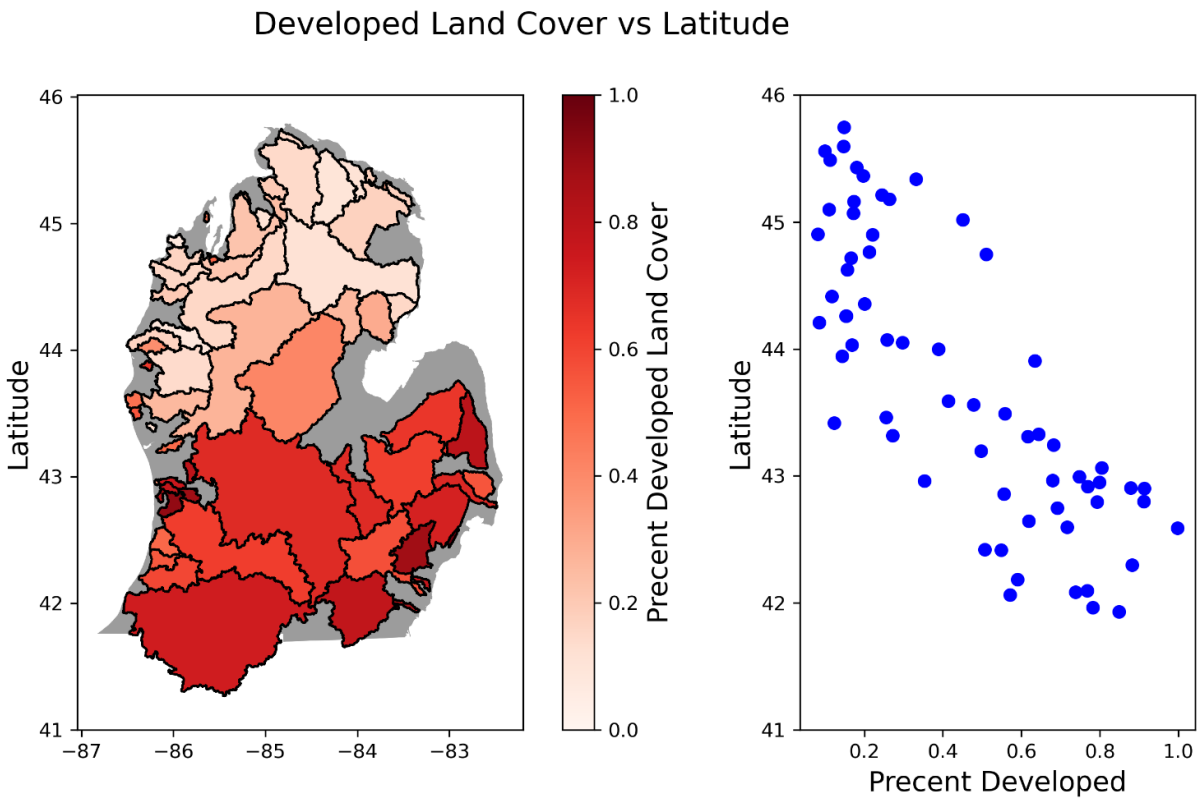

Figure A9: Distribution of Developed Land Cover wtihin the Study Domain . Figure showing the percentage of developed land (urban + agricultural) in each watershed (A) and versus latitude (B). The amount of developed land increased from north to south in the state.

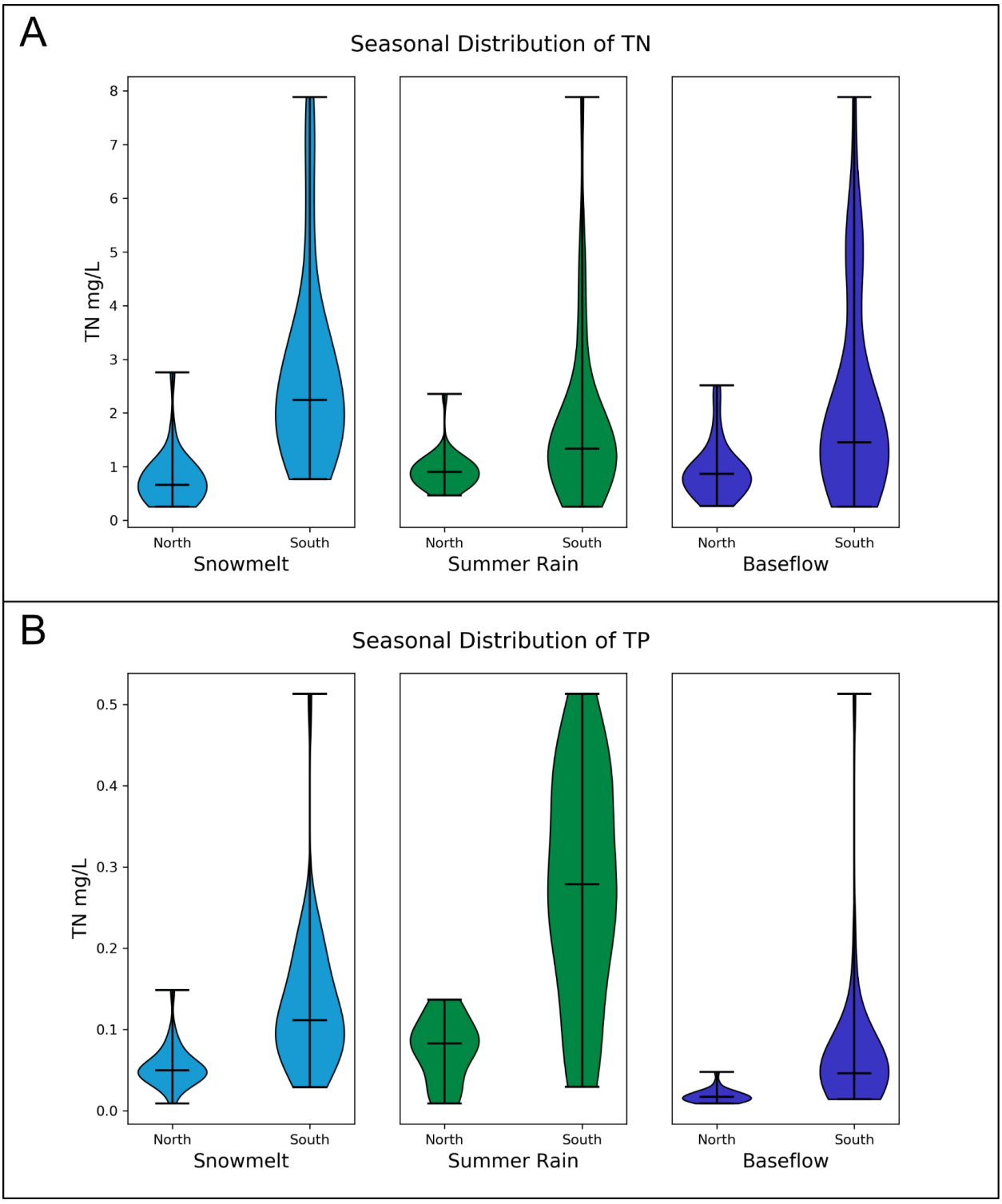

Figure A10: Distributions of TN and TP during the Three Seasons for the Northern and Southern Watersheds. Distributions of TN (A) and TP (B) for the northern (above 44 degrees latitude) and southern (below 44 degrees latitude) halves of the study region. Both the mean and maximum concentrations are greater in the southern half of the study region than the north, following gradients of increased landscape disturbance from north to south in the region.

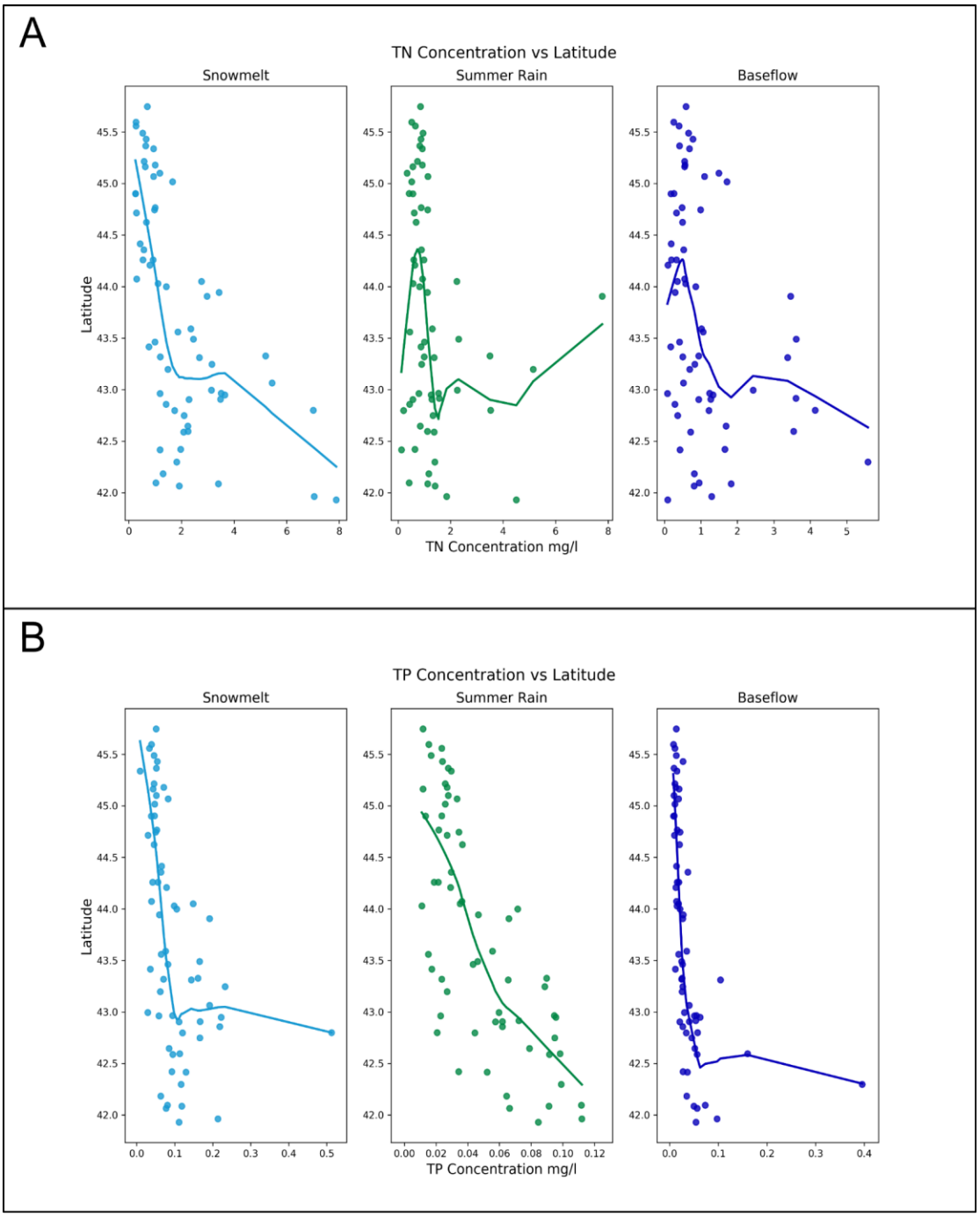

Figure A11: TN and TP Concentration Trends with Latitude for the Three Seasons. Concentrations of TN and TP plotted vs latitude fit with a nonparametric lowess model. Concentrations are uniformly low in the northern half of the region, while the range of concentrations increases in the southern region.

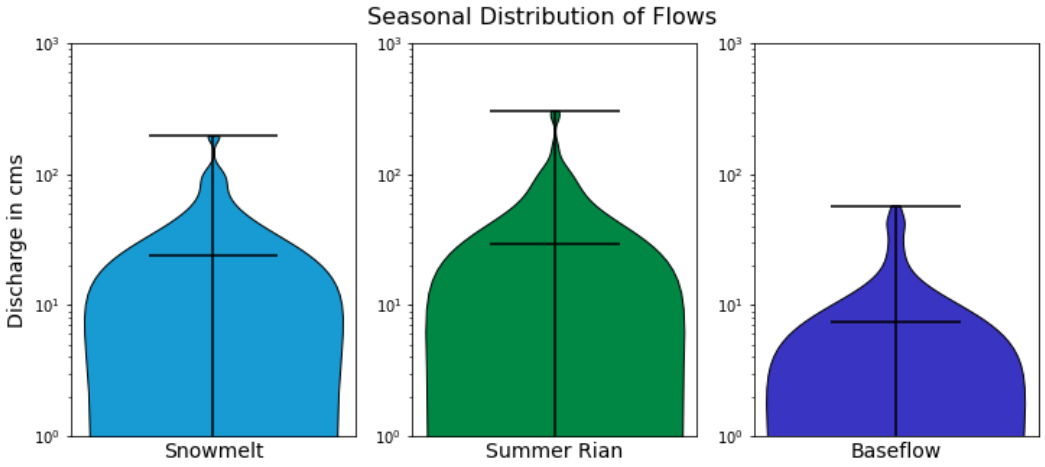

Figure A12: Streamflow Distributions during the Three Seasons. Seasonal distribution of discharge across the study watersheds, hash marks represent the maximum, median and minimum flows during each season. Flows are highest during summer rainfall, elevated during snowmelt and lowest during baseflow.

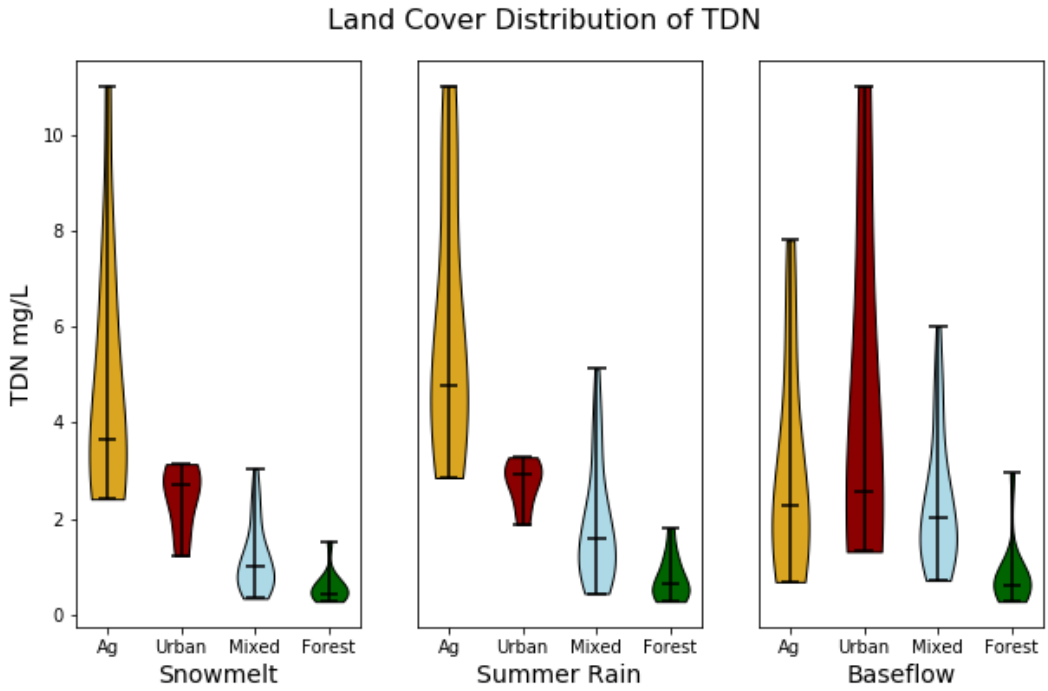

Figure A13: TDN Distribution with Land Cover. Distribution of TDN concentrations across the three seasons in our four classified watershed land cover types.

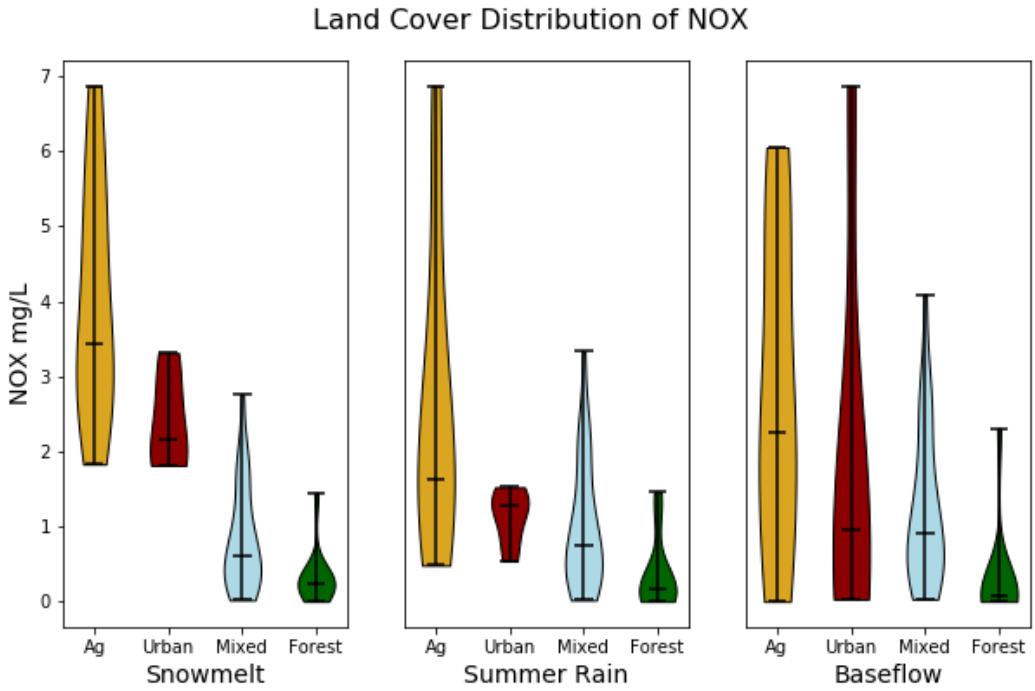

Figure A14: NO_x Distribution with Land Cover. Distribution of NO_x concentrations across the three seasons in our four classified watershed land cover types.

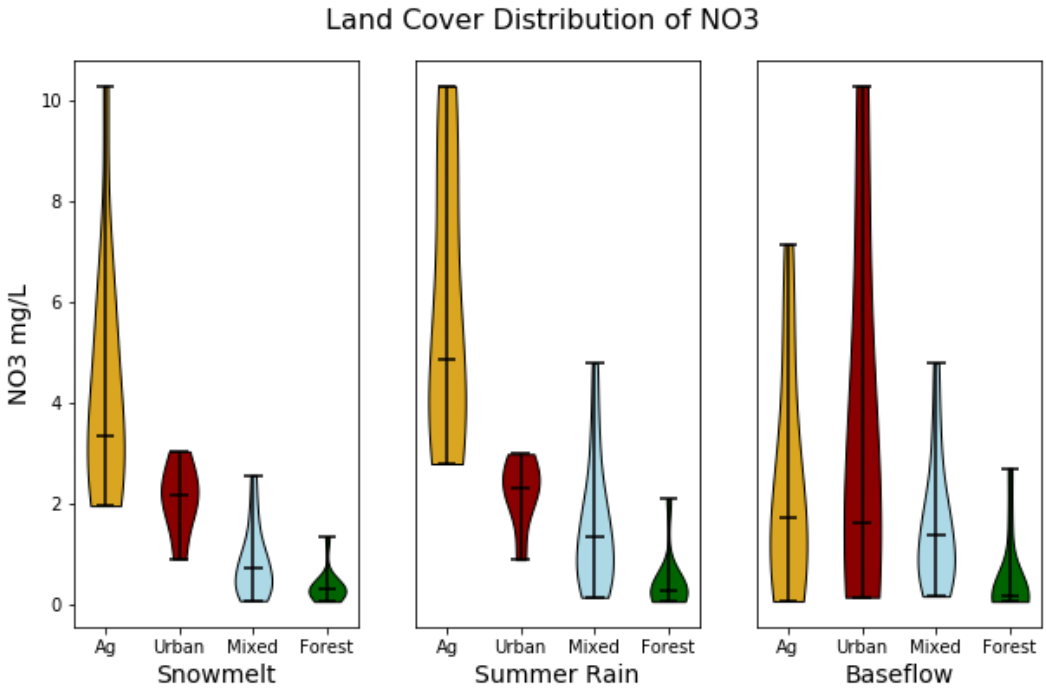

Figure A15: NO_3 Distribution with Land Cover. Distribution of NO_3 concentrations across the three seasons in our four classified watershed land cover types.

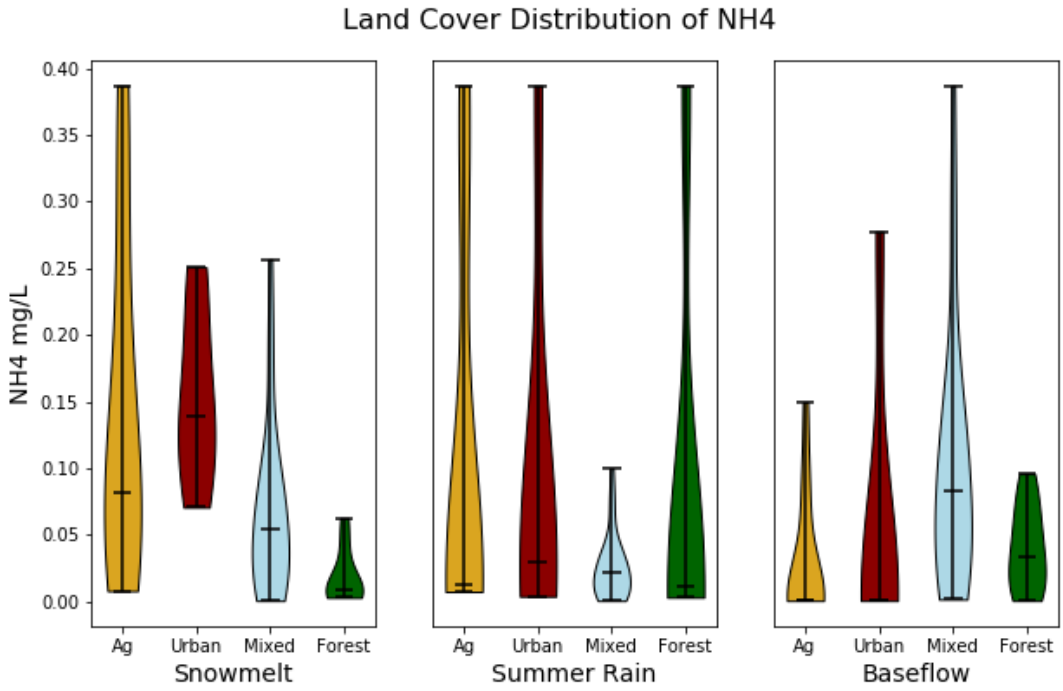

Figure A16: NH_4 Distribution with Land Cover. Distribution of NH_4 concentrations across the three seasons in our four classified watershed land cover types.

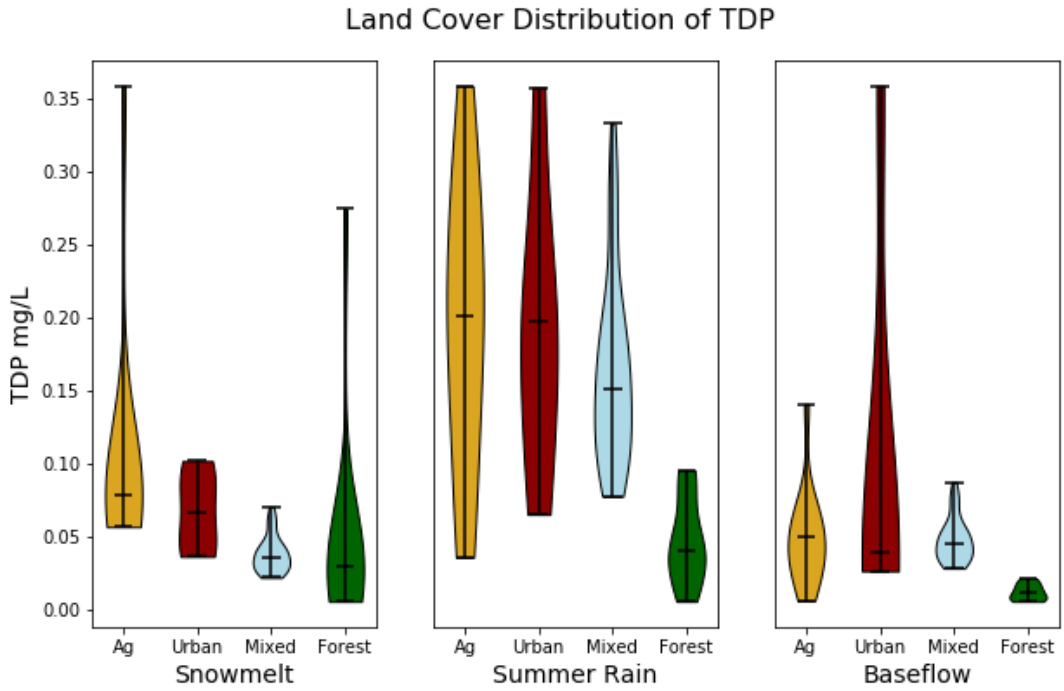

Figure A17: TDP Distribution with Land Cover. Distribution of TDP concentrations across the three seasons in our four classified watershed land cover types.

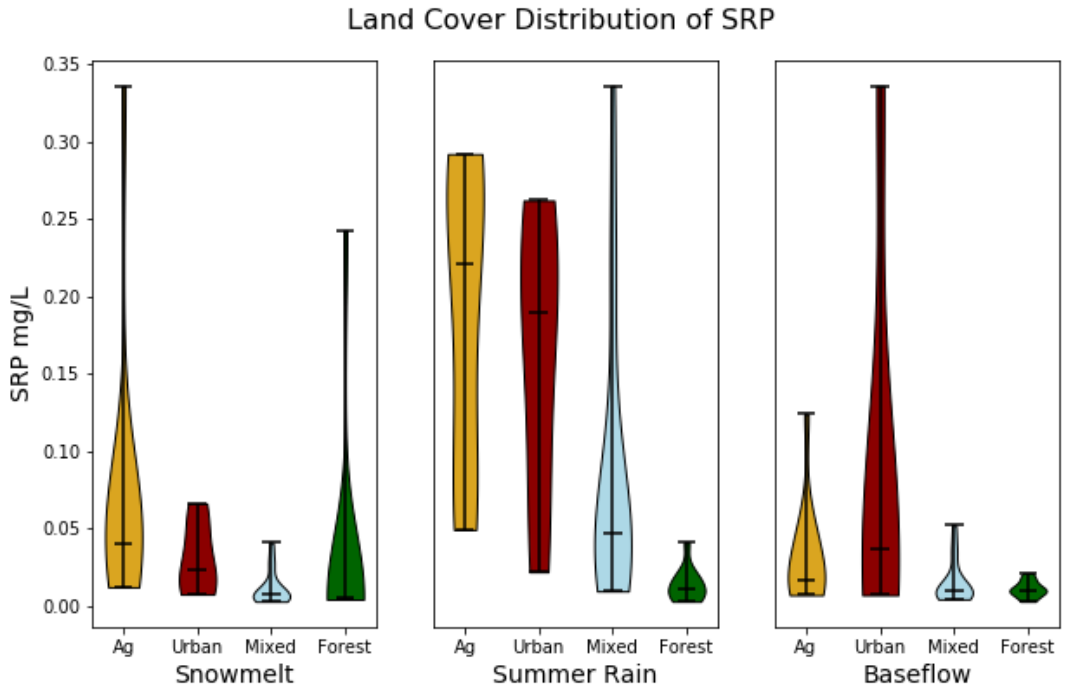

Figure A18: SRP Distributions with Land Cover. Distribution of SRP concentrations across the three seasons in our four classified watershed land cover types.

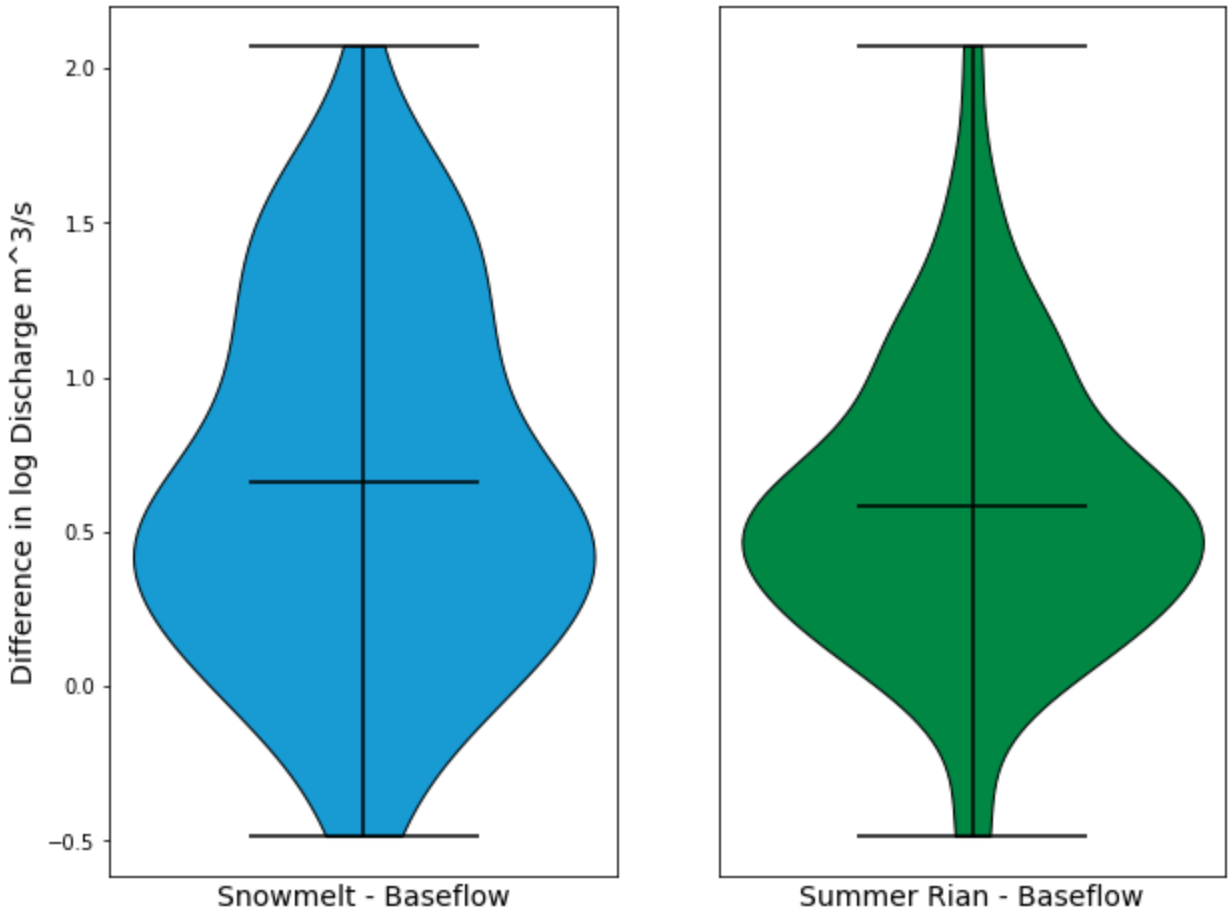

Figure A19: Differences in Discharge between Baseflow and High Flow Events. Distributions of differences in log streamflow between the events (snowmelt and summer rainfall) and baseflow. A majority of our sites during both events had flows higher than baseflow, indicating different hydrologic conditions were sampled.

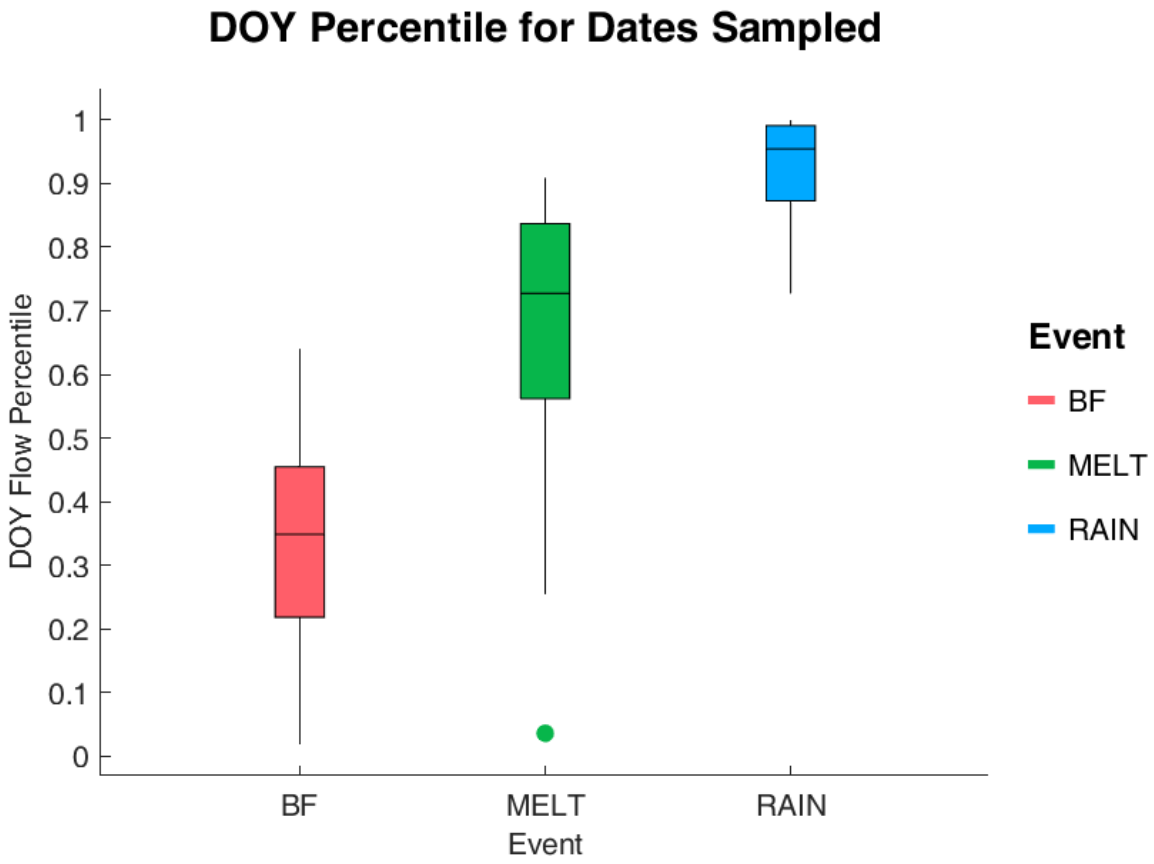

Figure A20: Box plots of Streamflow Percentiles Sampled During Each Event. Box plots of the distributions of day of year streamflow percentiles at the USGS gage locations sampled during the three seasonal sampling events. Results of this analysis suggest that: the baseflow event sampled conditions slightly drier than average, the snowmelt event captured slightly wetter than normal conditions, and the summer rain event was much wetter than average.

APPENDIX B: SUPPLEMENTARY INFORMATION FOR CHAPTER 3

B.1 Vertical Seepage Face Conductance Derivation

A conductance term C_{mf} is used by MODFLOW to approximate discharge Q_{mf} from a cell with a vertical seepage face using the head simulated by MODFLOW h_{mf} within that cell, as shown in Equation A1:

[A1] $$Q_{mf} = C_{mf} * h_{mf}$$

MODFLOW calculates a single head within each cell (h_{mf}), however in a cell containing a seepage face, some gradient between head at the cell face with incoming flow h_1 and the head at the cell face with the seepage condition h_2 must exist, as shown in the diagram below.

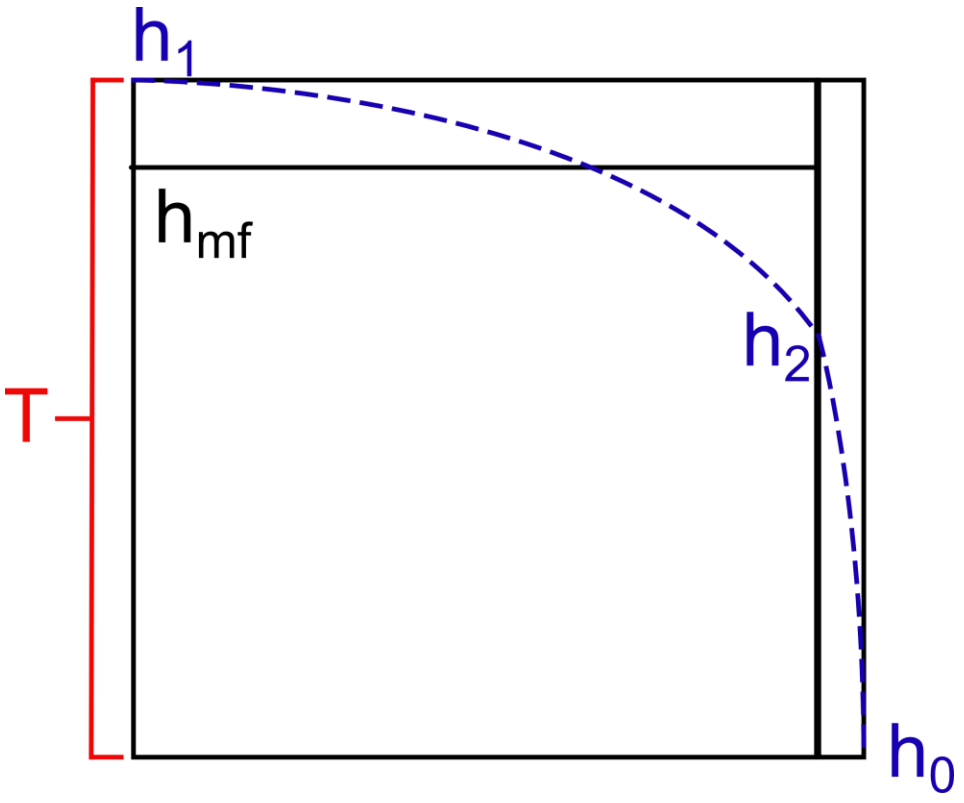

Figure A21: Vertical Seepage Face Conceptual Diagram. Conceptual relaptionship between the average head computed by MODFLOW h_{mf}, and the gradient in head a cell with a vertical seepage face from the cell face with incoming flow h_1 to the cell face with the drainage condition h_2.

The following process was used to derive C_{mf} such that within cell variations in head are considered with the calculation of Q_{mf}. Specifically, a combination of Darcy's law (shown in Equation A2) and the Dupuit-Forchheimer assumption (shown in Equation A3) were used to

approximate the saturated thickness of the cell at the seepage face (h_2).

Darcy's law (Equation A2) defines discharge through a porous media in two dimensions as:

[A2] $$Q = -K\frac{dh}{dL}T$$

Where: Q is discharge, K is hydraulic conductivity, dh is the change in head which occurs over the distance dL, and T is the saturated thickness of the aquifer.

The Dupuit-Forchheimer assumption is used to simplify the groundwater flow equation in an 2-D unconfined steady aquifer; assuming that groundwater flows predominantly in the horizontal direction and that discharge is proportional to saturated thickness such that:

[A3] $$Q_{DF} = \frac{K(h_2^2 - h_1^2)}{2L}$$

At the vertical seepage face, if we assume that head falls from h_2 directly interior of the seepage face, to h_0 directly outside the seepage face, across 1 unit length, then Q_{seep} becomes:

[A4] $$Q_{seep} = K\frac{h_2 - h_0}{dL} * h_2$$

If we assume that the head datum is the bottom of the saturated aquifer, then Equation A4 simplifies to:

[A5] $$Q_{seep} = K * h_2^2$$

Through the Continuity Equation, we know that the flux across the length L equals that across the seepage face $Q_{DF} = Q_{SEEP}$. Therefore:

[A6] $$Kh_2^2 = \frac{K(h_2^2 - h_1^2)}{2L}$$

Solving for h_2 yields:

[A7] $$h_2 = h_1 * \sqrt{\frac{1}{1+2L}}$$

Substituting h_2 from Equation A7 in A3 to solve for the Dupuit-Forchheimer discharge (Q_{DF}) in terms of cell width (W), cell length (L), K and h_1 as shown in Equation 7:

[A7] $$Q_{DF} = \frac{K}{2}\left(h_1^2 - h_1^2\left(\sqrt{\frac{1}{1+2L}}\right)^2\right) = \frac{K}{2}\left(h_1^2 - \frac{h_1^2}{1+2L}\right)$$

Assuming that in the case of a model with square cells, and a linear cell size (L) much greater than 1, the term $\sqrt{\frac{1}{1+2L}}$ is negligible, allowing us to simplify Equation A7 into Equation

A8:

[A8] $$Q_{DF} = \frac{K}{2} h_1^2$$

Hypothetically, MODFLOW is simulating the average head in a cell, thus we would like an expression of the average head in our system in terms of h_1. To do this, we integrate for $h(x)$, given by Equation A3: $h(x) = \sqrt{h_1^2 - \frac{2Q_{DF}}{k} x}$:

[A9] $$\bar{h} = \frac{1}{L} \int_0^L h(x) dx = \frac{1}{L} \int_0^L \sqrt{h_1^2 - \frac{2Q_{DF}}{K} x} dx$$

Using the method of substitutions, and assuming that the cell sizes are sufficiently large such that the quantity $1 + 2L \approx 2L$ this can be directly integrated to produce $\bar{h} = \frac{2}{3} h_1$. Thus the average head in the MODFLOW cell h_{MF} should be:

[A10] $$h_{MF} = \frac{2}{3} h_1$$

Finally, Equation 1 can be rewritten in terms of the seepage face conductance c_{sf}:

[A11] $$C_{sf} = \frac{Q_{MF}}{h_{MF}}$$

Assuming that the MODFLOW Discharge (Q_{MF}) equals the Dupuit-Forchheimer discharge from Equation A8, and substituting Equation A10 into Equation A11, yields:

[A12] $$C_{sf} = K * \frac{h_1^2/2}{\frac{2}{3} h_1}$$

Simplifying this equation yields the final equation for MODFLOW vertical seepage faces, shown in Equation A13:

[A13] $$C_{sf} = \frac{3}{4} K * h_1$$

Table A9: Summary Quaternary Geology Classes. Geology unit codes and names from the USGS Quadrangle maps, and their relationship to the summary model Quaternary geology classes.

USGS Geo Codes	USGS Map Units	LHM Model Class
al	Alluvium	Alluvium
lcr	Attenuated Lake Silt And Clay	Lacustrine fine
R	Bedrock	Bedrock
tc	Clayey Till	Till fine
tce(g)	Clayey Till	Till fine
tce(e)	Clayey Till	Till fine
tak	Clayey Till	Till fine
tae	Clayey Till	Till fine
tcb	Clayey Till	Till fine
tca	Clayey Till	Till fine
taj	Clayey Till	Till fine
tah	Clayey Till	Till fine
tad	Clayey Till	Till fine
ed	Dune Sand	Sand
eu	Eolian Sand And Silt	Sand
es	Eolian Sheet Sand	Sand
ks	Ice-Contact Sand	Sand
kg	Ice-Contact Sand And Gravel	Sand
lm	Lake Clay And Silt (Under Lakes Huron, Erie, And Ontario)	Lacustrine fine
lca	Lake Clay And Silt	Lacustrine fine
lcc	Lake Clay, Silt, Sand, And Gravel	Lacustrine coarse
lcb	Lake Clay, Silt, Sand, And Gravel (Under Lakes St. Clair)	Lacustrine coarse

Table A9 (cont'd)

lds	Lake Delta Sand And Gravel	Lacustrine coarse
lsa	Lake Sand and Gravel	Lacustrine coarse
ls	Lake Sand and Gravel (Under Lakes Huron, Erie, And Ontario)	Lacustrine coarse
lga	Lake Sandy Gravel	Lacustrine coarse
lc	Lake Silt And Clay	Lacustrine fine
tl	Loamy Till	Till medium
tlr	Loamy Till	Till medium
tkg	Loamy Till	Till medium
tki	Loamy Till	Till medium
tlg	Loamy Till	Till medium
tlh	Loamy Till	Till medium
f	Manmade	Artificial Fill
tdr	Noncalcareous Sandy Loamy Till, Attenuated Drift	Till medium
gs	Outwash Sand	Outwash
gg	Outwash Sand And Gravel	Outwash
hp	Peat	Peat and Muck
td	Sandy Loamy Till	Till medium
teb	Sandy Loamy Till	Till medium
tdb(g)	Sandy Loamy Till	Till medium
tdb(e)	Sandy Loamy Till	Till medium
tdb(s)	Sandy Loamy Till	Till medium
tdb	Sandy Loamy Till	Till medium
tde	Sandy Loamy Till	Till medium
ts	Sandy Till	Till coarse

Table A9 (cont'd)

tsr	Sandy Till, Attenuated Drift	Till coarse
hs	Swamp Deposit	Peat and Muck
Lake, river, island	Water	Water

Table A10: Quaternary Geology Unit Average Hydraulic Conductivity. Unit average horizontal hydraulic conductivity in the summary Quaternary geology classes.

LHM Model Class	Mean HK
Alluvium	4.35
Lacustrine coarse	17.90
Lacustrine fine	15.38
Outwash	67.15
Peat and Muck	23.00
Sand	58.17
Till coarse	15.94
Till fine	44.45
Till medium	63.01
Water	70.59
Artificial Fill	15.94
Bedrock	3.30

Table A11: Relationship between GLAHF Substrate and Quaternary Geology Class with Associated HK Values. GLHAF Substrate units were match to those in the Quaternary geology classes for the model surficial aquifer, and then average HK values form these Quaternary geology classes were assigned to the substrate types as shown below.

GLAHF Substrate Texture	GLAHF Substrate Description	Quaternary Geology Class	Mean HK
very coarse	<0 (Phi Units)	Lacustrine coarse	17.90
very coarse	>50% rock	Lacustrine coarse	17.90
fine	>6 (Phi Units)	Lacustrine fine	15.38
coarse	0.062 - 0.25 mm	Lacustrine coarse	17.90
fine	0.062 mm & smaller	Lacustrine fine	15.38
coarse	0.25 - 0.5 mm	Lacustrine coarse	17.90
very coarse	0.5 mm & larger	Lacustrine coarse	17.90
coarse	0-2 (Phi Units)	Lacustrine coarse	17.90
coarse	2-4 (Phi Units)	Lacustrine coarse	17.90
fine	4-6 (Phi Units)	Lacustrine fine	15.38
fine	artificial	Artificial Fill	15.94
very coarse	Assorted cobble/rock	Lacustrine coarse	17.90
very coarse	assumed hard	Bedrock	3.30
very coarse	Bedrock	Bedrock	3.30
very coarse	bedrock	Bedrock	3.30
very coarse	Bedrock and rubble	Bedrock	3.30
very coarse	Bedrock with cobble patches	Bedrock	3.30
fine	Clay ridges with sand	Lacustrine fine	15.38
coarse	Coarse Sand	Lacustrine coarse	17.90
coarse	coarse sand	Lacustrine coarse	17.90
very coarse	Cobble evenly distributed on sand	Till medium	63.01
very coarse	Cobble on bedrock	Bedrock	3.30

Table A11 (cont'd)

very coarse	Cobble patches on sand	Till medium	63.01
fine	cohesive clay	Lacustrine fine	15.38
fine	Dredge spoils	Lacustrine fine	15.38
coarse	fine sand	Lacustrine fine	17.90
coarse	Fine Sand	Lacustrine coarse	17.90
fine	Glaciolacustrine clay	Lacustrine fine	15.38
fine	glaciolacustrine clay	Lacustrine fine	15.38
fine	glaciolacustrine sediment	Lacustrine fine	15.38
very coarse	Gravel	Lacustrine coarse	17.90
very coarse	gravel	Lacustrine coarse	17.90
very coarse	hard	Bedrock	3.30
very coarse	Large cobble with sand	Lacustrine coarse	17.90
coarse	medium sand	Till medium	63.01
coarse	Medium Sand	Till medium	63.01
very coarse	Mixed Cobbles / Boulders	Till medium	63.01
very coarse	Mixed Gravels / Pebbles / Cobbles	Till medium	63.01
fine	mud	Lacustrine fine	15.38
fine	Mud	Lacustrine fine	15.38
fine	mud, silt	Lacustrine fine	15.38
fine	mud, silts	Lacustrine fine	15.38
fine	muds	Lacustrine fine	15.38
very coarse	rock	Till medium	63.01
very coarse	rubble	Till medium	63.01
very coarse	Rubble and Sand	Till medium	63.01

Table A11 (cont'd)

coarse	Sand	Till medium	63.01
coarse	sand	Till medium	63.01
very coarse	Sand and Gravel	Till medium	63.01
very coarse	Sand Infilled Cobbles to Boulders	Till medium	63.01
very coarse	Sand Infilled Pebbles to Cobbles	Till medium	63.01
very coarse	Sand on broken bedrock	Till medium	63.01
very coarse	Sand with cobble patches	Till medium	63.01
very coarse	Sand with scattered rubble	Till medium	63.01
very coarse	Sand and Rocks	Till medium	63.01
coarse	Sand/clay	Lacustrine coarse	17.90
coarse	sand/gravel	Till medium	63.01
fine	sand/mud	Lacustrine fine	15.38
very coarse	Sand/rock combination	Till medium	63.01
fine	Sandy Mud	Lacustrine fine	15.38
very coarse	Sandy Mud and Rocks	Till fine	
fine	silt	Lacustrine fine	15.38
fine	silt/clay	Lacustrine fine	15.38
very coarse	Small Cobbles	Till medium	63.01
very coarse	Smooth bedrock	Bedrock	
fine	soft	Lacustrine fine	15.38
very coarse	till and bedrock	Till medium	63.01
very coarse	till and/or bedrock	Till medium	63.01

Table A11 (cont'd)

fine	Type A basin sediments (muds)	Lacustrine fine	15.38
fine	Type B basin sediments (muds > 50%)	Lacustrine fine	15.38
fine	undefined	Lacustrine fine	15.38
very coarse	Undifferentiated till or bedrock	Till medium	63.01
fine	Unknown	Lacustrine fine	15.38

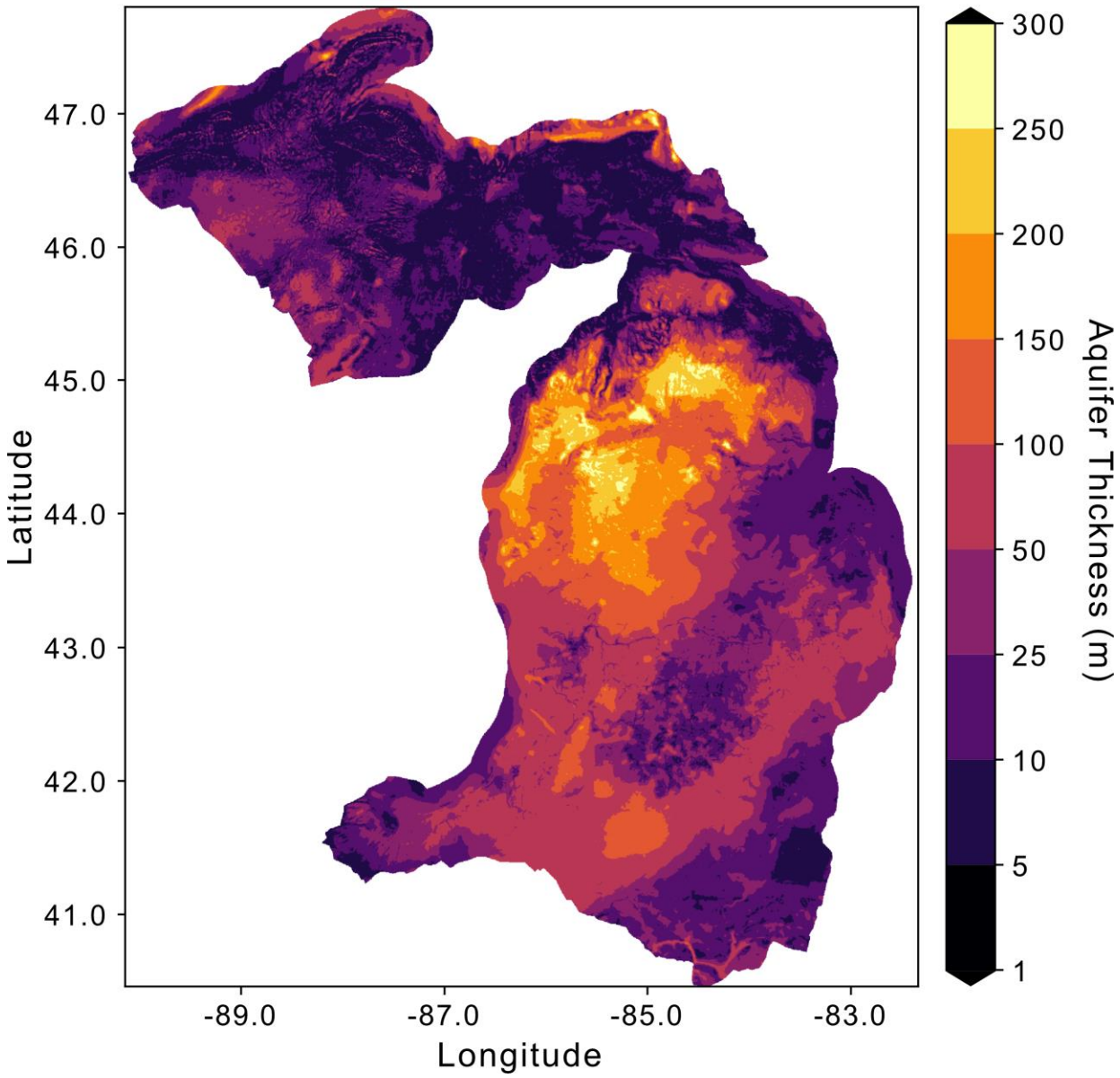

Figure A22: Surficial Aquifer Thickness. The surficial aquifer is thickest in the northern Lower Peninsula as a result of Quaternary glacial drift depots up to 350 m thick. The surficial aquifer is thinnest in the Upper Peninsula where bedrock units are near the surface, and in the Saginaw Bay and Maumee watershed regions.

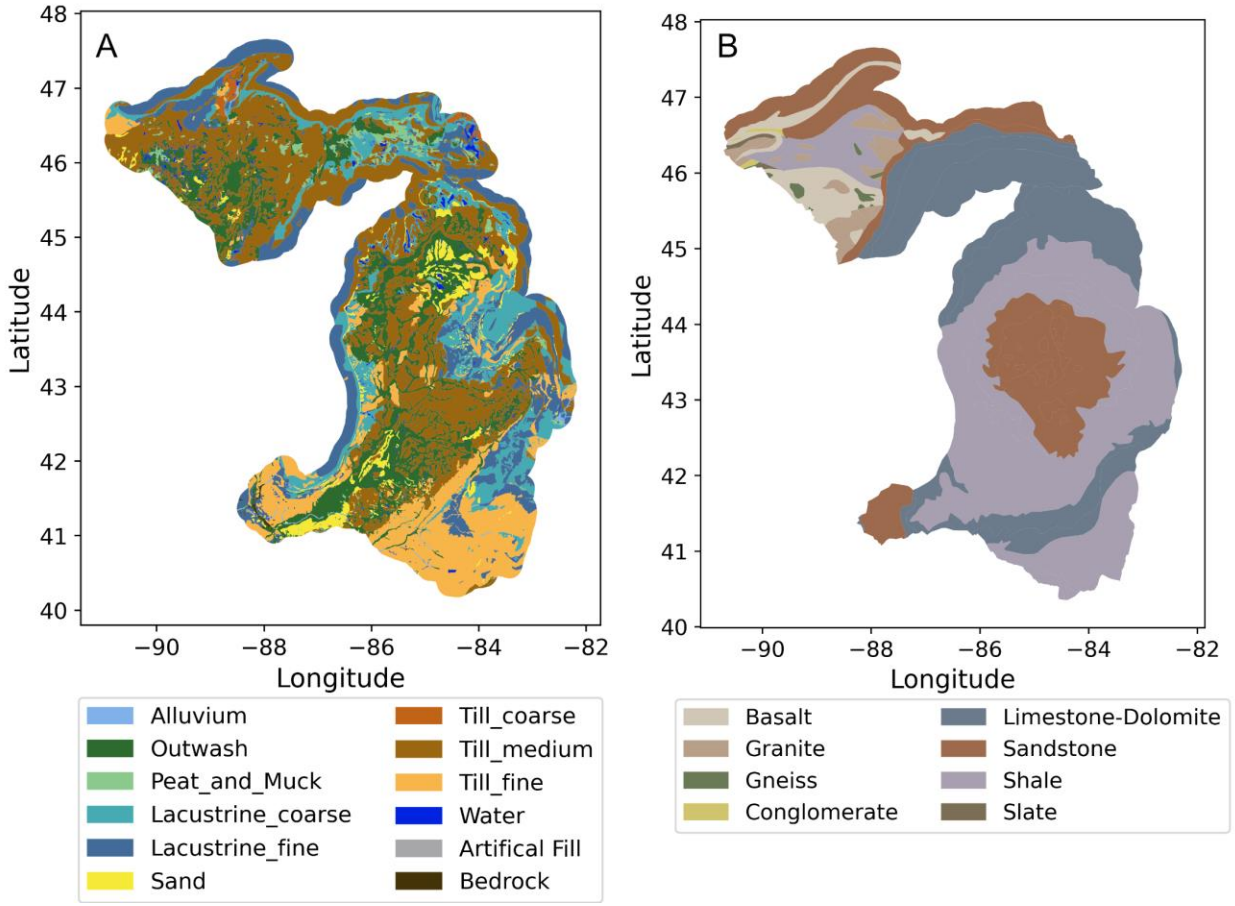

Figure A23: Surficial and Bedrock Geology for the Michigan Model Domain. Surficial (A) and bedrock (B) geology for the model region. Geologic unit classes present in the original datasets have been combined into summary classes for use in the model. Surficial geology is dominated by Quaternary glacial deposits including tills, outwash, and lacustrine deposits from glacial lakes. Bedrock geology across the eastern upper and all of the lower domain is dominated by units of the Michigan Basin, primarily limestone, dolomite, shale and sandstone. Bedrock in the western half of the upper domain includes Cambrian and Precambrian era volcanic and metamorphic units, including the southern extent of the Canadian Shield.

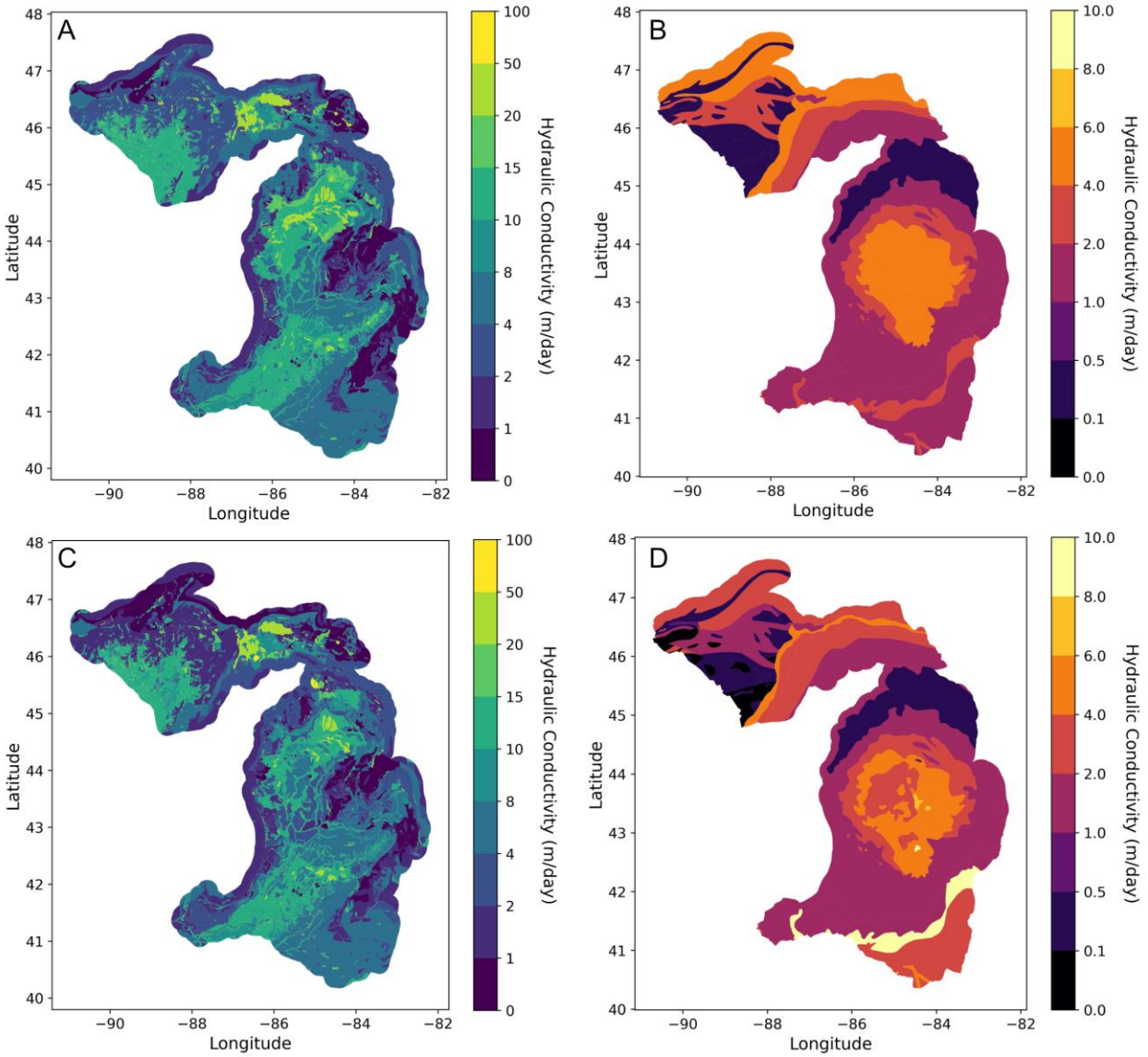

Figure A24: Uncalibrated and Calibrated Hydraulic Conductivity Maps. Model hydrogeologic properties including the (A) surface aquifer thickness (surface topography minus bedrock topography). Surficial aquifers are thickest in the Northern Lower Peninsula due to massive deposits of glacial outwash.

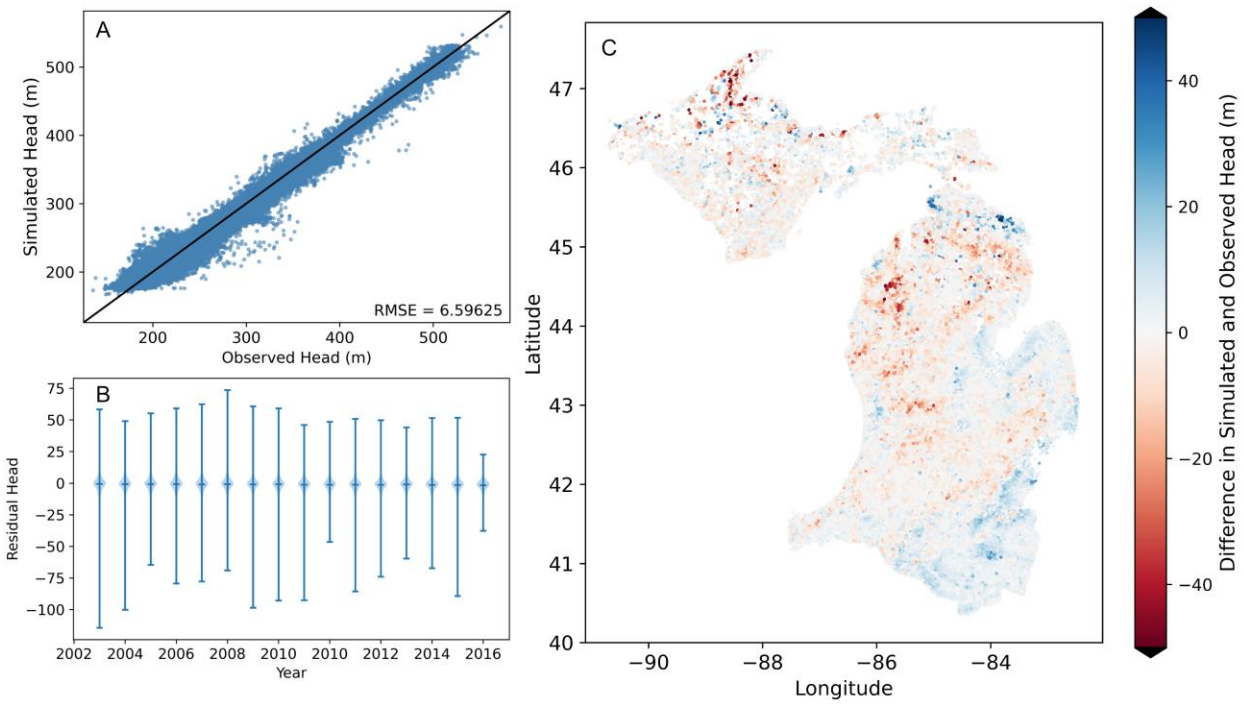

Figure A25: Simulated and Observed Groundwater Elevations. Model calibration results showing (A) simulated vs observed heads, (B) residuals binned to years, and (C) mapped differences in simulated and observed heads. Overprediction is biased slightly toward low-lying areas of the model, particularly in the northern Lower Peninsula and south-eastern proportion of the model domain. Underprediction is biased toward the mid-elevation portions of the northern Lower Peninsula characterized by deep glacial aquifers and to the western Upper Peninsula in regions of significant elevation and shallow surficial aquifers. No bias through time is observed in the simulated vs observed data, as shown in panel B.

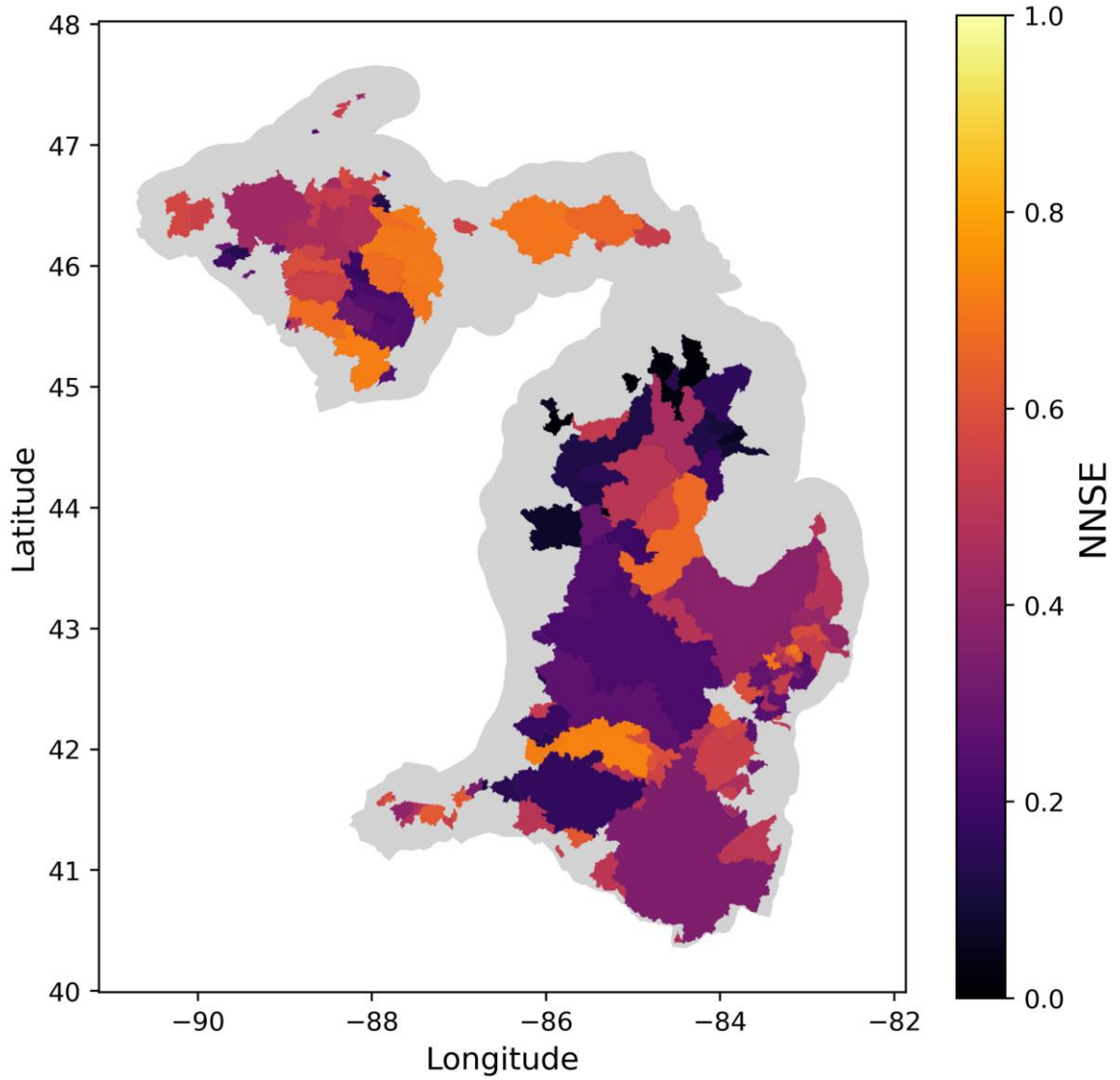

Figure A26: Simulated Streamflow Performance. Normalized Nash Sutcliffe efficiency for observation gage basins in the model domain. Highest NNES values occur in the central and eastern Upper Peninsula, and in a few watersheds in the Lower Peninsula. The lowest NNSE's are observed in the Northern Lower Peninsula, where overprediction in heads is greatest.

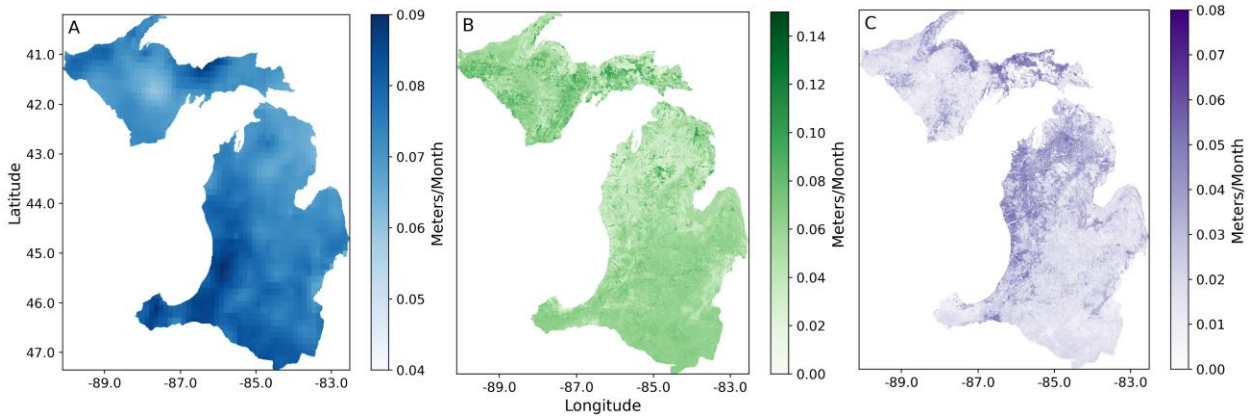

Figure A27: Average Precipitation, ET and Deep Percolation from the Surface Model. Surface model estimates of (A) precipitation, (B) ET and (C) deep percolation averaged over the model simulation period. The northern coastline of the Upper Peninsula along Lake Superior and the western coastline of the Lower Peninsula along Lake Michigan receive significant lake effect precipitation, which is visible in the patterns of deep percolation. ET patterns are influenced by precipitation, but also vegetation and soil characteristics..

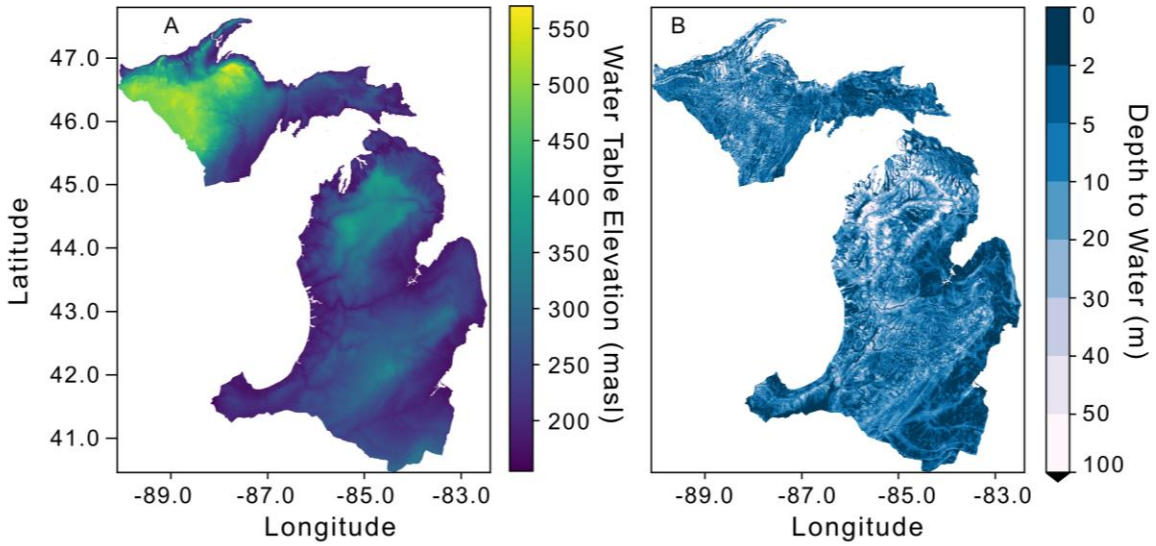

Figure A28: Average Water Table Elevation and Depth to Water from the Groundwater Model. Average water table elevation (A) and depth to water (B) during the model run. Water table elevations closely mirror surface elevations. Depth to water is greatest in the Northern Lower Peninsula, where deep glacial drift aquifers dominate, and shallowest in the western half of the lower domain, which is characterized by low permeability sediments and low relief.

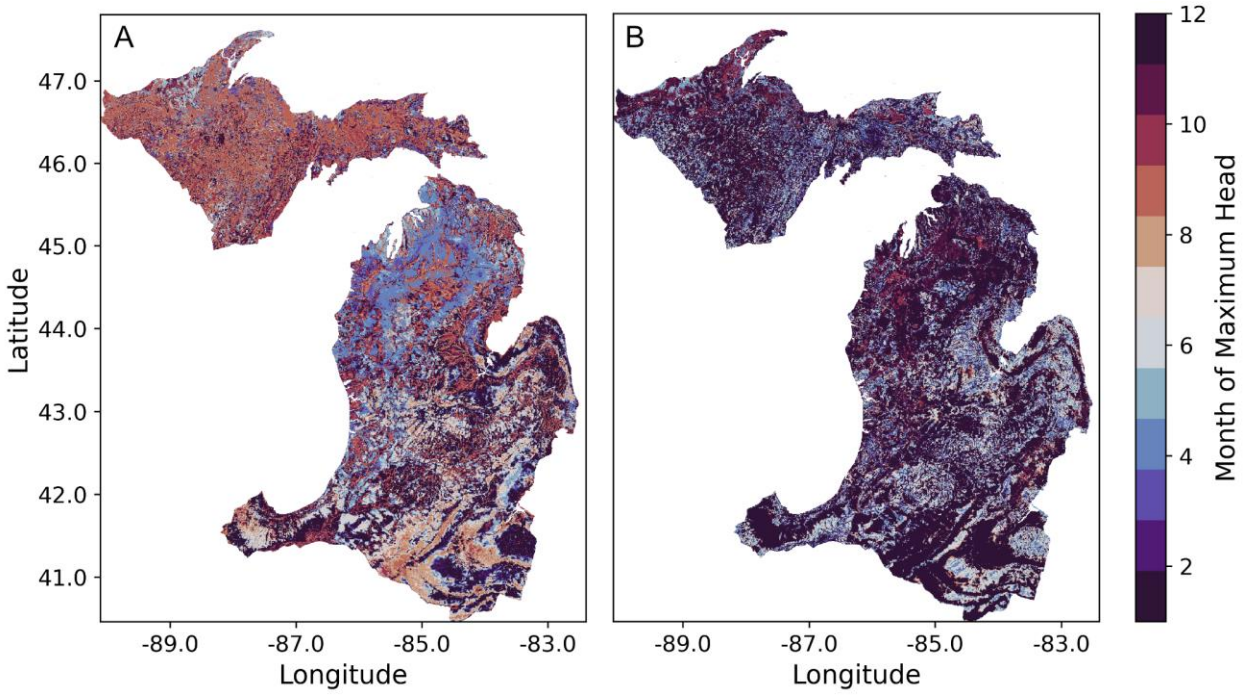

Figure A29: Month of Annual Minimum and Maximum Head Elevation. Month of (A) minimum and (B) maximum on average across the model years. The month of each year with the minimum (maximum) head was computed, and then the mode was taken for each pixel in the model domain. Minimum heads occur in fall for most of the upper domain. In the lower domain, minimum heads occur across a range from spring to fall in most of the domain. Parts of the southern lower domain including in the Saginaw Bay and Maumee Watershed experience minimum heads in the winter (December to January). Maximum head occur during winter (November to February) across most of the model region, with the exception of some portion of the lower domain, including in the Saginaw Bay and Maumee River basins, where maximum heads occur during the spring or early summer.

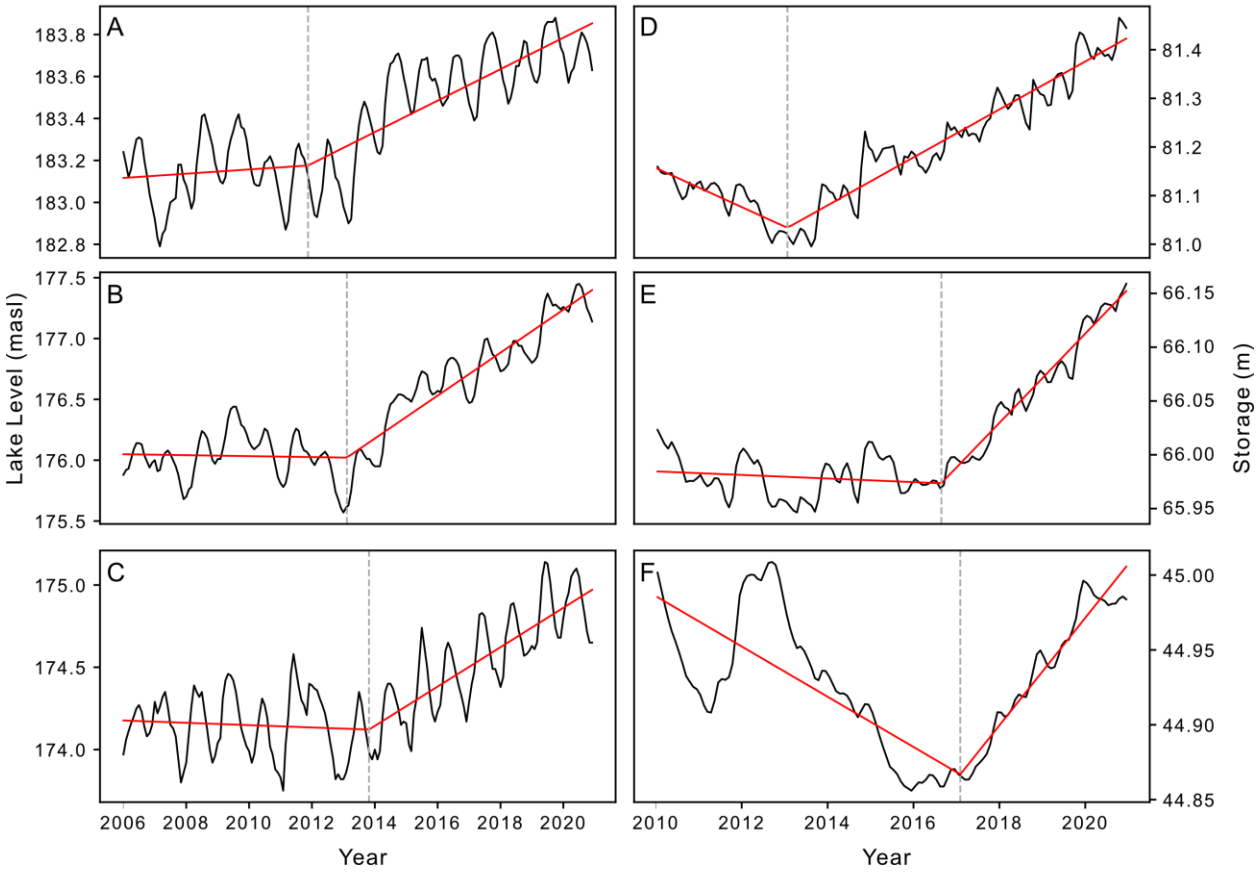

Figure A30: Segmented Linear Regression for Lake Eelvations and Simualted Groundwater Heads. Breakpoints identified by piecewise regression analysis indicating the year in which lake elevations (A-C) and groundwater storage (D-F) began their most recent increases. This analysis indicates a distinct delay between the rising lake elevations and increases in groundwater storage which increases north-south across the lakes and their associated basins.

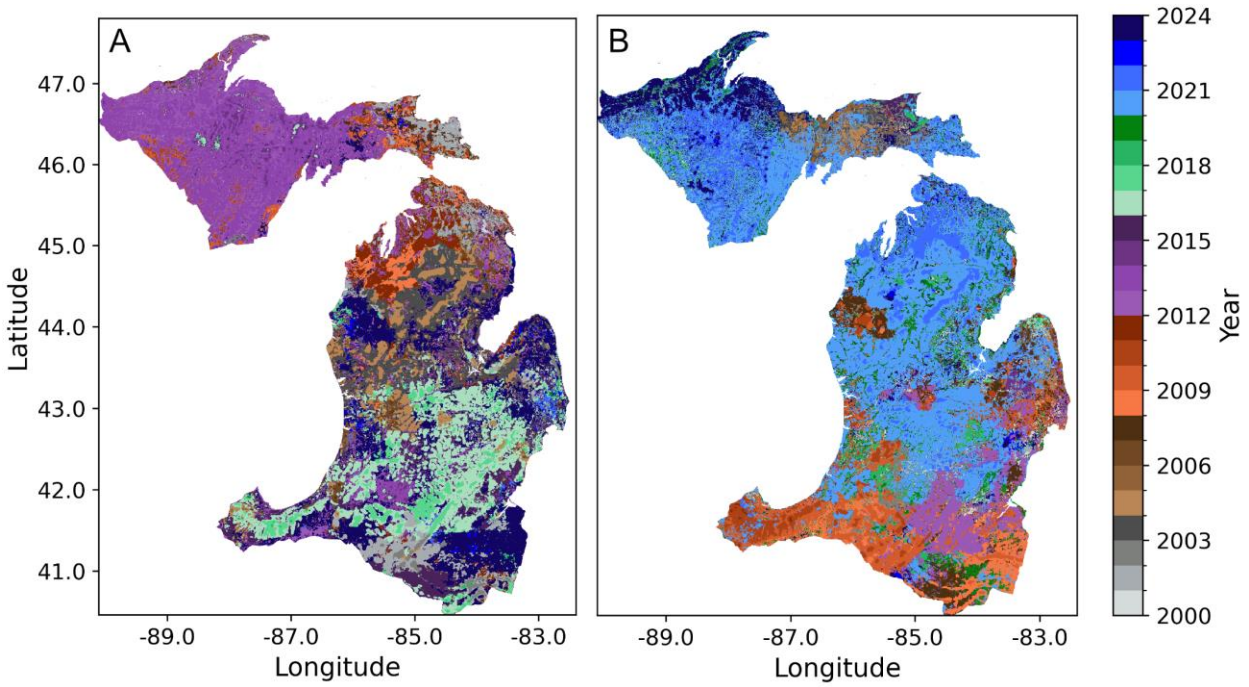

Figure A 31: Year of Minimum and Maximum Head Elevation. Year of (A) minimum and (B) maximum head elevations between 2000-2023. Across most of the upper domain, minimum heads occurred between 2009-2013. Minimum heads in the lower domain trends from ~2009 to between 2018-2024 north to south across most of the region. Maximum heads across a large portion of the domain occurred between the start of 2020 and the end of 2023. In the far southern portion of the basin, as well as in other isolated locations, maximum heads occurred much earlier between ~2009-2013.

APPENDIX C: SUPPLEMENTARY INFORMATION FOR CHAPTER 4

Table A12: NWI Palustrine Wetland Depth. Wetland depths assigned to palustrine wetlands based on the NWI Wetland Water Regimes, assuming an increasing depth with the degree of saturation and inundation.

NWI Water Regime Name	Depth
Seasonally Saturated	0
Continuously Saturated	0
Intermittently Flooded	0.25
Temporarily Flooded	0.5
Seasonally Flooded	0.75
Seasonally Flooded-Saturated	1
Semipermanently Flooded	1.5
Intermittently Exposed	2
Permanently Flooded	2.5
Artificially Flooded	2.5

Table A13: Effects of Mean Error Adjusted Head on Wetland Connectivity. Comparison of groundwater and surface water connectivity when assessed at the groundwater model (500m) and DEM (24.6m) resolution.

	500m Resolution		24.6m Resolution	
	Area km^2	Percent Change	Area km^2	Percent Change
Min SW Con	1897		495.38	
Max SW Con	5488		1871.84	
SW Con Change	3591	189.29	1462.36	277.86
Min GW Con	525.75		356.75	
Max GW Con	1161.25		573.7	
GW Con Change	635.5	120.87	216.95	60.81

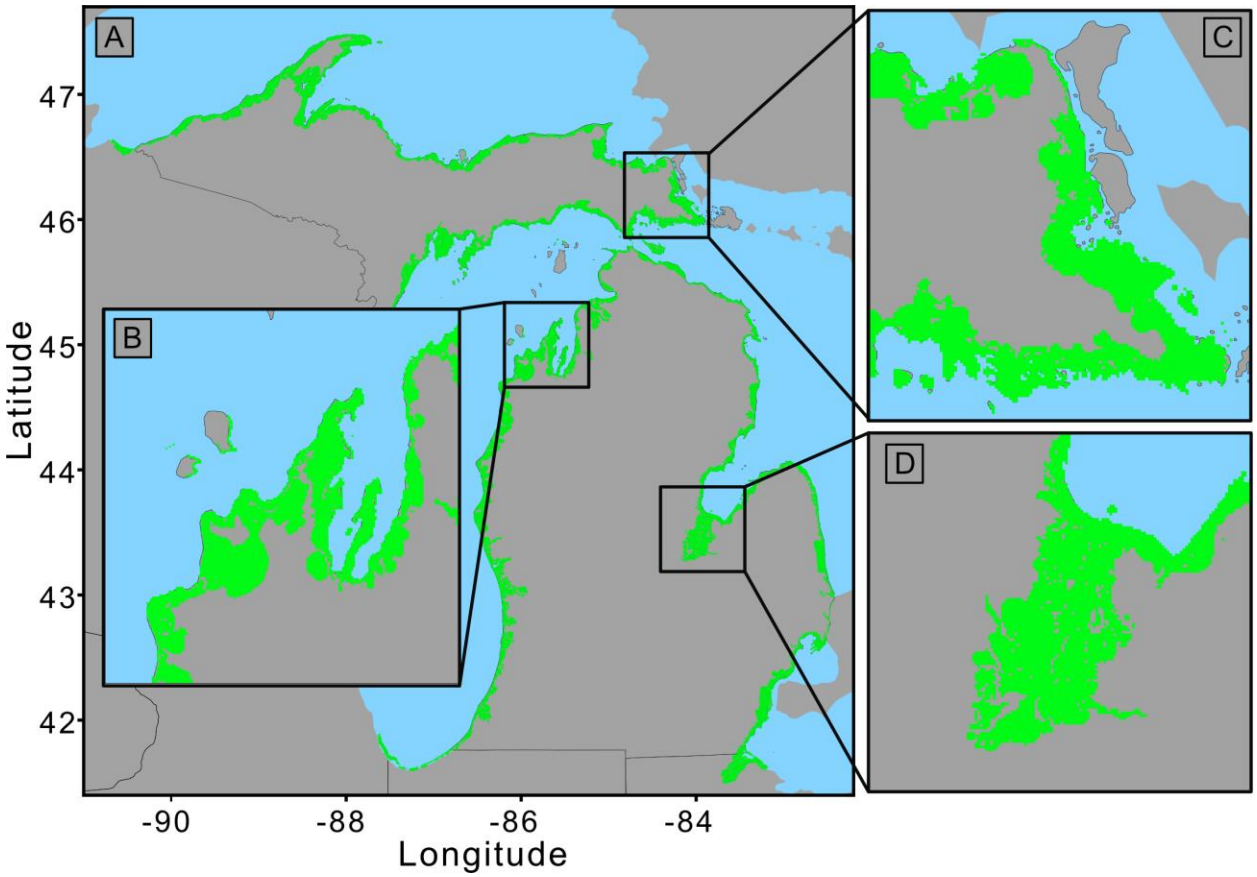

Figure A32: Coastal Wetland Zone Extent. The combined maximum extent of surface water inundated coastal wetlands and potential groundwater connected palustrine wetlands shown for the model region (A), Grand Traverse Bay region (B), eastern UP (C) and Lower Saginaw River (D). This layer was created by merging the area of maximum inundation with the area where heads were greater than 1cm different in the extreme lake level scenario runs. Both of these conditions were assessed at the groundwater model resolution. Quantification of wetland connectivity, and of groundwater model error for the purposes of uncertainty quantification in the sensitivity analysis were restricted to this area.

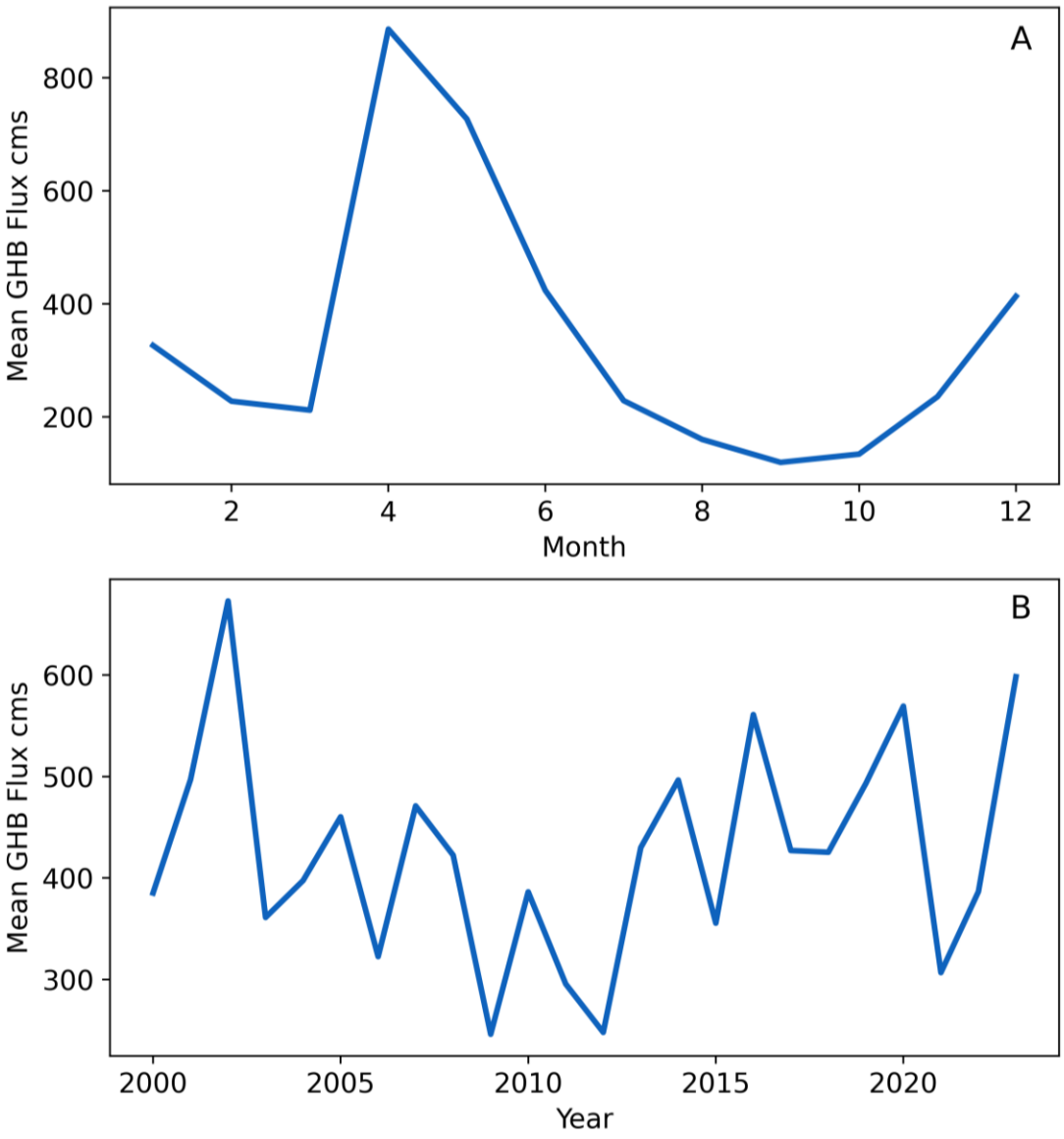

Figure A33: Average Monthly and Annual Average Groundwater Discharge to the Great Lakes. The average discharge through the general head boundary region for each month shows direct groundwater fluxes to the lake peak in April and are lowest in September. Annual average groundwater discharge (B) is lowest between 2009-2011, when the lakes and groundwater were both near their minimum conditions, and much higher at the beginning and end of the model period.

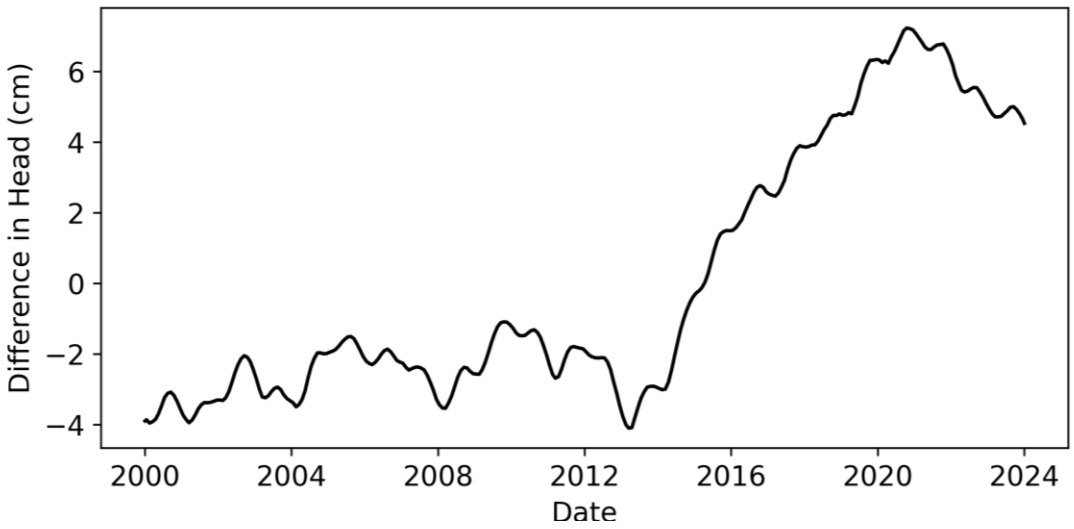

Figure A34: Difference in Simulated Heads with Transient and Fixed Lake Elevation Boundary Conditions. The difference between heads in the coastal wetland zone for the "base" and 'MED" scenarios suggest that without varying lake elevations, heads are over-predicted by roughly 4cm between 2000-2013 and underpredicted by between 1 and 6cm between 2014-2023.

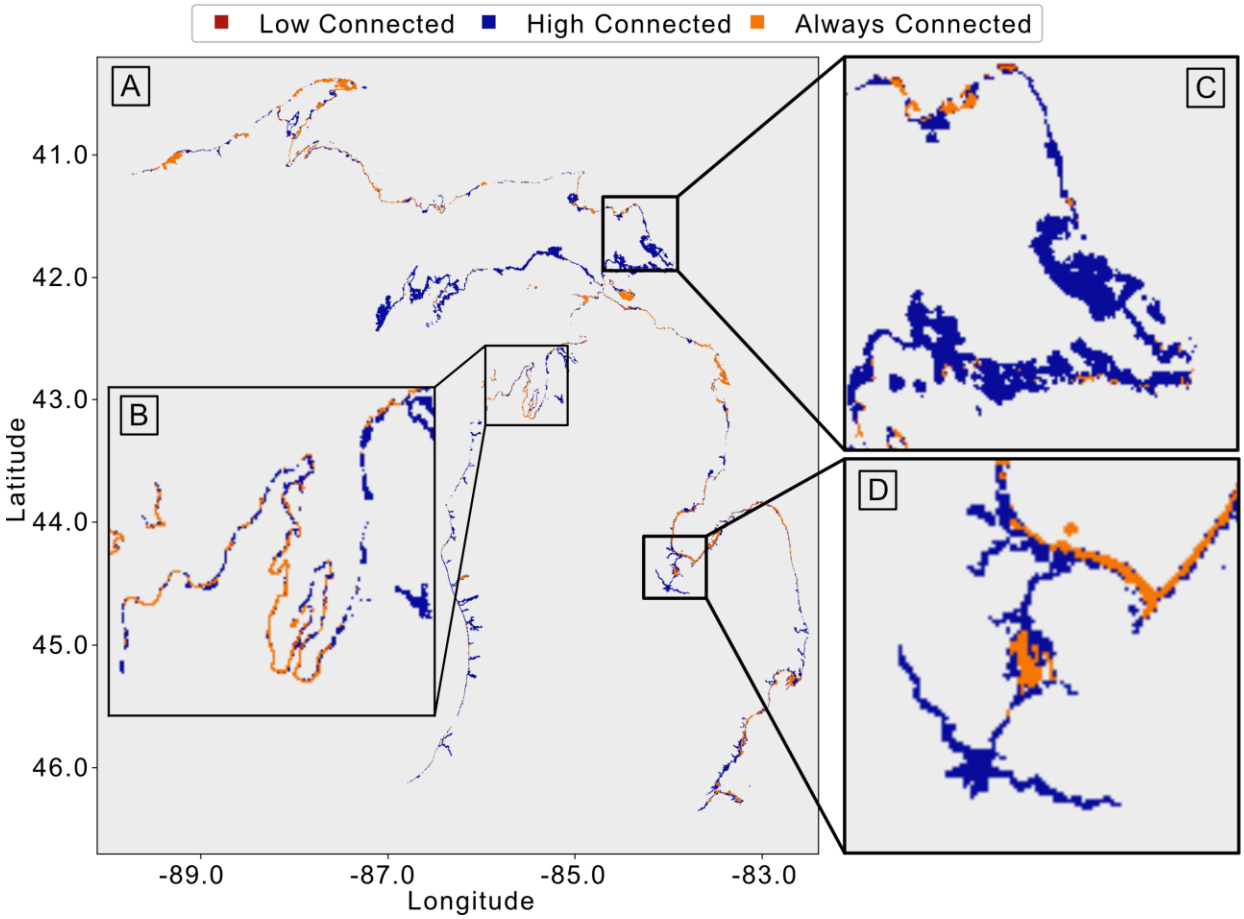

Figure A35: Surface Water Connectivity to Coastal Wetlands. Surface water connectivity to coastal wetlands for the low and high lake levels shown for the model region (A), Grand Traverse Bay region (B), Eastern UP (C) and Lower Saginaw River (D). Areas in red are only connected at low levels, those in blue connected only at high levels, and those in orange connected at both. Persistent connectivity is most widespread along the Lake Huron shoreline in the Lower Peninsula, while the Lake Michigan-Huron shoreline in the UP gains the most surface water connected wetland area at high lake levels.

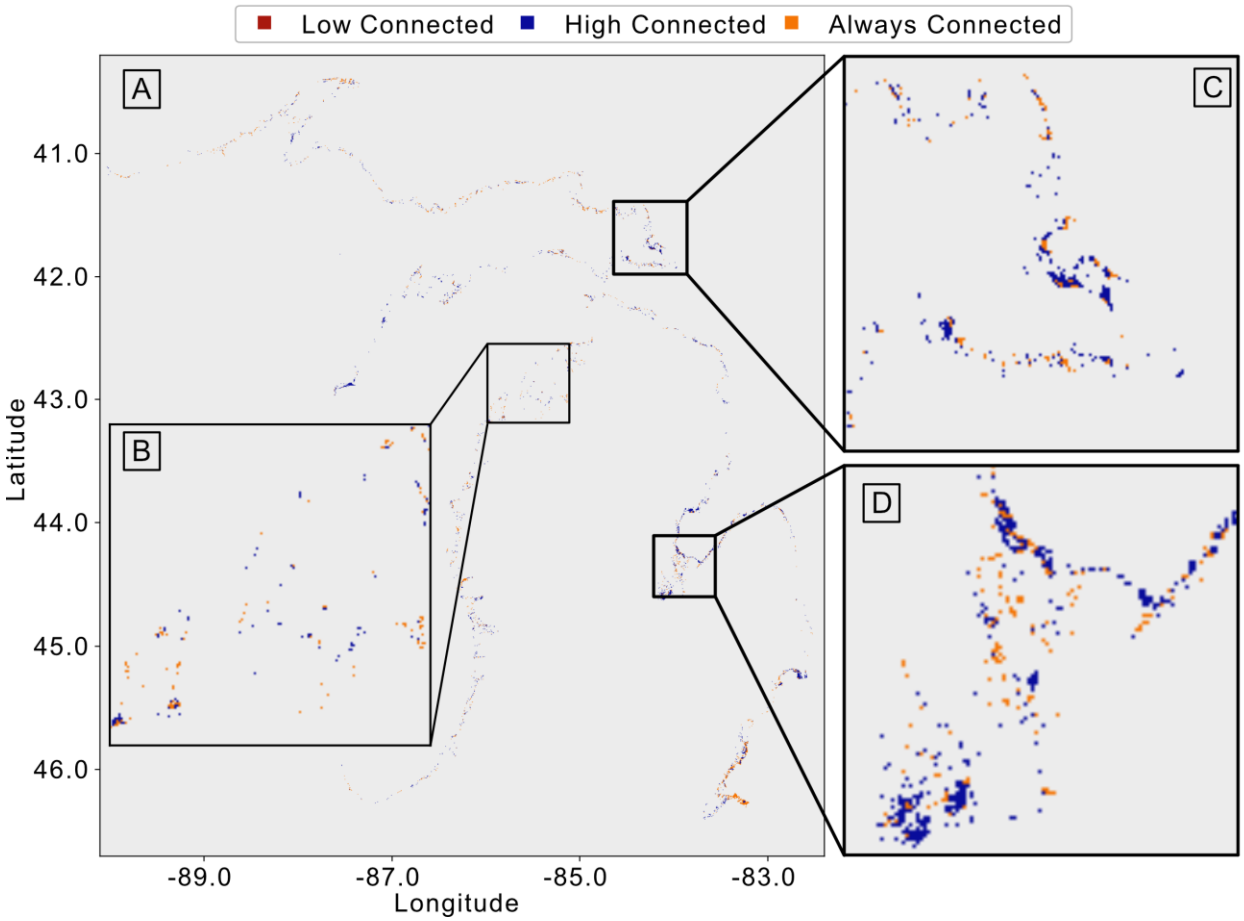

Figure A36: Groundwater Connectivity to Coastal Wetlands. Groundwater connectivity in coastal wetlands for the minimum and maximum head conditions shown for the model region (A), Grand Traverse Bay region (B), Eastern UP (C) and Lower Saginaw River (D). Areas in red are only connected at low levels, those in blue are connected only at high levels, and those in orange are connected at both. Groundwater connectivity is generally greater along the shorelines of the UP, and the Lake Huron shoreline in the LP. The Lake Michigan shoreline has generally lower groundwater-coastal wetland connectivity due to its generally higher relief along the shoreline.

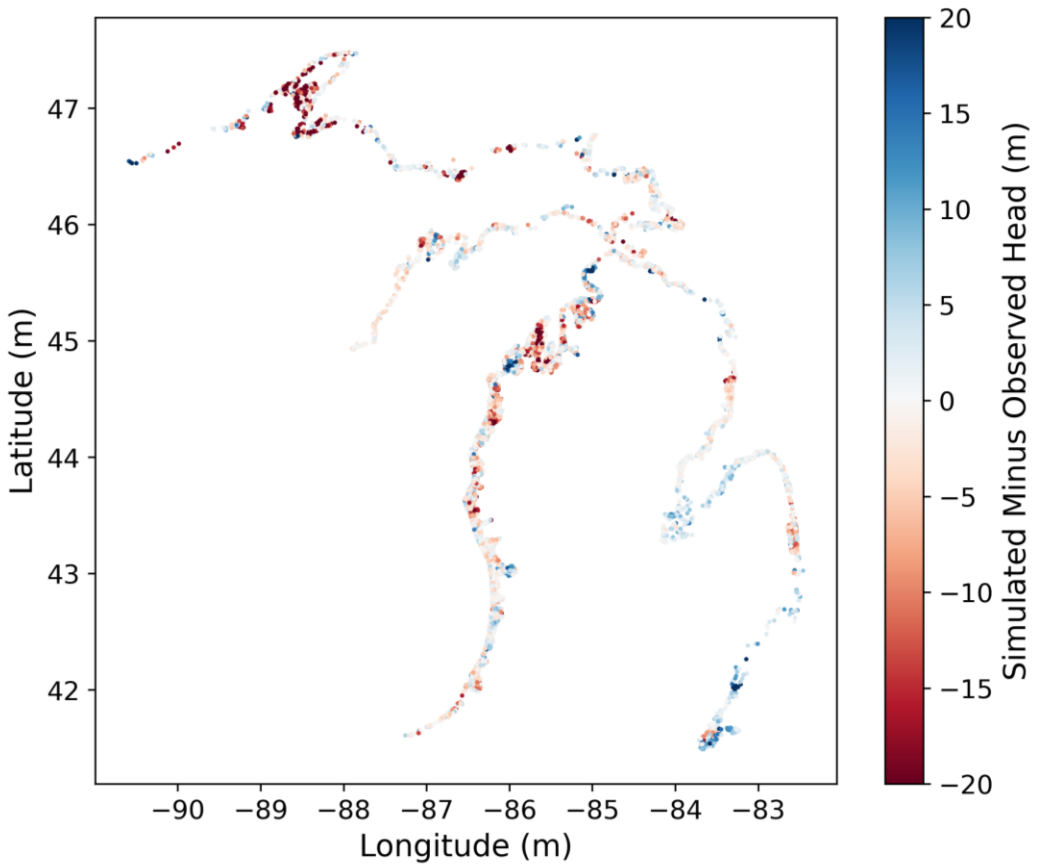

Figure A37: **Groundwater Model Error in the Coastal Wetland Zone.** Differences between simulated and observed heads in the coastal wetland zone where simulated heads are a median of 0.81 m below observed values. These areas are not evenly distributed; considerable areas of underprediction occur in the Grand Traverse Bay region, and in the Keweenaw Peninsula, while concentrated areas of overprediction occur along the Lake St. Clair and Lake Erie shorelines.

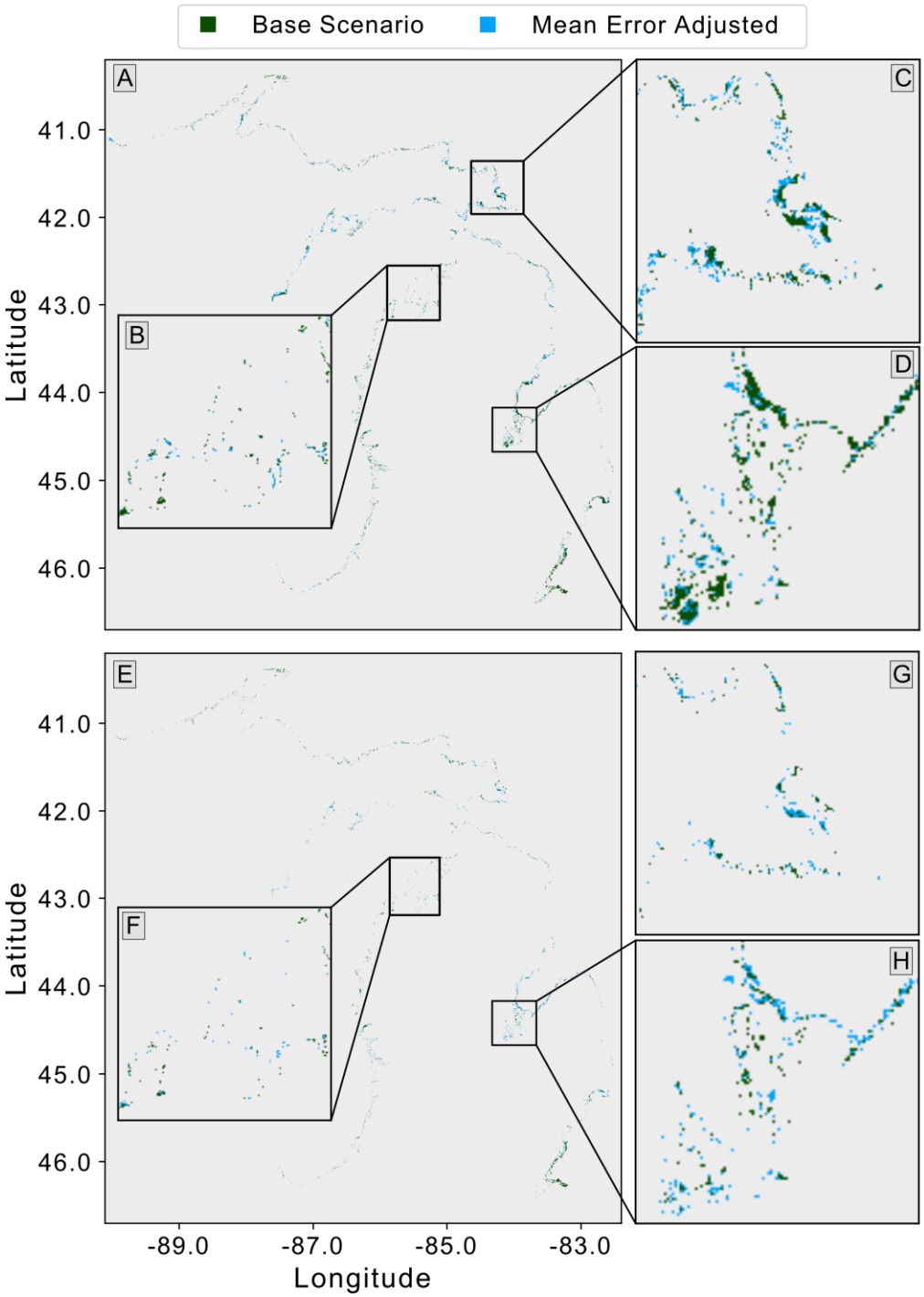

Figure A38: Sensitivity of Connected Wetland Area to Simulated Head Elevation. Changes in connectivity between the base scenario heads and those adjusted by the median error of -0.81 within the coastal groundwater zone, at the maximum (A-D) and minimum (E-H) head conditions. For both minimum and maximum conditions, the mean error adjusted head increases the estimated wetland connectivity, especially in the Eastern UP (Panels C&G) and Lower Saginaw River (Panels D&H). Connectivity in the Grand Traverse Bay region (Panels B&F) remains limited in both cases (base and mean error adjusted) and at both conditions (minimum and maximum).